2005-2010

CHINA NATIONAL REPORT ON

CRYOSPHERIC SCIENCE

Chinese National Committee for International Association of Cryospheric Science (IACS)

Lanzhou, China

December, 2010

CONTENTS

Preface

In July 2007, International Association of Cryospheric Science (IACS) was established during the 24th IUGG Conference, Perugia, Italy. IACS highlights the importance of cryospheric science in Earth system, especially when global warming is unequivocal nowadays.

In February 2008, the Chinese National Committee of IACS (CNC-IACS) was formed. It consists of 13 scientific advisors, 1 chairman, 5 vice-chairs and 44 committee members. The committee is divided into 8 working groups, they are: (1) snow and ice, (2) frozen ground, (3) cold regions hydrology, (4) cold regions ecology, (5) cryosphere and climate, (6) Observation, remote sensing and data base, (7)polar sciences and (8)sustainable development in cryospheric regions. CNC-IACS set up its secretariat in the State Key Laboratory of Cryospheric Sciences (SKLCS) in Cold and Arid Regions Environmental and Engineering Research Institute (CAREERI), Chinese Academy of Sciences (CAS), Lanzhou, China. CNC-IACS was soon approved by CNC-IUGG in early 2008.

Since establishment of CNC-IACS, several workshops and one conference have been organized. For example, annual workshops of CNC-IACS in 2008 (Beijing), 2009 (Beijing) and 2010 (Lijiang), an International Workshop (Xi'an, December 2009) on Changes in Surface and Ground water in the Tarim River Basin. an international joint conference (Lijiang, August 2010) by the WCRP/CliC and IUGG/IACS: Cryospheric Change and its Influences—Cryospheric Issues in Regional Sustainable Development. These workshops and conference have had fruitful outcomes, strengthened the ties between Chinese cryospheric communities with international ones.

CNC-IACS engaged the following researches in recent years: (1) new phase of glacier inventory in China using remote sensing data and in-situ calibration, (2) frozen ground investigations on Qinghai-Xizang (Tibet) Plateau, (3)Snow-cover monitoring and data-base building, (4)cryospheric models and the models of interspheric coupling, （5）disasters in cold regions, (6) polar cryospheric science, (7) adaptation strategy of cryospheric changes.

CNC-IACS also works closely with WCRP/CliC and Asia CliC to develop scientific understandings of the regional cryopshere in Asia especially high Asia regions. CNC-IACS is also very active in Global Cryospheric Watch (GCW) in WMO, designing the networks of cryospheric observations on the ground, with integration of remote sensing data and eventually as important inputs in various models.

This report summarizes the overall progress of CNC-IACS in the last 5 years. Basically divided 8 chapters by 8 working groups in CNC-IACS. Each chapter summarizes major results of group members' and beyond. We limit chapter's author only as working group's leader, but many colleagues contributed to it. The overall

report is edited by vice-Chair and also Secretary-general of CNC-IACS, Prof. Ding Yongjian, vice-Secretary-general, Dr. Xiao Cunde, and Secretary, Dr. Xie Aihong. I appreciate their hard work in the last months.

Qin Dahe

Chairman of Chinese National Committee of IACS

Chapter1. Advance of Studies on Changes in Glacier and Snow Cover in China

Wang Ninglian[1]， Kang Shichang[2,1]

(State Key Laboratory of Cryopsheric Sciences, Cold and Arid Regions Environmental and Engineering Research Institute, Chinese Academy of Sciences, Lanzhou 730000, China; Institute of Tibet Plateau Research, Chinese Academy of Sciences, Beijing 100871, China)

Dramatic changes in Cryosphere already happened in China during the last decades due to the global warming, especially glacier shrinkage prevailing over mountain regions in the western China. During the last 5 years, researchers have been focusing on the spatial and temporal variations in glacier and snow cover in China and hundred papers (or/and reports) have been published. Glacier changes in area, terminus, mass balance as well as their responses (or sensitivity) to climate changes and consequences (e.g. GLOFs) have been investigated in the west of China using remote sensing and in-situ observation data. Numerous results have also been achieved in reconstructing climate and environmental changes using ice core records from high alpine glaciers (cap) in China. This chapter is a review on those results.

1.1 GLACIER CHANGES IN CHINA

Based on the first Chinese Glacier Inventory, there are 46377 glaciers with an area of 59 406 km^2 and a total ice volume of 5 590 km^3 in China (Shi et al., 2005). All the glaciers are distributed in Western China (Fig 1.1). Glaciers in China can be categorized into three types: continental glacier, sub-continental glacier and maritime glacier (Shi et al., 2000). Continental glaciers are mainly located in the middle and west part of Kunlun Mountains, Qiangtang Plateau, eastern Pamirs, western Tanggula and Qilian Mountains. Sub-continental glaciers are distributed over Tian Shan, the northern slopes of the middle and west part of the Himalaya, northern slope of the Karakorum and Nyainqêntanglha Mountains. Maritime glaciers lie at southeast of Tibetan Plateau.

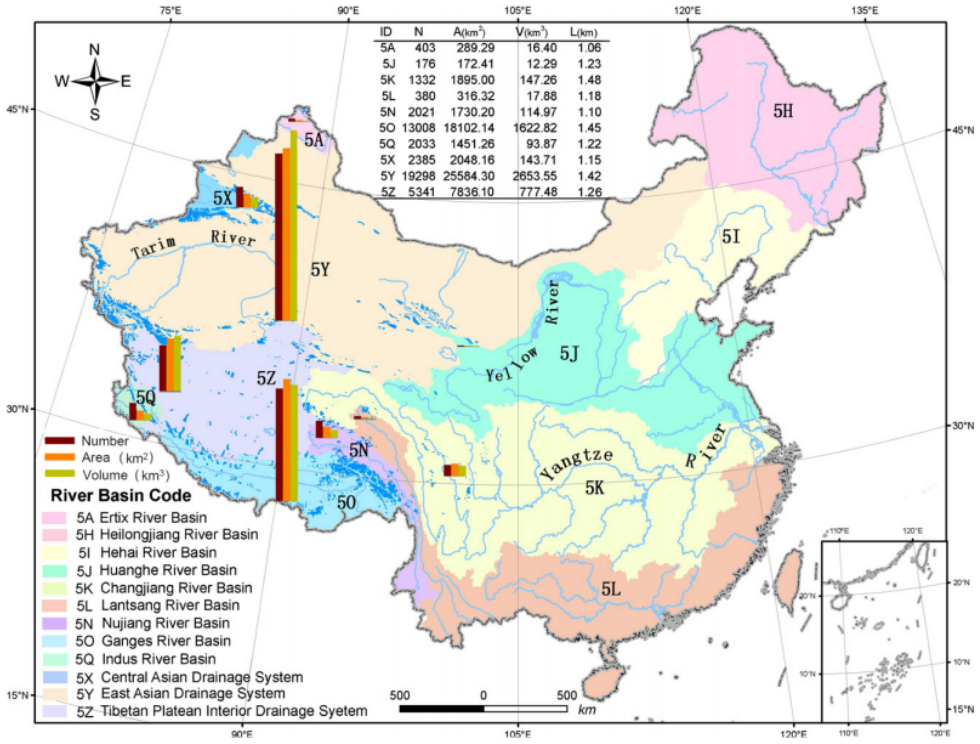

Fig 1.1. Distribution of glaciers in China (from Li et al., 2008)

Most of the glaciers are suffering recession under the global warming in China. According to the recent study, retreating glaciers reached 82.2% of the total glaciers in western China (Liu et al., 2006). Since Little Ice Age, the glacier area of western China has been decreased by 16 013 km^2, which is 21.2% of the whole glacier area (Shi, 2005). The retreating rate has been dramatically increased since 1990s in corresponding to the surface temperature rise. Because of the different glacier type and glacier size, glacier recession happened differently in China. Small glaciers retreat much more rapidly than large glaciers. Some of the small glaciers were even already disappeared (Liu et al., 2006). The amplitude of glacier retreat in the marginal regions is larger than those of interior regions in west China (Yao et al., 2007).

Multiple sources data have been used to detect the status of glacier change in China: (1) Topographic maps (1:50000 or 1: 100 000) derived from aerial photographs of 1960-70s; (2) Multi-temporal imagery as Landsat MSS /TM/ETM, SPOT, ASTER, CBERS and ALOS; (3) Ground survey data by GPRS and GPS. Based on these data, glacier change in length, area, mass balance and flow velocity has been deeply studied in China (Table 1.1- 3).

1.1.1 Glacier changes in Tianshan

Glacier area changes in China are presented in Table 1.1. From 1962 to 2006, the total area of glacier No. 1 at the headwater of Urumqi River in Tianshan decreased by 0.27 km^2 (14%), while it is 0.16 km^2 from 1992 to 2006. Glacier area was shrunk by 11% from 1959/1961 to 2001 on Mt. Karlik in the eastern Tianshan (Wang et al., 2008).

As shown in Table 1.2, east branch (EB) terminus of glacier No. 1 retreated by 38.7 m while west branch (WB) retreated by 64.1 m from 1993 to 2004. For the Glacier No.51, a sub-continental glacier, located on the northern slope of the Eren Habirgn Mountains, its terminus has been shrunk 84.51 m

from 1964 to 2006, and 49.00 m (1.40 m per year) and 35.51 m (5.07 m per year) for the periods of 1964-1999 and 1999-2006, respectively.

Glacier mass balance observation showed that glaciers in Tianshan have been downwasting recently (Table 1.3). For example, from 1958 to 2004, the annual glacier mass balance of glacier No. 1 was -233.6 mm while the accumulated net is -10746.5 mm (Wang et al., 2008). Correspondingly, the average glacier thickness decreased by 12 m which amounted to 2 062×10^4 m^3 glacier volume losses from 1959 to 2004 (Li et al., 2007a). According to the field measurement using B1 and B1+ Glacier Radar, the thickness of the Miaoergou flat-topped glacier in East Tianshan decreased around 5 m at the elevation of 4295-4357 m from 1981 to 2004 (Li et al.,2007b).

The glacier flow velocity measurements were carried out for the glacier No.1. In generally, the glacier flow velocity is decreasing for the EB and WB. During the period of 1980-2007, the annual flow velocity for EB and WB decreased by 0.8% and 2.0%, while the annual decreased rate is 3.4% and 7.3% from 1993 to 2007, respectively (Zhou et al., 2010).

1.1.2 Glacier changes in the Tarim Interior River basin (TIRB)

An investigation of the 3081 glaciers in the Tarim Interior River basin (TIRB) showed that the glacier area has lost 4.6 % from 1960 to 2001 (Liu et al., 2006). Meanwhile, from 1961 to 2006, the accumulated mass balance of the total glaciers in the TIRB is -6.4m. An increasing trend was also detected for the glacier downwasting in this region. From 1961 to 1990, the annual mass balance is -154.6 mm·a^{-1} while it increased to -240.1 mm·a^{-1} during the period of 1991-2006 (Gao et al., 2010). The glacier change shows a quite temporal and spatial difference in this region. The results from the 7665 glaciers in seven sub-basins of TIRB showed that the total glacier area was reduced by 3.3% from the 1960s/1970s to 1999/2001. Glaciers with area 1–5 km^2 accounted for 48.3% area loss in the TIRB and the maximum contribution of area shrinkage occurred at 4900–5400 m. Furthermore, the glacier area reduction varied from 0.7% to 7.9% among the seven sub-basins of the TIRB during the study period (Shangguan et al., 2009).

1.1.3 Glacier Changes in Qilian Mountains

There are 2815 glaciers covering a total area of 1931 km^2 with the ice volume of 93 km^3 in the Qilian Mountains. Most glaciers (69% of the total area) distribute on the north slope of the mountain. The Laohugou No.12 Glacier is the largest valley glacier with 10 km in length and 21.9 km^2 in area. Dunde ice cap is the largest flat-topped ice mass with the area of 57.07 km^2 (Shi et al., 2005).

A comparison of glacier termini from Landsat Thematic Mapper (TM) images acquired in 2000 and 2001 and aerial photographs taken in 1956, 1966 and 1972 indicated that the 33 glaciers monitored on the northeastern slope of the eastern end of the mountains were all receding, with a mean length reduction of 11.5 m a^{-1} (Liu et al., 2003). Another study from 244 glaciers in the Lenglong Range of Eastern Qilian Mountains indicated that all glaciers have been shrinking, and 27 glaciers disappeared by 2007. From the first CGI to 2007, the total area lost was about 24.286 km^2, accounting for 23.57% (0.67% a^{-1}) of the glacierized area (Cao et al., 2010). The glacier area in the Yeniugou River watershed, source of the Heihe River, had decreased by about 9.29% (0.54%· a^{-1}) from 1956 to 1970/1973 and 18.23% (0.60%·a^{-1}) from 1970/1973 to 2003. The number of glaciers in the Yeniugou River basin had decreased from 165 in 1956 to 144 in 2003. Glacier volume had decreased about 229×10^7 m^3 from

1956 to 1970/1973(13×10^7 m^3a^{-1}) and 419×10^7 m^3 from 1970/1973 to 2003(14×10^7 m^3a^{-1}) (Yang et al., 2007).

Mass balance of the Qiyi Glacier in the Qilian Mountains was -810 mm in 2001/2002 and -316 mm in 2002/2003, respectively, suggesting that the glacier was thinning dramatically. However, the glacier experienced positive mass balance of about 360 mm per year in the 1970s and 4 mm per year in the 1980s (Pu et al., 2005).

Table 1.1 Changes in glacier area in China

Study area and location	Data used	period	Glacier number	Area at the start of record (km^2)	Area at the end of record (km^2)	Area change (%)	reference
Yeniugou Watershed of Heihe River Basin. Qilian Mts.	Aerial-photograph(1956), Topographic map(1970/1973), ASTER(2003)	1956-2003	165	63.08	46.86	-25.7	Yang et al.(2007)
Lenglongling Range , Qilian Mts.	Aerial photography (1956, 1972), topographic map (1973), TM(1994), CBERS(2000), ASTER(2007)	1972-2007	244	103.02	78.734	-23.57	Cao et al.(2010)
Mt. Karlik, eastern Tianshan	Aerial photograph (1972), Topographic map (1959/1961), TM(1992), ETM+(2001)	1959-2001	122	125.89	111.54	-11.4	Wang et al. (2008)
Tarim basin	Topographic map(1960,70s), TM/ETM+(1999-2001)	1963-1999	3081	9998.5	9542.3	-4.6	Liu et al.(2006)
Karamilan-Keriya River,Tarim basin	Topographic map(1970s), TM/ETM+(1999-2001)	1970-2000	895	1374.18	1334.91	-2.9	Xu et al.(2006)
Kaidu River basin, Middle Tianshan	Topographic map(1963), ETM+(2000)	1963-2000	70	55	48	-13	Li et al.(2006)
Mt. Muztag Ata-kongur Tagh, the Pamir Plateau	Aerial photograph(1962-66), ASTER(2001)	1962/ 1966-2001	379	1092.7	1025.8	-6.2	Shangguan et al. (2005)
Mt. Muztahgata	Aerial photograph(1965), ASTER(2001)	1965-2001	128	377.21	373.04	-1.1	Cai et al.(2006)
Nam Co Basin, Mt. Nyainquentanglha	aero-photo topographic map(1970), TM(1991), ETM (2000)	1970-2000	N/A	167.62	141.88	-15.4	Wu et al.(2007)

Mt. Nyainqentanglha	Topographic map(1970), TM(1991), ETM+(2000), ASTER(2007)	1970-2007	N/A	203.3	166.2	-18.2	Chen et al.(2009)
Western Nyainqêntanglha Mts.	Aerial photography(1970), ETM+(2000), ASTER(2001)	1970-2000	870	917.8	865.7	-5.7	Shangguan et al. (2008)
Mt. Geladandong, the upper Yangtze River	Aerial photograph(1969), ETM+(2002)	1969-2002	N/A	889.31±0.02	846.81±0.0007	-4.8	Ye et al.(2006b)
A'nêmaqên Range, the upper Yellow River	Aerial photography(1966), TM(2000)	1966-2000	57	125.50	103.80	-17.3	Lu et al.(2005)
Gongga Mts.	Topographic map(1966), ETM+(2002), DEM(1989)	1966-2002	74	253.026	236.936	-6.36	Zhang et al.(2010)
Gangrigabu Mts.,	Topographic map(1980), CBERS(2001)	1980-2001	88	797.78	795.76	-0.25	Liu et al.(2005)
Central and Western Qangtang Plateau	Topographic map(1970, 1971), TM(1990, 1992), ETM+(1999, 2001, 2002)	LIA-2000	108	573.67	556.40	-3	Li et al.(2009)
Ranwu Lake Watershed	Topographic map(1980), Landsat TM(1988), ETM+(2001), CBERS(2005)	1980-2005	N/A	496.64	466.94	-5.98	Xin et al.(2009)
Kangwure Glacier, Himalayas	GPS, GPR data(2007, 2008), topographic map(1974), AOLS imagery (2008)	1974-2008	1	2.98	1.96	-34.2	Ma et al.(2010)
Mt.omolangma, Himalayas	MSS(1976,1977), TM(1988, 1989, 1990, 1992, 2006)	1976-2006	N/A	3212.08	2710.17	-15.6	Nie et al.(2010)
Ninachu river basin, Himalayas	Topographic map(1980), TM(1990), ETM+(2000), CBERS(2005)	1980-2005	84	182.77	169.36	-7.34	Li et al.(2010)
Mapam Yumco Basin, Himalayas	Topographic map(1974), TM(1990), ETM+(1999, 2000), ASTER(2003)	1974-2003	N/A	107.92	100.39	-6.98	Ye et al.(2008)
Pumqu River basin, Himalayas	Topographic map(1970,80s), ASTER and CBERS(2001)	1970s-2001	999	1462±9	1330±8	-9.0	Jin et al.(2005)

Reqiang Glacier, Mt. Xixiapama, Himalayas	MSS(1977and1984), TM(1990,1996), ETM+(2000), ASTER(2003)	1977-2003	1	6.92	5.34	-22.9	Che et al.,2005
Jicongpu Glacier, Mt. Xixiapama Himalayas	MSS(1977 and 1984), TM(1990,1996), ETM+(2000), ASTER(2003)	1977-2003	1	20.28	18.81	-7.3	Che et al.,2005
Mt. Naimona'nyi, western Himalayas	MSS(1976), TM(1990, 1999), ASTER(2003)	1976-2003	N/A	87.04	79.39	-8.8	Ye et al.(2006a)
Mapam Yumco Basin	aero-photo topographic map(1974), TM(1990), ETM+(1999), ASTER(2003)	1974-2003	N/A	107.35	100.08	-6.77	Guo et al.(2007)
Yamzhog Yumco basin	topographic maps(1980), TM(1988/1990), ETM+(2000)	1980-2000	N/A	218	215	-1.5	Ye et al.(2007)
Mt. Qomolangma Himalayas	MSS(1976), TM(1992), ETM+(2000), ASTER(2003), ALOS(2008)	1974-2008	74	144.14	129.13	-10.41	Ye et al.(2009)

Table 1.2 Changes in glacier terminus in China

Study area	Glacier	Velocity/m·a^{-1}	Period	Method	reference
Mt. Nyainqentanglha	Zhadang	-10.3	1970-2007	Field surveyed by GPS (1970, 1999, 2007)	Kang et al.,2007
	Lanong	-11.1	1970-2007		
	Panu	-10.2	1970-2007		
	Gurenhekou Glacier	-17.0	2005-2006	Field observation by stakes	Pu et al.,2006
Tianshan	Glacier No.51 at Haxilegen	-1.97	1964-2006	Topographic map(1964), GPS	Jiao et al.,2009
	Ürümq Glacier No.1	-4.22	1962-2004	GPS field survey	Wang et al.,2008
Gongga Mts.	Hailuogou	-22.45	1996-2008		Zhang et al.,2010

	Yanzigou	-11.76	1996-2008		
	Xiao Gongba	-5	1996-2008		
	Hailuogou	-25	2004-2006		Li et al.,2009
Gangrigabu Mts	Azha	-65	1980-2006	Field survey	Yang et al.,2008
	Palong No.4	-15.1	1980-2006		
	Palong No.10	-10.2	2006-2008		
Kangri Karpo	No.4, 10, 12, 94	-14.6 to -19.0	2006-2007		
Ranwu Lake Watershed	Yalong	-73	1980-2005	Topographic map(1980), Landsat TM(1988), ETM+(2001),CBERS(2005)	Xin et al.,2009
Himalaya	Naimona'nyi Glacier	-7.8	2004-2006	Field surveyed	Yao et al.,2007
	Kangwure Glacier	-9	1974-2008	GPS(2008), aero-photo topographic map(1974)	Ma et al.,2010
Mt. Xixabangma	Jicong Pu Glacie	-48	1977-2003	MSS(1977,1984), TM(1990,1996), ETM+(2000), ASTER(2003)	Che et al.,2005
	Reqiang Glacier	-71	1977-2003	MSS(1977,1984), TM(1990,1996), ETM+(2000), ASTER(2003)	
Mt. Qomolangma	Reqiang	-65.9±5.87	1976-2006	Remote Sensing	Nie et al.,2010

Table 1.3 Changes in glacier mass balance in China

Study area	Data used	period	Total Mass blance	Per year mass blance	reference
Glacier No.1, Tianshan	Field observation	1959-2004	-10789mm	-235mm	Li et al. (2007)
		1980-2006	-12115.4mm	-448.7 mm	Zhou,et al. (2010)
Tarim Interior River basin	Monthly precipitation and air temperature,90-m resolution DEM, digital vector map of glaciers (1970)	1961-2006	-7.5m	-163.1mm	Gao et al. (2010)
Watershed of Sary Jaz-Kumarik Rivers, Tianshan	Restore data by analysis	1956-2006	-9.7m	-194mm	Shen et al. (2009)
Keqicar Baxi Glacier, Tianshan	Model simulation	2003-2005	-878mm	-439mm	Zhang et al. (2006)
Zhadang Glacier	Field observation by Stakes,Topographic map	2006-2006	-1547.57mm	-1547.57mm	Zhou et al. (2007)
Naimona'nyi Glacier	Field observation by Stakes, Topographic map	2004-2006	-1316mm	-658mm	Yao et al.,2007
Hailuogou	Restore data by analysis	1959-2004	-10825.5mm	-240.6mm	Li et al.(2009)
Baishui No.1 Glacier, Mt. Yulong	Field observation	1959-2004	-18000mm	-360mm	Li et al.(2008)
Glacier No.12, Kangri Karpo	Field observation	2006-2007	-1.58m	-1.58m	Yang et al., (2008)
the Upper Stream of Yarkant River, Karakorum Mountains	monthly precipitation and air temperature, 90-m resolution DEM, digital vector map of glaciers(1970)	1961-2006	-7.5m	-163.1mm	Gao et al. (2010)

1.1.4 Glacier Changes in Karakoram and East Pamir

The north slope of Karakoram is one of the most densely glacierized areas in China. A careful analysis based on maps and Landsat Enhanced Thematic Mapper Plus (ETM+) imagery indicated that glacier changes in this region are complicated; some of the large glaciers were in a steady state (equilibrium) or have advanced or even surged during recent decades (Shangguan and others, 2004b). For example, from 1965 to 2001, the total glacier area had decreased for about 1.11% in Mt. Muztagta, while the advancing glaciers happened in the west and south of the mountain (Cai et al., 2006). A recent study on the glacier change in the Upper Stream of Yarkant River which is located in the north slopes of the Karakorum Mountains indicated that the mean annual glacier mass balance during 1961—2006 was -163.1 mm per year and the total glacier mass loss was -7.5 m in thickness within 46 years. The equilibrium line altitude rose about 64.2 m from 1991 to 2006 comparing with the mean value over the period of 1961—1990 (Gao et al., 2010).

According to the Glacier Inventory of China (Yang et al., 1989; Liu et al., 2001), there are 1277 glaciers with a total area of 2670.61km^2 in Eastern Pamir in Chinese territory. The area of Zulumart glacier which is the biggest glacier in the East Pamir has reduced 8.3% during 1978–1990 and 10% in 1990–2001. For the whole region in East Pamir, the glacier area has decreased 7.8% in the period of 1978–1990 and 11.6% for 1990–2001. The results from length measurements of 44 glaciers showed that the mean glacier recession rate was 4.4 ma^{-1} from 1972 to 1980, and then increased almost twice to 8.3 m a^{-1} during 1980–1991. However, the glacier length recession rate changed to 6 m a^{-1} showing a depressing trend in the period of 1991–2003 (Khromova et al., 2006).

1.1.5 Glacies Changes in the western Nyainqêntanglha Mountains

Glacier area in the Nam Co Basin in the northern slope of Nyainqêntanglha Mountains decreased from 167.62 km^2 to 141.88 km^2 from 1970 to 2000. The annual reducing rate of the glacier area was 0.97 and 0.80 km^2 a^{-1} for the two periods 1991-2000 and in 1970-1991, respectively (Wu et al., 2007). During the period of 1970-2007, the glacier area reduced 37.1 km^2 which accounted for 18.2% of the whole glacier area in the Nam Co Basin. The annual glacier change ratio is -1.0 km^2 a^{-1} (Chen et al., 2009). The area and volume of 870 glaciers in the western part of Nyainqêntanglha Mountains has decreased 5.7 % and 7 % from 1970 to 2000, respectively. Glaciers in the area rank of 1~5 km^2 contribute to 56.7% (19.5 km^2) of the total area loss (Shangguan et al., 2008).

Glacier terminus change was investigated on Gurenhekou Glacier which lies in the southern slope of Mt. Nyainqêntanglha in different periods. The glacier shrinking rate was about 7.0 m·a^{-1} from the Little Ice Age to 1970 and changed to 8.3 m·a^{-1} from 1970 to 2004. Based on the GPS measurement, the glacier shrinking rate was about 9.5 m·a^{-1} for the periods 2004-2005 and 17.0 m·a^{-1} for the period of 2005-2006 (Pu et al., 2006). The termini of Zhandang glacier and Lanong glacier had retreated 381.8 m and 489.5 m with the annual change ratio of 10.3m a^{-1} and 13.4 m a^{-1} from 1970 to 2007, respectively (Kang et al., 2007).

According to the glacier mass balance observation on the Zhadang Glacier in 2005/2006, the mass balance of the glacier was calculated to be negative -1 547.57 mm (mm w.e.). It is suggested that the glacier was suffering downwasting dramatically (Zhou et al., 2007). Kang et al. (2009) presented that a large deficit mass balance occurred during the mass balance years 2005/06 and 2006/07, but in 2007/08 there was a surplus mass balance and retreat of the glacier terminus slowed in 2008.

1.1.6 Glacier Changes in Himalayas

The Himalayas is a prominent area among many parts of the world where climate change greatly influences the glacier retreat. As shown in Table 1.1 and 1.2, the terminus position of Kangwure Glacier in the middle of Himalayas has retreated 303 m from 1970 to 2008. Meanwhile, the glacier area declined from to 2.98 km^2 to 1.96 km^2 which decreased by 34.2%. The volume declined from 0.0998 km^3 to 0.0517 km^3 which decreased by 48.2%. The average thickness decreased by 7.5m (Ma et al., 2010). The glacier area of Boiqu River Basin in the Middle Himalayas has decreased by 20% from 1987 to 2001 (Chen, et al., 2005). From 1980 to 2005, the debris-free glacierized area in the Nianchu River Basin shrank by 7.3 % (13.42km^2). (Li et al., 2010)

The glacier area of Mt. Qomolangma region in the central Himalayas has reduced by 15.6% of that in

1976 during the period 1970-2006. The rate of glacier retreat was higher in sub-basins on the southern slopes (16.79%) of the Himalayas than on the northern slopes (14.40%) (Nie et al., 2010). The glacier area of the Rongbuk river catchments in the northern slopes of the Mt. Qomolangma was 144.14 km^2 in 1974 and decreased to 129.13 km^2 in 2008 which decreased 10.41% of that in 1974 (Ye et al., 2009).

The variation of glaciers in the western Himalayan region is not dramatic comparing with other regions in western China. From 1976 to 2003, glacier area decreased from 84.41km^2 to 77.29 km^2. The annual glacier areas reducing rate is 0.17, 0.19 and 0.77 km^2 a^{-1} for the three periods 1976–1990, 1990–1999 and 1999–2003, respectively, suggesting that glacier retreat has been accelerated (Ye et al., 2006). Glaciers area in the MapamYumco Basin reduced 7.53 km^2 (6.98%) from 1974 to 2003 (Ye et al., 2008). The glacier average retreating rate in Naimona'nyi was 5.5 $m \cdot a^{-1}$ in the past 30 years before 2006 and 7.7 $m \cdot a^{-1}$ from 2004 to 2006, which also indicates an accelerating glacier recession. The mean annual mass balance was -658 mm w.e.q. and the surface elevation decreased 1.35 m at 6 050 m a.s.l and 2.85 m at 4 800 m a.s.l due to strong surface ablation from 2004 to 2006 (Yao et al., 2007). Volume of Glacier in Mt. Naimona'nyi Region has decreased by 3.060 km^3 (0.1224 $km^3 \cdot a^{-1}$) from 1976 to 2001 (Wang et al., 2010).

Jicongpu glacier and Reqiang glacier are located on the East slopes of Mt. Xixabangma. From 1977 to 2003, the area of Jicongpu glacier has decreased by 7.29 % whiles the glacier length decreased by 16.60 %. The area of Reqiang glacier has decreased by 22.90 % and glacier length retreated by 27.56 % in the same period (Che et al., 2005).

1.1.7 Glacier Changes in Southeast Tibetan Plateau

Field observation measurements are carried on over the Gongga Mountains and Gangrigabu Mountains (Table 1.1). From 1966 to 2008, glacier terminus retreating had been detected for the Hailuogou Glacier, the Yanzigou glacier the Xiao Gongba Glacier. Although the terminus of the Da Gongba Glacier did not change, the ice storage was in reduction (Zhang et al., 2010). A dramatic recession happed in Hailuogou glacier. The terminal elevation of Hailuogou glacier has increased 150 m in last 45 years from 1930 to 2006. Its accumulative mass balance is -10 825.5 mm w.e. with an annual value -240.6 $mm \cdot a^{-1}$ w.e. (Li et al., 2009). Between 2006 and 2007, the termini of glacier Palong No.4, No.10, No.12 and No.9 have retreated 5.2m, 4.15m, 2.9m and 3.75 m, respectively (Yang et al., 2008). For the Yulong Mountain, the terminus elevation of Baishui Glacier No. 1 is 4200 m in 1999, 4245m in 2003, and 4300m in 2006 (Pang et al., 2007).

Results on the glacier changes in the Gangrigabu Mountains from 102 glaciers showed that the glacier area had lost 13.8% of the total area and 9.8% of the total ice volume from the 1920s to 1980s with a total areal and ice volumetric decreases of 47.9 $km^2$and 6.95 km^3. It is estimated that all glaciers in the region have lost 13.8% of their total area and 9.8% of the total ice volume during the same period. Since 1980, glaciers in this region have experienced an ice mass loss process based on the analysis of 88 selected glaciers (Liu et al., 2005).

In Gongga Mountains, the overall glacierized area has decreased by 6.36% with an annual decreasing rate of 0.447$km^2 \cdot a^{-1}$ from 1966 to 2002. The number of glaciers in the east mountain increased from 33 to 36 while the glacier area reduced 7.20 km^2 which is about 4.71% of the total glacier area. In the west range, the number of glaciers reduced from 41 to 39 with a reducing glacier area of 7.89 km^2 (7.97%) (Zhang et al., 2010). From 1980 to 2005, the glacier area around Ranwu Lake has lost 29.7 km^2 (5.98%) (Xin et al., 2009).

1.1.8 Glacier Changes in inland Tibetan Plateau

In the Central and Western Qangtang Plateau, the glacier area had lost 17.27 km^2 (3.01 %) from the LIA to the 2000s (Li et al., 2009). The change of glacier area in the Geladandong mountain region is not as large as it in other regions on the Tibetan Plateau. Several glaciers in this region even have advanced during the past 30 years from 1973 to 2002. The total glacier area has decreased from 889 km^2 to 847 km^2 from 1969 to 2002 with an annual reducing rate of 1.29km^2 a^{-1}. Glacier area reducing rates in three different periods (1969–76, 1976–92 and 1992–2002) are 0.68km^2 a^{-1}, 0.96 km^2 a^{-1} and 2.24 km^2 a^{-1}, respectively, suggesting an accelerated glacier retreating trend in recent years (Ye et al., 2006).

The annual mass balance of the Xiao Dongkemadi glacier changed from a positive mass balance with a value of 525 mm water equivalent in 1988/1989 to a negative value of -701 mm water equivalent in 1997/1998. The 9 years' (1994–2002) accumulated mass balance was -3119 mm in water equivalent with

an average glacier surface downwasting about 3.5 m (Pu et al., 2008).

1.2 SENSITIVITY OF GLACIER CHANGES IN RESPONSE TO CLIMATE CHANGE

1.2.1 Sensitivity of glacier mass balance

The glacier mass balance is the difference between accumulation and ablation, and is the comprehensive reflection of the hydrothermal regime for the survival of a glacier. Therefore, it has significant influence on the physical characteristics and behaviors of a glacier. Under the impact of climatic warming, the glaciers in the High Asia in China have been retreating continuously with negative glacial mass balance in recent several decades, and glacier retreating became more intensive in the past 10 years (Yao et al., 2004). Glacier fluctuations and current glacier retreat have consequences on the local to global scale natural and societal environment, such as changing water and tourist resources, global sea level, as well as glacier-related risks. In order to evaluate and quantify glacier changes, sensitivity of glacier mass balance to climate must be well understood. In case of the data scarcity in glacier regions, glacier surface mass balance (SMB) has often been modeled only by using the most accessible meteorological data, e.g., air temperature and precipitation. A common procedure is to calibrate a mass balance model using historic climate and mass balance data (e.g., degree-days models or one regression formula), and then to run the model with a perturbated climate using either hypothetical or model-predicted climate changes. Thus, the analysis of the mass balance variations correlated with climate changes is the groundwork for the analysis of the sensitivity of mass balance to climate.

In 1959, Chinese Academy of Sciences and Xinjiang Water Conservancy Bureau established a glaciological observation station on the Glacier No.1 at the headwater of the Urumqi River in Tianshan Mts., and began to monitor mass balance, terminus variation, ice formation zone, snow/firn densification, ice movement, ice temperature, heat budget, glacio-hydrometeorology, etc.. The station has been run by Chinese Academy of Sciences since 1961. Unfortunately, the measurements on this glacier were interrupted in 1967. The conventional observations were resumed in 1979. And several hydrometeorological/meteorological stations were also established in the river basin. One of the hydrometeorological stations (43º06′N, 87º15′E, 3693 m a.s.l., named Glacier No.1 Hydrometeorological Station, in short, G1HS) was very close to the Glacier No.1, about 200 m down the tongue of the glacier. Temperature and precipitation observations at G1HS provide an opportunity to analyze the impact of climate change on this glacier. At present, there are few glaciers (around 10) monitored in China. Of these, the Glacier No.1 is the only one with continuous measurements for more than 40 years (Wang et al., 2007). Most other glaciers have datasets only covering several years. These datasets limit the testing of their sensitivities to climate change in different regions, which might explain spatial and temporal variations in glaciers in China.

To detect the mass balance trend of the Glacier No.1 in the past 40 years (Fig 1.2), the cumulative sum of the mass balance departures from –129 mm w.e./yr, the mean mass balance over the 30-year climatological reference period (1961-1990), are calculated and presented in Fig 1.3 (Wang et al., 2007) . It is clear that the trend of the mass balance shows a shift in the late 1970s, i.e. the mass balance of the glacier has changed toward a significant deceasing trend since then and further accelerated after the early 1990s.

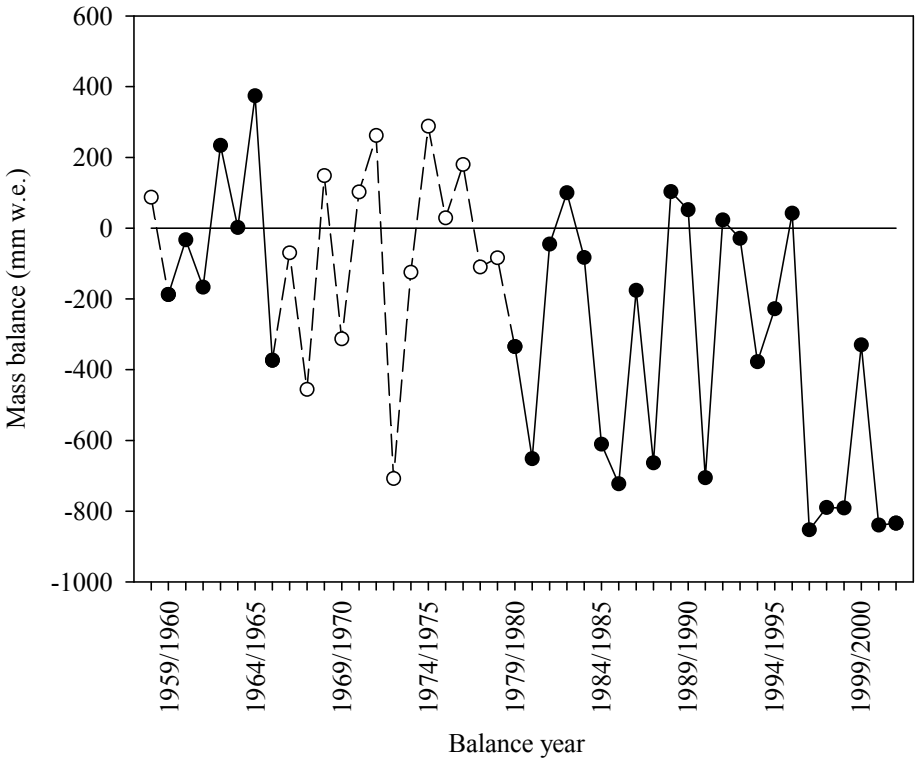

Fig 1.2. Variations in mass balance of the Glacier No.1 at the headwater of the Urumqi River, Tianshan Mts., in the past 40 years. Solid curve with solid circles represents the observation data; dashed curve with open circles is the interpolation values estimated by the correlation between the observed mass balance and meteorological data (Wang et al., 2007).

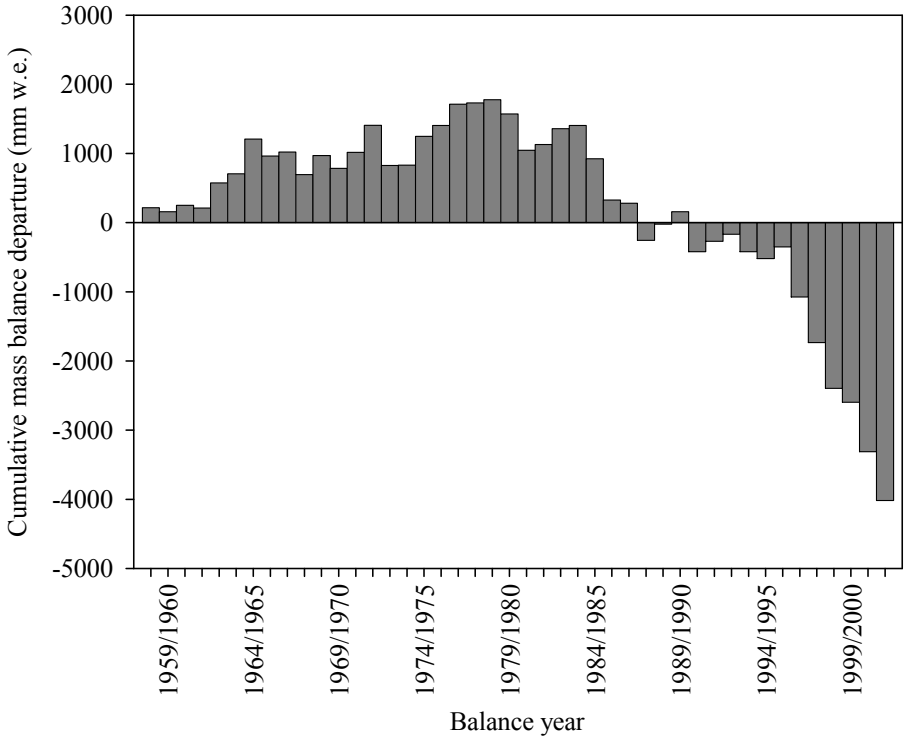

Fig 1.3. Cumulative departures of the Glacier No.1 mass balance relative to its mean in 1961-1990 "climatological normal" period.(Wang et al., 2007)

Wang et al. (2007) investigated the correlations between climatic factors (only temperature and precipitation considered) observed at G1HS and mass balance measured on the Glacier No.1 to understand major causes of the glacier variation (Table 1.4, 5). The results implied that precipitation might not be a major factor influencing the behavior of the Glacier No.1, however, the annual mass balance is closely correlated with summer air temperature (see Table 1.5). Fig 1.4 suggests that air temperatures in June, July and August are positive, and the temperature in July is highest. Thus, if summer mean temperature is calculated by assigning weights of 0.25, 0.5 and 0.25 to June, July and August temperatures, respectively, the correlation coefficient between the annual mass balance and summer mean temperature can reach –0.721. This means that summer temperature is the major cause of the variations in the mass balance.

Table 1.4. Correlation coefficients between the annual mass balance of the Glacier No.1 and precipitations at G1HS during the different periods of the balance year (1979/1980 through 2001/2002) (After Wang et al., 2007)

	Sep.	Oct.	Nov.	Dec.	Jan.	Feb.	Mar.	Apr.	May	Jun.	Jul.	Aug.	Jun.-Agu.	Year
CC*	-0.014	0.085	-0.054	0.005	-0.292	-0.039	0.138	0.191	-0.005	0.122	0.086	-0.236	-0.032	0.165

* There is no correlation coefficient with 99 % significance level.

Table 1.5. Correlation coefficients between the annual mass balance of the Glacier No.1 and air temperatures at G1HS during the different periods of the balance year (1979/1980 through 2001/2002) (After Wang et al., 2007)

	Sep.	Oct.	Nov.	Dec.	Jan.	Feb.	Mar.	Apr.	May	Jun.	Jul.	Aug.	Jun.-Agu.	Year
CC	-0.112	-0.073	-0.060	0.427	-0.136	-0.143	-0.322	-0.430	-0.142	-0.385	-0.663*	-.0350	-0.658*	-0.407

* 99 % significance level.

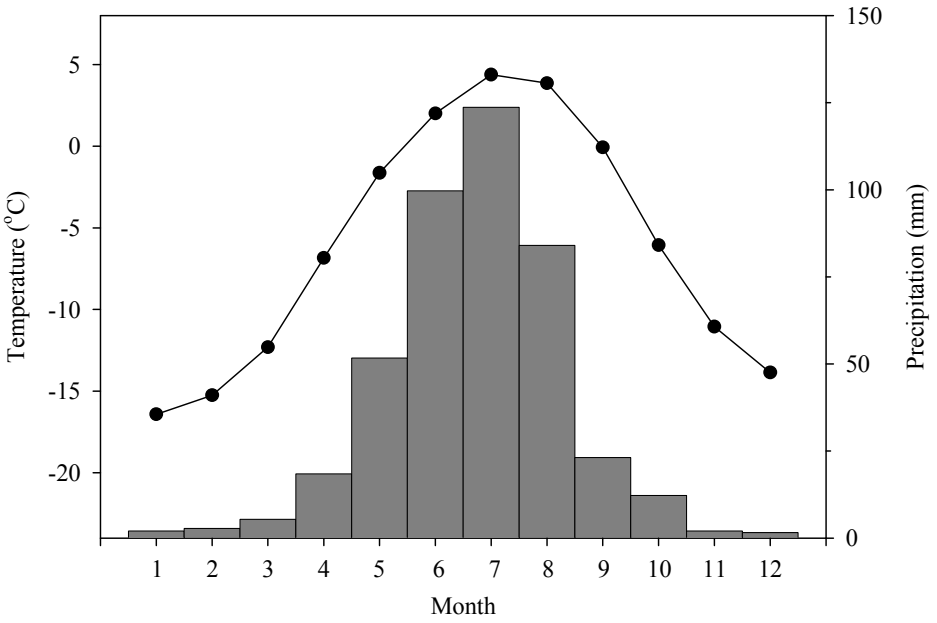

Fig 1.4. Seasonal variations in air temperature (line) and precipitation observed (bar) at G1HS during 1980 through 2002.(Wang et al., 2007)

In the recent years, many other researches investigated the characteristics of mass balance on the Urumqi Glacier NO.1 (Han et al., 2006; Jing et al., 2006; Li et al., 2007). All those results also showed that the mass balance on the glacier were more sensitive to summer temperature changes than the precipitation. Similar to the results on Glacier NO.1, the glacier mass balance in other regions of China (e.g., Qiyi Glacier in Qilian Mountains, Xiao Dongkemadi Glacier in the Tanggula Mountains, etc.) also suggested particular sensitivity to summer temperature change (Pu et al., 2005; Liu et al., 2006; Pu et al., 2008).

Over long periods of time, glaciers are generally modeled as bulk and distributed mass balance is ignored. Many sophisticated models exist to study different aspects of glaciers. Accurate testing of the sensitivity of the glaciers mass balance requests that physically-based and spatially distributed models are developed and used. Jiang and others (Jiang et al., 2010) applied a distributed energy and mass balance model to analyze the mass balance sensitivity of Qiyi glacier in the Qilian Mountains to climatic change. The climate sensitivity test (see Table 1.6) showed that the mass balance on Qiyi glacier was more sensitive to summer air temperature than precipitation, and the response of mass balance to air temperature change was nonlinear whereas the response to precipitation change was linear. The negative mass balance trend of the glacier can not be reversed when precipitation increases by 20% and the air temperature rises by 1℃. Another study on Xibu glacier in the Nyainqêntanglha mountain range also showed the similar results that the mass balance was particularly sensitive to air temperature in wet season (May-September, i.e. the warm season)(Caidong et al., 2010).

Table 1.6. The climate sensitivity tests for the cumulative mass balance on Qiyi Glacier for the period of July 1–October 9, 2007. (Jiang et al., 2010)

Test case	Air temperature forcing (°C)	Precipitation forcing (%)	Mass balance (mm w.e.)	Mass balance change rate(%)
0	0	0	–604	0.0
2–1	+1	0	–1022	–69.1
2–2	–1	0	–266	56.0
2–3	0	+20	–560	7.3
2–4	0	-20	–648	–7.3
2–5	+1	+20	–987	–63.4

2–6	–1	-20	–315	47.9

"case 0" was used as the reference value to calculate the change rates of

1.2.2 Sensitivity of ELA

The equilibrium line altitude (ELA) is a theoretical line on a glacier at which annual mass accumulation equals annual mass loss. Glacier behaviors such as advancing or retreating are controlled by the variations in ELA. Relative to its steady state, a glacier advances when its ELA falls, and retreats when its ELA rises, or melts entirely when its ELA rises above the summit. In contrast to variations in glacier length or area, variations in ELA respond almost simultaneously to climate change. Reconstructions of ELAs in many regions using various methods, such as the accumulation area ratio (AAR), balance ratio (BR), altitude of lateral moraines (ALM), cirque floor altitude (CFA) and toe-to headwall altitude ratio (THAR), have made a great contribution to the study of past climatic and environmental changes. The sensitivity of ELA to climate change is a vital issue for predicting glacier behavior, and is the basis for quantitative reconstructions of past climate change using data on glacier variations. Therefore, studies on ELA variations and their sensitivity to climate change are important for understanding correlations between glacier behavior and climate change.

In recent years, many studies have analyzed variations in glacier areas and lengths, but few have focused on ELA variations. With global warming, studying ELA variations is of prime importance. Glacier No.1 in the Tianshan Mountains has the longest ELA dataset of about approximately 50 years in China, including interpolation data. Most other glaciers have short term datasets in China. These datasets limit the comparison of long-term ELAs' variations and their sensitivities to climate change in different regions, which might explain spatial and temporal variations in glaciers in China. Wang et al. (Wang et al., 2010) established a correlation between ELA of the Qiyi Glacier and climatic factors (air temperature and precipitation) based on intermittent observation data in the past several decades, reconstructed ELA variations over the past 50 years, and analyzed their sensitivity to climate change. They also predicted future behavior of the Qiyi Glacier using a model of the response of glacier steady-state length to climate change (Wang et al., 1996) .

The Qiyi Glacier (39° 14.22′ N, 97° 45.34′ E) is located in the Tuolai Range in the Qilian Mts (Fig 1.5). Its melt water feeds into the Liugouquan Creek, a tributary of the Beida River. The glacier is a cirque-valley glacier, and is classified as sub-continental glacier type based on its physical properties. The glacier was the first to be subjected to modern Chinese glaciological studies in 1958, and its name, Qiyi Glacier (July 1st Glacier), commemorates Chinese glaciologists climbing on it on July 1st of that year. Thereafter, especially during the periods 1975 through 1978 and 1985 through 1988, many observations were conducted on the glacier such as mass balance, ELA, ice formation processes, glacial movement, terminus variation, ice thickness, melt water runoff, and glaciological meteorology. Since 2001, we conducted further observations on mass balance, ELA, melt water runoff and glaciological meteorology (Pu et al., 2005). Climate in the Tuolai Range is affected mostly by westerly wind circulation, and is also influenced occasionally by the Asian monsoon in summertime. Meteorological observations in the Qiyi Glacier's catchment during the period from September 2006 to September 2008 showed (Wang et al., 2009): (1) precipitation occurred mainly in summer; (2) there was a zone of maximum precipitation at ~4500–4700 m a.s.l. with an annual precipitation of 485 mm. The ELA of the Qiyi Glacier was determined by using the altitudinal profile of the annual mass balance by measuring sticks. The observed ELAs in different periods are presented in Table 1.7.

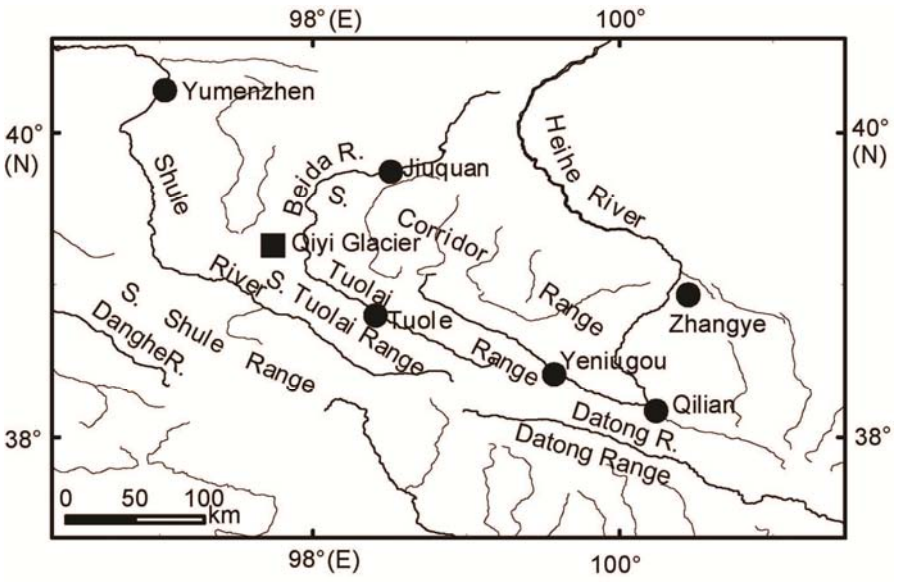

Fig 1.5. Location of the Qiyi glacier

Table 1.7. Observations of the Qiyi Glacier ELA over the past 30 years. (Wang et al., 2010)

Balance year	ELA(m a.s.l.)
1973/1974	4580
1974/1975	4650
1975/1976	4550
1976/1977	4620
1983/1984	4600
1984/1985	4710
1985/1986	4810
1986/1987	4690
1987/1988	4730
2001/2002	5012
2002/2003	4939
2003/2004	4973
2004/2005	4869
2005/2006	5131
2006/2007	4855
2007/2008	4772

Using the 16-year Qiyi Glacier ELA observations (Table 1.7) in combination with glacier catchment climate data, it is possible to derive a correlation model between ELA and climatic factors. With this, past ELA variations can be constructed, and ELA sensitivity to climate change can be analyzed. Because available meteorological stations are far from the Qiyi Glacier (see Fig 1.5), and the topographic influence on climate (especially precipitation) is notable, we could not directly determine the climatology of the glacier catchment from any one of the meteorological stations. Therefore, selecting an appropriate station is vital. Tables 8 and 9 present the correlation coefficients of air temperatures and precipitations, respectively, among meteorological stations around the Qiyi Glacier, i.e. Tuole station (3368 m a.s.l.), Yeniugou station (3320 m a.s.l.), Qilian station (2789 m a.s.l.), Yumenzhen station (1527 m a.s.l.), Jiuquan station (1478.2 m a.s.l.) and Zhangye station (1483.7 m a.s.l.) (Fig 1.5). Correlation coefficients among stations either only in mountainous area or only on the piedmont plain are higher than those among the stations in mountainous area and piedmont plain. This demonstrates that climate change, especially the precipitation variability, in the mountainous area is different from that on the piedmont plain. We should select the meteorological data observed at the mountain stations to calculate climatic conditions on the Qiyi Glacier. Table 1.9 also shows that the shorter the distance among stations, the higher the correlation coefficients. Consequently, we used meteorological data from Tuole station, the closest mountain station to the Qiyi Glacier, and altitudinal gradients of air temperature and precipitation measured in the glacier catchment, to calculate the climatic data on the glacier.

Table 1.8. Correlation coefficients of annual mean air temperatures among meteorological stations around the Qiyi Glacier (1960–2007)[a] (Wang et al., 2010)

		Plain station		Mountain station		
		Jiuquan	Zhangye	Tuole	Yeniugou	Qilian
Plain station	Yumenzhen	0.981	0.960	0.814	0.709	0.825
	Jiuquan		0.943	0.786	0.688	0.795
	Zhangye			0.850	0.758	0.899
Mountain station	Tuole				0.931	0.927
	Yeniugou					0.916

a) Significances of all correlation coefficients are at the 0.001 level.

Table 1.9. Correlation coefficients of annual precipitation among meteorological stations around the Qiyi Glacier (1960–2007) [a] (Wang et al., 2010)

		Plain station		Mountain station		
		Jiuquan	Zhangye	Tuole	Yeniugou	Qilian
Plain station	Yumenzhen	0.748*	0.548*	0.272	0.055	0.017
	Jiuquan		0.673*	0.434	0.274	0.224
	Zhangye			0.573*	0.497	0.375
Mountain station	Tuole				0.634*	0.455
	Yeniugou					0.694*

a) * Significant at the 0.001 level

Based on the above observations of the equilibrium line altitude (ELA) of the Qiyi Glacier in the Qilian Mountains, a statistical model between ELA and its major influencing factors such as, warm season air temperature (T_w, air temperature averages for September, July and August) and cold season precipitation (P_c, total precipitation in the period January through March) was established as Formula 1:

$$ELA = 5357 + 172.1T_w - 14.5P_c, \ (\mathrm{R}=0.837, \mathrm{n}=15) \quad (1)$$

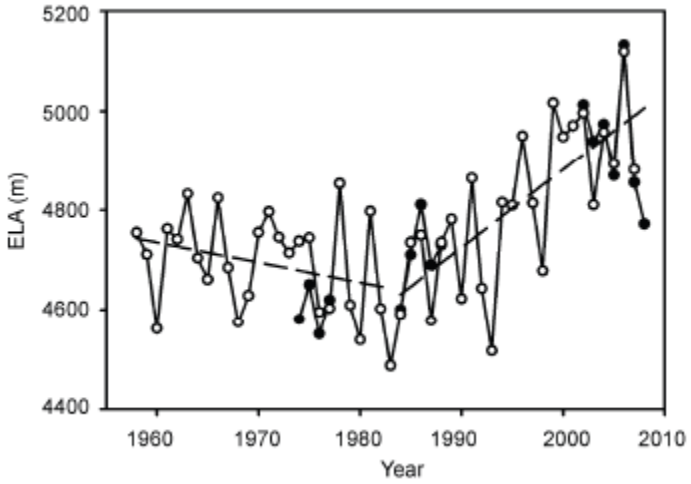

Fig 1.6. Variations in the Qiyi Glacier ELA from 1958 to 2008. Closed circles represent observed values, open circles represent calculated values, and the dashed lines are linear trends of the variations in ELA in different periods.(Wang et al., 2010)

The reconstruction of the Qiyi Glacier ELAs over the past 50 years, which was derived from Formula (1), was shown in Fig 1.6. We investigated the sensitivities of the Qiyi Glacier ELA to variabilities in warm season air temperature and cold season precipitation using formula (1). The results showed that the Qiyi Glacier ELA ascends (descends) 172 m when warm season air temperature increases (decreases) by 1°C, and ELA ascends (descends) 62 m when cold season precipitation decreases (increases) by 10%. A similar study on Glacier No.1 in the Tianshan Mts showed that ELAs of its east and west branches ascend (descend) 238 and 122 m, respectively, when summer air temperature increases (decreases) by 1°C, while ELAs ascend (descend) 29 and 10 m, respectively, when annual precipitation decreases (increases) by 10%. In the period 1958–2008, the glacier ELA showed a general increasing trend, ascending 230 m and reaching its highest altitude in 2006 at 5131 m a.s.l., close to the glacier summit. Recently a study on the sensitivity of

Xibu glacier in the Nyainqêntanglha Mts to climate change by energy balance method showed that a temperature change of ±1℃ or a precipitation change of ±35% changes the equilibrium-line altitude (ELA) by 140±125 m (Caidong et al., 2010). These studies show that ELAs sensitivities to climate change in the same region or in different regions vary. This is possibly one of the major external causes for differing responses of glacier terminuses in the same or different regions to the same climate change (internal causes are related to glaciers' dimension and dynamics).

1.2.3 Sensitivity of glacier length

In recent years, many studies have analyzed variations in glacier lengths or terminus by remote sensing; and only few have focused on the sensitivity of glacier length/terminus to climate change. A statistical model of the response of glacier steady state length to climate change was already established based on observation data from glaciers around the world (Wang et al., 1996). In the model, the influencing factors on glacier length were the positive difference of glaciation (H_0, i.e., the altitudinal difference between ELA_0 and glacier summit), glacial surface slope (α, defined as the ratio of the difference of glaciation to glacier length), ratio of altitudinal gradients of mass balances in the accumulation area and the ablation area ($(bc/ba)_0$), and accumulation area ratio (AAR_0). The subscripts of "0" in the above factors indicate that the values of these factors were obtained under the condition where glacial mass balance is zero. When assessing the steady state lengths of a given glacier (L_0) under different climatic scenarios, a correction coefficient (C) should be added into the model (Wang et al., 1996; Wang et al., 1997) :

$$L_0 = C \cdot e^{-7.5604} \cdot H_0^{0.7325} \cdot AAR_0^{0.6424} \cdot (b_c / b_a)_0^{0.0997} \cdot \alpha^{-1.2724} \quad (2)$$

On the basis of the Qiyi Glacier observation data, Wang et al. (2010) calculated the values of parameter H_0 (ELA_0=4693 m) as 452 m, AAR_0 as 58%, and $(bc/ba)_0$ as 0.3366. The value of C was 0.9892, estimated by comparing the actual length with the calculated steady state length of the Qiyi glacier. When calculating the responses of the steady state length of the Qiyi Glacier to climate changes, H_0 was evaluated by ELAs under the different climatic scenarios, and α (its present value is 0.2197) was evaluated according to local topography and location of the terminus predicted by the new steady state length of the glacier. Table 1.10 shows the steady state lengths (L_0) of the Qiyi Glacier under the different climatic scenarios. If the future climate is similar to the average climatic conditions of 2001 to 2008, the Qiyi Glacier will not reach its steady state until it retreats by 2.08 km. If warm season air temperature decreases by 1°C in the future, the glacier will not stabilize until it retreats by 0.27 km. Relative to the Qiyi Glacier's steady state length (1.58 km) under average climatic condition from 2001 to 2008, the retreat caused by a 1°C rise in warm season air temperature (i.e., 1.58 km–0.37 km=1.21 km) would be smaller than the advance caused by a 1°C decrease (i.e., 3.39 km–1.58 km=1.81 km). Moreover, the retreat caused by a 10% decrease in cold season precipitation would also be smaller than the advance caused by a 10% increment. This suggests that even though ELA response to climate change is linear, the response of the steady state length to climate change is nonlinear. These phenomena might be related mostly to geomorphological features along the glacier's valley and the altitudinal profile of the glacial mass balance. The slope becomes steeper towards the upper part of the Qiyi Glacier. This means, when ELA rise or fall by the same amount relative to an ELA_0, there might be a large increase in the accumulation area caused by a fall in ELA, whereas only a small reduction in the accumulation area caused by a rise in ELA. This could result in a large advance and a relatively small retreat, respectively. In addition, due to the altitudinal gradient of the glacial mass balance increasing towards the lower part of the Qiyi Glacier, reflected by $(bc/ba)_0<1$, the fall in ELA could result in much mass accumulation which might also cause glacier advance. For most valley glaciers, their geomorphological features and altitudinal mass balance profiles are similar to that of the Qiyi glacier. Therefore, the response characteristics of the Qiyi Glacier length to climate change might be representative for most valley glaciers.

Table 1.10. Steady state lengths of the Qiyi Glacier under different climatic scenarios[a] (Wang et al., 2010)

	Average climatic condition of 2001–2008	Warm season air Temperature*		Cold season precipitation*	
		+1°C	–1°C	+10%	–10%
ELA (m a.s.l.)	4935	5107	4763	4873	4997
L0(km)	1.58	0.37	3.39	2.20	1.10
Variational amount** (km)	–2.08	–3.29	–0.27	–1.46	–2.56

a) * Relative to average climatic condition from 2001 to 2008; ** Relative to the present length, i.e., 3.66 km.

1.3 INVESTIGATION OF GLOFS AND THEIR RISK ASSESSMENT

With global warming and glaciers melting, glacial lakes are widespread and glacial lake outburst floods (GLOFs) are becoming one of the serious natural disasters in western China. Tibet is the region suffering from the most severe hazards resulted from glacial lakes. Among them, the most frequent are debris flows and floods caused by glacial lakes outburst, especially the end moraine lakes. Such events, with an unexpected occurrence, high peak discharge, and great power of destruction, have brought out tremendous loss to the lower parts of the lakes. In addition, the debris flows blocking the rivers often invite the secondary hazardous events causing even more severe disasters.

1.3.1 Tibet-Himalayas region

Since the 1930s, there have been 18 outburst events of 15 glacial lakes in Tibet. These events are discussed in details by Liu et al. (2008). It is reveled that these glacial lakes are mainly distributed in the transit region from the marine glaciers to the continental glaciers; the breaks of glacial lakes are controlled mainly by the climate conditions, especially as a response to the variety of weather. These occurrences are coinciding with the abnormal years. Recent surveys suggest that the potentiality of glacial lake outbreak is increasing in the near future. The properties of hydrograph of the flood and debris flow are also analyzed (Liu et al., 2008).

The criteria for glacial lake inventory were set up with two phases of glacial lake inventories work of the Tibet-Himalayas carried out on the basis of the 278 topography maps (1970s-1980s), 38 ASTER images (2004-2008, including 7 Land-sat Thematic Map per images from 2004-2008 were used to fill the minor maps between ASTER images), the DEMs and slope maps generated from the 278 topography maps and so on. In comparison to the two phases of glacial lake inventories data, Wang and others (Wang et al., 2010) found that the glacial lake variations are characterized by a general trend of "the decrease in the number and the increase in area of glacial lakes" in the Tibet-Himalayas during the past 30 years. Further analysis shows that, in recent 30 years, (1) the number of glacial lake decreased from 1750 to 1680 (with a rate of 4%) whereas the area of glacial lake increased from 166.48 km^2 to 215.28 km^2 (with a rate of 29%); (2) a total of 294 glacial lakes disappeared and 224 glacial lakes formed; (3) among the 6 types of glacial lakes, 66% that disappeared were glacial lakes and 88% of newly formed glacial lakes were moraine-dammed ones; (4) the glacial lakes varied more significantly at the edge of survival glaciers due to the fact that the climate was warming and glaciers were retreating in the region. Wang and others (Wang et al., 2009) also takes the Himalayan region of China as an ideal study area to investigate the potentially dangerous glacial lakes. The 143 potentially dangerous glacial lakes were first identified by six indices in the study area. Then, the probabilities of three types of possible breaching modes (i.e. ice avalanche, glacier slide, ice melting) were quantitatively graded on the basis of the criteria of the probabilities of moraine-dammed lake breaching modes. Breach probabilities of the 143 potentially dangerous glacial lakes were further calculated by means of decision-making trees methods.

There are many glacial lakes in the Poiqu River basin, Nyalam County, Tibet Autonomous Region. The distribution and area of glacial lakes are based on the interpretation of the remote sensing data of Landsat satellite 2000/2001. Compared with the data of 1987, Chen and others (Chen et al., 2007) found that their number and area are changed greatly: the area of glacial lakes increased by 46 % and the number of the lakes in area over 0.02 km^2 increased by 11%. Especially, the Galongco and Gangxico are increased by 104% and 118%, respectively. Field investigation revealed the overall conditions of some key lakes, which mostly depend on the stability of moraine dams and the impact of glaciers. Using direct distinguishing and risk indices of glacial lake outburst, respectively, two types of risk assessments have been completed. Risk assessment shows that there are nine glacial lakes at high dangerous degree, three at middle degree, two at sTable 1.state, and the other 35 at relative sTable 1.state. In this basin, there are some highly dangerous regions, e.g., the lower reaches of Chongdui gully, Keya gully and the confluence spot of Keya gully and Poiqu River; some middle degree dangerous regions, e.g., the lower reaches of Tajiling gully, Rujia gully and Zhangzang gully; and some safe regions. In order to mitigate harm to Nyalam and Zham port, a series of countermeasures are put forward, such as: 1) designing mitigation programme on the base of risk assessment, 2) pre-warning and emergency programme, 3) periodical professional measure, and 4) public warning and prevention system.

Wang et al. (Wang et al., 2008) used the topographic maps, aerial photographs, Landsat TM images, and compilations of other relevant data to analyze the changes of the lakes near S301 highway which joins

Naqu and the Ngari area on the Tibetan Plateau from 1970 to 2000, and to investigate the impact of the lake changes on the road. The results suggested that most of the lakes have expanded and affected the safety of the S301 highway due to global warming, glaciers melting and permafrost degradation.

The Plateau Tibetan holds over 1000 lakes and accounts for roughly 50% of the total lake areas in China. Lakes on the Tibetan Plateau play critical roles in the water cycle and ecological and environment systems of the Plateau. A better understanding of lake variations on the Tibetan Plateau is important for evaluating climate change on Tibetan Plateau under global warming. Lu and others (Lu et al., 2006) used topographic maps, aerial photographs, Landsat TM images, and compilations of other relevant data to set up one syntheses method using remote sensing, and use the method to analyze the changes of the lakes on the Tibetan Plateau from 1970 to 2000. The results showed that the selection of the method to study the lakes variation from 1970 to 2000 is feasible.

1.3.2 Xingjiang Uygur Autonomous Region

Mountain region in Xinjiang is prone to rapid onset flood disaster due to glacier-dammed lake. Investigation on three typical rivers (Ye'erqiang River, Kunmalike River, and Four-trees River) showed that the predicable flood sequence had a positive correlation with storage capacity of glacier-dammed lake (Chen et al., 2005). According to an analysis on the characteristics of geographic environment of A'ertai Mts, Qilian Mts and Tibet, it is thought that circumjacent area of Tarim Basin is exposed to rapid onset flood by glacier-dammed lakes.

In order to understand the glacial lake outburst and find a reasonable assessment way for the glacial lake outburst assessment, Tie and Tang (Tie and Tang, 2009) summarizes main methods for glacial lake outburst assessment developed by the researchers from all over the world, explains some problems existing in current studies, and analyzes the advantages and disadvantages of each methods. Finally, some new ways in the future research are discussed, which gives some information and suggestions for the future study.

1.4 CLIMATE AND ENVIRONMENTAL CHANGES RETRIEVED FROM ICE CORES

The development and interpretation of paleoclimate records is especially significant given the critical role that the highlands of central Asia play in the development and intensity of the Asian monsoon, and the importance of the Asian summer monsoon in providing life sustaining rain to a considerable portion of the worlds' population. The physical and chemical analysis of ice cores recovered from glaciers on the western China provides some of the best high-resolution records of past climate and environmental changes in the region. During the past five years, new ice cores have been retrieved from the Tibetan Plateau (TP) and decadal to centennial climate and environmental changes have been achieved.

1.4.1 Decadal to millennial temperature changes

Temperature reconstruction, a key to understand the past climate change, is the principle for high-resolution ice core records. A 70-year history of summer air temperature has been recovered using an ice core $\delta^{18}O$ record retrieved from a plat portion of the firn area in the Guoqu Glacier at Mt. Geladaindong (the source region of Yangtze River) in TP (Kang et al., 2007a; Zhang et al., 2007). Summer temperature was relatively low in 1940s and high during 1950s to the middle of 1960s. The lowest temperature occurred in the middle of 1970s. The temperature was comparatively low in 1980s and dramatically increased since 1990s, keeping the trend to the beginning of the 21st century (Fig 1.7). The warming rate recorded in the ice core with 0.5℃/10a since 1970s is much higher than that in the central TP and the Northern Hemisphere (NH). The warming rate of 1.1℃/10a since 1990s is also higher compared to the central TP and the NH, reflecting an accelerated warming and a more sensitive response to global warming in the high elevation region (Kang et al., 2007). The shallow ice core from Muztagata, the eastern Pamirs, suggest that the annual fluctuations of $\delta^{18}O$ in the ice core are in good agreement with the annual air temperature changes at the nearby meteorological station Taxkorgen, indicating that the isotopic record from this ice core is a reliable temperature trend indicator (Tian et al., 2006). The most important discovery from the $\delta^{18}O$ variation of the ice core is a rapid warming trend in the 1990s, which is consistent with a general global warming trend.

Ice core $\delta^{18}O$ records from four ice cores (Puruogangri, Dasuopu, Guliya and Dunde) in the TP

provide an overall perspective on climatic warming during the 20th century in a region (Yao et al., 2006a, b; Yang et al., 2007). The $\delta^{18}O$ changes vary with regions on the plateau (Yao et al., 2006b) (Fig 1.8). The average $\delta^{18}O$ and surface air temperature over the TP show very similar fluctuations since 1955, which provides new evidence that the $\delta^{18}O$ in the ice cores is, at least in part, a temperature signal (Yao et al., 2006a). Nevertheless, differences and similarities exist among the four records. Some climatic events, particularly the major cooling episodes, are synchronously recorded in Puruogangri and Dasuopu, as well as the Bange station (Yao et al., 2006b). Climate warming recorded in the ice cores in the past 100 years is consistent with the stations' records over the TP and NH (Yao et al., 2006b) (Fig 1.9).

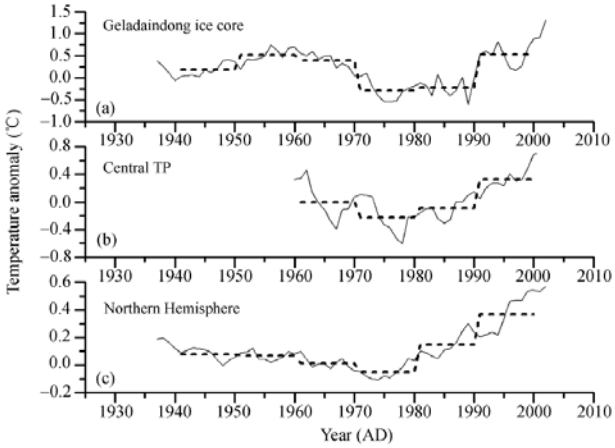

Fig 1.7. Comparisons of summer temperature anomaly reconstructed using the ice core $\delta^{18}O$ records with that of central TP and NH. Fine lines represent annual values and dash coarse lines the average values in different periods. (Kang et al., 2007a)

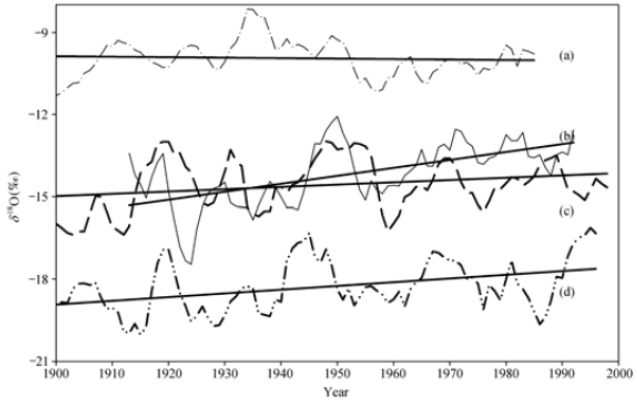

Fig 1.8. Comparison among the Dunde (a), Guliya (b), Puruogangri (c), and Dasuopu (d) ice core. The straight line indicates the linear trend (Yao et al., 2006b).

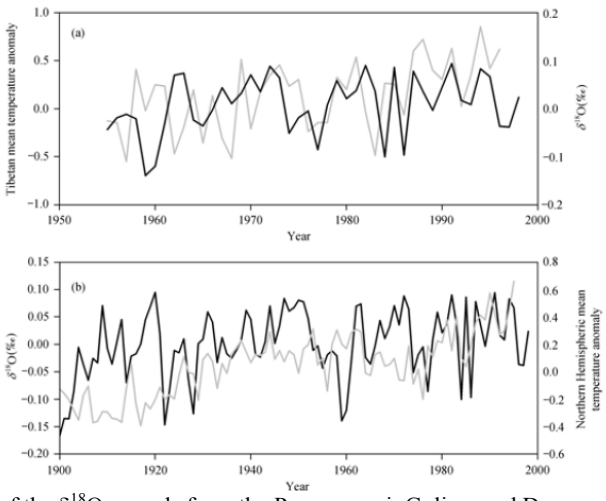

Fig 1.9. Variations of mean of the $\delta^{18}O$ records from the Puruogangri, Guliya, and Dasuopu ice cores (black line) and comparison with direct temperature measurements from the Tibetan Plateau (grey line) (a) and the North Hemisphere (grey line) (b) (Yao et al., 2006b).

Puruogangri ice core records detail regional temperature and moisture variability since AD 1600. The post-1920 period is characterized by above-average annual net balance, contemporaneous with the greatest $\delta^{18}O$ enrichment for the last 400 years as well as consistent with the isotopically inferred warming observed in other TP ice-core records (Fig 1.10) (Thompson et al., 2006). For the period 1860-2000 AD, 5-yearly averaged Puruogangri ice core $\delta^{18}O$ and a summer temperature reconstruction derived from pollen data from the same ice core were compared. The statistical results provide compelling evidence that ice core $\delta^{18}O$ variations represent summer temperature changes for the central TP, and hence regional temperature history during the past 600 years was revealed. Common cold periods were identified in the 15th century, 1625-1645 AD, 1660-1700 AD, 1725-1775 AD, 1795-1830 AD, 1850-1870 AD, 1890-1920 AD, 1940-1950 AD, and 1975-1985 AD. The period 1725-1775 AD was one of the most prolonged cool periods during the past 400 years that corresponded to maximum Little Ice Age (LIA) glacier advancement of monsoonal temperate glaciers of the TP (Yang et al., 2009). On longer timescales, the aerosol history reveals large and abrupt events in Puruogangri ice core, one of which is dated 4.7 kyr BP and occured close to the time of a drought that extended throughout the tropics and might have been associated with centuries-long weakening of the Asian/Indian/African monsoon system (Thompson et al., 2006). The Puruogangri climate history, combined with the other TP ice-core records, has the potential to provide valuable information on variations in the strength of the monsoon across the TP during the Holocene.

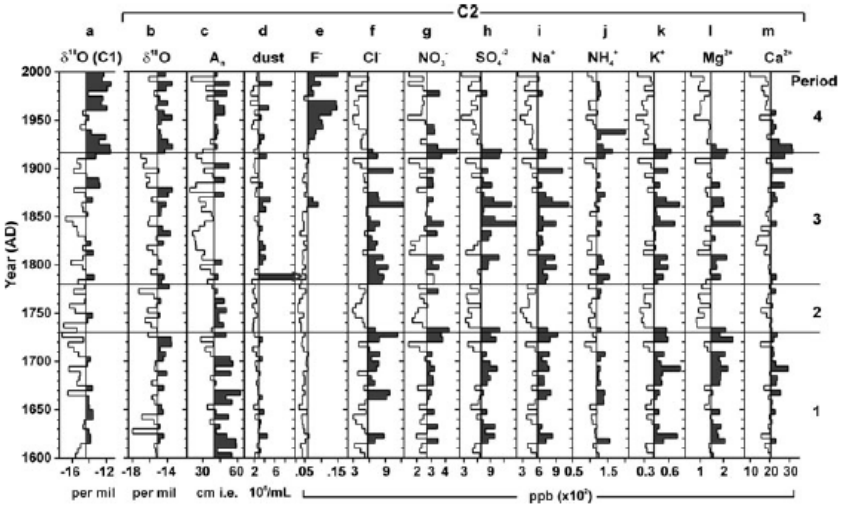

Fig 1.10. Five year averages for the last 400 years shown for $\delta^{18}O$ in both Puruogangri ice core-1 and core-2, along with the concentrations of insoluble dust and soluble species from core-2. (Thompson et al., 2006)

Temperature variation on the TP over the last 1000 years has been inferred using a composite $\delta^{18}O$ record from the four ice cores (Yao et al., 2007), indicating that the temperature change on the whole TP is similar to that in the NH on multi-decadal timescales except that there is no decreasing trend from AD 1000 to the late 19th century in the former. The $\delta^{18}O$ composite record from the northern TP, however, indicates a cooling trend from AD 1000 to the late 19th century, which is more consistent with the NH temperature reconstruction. The $\delta^{18}O$ composite record reveals the existence of the Medieval Warm Period (MWP) and the LIA on the TP. The LIA is not the coldest period during the last millennium in the TP unlike in other regions in the NH. The record of $\delta^{18}O$ since 1129 AD in the Malan ice core indicates that the warm-season air temperature variations display a general increasing trend. The 20th-century warming was within the range of natural climate variability, and the warmest century was the 17th century with warmest decade as the 1610s, over the entire study period (Fig 1.11) (Wang et al., 2006). The MWP and LIA were also reflected by the Malan ice core record. The present study indicates that the 20th-century warming is abrupt on the TP, and is warmer than at any time during the past 1000 years. Moreover, the two Himalayan ice cores display a factor-two decreasing trend of air content over the past two millennia, in contrast to the relatively sTable 1.values in Greenland and Antarctica ice cores over the same period. The reconstruction points toward an unprecedented warming trend in the 20th century, however does not depict the usual trends associated with MWP, or LIA (Hou et al., 2007).

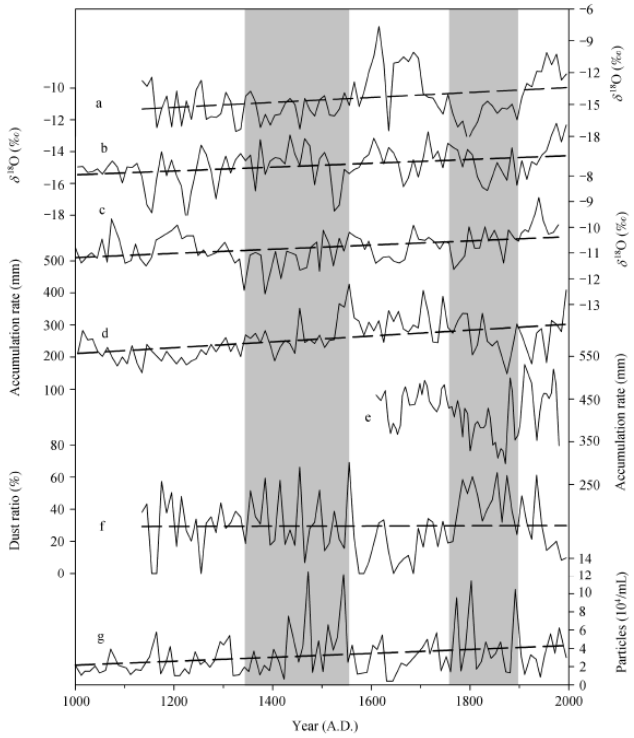

Fig 1.11. Comparison of climatic and environmental records in different ice cores from the northern Tibetan Plateau. (a): $\delta^{18}O$ in the Malan ice core; (b): $\delta^{18}O$ in the Guliya ice core; (c): $\delta^{18}O$ in the Dunde ice core; (d): accumulation rate in the Guliya ice core; (e): accumulation rate in the Dunde ice core; (f): dust ratio in the Malan ice core; (g): particle concentration in the Guliya ice core. The grey columns represents the periods with cold and dry climate and high dust concentrations. (Wang et al., 2006)

1.4.2 Decadal to centennial precipitation variability

Previous work suggested that ice core accumulation records could represent the regional precipitation change, and also be closely related with the atmospheric circulation. Annual accumulation records covering the period 1952-1998 AD were reconstructed from the Lanong ice core on the eastern saddle of Mt.

Nyainqentanglha, southern TP (Kang et al., 2007b). During the last 47 years, the average annual accumulation is 517 mm (water equivalent) at the coring site, which is slightly higher than that at Dangxiong (400 mm) and Lhasa (432 mm). Since the 1950s, there is an increasing trend in annual accumulation with a dramatic increase occurring in the late 1980s. Linear correlation analysis between annual accumulation and climate components (NCEP/ NCAR Reanalysis data) indicates that annual accumulation variations are closely correlated with sea-surface and 500 mb air temperature over the North Indian Ocean and atmospheric circulation (surface pressure and geopotential height) over Asia ($r > 0.34$, $P < 0.01$). An intensification of atmospheric circulation and increase of sea surface and air temperatures, resulting in intensified moisture availability and moisture transport, have been a major cause for the increase of ice core accumulation over the Mt. Nyainquentanglha region since the 1980s (Kang et al., 2007b).

Variations of annual accumulation in the Tanggula ice core (1950-2004) suggested three different phases (1950-1967 for increasing, 1968-1991for hovering, and 1992-2004 for decreasing, respectively) (Zheng et al., 2010). Annual accumulation reconstructed from a Geladaindong ice core covering a duration of 1935-2004 showed that precipitation in the Geladaindong region was low between 1930s and early 1960s with the lowest value occurred in the later 1950s (Zhang et al., 2007). Since 1960s, precipitation increased dramatically and reached the maximum around 1980s, then decreased slightly in 1990s (Fig 1.12). By using Mann-Kendall rank statistical test method, a change point for precipitation was determined in 1967. Analysis of the atmospheric circulation over the TP suggested that, compared with the southwest wind during the low precipitation period (before 1967), it extended about 2 latitudes northward during high precipitation period (after 1967). Moreover, during the high precipitation, the trough over the Bal Karshi Lake was also enhanced, and both the meridional wind and vapor transportation displayed a remarkable aggrandizement.

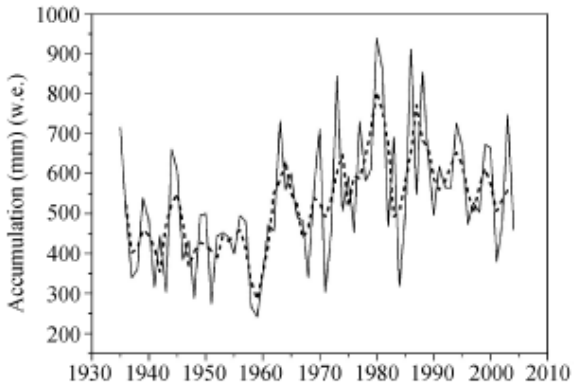

Fig 1.12. Variations of accumulation in the Geladaindong ice core for recent 70 years. Dashed line represents the 3-year smoothing average.

The profile of East Rongbuk ice core, annual-layer thickness data spanning 1534-2001AD, clearly showed that the mean accumulation rate had changed every 50-100 years (Kaspari et al., 2008). The mean annual accumulation rate decreased from ~0.8 m ice equivalent in the 1500s to ~0.3m in the mid-1800s (Table 1.11). From ~1880 to ~1970 this rate was increased. However, it has decreased since ~1970. Comparison of six other records from the Himalaya and the TP suggested that the changes in accumulation in East Rongbuk Col were broadly consistent with a regional pattern over much of the plateau (Fig 1.13). This suggests that there may be an overarching mechanism controlling precipitation and mass balance over this area.

Table 1.11. Accumulation rates (m a^{-1}) during time intervals (AD) for the values of m shown in the left hand column. (Kaspari et al., 2008)

M	2000BC-AD1535	1535-1620	1620-1720	1720-1835	1835-1935	1935-2000
1.01	0.52	0.55	0.42	0.39	0.29	0.64
1.11(by least squares)	0.53	0.77	0.53	0.46	0.33	0.69
1.11(model)	0.52	0.80	0.50	0.44	0.30	0.66
1.21	0.52	1.10	0.58	0.49	0.31	0.68

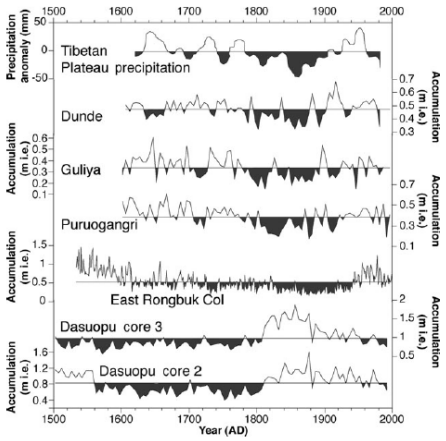

Fig 1.13. Reconstructed Tibetan Plateau precipitation record from tree rings and ice-core accumulation-rate time series from Dunde, Guliya, Puruogangri, East Rongbuk Col and Dasuopu. The horizontal line through each time series is the average, and the gray shaded regions denote below-average accumulation. (Kaspari et al., 2008)

The 400-year annual accumulation record was reconstructed from Puruogangri ice core (Yao et al., 2008). The result shows that the central TP experienced a drier period with an average annual precipitation of ~300mm in the 19th century, compared to ~450 mm in the wetter periods during 1700~1780 and the 20th century. This pattern agrees with precipitation reconstructions from the Dunde and Guliya ice cores on the northern Plateau but differs from that found in the Dasuopu ice cores from the southern Plateau (Fig 1.14). The north-south contrasts in precipitation reconstruction reveals difference in moisture origin between the south TP dominated by the Asian monsoon and the north TP dominated by the continental recycling and the westerlies.

In the southern TP, precipitation is closely related to the South Asian monsoon (Indian summer monsoon). Variations in the monsoon can result in severe droughts and torrential rains. Modern South Asian monsoon variability is linked with sea surface temperature anomalies, Eurasian snow cover, soil moisture, and the El Nino Southern Oscillation. A highly resolved Mt. Everest ice core reveals a decrease in marine and increase in continental air masses related to relatively high summer surface pressure over Mongolia, and reduction in northward incursions of the summer South Asian monsoon since ~1400 AD (Fig 1.15) (Kasparti et al., 2007). Changes in monsoon strength are associated with solar output and the solar activity can alter the south-north seesaw of convective activity in the Indian region. During periods of high solar activity, increased

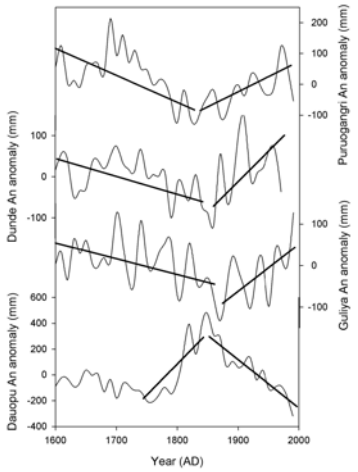

Fig 1.14. Decadal changes of precipitation based on glacial accumulation reconstructed from Puruogangri ice core,

Dunde ice core, Guliya ice core and Dasuopu ice core. The thick lines are linear trends of accumulation in different periods. (Yao et al., 2008)

equatorial convection result in increased monsoon strength in southern regions of monsoon influence. Conversely, the decrease in solar irradiance at ~1400 AD coincides with reduced monsoon strength at all four proxy record sites (Fig 1.15). These regional differences are consistent with a south-north seesaw in convective activity in the Asian monsoon region, and reflect a southward shift in the mean summer position of the monsoon trough since ~1400 AD. During post ~1400 AD, the monsoon intensifies in southern regions but remains relatively weak in the Everest region. These south-north differences are consistent with the previously mentioned seesaw pattern in monsoon strength. The mechanism for how variations in solar irradiance affect the monsoon is not well understood because solar irradiance variations are small, and are not likely to have directly caused large differences in sensible heating of the TP. The change in monsoonal circulation at 1400 AD is synchronous with a reduction in solar irradiance and the onset of the LIA. This demonstrates a hemispheric scale circulation reorganization at this time, and the potential for future large shifts in monsoonal circulation.

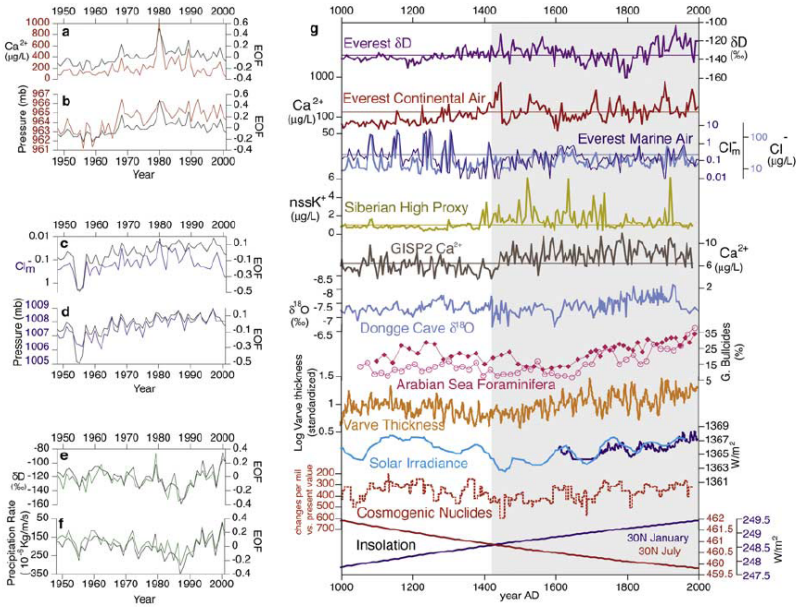

Fig 1.15. Calibration of the Everest ice core and instrumental records, and proxy data from 1000~2000 AD. (a) Everest mean annual Ca^{2+}(ppb) (red) and (b) NCEP May-October surface pressure (mb) (red) and their common first EOF (black) representing 75% of the variance in the two time series; (c) Everest mean annual Cl_m^- (blue) and (d) NCEP May-October surface pressure (mb) (blue) and their common first EOF (black) representing 76% of the variance in the two time series; (e) Everest mean annual dD (%) (green) and (f) NCEP June-September precipitation rate (10^{-6} kg/m/s) (green) and their common first EOF (black) representing 71% of the variance in the two time series. (g) Proxy data. Lines through the data sets are the mean values from 1000~2000 AD, and the shaded region highlights the LIA. (Kaspari et al., 2007)

1.4.3 Variations of major ions and elements

Glaciochemistry in snow and ice provides a valuable record of atmospheric environment and circulation, and allow evaluation of past climate change. Seasonal and spatial variations of major ions and elements in snow and ice are the basic knowledge for interpretation of ice core ion records. Investigations in Himalayas suggest that major ions have a significant seasonal variation, with high concentrations during the non-monsoon season and relatively low concentrations during the monsoon season (Kang et al., 2007c; Liu et al., 2010).

Major ions of a 32.4m shallow ice core recovered from Mt. Tanggula shows that the ion chemistry of the upper 14.5 m, covering the last 55 years, is characterized by mineral dust (HCO_3^- , Ca^{2+}, SO_4^{2-}, Na^+, Cl^- and K^+), anthropogenic species (SO_4^{2-}, NH_4^+ and NO_3^-) and soil and biogenic emissions (NO_3^- and NH_4^+)

(Zheng et al., 2010). Ca^{2+} is the dominant cation in the core with a medium value of 33.5 μeq L^{-1}, accounting for 64.5% of the total cations, and HCO_3^- is the predominant anion, accounting for 80.2% of the total anions. Compared with ice core records from Altai and Himalayas (Table 1.12) in the north and south of the TP, respectively, major ion concentrations (except SO_4^{2-}, NH_4^+ and NO_3^-) in Tanggula ice core are much higher due to pronounced regional crustal aerosol inputs. Increasing SO_4^{2-} concentrations in the most recent 50 years are attributed to anthropogenic contributions; but mineral dust is still the major source for SO_4^{2-} in the central TP. The noTable 1.relationship between increasing NH temperature and NO_3^- and NH_4^+ concentrations suggests that recent temperature increase in TP might have been enhancing biological activity and associated NO_3^- and NH_4^+ emissions from the regional terrestrial ecosystems (Zheng et al., 2010).

Table 1.12. Median concentrations and percentage of major ions in ice cores from Belukha, Tanggula, and East Rongbuk in high Aisa. (Zheng et al., 2010)

Ice core	Belukha, Altai (Olivier et al., 2003)		Tanggula , central Tibetan Plateau (this work)		East Rongbuk, Himalayas (Kang et al., 2002)	
Period of record	1940–2000		1950–2004		1846–1997	
Location	49°38.4′N, 86°34.7′E		33°7.1′N, 92°5.4′E		27°59.2′N, 86°54.9′E	
	4062 m a.s.l		5743 m a.s.l		6450 m a.s.l	
	Median	Percentage	Median	Percentage	Median	Percentage
SO_4^{2-}	11.0	23.1	2.9	5.0	1.9	10.3
Cl^-	0.9	1.9	1.8	2.8	0.5	2.6
NO_3^-	4.3	9.0	1.8	2.7	0.7	3.5
HCO_3^-	7.6	16.0	26.3	39.6	6.4	33.6
Na^+	1.0	2.1	2.8	4.5	0.5	2.7
NH_4^+	11.4	23.9	6.1	7.3	3.0	15.9
K^+	0.4	0.8	0.3	0.4	0.2	1.1
Mg^{2+}	1.6	3.4	2.6	4.2	0.4	2.3
Ca^{2+}	9.4	19.7	21.4	33.5	5.3	28.0
Total	47.6		65.9		19.0	

Percentage: current ion to total ions.

Major and trace elements in the Everest snow/ice show that crustal elements are dominated, suggesting that Everest snow chemistry is mainly influenced by crustal aerosols from local rock or prevalent spring dust storms over southern/central Asia. Seasonal variability in snow/firn elements show that high elemental concentrations occur during the non-monsoon season and low values during the monsoon season (Fig 1.16). Ca, Cr, Cs, and Sr display the most distinct seasonal variations. Elemental concentrations (especially for heavy metals) at Mt. Everest are comparable with polar sites, generally lower than in suburban areas, and far lower than in large cities. This indicates that the atmospheric environment in the Everest is on the global background level (Kang et al., 2007c).

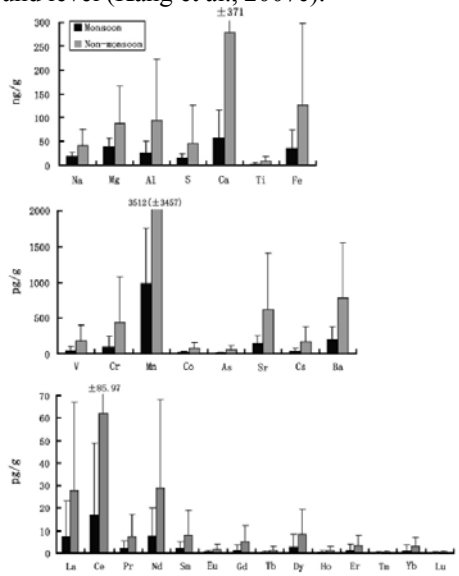

Fig 1.16. Comparison of element concentrations in snow/ice between monsoon and non-monsoon seasons at Mt. Everest

Rare earth element (REE) concentrations in Everest snow/ice seem to be comparable with those

measured in modern and Last Glacial Maximum snow/ice samples from Greenland and Antarctica, and with precipitation samples from Japan and the East China Sea. When normalized to a shale standard, the Mt. Everest REEs exhibit a consistent shale-like pattern with a slight enrichment of middle REEs during both seasons. However, individual monsoon REE patterns show differences, possibly resulting from diversified sources. Non-monsoon REE patterns are sTable 1.and are associated with the westerlies. Investigation of potential sources for the Everest REEs suggests an absence of anthropogenic contributions and minimal input from local provenances (Fig 1.17). REEs in Mt. Everest samples are most likely representative of a sTable 1.well-mixed REE background of the upper troposphere consisting of a mixture of aerosols transported by the atmospheric circulation from the west windward arid regions such as the Thar Desert, West Asia, the Sahara Desert and other uncertain provenances (Zhang et al., 2009).

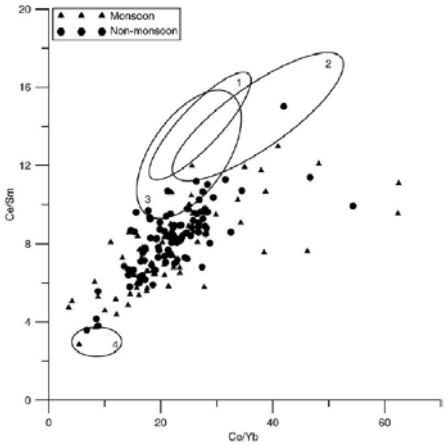

Fig 1.17. REE ratios of Everest snow/ice samples compared with those from other potential source regions. [1] Aerosol from the Sahara; [2] Taklimakan sand; [3] China loess; [4] Thar Desert. (Zhang et al., 2009)

REE compositions of dust extracted from shallow ice core from the Dunde ice cap provide a framework to trace the source of Dunde dust (Wu et al., 2009). Trace and REE parameters of Dunde dust show characteristics of a typical eolian deposit, with an average La/Th ratio of 2.6, a Th/Uratio of 3.7, and a strong negative Eu anomaly (0.61). The dirty layers in the ice core section have the same element characteristics as in the clear layers, indicating that the dust in Dunde is well-mixed and has a sTable 1.composition. Trace element and REE ratio plots (Fig 1.18) show that Dunde dust has a similar composition to the finer fraction materials in the Taklimakan desert, suggesting that the Tarim Basin might be an important source region for Dunde dust under the present circulation, but does not favor a material contribution from Badain Jaran. The results reveal distinct differences in composition between Dunde dust and Chinese loess materials with an indication of different sources.

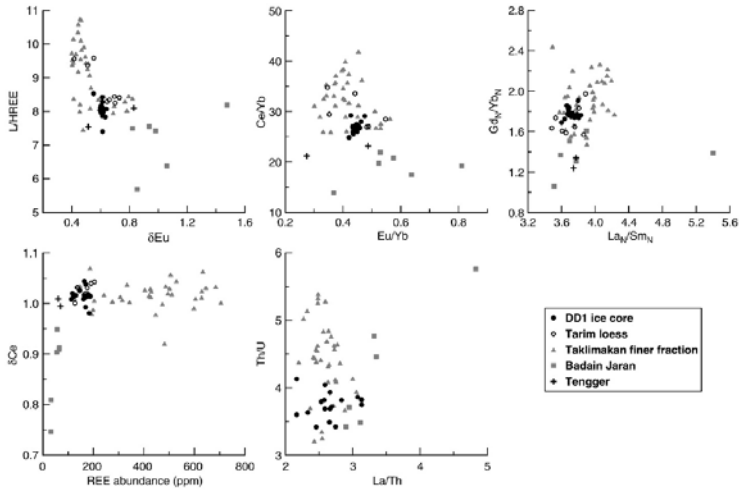

Fig 1.18. Trace and REE parameters for dust samples from Dunde dust, Taklimakan finer fraction of eolian sediment, Tarim Basin loess, Tengger and Badain Jaran eolian sediment. (Wu et al., 2009)

High-resolution major and trace elements (Sr, Cs, Ba, La, Ce, Pr, Nd, Sm, Eu, Tb, Dy, Ho, Er, Tm, Yb, Lu, Bi, U, Tl, Al, S, Ca, Ti, V, Cr, Mn, Fe, and Co) are also quantified in Mt. Everest ice core (6518 m a.s.l.) spanning the period of 1650~2002 AD that provides the first Asian record of trace element concentrations from the pre-industrial era, and the first continuous high-resolution Asian record from which natural baseline concentrations and subsequent changes due to anthropogenic activities can be examined (Kaspari et al., 2009a). Modern concentrations of most elements remain within the pre-industrial range; however, Bi, U, and Cs concentrations and their enrichment factors (EF) have increased since the 1950s, and S and Ca concentrations and their EFs have increased since the late 1980s (Fig 1.19). A comparison of the Bi, U, Cs, S, and Ca data with other ice core records and production data indicates that the increase in atmospheric concentrations of trace elements is widespread, however the enrichment varies regionally. Likely sources for the recent enrichment of these elements include mining, metal smelting, oil and coal combustion, end uses for Bi, and mining and refinement for U and Cs. Although the source of the synchronous enrichment of Ca and S is less certain, it may be related to the land use and environmental change (Kaspari et al., 2009a).

Muztagata ice core also provides a Pb concentration record from 1955 to 2000 (Li et al., 2009). The result reveals increasing Pb concentrations from 1955 to 1993, with two Pb concentration peaks in 1980 and 1993. After 1993, Pb concentrations in ice core show an obviously declining trend. The lead in the Muztagata ice core was a result of anthropogenic emissions from central Asia, while the local emission had little contribution (Li et al., 2009).

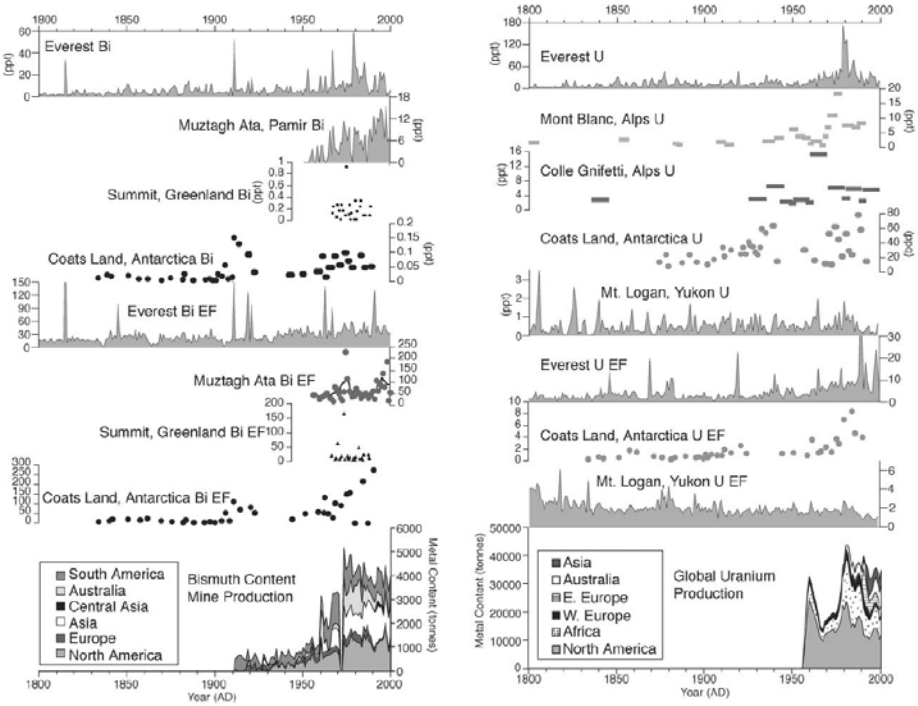

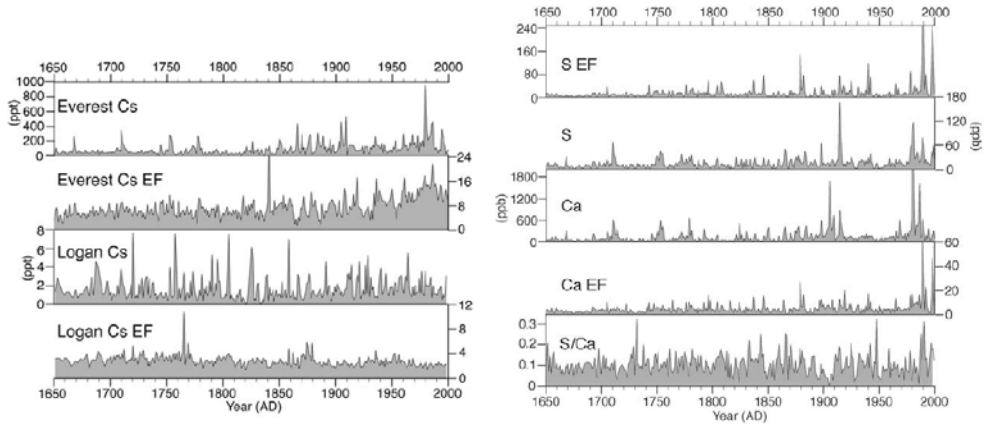

Fig 1.19. Mt. Everest Bi, U, Cs, S, Ca and Bi EF, U EF, Cs EF, S EF, Ca EF and other ice cores discussed in the text. (Kaspari et al., 2009a)

1.4.4 Atmospheric dust variability

Assessing the dust loading of the atmosphere is important because dust aerosols can affect climate, global biogeochemical cycles, the hydrologic cycle, and human health. Dust aerosols impact the climate system by altering the earth's radiative balance. Ice cores recovered from appropriately chosen sites are an ideal archive for reconstructing past atmospheric dust aerosol loading, transport, and chemical composition prior to the instrumental record. A Mt. Everest ice core, spanning the period of 1650–2002 A.D., is used to investigate the sources of and variations in atmospheric dust through time (Kaspari et al., 2009b). Significant correlations between the Everest dust record and dust observations at stations (Fig 1.20) suggest that the Everest record is representative of regional variations in atmospheric dust loading. A significant correlation of Everest dust concentrations and the Total Ozone Mapping Spectrometer (TOMS) aerosol index indicates that the dominant winter sources of dust are the Arabian Peninsula, Thar Desert, and northern Sahara. Factors that contribute to dust generation at the surface include soil moisture and temperature, and the long-range transport of dust aerosols appears to be sensitive to the strength of 500-mb zonal winds. There are periods of high dust concentration throughout the 350-yr Mount Everest dust record; however, there is an increment since the early 1800s (Fig 1.21). The record was examined for recent increases in dust emissions associated with anthropogenic activities, but no recent dust variations can be conclusively attributed to anthropogenic inputs of dust (Kaspari et al., 2009b).

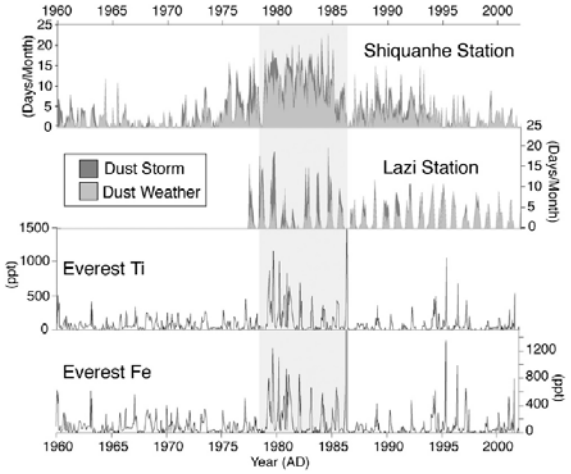

Fig 1.20. Dust variability from station dust data (Chinese Meteorological Administration), and the Mount Everest ice core glaciochemical record. A dust storm day has strong and turbulent wind and horizontal visibility is <1km, whereas a dust weather day has moderate winds and horizontal visibility is ~1-10km. (Kaspari et al., 2009b)

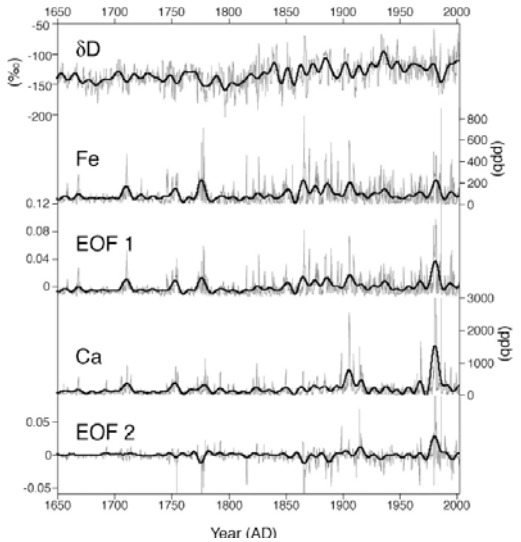

Fig 1.21. Mt. Everest δD, Fe, EOF1, Ca, and EOF2 data resampled to four samples per year (gray) with a 10-yr low pass filter (black) from the period A.D. 1650-2000 (Kaspari et al., 2009b)

Comparisons of dust particle record from the other Everest 40-m ice core (Xu et al., 2007) with winter (DJFM) precipitation from 26 meteorological stations distributed throughout Pakistan and winter (DJFM) North Atlantic Oscillation (NAO) show a significant inverse correlation between westerly strength (NAO) and dust concentrations (r^2=−0.46, P<0.01, n=51) (Fig 1.22), suggesting that westerlies may play an important role in controlling Himalayan ice-core dust concentration. Although variations in precipitation are not distinctly correlated with dust concentrations and NAO in decadal scale, low (high) precipitation is in phase with high (low) dust concentrations and low (high) NAO index values, indicating that precipitation during winter may be another factor controlling the dust storm activity in central Asia.

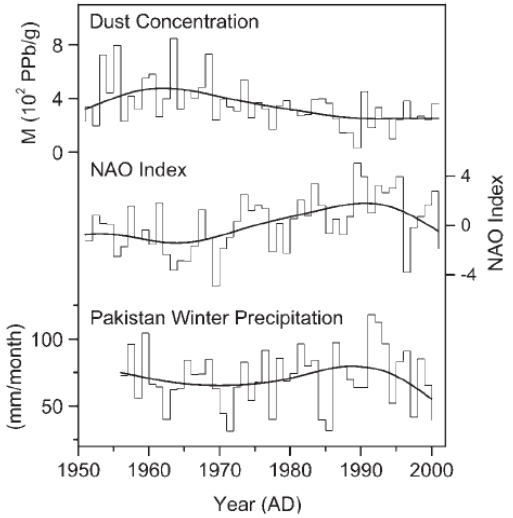

Fig 1.22. Comparisons of dust record from the 40-m ER ice core, the winter (DJFM) NAO index and Pakistan winter (DJFM) precipitation. The solid thick lines represent the 11-yr running mean. (Xu et al., 2007, 2010)

To identify the sources of the particles at Everest, Sr-Nd-Pb isotopic tracer was applied (Xu et al., 2009). The results (Fig 1.23) show that the particles in the dirty layers originate mainly from local sources, whereas the particles in the non-dirty layers are consistent with the features of dust from the arid regions in northwestern India. The HYSPLIT model shows that the air trajectory goes first through northwestern India before reaching the drilling site of ice core when dust storms occur in northwestern India, confirming northwestern India as a possible source of dust on Everest (Xu et al., 2009).

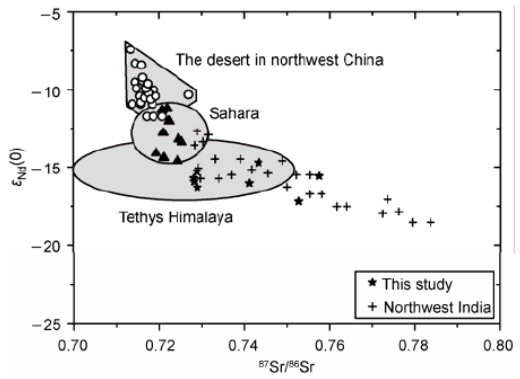

Fig 1.23. Comparison of the Sr-Nd isotopic compositions between the ER ice core samples and that of the potential source areas

The dust particle record on the Everest ice core since AD 1500 shows a significant positive relationship between the dust concentration and reconstructed air temperatures during this period (Xu et al., 2010) (Fig 1.24). This result suggests a likely cold-humid and warm-dry climatic pattern in the dust source regions, namely central Asia. Intervals around 16th, 18th, mid-19th, and post-20th century are characteristic of relatively high dust concentrations. During the LIA, dust accumulation was positively correlated with reconstructed temperatures. A conceptual model relating to the variability of westerlies and corresponding winter precipitation was then used to explain this relationship. During cold periods of LIA, the westerlies were enhanced, resulting in higher than normal precipitation and increased seasonal snow cover in central Asia, thus decreasing dust concentrations. During the relatively warm periods of LIA, the intensity of westerlies weakened, resulting in low precipitation in the winter and spring seasons and significantly reduced seasonal snow cover. As a consequence, dust concentrations increased. This is associated with the variability in the strength of the westerlies and its corresponding precipitation (Xu et al., 2010).

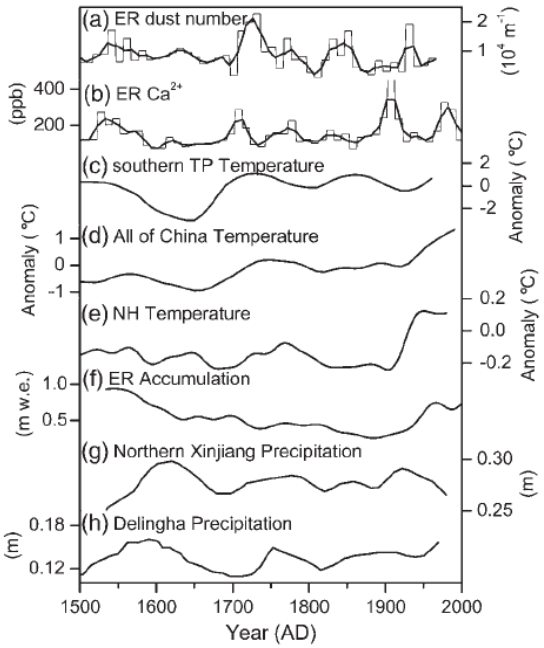

Fig 1.24. Profiles of 10-yr averages of (a) dust number, (b) Ca^{2+}, and (f) accumulation in the Everest ice core. The thick lines represent the 31-yr running mean. Regional to hemispheric temperature variations from (c) southern TP, (d) all of China, and (e) the Northern Hemisphere (NH). Reconstructed precipitation based on tree rings from (g) northern Xinjiang and (h) Delingha. (Xu et al., 2010)

In central TP, a Mt. Geladaindong (GL) ice core dust proxy was recovered spanning the period of

1940-2005 AD (Kang et al., 2010). The crustal source ions vary seasonally with peaks in dust concentrations occurring during the winter and spring which are consistent with atmospheric dust observations at local meteorological stations. The 1980s and 1970s were taken as case periods for low and high atmospheric dust loading (Table 1.13), respectively. These two periods reflect shifts in spring atmospheric circulation (a weakening of zonal and meridional winds) from the 1970s (a period of enhanced dust aerosol transportation to central TP) to the 1980s (a period of diminished dust aerosol transportation to central TP), especially a significant decrease of meridional wind speeds in the 1980s (Fig 1.25). GL ice core dust proxies (Ca^{2+} and K^{+}) are also correlated with Total Ozone Mapping Spectrometer (TOMS) Aerosol Index (AI) data in spring over the TP and in the northwestern China (especially for K^{+}). Thus variability of crustal ions in central TP ice core provides a proxy for reconstructing a history of atmospheric dust loading not only on the TP, but also in northwestern China.

Table 1.13. Decadal mean ion concentrations (±Sta.Dev.) in the Geladaindong ice core. (unit: ng/g) (Kang et al., 2010)

	1940s	1950s	1960s	1970s	1980s	1990s
Ca^{2+}	708.50 ± 299.52	757.01 ± 322.07	1031.81 ± 318.02	1857.64 ± 1060.54	455.96 ± 438.35	1153.44 ± 657.93
K^{+}	15.19 ± 5.02	21.40 ± 5.40	32.46 ± 9.91	49.83 ± 31.52	15.25 ± 7.31	40.32 ± 31.67
Na^{+}	126.46 ± 51.40	230.06 ± 56.19	400.37 ± 129.03	540.60 ± 362.15	85.25 ± 78.39	386.41 ± 530.71
Mg^{2+}	37.40 ± 8.75	65.41 ± 14.26	109.67 ± 33.73	166.38 ± 95.72	40.47 ± 37.61	118.86 ± 61.34
Cl^{-}	225.23 ± 72.16	325.02 ± 83.80	444.17 ± 94.16	640.06 ± 472.30	104.76 ± 93.70	384.07 ± 448.76
NO_3^{-}	131.70 ± 37.61	176.07 ± 47.62	245.90 ± 75.83	358.42 ± 207.04	117.85 ± 91.82	219.37 ± 208.69
SO_4^{2-}	142.91 ± 48.44	207.21 ± 60.00	470.39 ± 184.32	782.77 ± 569.90	154.37 ± 114.50	510.56 ± 706.20

After analyzing the dust layers in the Malan ice core in the northern TP, it was found that dirty ratio in this core might be a good proxy for dust event frequency (Wang et al., 2005, 2006b). The variations in the dirty ratio displayed a decreasing trend over the past 200 years (Fig 1.26), which implies that dust events became less frequent during the study period. The decreasing trend in the variations in dust event frequency might be caused mostly by the natural processes, including increasing precipitation and weakening westerly which might be related with global warming. Furthermore, statistical analysis of the variations in the dust ratios and $\delta^{18}O$ in the Malan ice core shows a strong negative correlation between them (Fig 1.26), suggesting that dust events occur more frequently in cold periods than in warm periods (Wang et al., 2006b). Precipitation in the northern TP and its vicinity showed an increasing trend over the past 200 years (Fig 1.26) (Wang et al., 2005), which is another important reason for the deceasing trend of dust event frequency over the past 200 years in Malan ice core.

Based on the oxygen isotope ratio and microparticle record in ice cores recovered at Mt. Muztagata, Eastern Pamirs, the seasonal variations of atmospheric dust have been reconstructed for the past four decades (Wu et al., 2008). The statistical analyses indicate that 50%~60% high dust concentration samples occurred during the season with high oxygen isotope values (summer), while low dust storm frequency during spring and winter (Table 1.14). Back-trajectory analysis shows that the air mass hitting Muztagata predominately came from West Asia (such as Iran-Afghanistan Plateau) and Central Asia, which are the main dust source area for Muztagata. Dust storms in those source areas most frequently occur during summer (from May to August), whereas frequent dust storm events in northern China occur mainly during spring (March to May). The results indicate that dust storms have different seasonality in different regions within Asia.

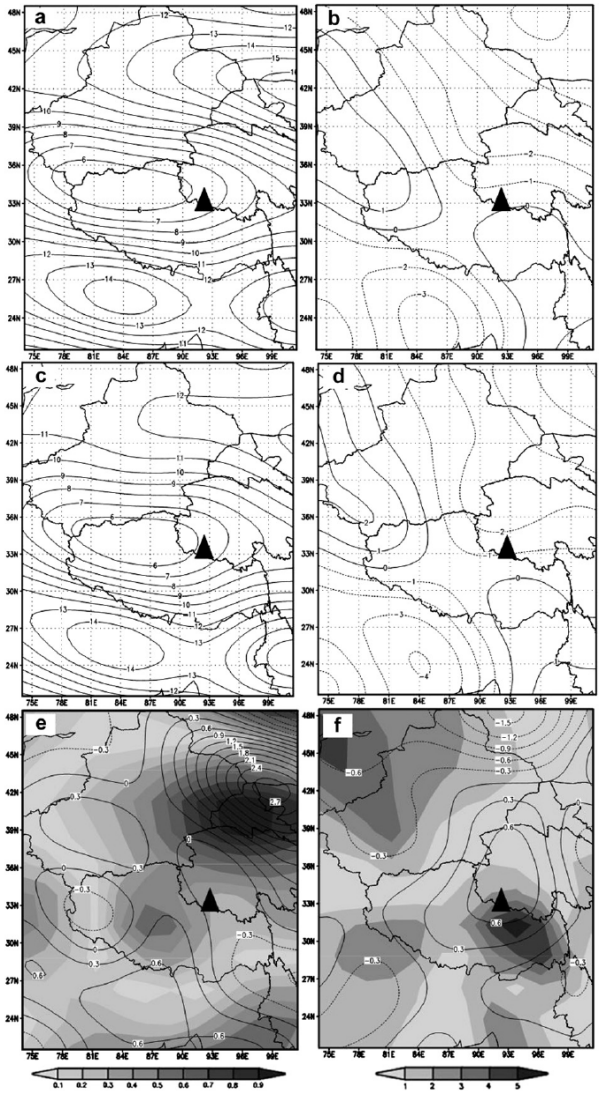

Fig 1.25. Mean 500 hPa zonal (a/c) and meridional (b/d) wind speeds in the 1970s/1980s and differences of mean zonal (e) and meridional (f) wind speeds during spring (MAM) between the 1980s and the 1970s (1970s' value minus 1980s') (t-test values for the significance levels shown in grayscale; $t > 2.26$, $p < 0.05$, $n = 10$). Triangle represents the ice coring site. (Kang et al., 2010)

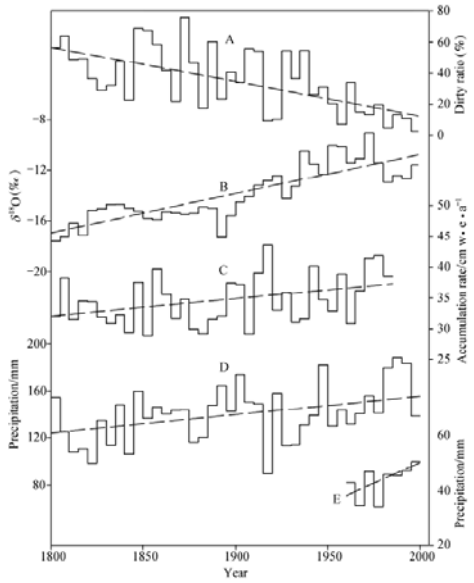

Fig 1.26. Comparison of dirty ratio in the Malan ice core with some climatic records from the northern Tibetan Plateau and its vicinity over the past 200 years. All these set are 5-year mean. A- the dirty ratio in the Malan ice core; B- $\delta^{18}O$ in the Malan ice core; C- accumulation rate recorded in the Dunde ice core; D- precipitation revealed by the tree-ring records at Delingha, Qinghai; E- precipitation in south Xinjiang. (Wang et al., 2005)

Table 1.14. Statistical results for high dust concentration cases (frequency) in the Muztagata 7010 m and 6350 m ice cores. (Wu et al., 2008)

$\delta^{18}O$ period (season)	7010 m Core 3 (from 1970－2002 A.D.)			6350 m (from 1957－2000 A.D.)	
	>10000 μg kg^{-1} event (%)	>15000 μg kg^{-1} event (%)	>20000 μg kg^{-1} event (%)	>15000 μg kg^{-1} event (%)	>20000 μg kg^{-1} event (%)
Increasing (spring)	18 (19%)	11 (31%)	6 (30%)	15 (16%)	10 (17%)
Maximum (summer)	43 (46%)	18 (52%)	10 (50%)	56 (62%)	39 (66%)
Decreasing/minimum (winter)	33 (35%)	6 (17%)	4 (20%)	20 (22%)	10 (17 %)
Total	94 (100%)	35 (100%)	20 (100%)	91 (100%)	59 (100 %)

Atmospheric dust loading and its variation display large spatial and temporal differences in TP. The ice core records indicated that the mean dust concentration in the past 150 years was one or two times higher in the Guliya and Dunde ice cores from the northern TP compared to the Dasuopu ice core from the southern TP (Wang et al., 2006c). Over the last millennium, the Dasuopu ice core record shows that the 1270s~1380s and 1870s~1990s were the two epochs with high dust concentration (Fig 1.27). However, the Malan ice core from the northern TP indicates that high dust loading occurred during the 1130s~1550s and 1770s~1940s. The Dunde dust content shows a decreasing trend since the early 1700s. During the LIA, it was slightly higher corresponding to the cold period (Yang et al., 2006). Interestingly, climatic and environmental records of the ice cores from the TP reflected that the correlation between dust concentration and air temperature was strongly positive in the southern Plateau but negative in the northern Plateau over the last millennium. This implies that climatic and environmental changes showed considerable differences in different parts of the plateau (Wang et al., 2006c).

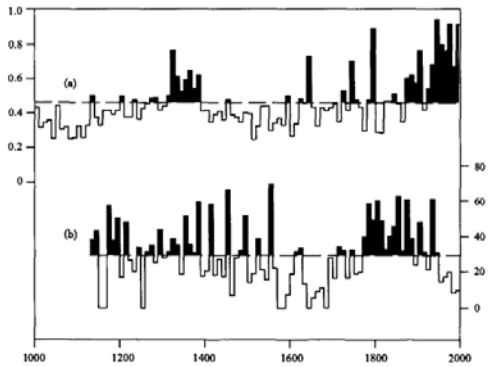

Fig 1.27. Comparison of the variations of decadal mean dust concentration in the Dasuopu ice core from the southern Tibetan Plateau (a) with the variations of decadal mean dust ratio in the Malan ice core from the northern Tibetan Plateau (b) over the last millennium. (Wang et al., 2006c)

1.4.5 Black carbon variability

Black carbon (BC) plays an important role in the earth climate system. BC particles suspended in the atmosphere could result in very complex radiative effects by acting as the light absorber and veil. A recent continuous measurement on BC in a 40m shallow ice core retrieved from the Everest ice core provided the first historical record of BC deposition during the past 50 yrs in the high Himalayas (Ming et al., 2008). Apparent increasing trend (smooth average) of BC concentrations was revealed since the mid-1990s. Seasonal variability of BC concentrations in the ice core indicated higher concentrations in monsoon seasons compared to non-monsoon seasons. Backward air trajectory analysis by the HYSPLIT model indicated that South Asia's BC emissions had significant impacts on the BC deposition on Everest region. The estimated average atmospheric BC concentration in the region was about 80 ng m^{-3} during 1951~2001. A significant increasing trend of the radiative forcing simulated by the SNICAR model appeared since 1990, which even exceeded 4.5Wm^{-2} in the summer of 2001. It was suggested that such an amplitude of BC concentrations in the atmosphere over the Himalayas and consequently in the ice in the glaciers could not be neglected when assessing the dual warming effects on glacier melting in the Himalayas.

Xu et al. (2009b) represented the BC variability through the whole TP using the ice core records (Fig 1.28). Relatively high black soot concentrations occurred in the 1950s~1960s at all Tibetan locations except the Zuoqiupu. Black soot on the TP glaciers was deposited primarily from two directions: west and south. The northern and northwestern plateau is under control of the westerly jet stream all year, so its upwind sources are principally Europe and the Middle East. Glaciers in the southern part of the plateau receive deposits from the west in winter and the south in summer. Lack of a noTable 1.1950s~1960s peak at the Zuoqiupu may be due to the circuitous path required for European air to reach that location on the eastern plateau, and thus the greater proportion of Asian aerosols there. Decreased BC and organic carbon (OC) concentrations on the northwestern and central plateau in the 1970s~1980s, relative to 1950s~1960s, are consistent with declining European sources due to environmental regulations. Overall, there is an evidence of increasing BC and OC concentrations on southern Tibetan glaciers (Zuoqiupu, Noijin Kangsang, and East Rongbuk) (Fig 1.28) since 1990. This post-1990 difference between southern and northern glaciers reflects regional differences in source strength and transport pathways for atmospheric black soot between Europe and Asia, including regional differences in the degree of environmental regulation.

Seasonal variation of BC probably maximizes its impact on snowmelt. Lowest BC concentration is during the monsoon season, whereas the highest concentration is associated with the South Asian Haze, which peaks during November-March, spreading northeastward along the south side of the Himalayas. Thus, highest black soot concentration in unmelted snow occurs at the time of maximum snow extent, accelerating spring melt and lengthening the melting season. In addition, the ice cores used to measure black soot concentration are obtained in the accumulation zone of the glaciers; i.e., in regions where snow melt is negligible. In the ablation zone on the glaciers, the melting process tends to increase the concentration of black soot on the glacier surface, thus increasing the impact of black soot on glacier melt (Xu et al., 2009b).

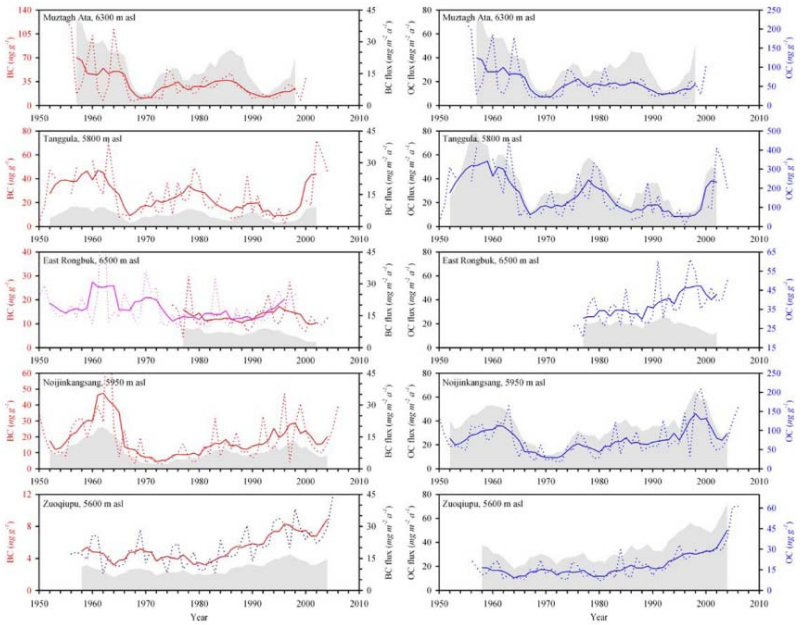

Fig 1.28. BC and OC in the five ice cores. Dotted line is annual concentration (ng g^{-1}), solid line is 5-year running mean, and gray shaded region is the integrated annual deposition. (Xu et al., 2009b)

1.4.6 Volcanic activity records

Volcanic eruptions eject large amounts of gas (mainly sulphur dioxide) and dust (generally silicate ash) into the atmosphere that can be transported via atmospheric circulation and deposited on the surface of glaciers. This provides a useful method to study the past volcanism by ice core records. Continuous Bi profile of the Everest ice core reveals nine major volcanic events since AD 1800 (Xu et al., 2009c) (Fig 1.29). Compared with Volcanic Explosivity Index (VEI), it shows that the concentrations of Bi in the ice core can reflect the major volcanic events within the key areas. This provides a good horizon layer for ice core dating, as well as a basis for reconstructing a long sequence of volcanic records from the TP ice cores.

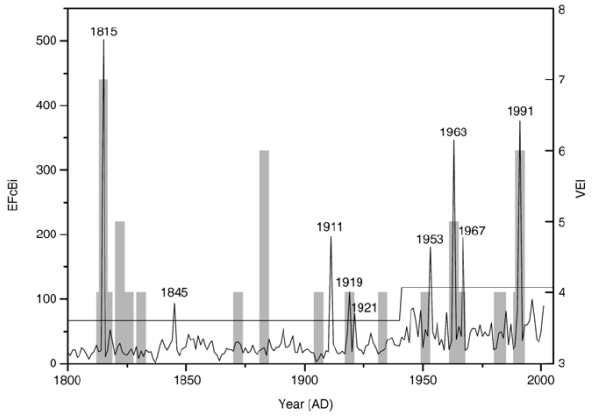

Fig 1.29. Comparison between EFc Bi in the Everest ice core and VEI of the volcanic events with VEI≥4 in regions 1 and 2 since AD 1800. The fine curve stands for EFc Bi, the horizontal line for the average-plus-2 times standard deviation (σ) before and after1940, and histogram for the VEI. (Xu et al., 2009c)

1.4.7 Changes in persistent organic pollutants

High mountains may serve as "cold traps" for persistent organic pollutants (POPs) and ice cores can provide long-term records of atmospheric deposition of pollutants. DDT, hexachlorocyclohexanes (HCHs)

and polycyclic aromatic hydrocarbons (PAHs) were analyzed and the deposition fluxes of these pollutants were investigated from the Everest ice core (Wang et al., 2008). Concentrations of total DDTs reached maxima of approximately 2 ng l^{-1} in mid-1970s, which is corresponding to the peak of malaria cases in India (in 1976) (Fig 1.30). The decrease of DDT concentration after 1990s was in-line with the ban of DDT in India (in 1989). High level of a-HCH was observed in early 1970s and it showed a decrease to undetecTable 1.level at the end of 1990s, which is in agreement with the period when India banned the usage of HCH (in 1997). Concentrations of total PAHs sharply increased after 1990 and the peak (approximately 100 ng l^{-1}) was found at the end of 1990s, when India entered the rapid industrialization (urbanization). PAHs in the ice core are dominantly pyrogenic in source, and are mainly from incomplete combustion of coal and biomass burning. Close correlations among concentrations of PAHs, nssSO_4^{2-} and microparticles in snow pit samples showed that the origin of the PAHs and nssSO_4^{2-} is often the same and they may be absorbed by particles and transported to high mountain regions by atmospheric circulation.

Concentrations of DDT and HCH in the Everest ice core were associated with the El Nino-Southern Oscillation. Decrease in the deposition flux of a-HCH from 1980 to 1990 appears inconsistent with its annual emission trend in neighboring country (India). Using the a-HCH annual India emission and the multivariate ENSO index (MEI) as the independent variables, and the logarithm of 5-year averaged deposition flux of a-HCH for 1970-1990 as the dependent variables, a multivariate regression model showed that the annual Indian emission and the MEI explain 62% of the deposition variance of a-HCH. Therefore, the stronger the Indian monsoon is, the higher the POPs concentrations will be. The weakening Indian Monsoon impacted by El Nino episode would abate the influence of continued increase of pollutants emission in India. This counteract is likely to cause the decreased concentration of DDT/a-HCH after 1976 (Wang et al., 2010). Concentrations of DDTs in Mt. Muztagata ice core tended to increase during the positive Siberia High phase that result in southwards incursion of cold air from the polar areas to the mid-latitude. These associations suggested that there are some linkages between climate variations and the global distribution of persistent organic pollutants (Wang et al., 2010).

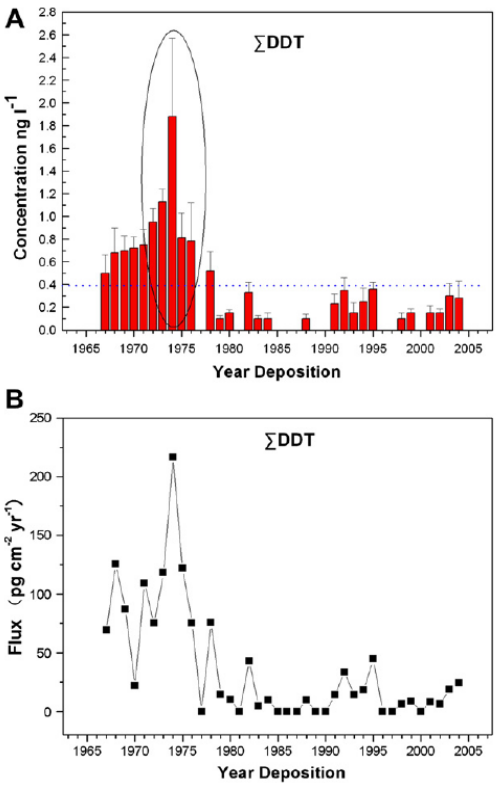

Fig 1.30. Concentration (A) and deposition flux (B) of DDT in the ice core from the Mt.Everest, The Himalayas). (Wang et al., 2008)

1.4.8 Microorganisms records

With rapid development of microbiology on extreme environment, many microorganisms have been found on ice cores around the world. The results of culturable bacteria preserved in the Everest ice core show that the average concentrations of culturable bacteria are 5.0, 0.8, 0.1 and 0.7 CFU mL^{-1} for the snow deposited during the pre-monsoon, monsoon, post-monsoon and winter seasons, respectively (Zhang et al., 2007c). The high concentration of culturable bacteria at Everest in the pre-monsoon season is attributed to the transportation of continental dust stirred up by the frequent dust storms during spring. This is also confirmed by the spatial distribution of culturable bacteria in Tibetan glaciers (Fig 1.31). Continental dust originated from the Northwest China accounts for the high abundance of culturable bacteria in the northern TP, whereas monsoon moisture exerts great influence on culturable bacteria with low abundance in the southern plateau. The numbers of representatives with different ARDRA patterns from RFLP analysis are 10, 15, 1 and 2 in the pre-monsoon, monsoon, post-monsoon and winter seasons, respectively, suggesting that culturable bacteria during monsoon season are more diverse compared to other seasons, possibly due to their derivation from both marine air masses and local or regional continental sources. The culturable bacteria deposited during the other seasons are from only one possible origin that is transported by westerlies (Liu et al., 2006, 2007; Zhang et al., 2007c).

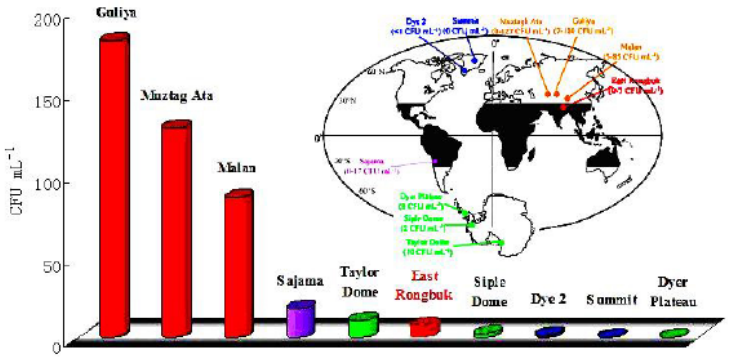

Fig 1.31. Concentration of culturable bacteria recovered from the Everest (red) compared with other Tibetan (orange), Sajama, Bolivia (purple), Arctic (blue) and Antarctic (green) ice cores. (Zhang et al., 2007c)

Bacterial diversity and cell abundance in the snow of the four glaciers (Guoqu, Zadang, East Rongbuk and Palong No. 4) located in different climatic zones of the TP were investigated through culture-independent molecular analysis of 16S rRNA gene clone library and flow cytometry approaches (Liu et al., 2009). Cell abundance ranged from 0.68×10^3 to 720×10^3 cells mL^{-1}, with higher values in the northern glaciers than in the southern ones. Most of them were more similar to those in the Antarctica compared to the Arctic and other high mountains. Cell abundance was related with the input dust concentration but did not show obvious correlation with the nutrient condition. Bacterial diversity was unexpectedly high in the snow habitats of the world's highest plateau. Bacterial 16S rRNA gene sequences were affiliated to 13 phyla and 82 genera. Among them, 15 common genera were distributed widely in glaciers located at different regions of the plateau, implying that the same selective mechanism occurs at plateau. Bacterial diversity in the snow at different glaciers was related to the surrounding environments. The Guoqu Glacier, to the north near the desert zone and with the lowest temperature, preserved more bacteria closely related to a cold environment and soil than the other glaciers. However, in the Palong No. 4 Glacier located in the south warm region around vegetation, most bacteria were phylogenetically related to plant-associated bacteria (Liu et al., 2009).

Main bacteria isolated from the Muztagata ice core was investigated by means of cultivation and 16S rRNA sequence analysis (Xiang et al., 2005a). The amount of culturable bacteria was more in dirty layer than in clean ice, which suggests the close corresponding relationship between high input of the bacteria deposited by wind and snowflow. Small subunit 16S rRNA sequences, growth temperatures, and phylogenetic relationships also have been established for 129 bacterial isolates recovered under aerobic growth conditions from different regions of the ice core (Xiang et al., 2005b). Only 11% were

psychrophiles (grew at 2°C or -2°C up to ~20°C), although the majority (82%) were psychrotolerant (grew at 2°C or -2°C up to 37°C). The majority of the isolates had 16S rRNA sequences similar to previously determined sequences, ranging from 85% to 100% identical to database sequences. Based on their 16S rRNA sequences, 42.6% of the isolates were high-G+C (HGC) gram-positive bacteria, 23.3% were γ-Proteobacteria, 14.7% were α-Proteobacteria, 14.7% were Flavobacteria, and 4.7% were low-G+C (LGC) gram-positive bacteria.

The microorganisms in the Malan ice core are identified as α, β, and γ-*Proteobacteia*, and the LGC, HGC, and CFB group by means of the results of 16S rRNA sequence analysis and physiological characteristics, while the eukaryotes in the ice core are mainly composed of *Chlamydomonas* sp. and *Pseudochlorella* sp. based on the phylogenetic examination of the 16S rRNA gene (Yao et al., 2006c). The microbial populations showed observable differences at different depths in the ice core, reflecting the effects of climatic and environmental changes on the distribution of the microorganisms in the glacier. Examination of the Malan ice core revealed four general periods of microbial concentration corresponding to four phases of temperature revealed by $\delta^{18}O$ values in the core. Observations also indicated that microorganism concentrations tend to be negatively correlated with the temperature at a relatively long timescale and, to some extent, positively correlated with mineral concentrations.

Seventy year history of annual bacterial abundances was retrieved from a Mt. Geladaindong ice core on the central TP (Yao et al., 2008). The bacterial abundance was lowest in 1938 and highest in 1997. Analyses of correlations between bacterial abundance and $\delta^{18}O$ and Ca^{2+} concentrations indicate that bacterial abundance correlates positively with both temperature and amount of dust transported onto the glacier (Fig 1.32). These correlations imply that both higher temperatures and more frequent dust deposition influence bacterial abundance in the Geladaindong ice core. Bacterial genetic diversity also changes seasonally, and the diversity during the monsoon season appears much higher than during the non-monsoon season. Bacterial sequences representing the monsoon season were related to bacteria originating from various environmental conditions, whereas the sequences representing the non-monsoon season were typically related to microorganisms coming from cold environments and soils. The Geladaindong ice core record suggests bacterial abundance as a potential indicator for paleoclimate and paleoenvironment reconstruction (Yao et al., 2008).

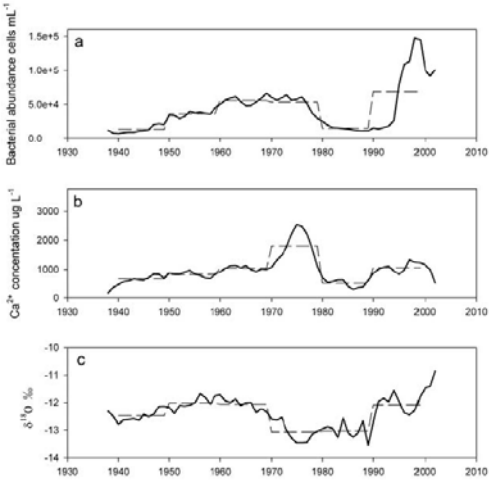

Fig 1.32. Annual variations and 10 year average values of (a) bacterial abundance, (b) Ca^{2+} concentration, and (c) $\delta^{18}O$ value in the Geladandong ice core from 1935 to 2004. Fine line represents annual values and coarse line the 10 year average values.

1.4.9 Air content in ice cores

Air bubbles trapped in ice is a source of abundant climate information and could be used for the reconstruction of regional and global climate change. Because the air content in ice is highly sensitive to the variation of physical character of ice and the transformation of ice formation zones (both induced by climate and environment changes), it also could provide a feasible means to reconstruct the regional and global paleo-climate evolution.

Two Everest ice cores displayed a large decrease of air content over the last two millennia from mean values ~0.050 cm^3/g to ~0.028 cm^3/g (Hou et al., 2007). Most of the decrease took place over the last 200-300 years. Air content decreased in parallel with a larger deviation around the mean value, which may reflect the thinning of annual layers with depth, as shallower samples partly depicts the seasonal variability of air content (Fig 1.33a) whereas the deepest samples integrates this variability through multi-annual depth resolution. The gas content profile (Fig 1.33b) thus suggests unprecedented warm summer temperatures at the altitude of the drill site for the 20th century (Hou et al., 2007).

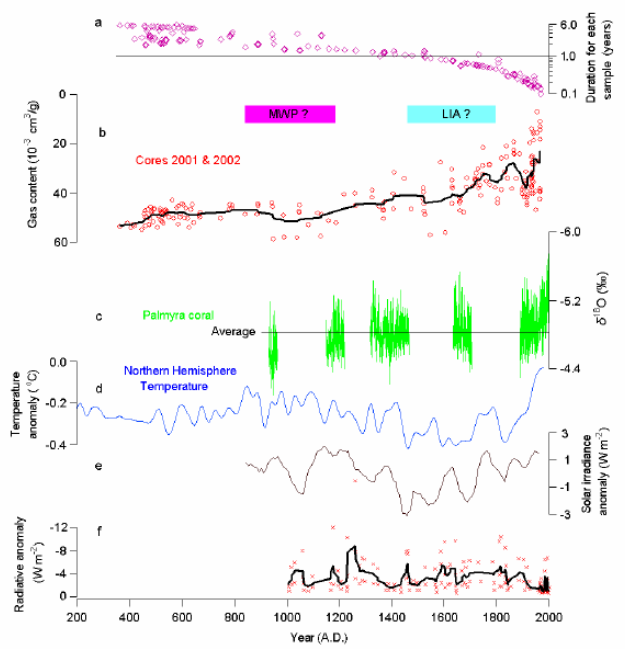

Fig 1.33. (a): Average age representativity of each sample; (b): Air content time series, with a binomial smoothing trend (thick black line). Note that the air content is plotted as a function of the age of ice, because in this case it is affected by surface processes. (c): The monthly resolved Palmyra coral $\delta^{18}O$ records. The black horizon represents the average of all the coral dataset. (d): Temperature reconstruction of North Hemisphere. (e) Reconstruction of solar irradiance anomalies. (f): Radiative forcing associated with volcanic eruptions recorded in ice core, with a binomial smoothing trend (thick black line). The approximate timing and duration of the "Little Ice Age" and the "Medieval Warm Period" are marked by horizontal bars. (Hou et al., 2007)

The ice core air content recovered from the refrozen-recrystallization ice formation zone in the Dasuopu Glacier was investigated, where the air content in ice showed significant fluctuations both in the seasonal and long-time series (Li et al., 2010). The air content was low in summer and high in winter, and fluctuated around the mean value of 0.05 cm^3/g ice from 1571 AD to 1927 AD. The correlation of the air content in ice with the climatic and environmental factors was discussed combining with the dating results. This result, over about 400 years, showed that the air content in ice was mainly dominated by the insolation intensity rather than the temperature and other environmental factors in the southern TP (Li et al., 2010).

1.5 CHANGES IN SNOW COVER OVER CHINA

Snow cover is one of the important components in cryosphere with widest distribution and distinct seasonal and interannual variability. Based on the available data set, the snow cover area lasting no less than 60 days in a year was originally estimated at 4.2×10^7 km^2 via in-situ measurements ending in 1970 or

1980 from 1600 ground-based meteorological stations in China. The application of passive microwave remote sensing data since 1979 increased the accuracy of snow cover monitoring. Based on the improved retrieval algorithm being suiTable 1.in China (Che et al., 2008), the more reliable estimation for the snow covered area is 3.4×10^7 km^2 in average (Li et al., 2008). Meanwhile, the annual mean snow depth in China is estimated at 4.1 cm with obvious discrepancies in spatial distribution, with a maximum value of 12.0 cm (Fig 1.34). When converting to snow water equivalent (SWE), according to a snow density of 0.16 g/cm^3, the annual mean SWE in China during 1978–2006 is estimated at 6.6 mm with a maximum of 19.2 mm spatially.

In the northwestern China, the distribution of snow depth varies with the altitude. The deepest snowpack occurs in Altai Mts., and then in Tianshan, Pamir, Karakoram and Kunlun Mts. (Xiao et al., 2007), and the accumulated snow depth is greatest in the southern Altai Mts. (Wang et al., 2009). The snow cover in Xinjiang Uygur Autonomous Region (briefly Xinjiang) usually begins in September and ends in the next May, reaching its maximum in February or March. The snow cover over Tianshan Mts. and Pamir lasts till June, sometimes extending to August (Zhang et al., 2008). In the northeastern China, the snow cover duration is usually seven months, from October to the next April, and only snow cover in the northern Greater Khingan Mts. can last till May with its maximum in February or March. Over the Tibetan Plateau (TP), the snow cover may occur in any month of a year, and the snow cover extent usually reaches its maximum and minimum in January and July, respectively. Analysis from ground-based measurements indicated that there are four main regions with deeper snow, namely, the middle part of the TP, the southeastern TP, the Himalayas, and the Pamir (Ma, 2008). The changes of snow cover over the TP are dominated by the snow cover in the southeastern TP.

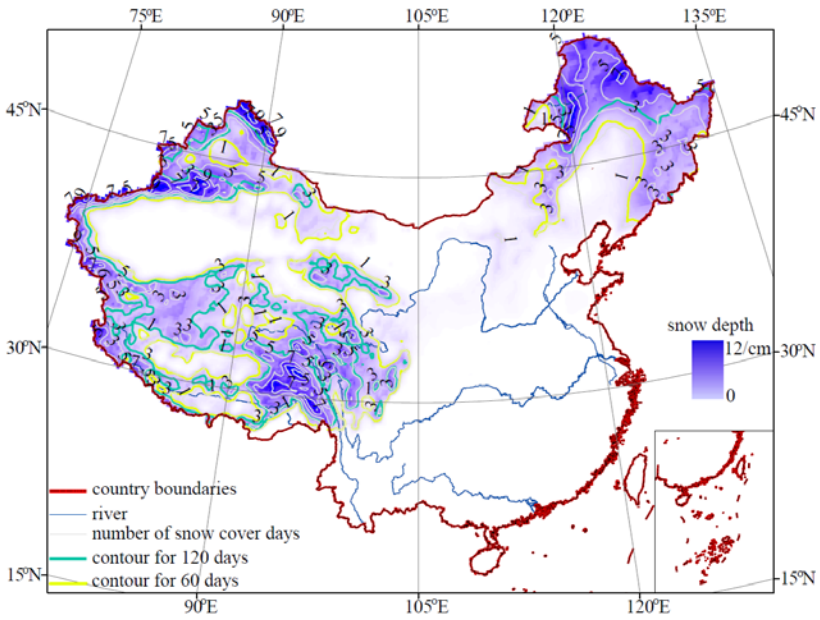

Fig 1.34. 1979–2006 annual mean snow depth and the number of snow cover days retrieved from SMMR and SSM/I remote sending data (Li et al., 2008).

The numbers within the Fig 1.denote snow depth.

There are generally three changing patterns for snow cover over China during 1961–2004 (Wang et al., 2009). Firstly, both snow depth and the number of snow cover days (SCD) exhibited increasing or decreasing trends. Secondly, snow depth increased slowly, but SCD decreased. Thirdly, snow depth decreased with an increase in SCD, which is opposite to the second pattern. By 2071–2100, except for an increasing winter mean SWE in a small fraction of China, such as the Greater Khingan Range, the eastern Tianshan Mts., and part of Qilian Mts. (Fig 1.35), the winter mean SWE over most of the northeastern and northwestern China and the TP will decrease under SRES A2 compared with that in 1961–1990 (Shi et al., 2010). The maximum SWE and the maximum continuous SCD in the southern China, especially in part of the eastern Jiangxi Province, will also increase due to the longer snowfall hours and greater snowfall intensities (Song, 2008).

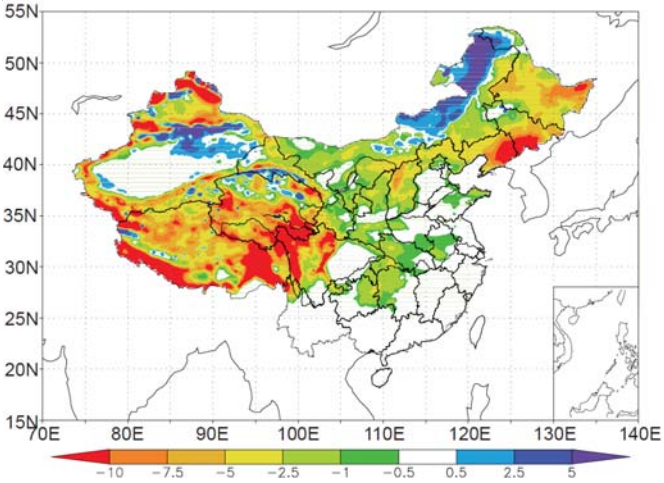

Fig 1.35. Differences of snow water equivalent over China in winter between 2071–2100 and 1961–1990 simulated by a high resolution RCM under SRES A2 (unit: mm) (Shi et al., 2010).

The time series for observed annual mean snow depth over the TP during 1958–2009, as shown in Fig 1.36, presents distinct fluctuations. The snow depth increased slowly before the end of 1990s, and the amplitude for interannual variation became greatest during 1980s and 1990s. However, the annual mean snow depth over the TP dropped down sharply after that period, and has always been low till the year 2009. Similarly, the snow covered area over the TP increased slightly during 1980s and 1990s (Qin et al., 2006), but decreased later until 2005 (Wang et al., 2007). The sensitivity of SCD to air temperature and the number of stations with “at-risk” snow over the TP will both increase with the warming climate (Ma et al., 2010a; 2010b). In the northern Xinjiang, observed maximum snow depth (MSD) from 20 meteorological stations showed significant increasing trend during 1961–2006, and the increasing amount for annual mean MSD was about 0.8%/a (Wang et al., 2009). The MSD over Tianshan Mts. also presented significant increasing trend during 1967–2000, and the corresponding rate was 1.43%/a (Gao et al., 2005). However, the increment of SCD in the northern Xinjiang mainly occurred between 1960s and 1980s, and the SCD decreased since 1990s (Wang et al., 2009). During 1961–2006, the observed beginning date of snow cover

delayed almost in all 32 stations in the northern Xinjiang. However, the ending date became advanced only in stations higher than 1000 m, but delayed in stations lower than 1000 m (Zhao et al., 2010). In the northeastern China, there is no significant change in the trend for snow depth, but the amplitude of fluctuation increased since 1990s (Qin et al., 2006). The regions with deeper snow, such as the Greater Khingan Mts., the Lesser Khingan Mts., and the Xilin Gol League, were the places that suffered greater seasonal and interannual variations (Xiao et al., 2007). During 1961–2006, the starting date and the ending date of snow cover in Heilongjiang province were delayed and advanced at rates of 1.9 d/10a and 1.6 d/10a, respectively, and the changes mainly occurred in the plain regions in lower latitude (Li et al., 2009a).

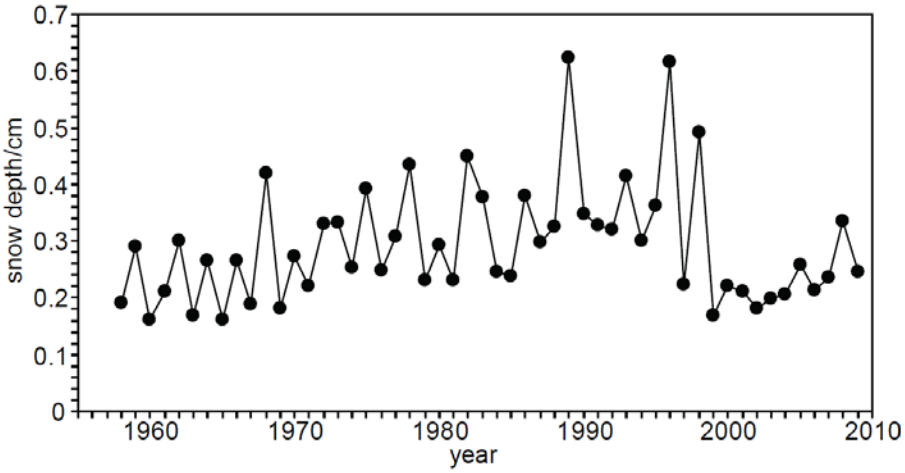

Fig 1.36. Variations of observed annual mean snow depth over the Qinghai-Tibetan Plateau during 1958–2009 (updated by Ma, 2008).

Snow cover over the TP is always considered as one of the important factors that affects the summer climate in the eastern China. The response of soil moisture to snow cover over the TP in the late spring and early summer was proved to be an important mechanism that snow cover acts on the summer climate (Zhao et al., 2007). Additionally, the snow cover over Eurasia also plays important role on the changes of summer rainfall in the eastern China. The leading mode of EOF showed that there was less SWE in most of Eurasia and more in parts of East Asia and the TP from 1970s to 1990s. This pattern is favorable to arouse wave train in higher latitude resulting in higher and lower pressure over North China and South China, respectively (Zhang et al., 2008). Correspondingly, the rainfall in the southern and southeastern China was more than normal, whereas the rainfall in the upper reaches of the Yellow River was less (Wu et al., 2009). Hereinto, the albedo effect and the soil moisture effect of Eurasian snow cover on climate are proved to be more important in spring and summer, respectively (Li et al., 2009b). Therefore, the rain belt pattern shifting to “flood in the South and arid in the North” since 1980s is closely related to both the increasing over the TP and the decreasing of snow cover in most of Eurasia.

Additionally, the advancing of snowmelt runoff process and the extending of snow melting period in the mountain areas of the northwestern China in spring have changed the seasonal distribution of water

resources. The runoff in spring was increasing inversely in some rivers although their corresponding annual total runoff was decreasing (Wang and Li, 2005), and the increasing amount was determined by the recharge rate of the melting snow. For Kelan River in Xinjiang, the total monthly runoff increased about 15% during 1958–2005. The proportion of runoff in snow melting season, from April to June, vs. annual total runoff increased from 60% to 70%, and the maximum runoff shifted one month ahead, from June to May (Shen et al., 2007). In the reaches of Heihe River, the increased snowmelt runoff enhanced the monthly runoff from March to July significantly in 1981–2000 (Wang and Li, 2005). Moreover, the increasing runoff in spring also increased the risk of spring flood disaster. The measured annual maximum peak flow in Kelan River was around 200 m^3/s during 1970s–1980s, and increased to 350 m^3/s since 1990s (Shen et al., 2007).

Snow disasters of different degrees occur in China every year, and the heavy snow disasters in some mountain areas, such as Tanggula, Bayan Har, Himalaya, and Altai Mts., are estimated to be intensified by 2050 (Ding and Pan, 2005). The enhancement of human activities, especially the severe overgrazing in pastures, is one of the main reasons that snow disasters increased continually (Liu et al., 2008).

References

1) Cai Dihua, Ma Jinhui, Nian Yanyun, Liu Shiyin, Shangguan Donghui. The study of glacier change using remote sensing in Mt.Muztagta. 2006. *Journal of Lanzhou University (Natural Sciences)*. 42(1):13-17. (In Chinese with English abstract)
2) Caidong Caidong, Sorteberg Asgeir, 2010. Modeled mass balance of Xibu glacier, Tibetan Plateau: sensitivity to climate change. *Journal of Glaciology,* 56: 235-248.
3) Cao Bo, Pan Baotian, Gao Hongshan, Jiang Shaofei, Wen Yuhua, Shangguan Donghui. 2010. Glacier Variation in the Lenglongling Range of Eastern Qilian Mountains from 1972 to 2007. *Journal of Glaciology and Geocryology*, 32(2):242-248. (In Chinese with English abstract)
4) Che Tao, Li Xin, Jin Rui, Armstrong R, Zhang Tingjun. 2008. Snow depth derived from passive microwave remote sensing data in China. *Annals of Glaciology*, 49 (1): 145–154, doi: 10.3189/172756408787814690.
5) Che Tao, Li Xin, P K Mool, Xu Jianchu. 2005. Monitoring Glaciers and Associated Glacial Lakes on the East Slopes of Mount Xixabangma from Remote Sensing Images. *Journal of Glaciology and Geocryology*, 27(6):801-805. (In Chinese with English abstract)
6) Chen Feng, Kang Shichang, Zhang Yongjun, You Qinglong. 2009. Glaciers and Lake Change in Response to Climate Change in theNam Co Basin, Tibet. *Journal of Mountain Science*, 27(6):641-647. (In Chinese with English abstract)
7) Chen Gongbi. 2005. Rapid onset flood disaster due to glacier-dammed lake in Alpine Area, Xinjiang Province, Western China. *Journal of Catastrophology*, 20(1):45-49.
8) Chen Xiaoqing, Cui Peng, Yang Zhong, and Qi Yong-qing. 2007. Risk Assessment of Glacial Lake Outburst in the Poiqu River Basin of Tibet Autonomous Region. *Journal of glaciology and geocryology*, 29(4):509-516.
9) Chen Xiaoqing, Cui Peng, Yang Zhon, Qi Yongqing. 2005. Change in Glaciers and Glacier Lakes in Boiqu River Basin, Middle Himalayas during Last 15 Years. *Journal of Glaciology and Geocryology*, 27(6):793-800. (In Chinese with English abstract)
10) Ding Yongjian, Pan Jiahua. 2005. Assessment of the impact of climate and environmental changes on ecosystem and social economy. In: Qin Dahe, Chen Yiyu, Li Xueyong [eds]. Assessment of Climate and Environment Changes in China (II): Measures to adapt and mitigate the effects of climate and environment changes. Beijing: Science Press 92–159. (In Chinese with English abstract)
11) Du Wentao, Qin Xiang, Liu Yushuo, Wang Xufeng. Variation of the Laohugou Glacier No.12 in the Qilian Mountains. *Journal of Glaciology and Geocryology*, 2008, 30(3):373-379. (In Chinese with English abstract)
12) Gao Weidong, Wei Wenshou, Zhang Xuli. 2005. Climate Changes and Seasonal Snow Cover Variability in the Western Tianshan Mountains, Xinjiang in 1967-2000. *Journal of Glaciology and Geocryology*, 27 (1): 68–73. (In Chinese with English abstract)
13) Gao Xin, Ye Baishen, Zhang Shiqiang, Qiao Chengjun, Zhang Xiaowen. 2010. The Variation of Quantity of Glacier melting water in Tarlimu watershed and impact on discharge during 1961 to 2006.*Chinese Science*, 40(5): 654-665. (In Chinese)
14) Gao Xin, Zhang Shiqiang, Ye Baisheng, Qiao Chengjun. 2010. Glacier Runoff Change in the Upper Stream of Yarkant River and Its Impact on River Runoff during 1961—2006. *Journal of Glaciology and Geocryology*, 32(3):445-453. (In Chinese with English abstract)
15) Han Tianding, Ding Yongjian, Ye Bbaisheng, Liu Shiyin, and Jiao Keqin, 2006. Mass-balance characteristics of Urumqi glacier No. 1, Tien Shan, China. *Annals Of Glaciology,* 43: 323-328.
16) Hou Shugui, Chappellaz J, Jouzel J, et al., 2007. Summer temperature trend over the past two millennia using air content in Himalayan ice. *Climate of the Past*, 3: 89-95.
17) Hou Shugui, Li Yuansheng, Xiao Cunde, Pang Hongxi, Xu Jianzhong. 2009. Preliminary results of the close-off depth and the sTable 1.isotopic records along a 109.91m ice core from Dome A, Antarctica. *Science in China (Series D: Earth Sciences)*, 52(10): 1502-1509, doi: 10.1007/s11430-009 -0039-6.
18) Jiang Xi, Wang Ninglian, He Jianqiao, Wu Xiaobo, and Song Gaoju, 2010. A distributed surface energy and mass balance model and its application to a mountain glacier in China. *Chinese Science Bulletin,* 55: 2079-2087.

19) Jiao Keqin, Jin Zhefan, Cheng Peng, Han Tianding, Liu Shengmei. 2009. Monitoring results on the Glacier No. 51 at Haxilegen in the Kuytun River Basin, Tianshan Mountains. *Arid Land Geography*, 32(5):733-738. (In Chinese with English abstract)
20) Jing Zhefan, Jiao Keqin, Yao Tandong, Wang Ninglian, and Li Zhen, 2006. Mass balance and recession of Urumqi glacier No. 1, Tien Shan, China, over the last 45 years. *Annals Of Glaciology,* 43: 214-217.
21) Kang Shichang, Chen Feng, Ye Qinghua, Jing Zhefan, Qin Dahe, Ren Jiawen. 2007. Glacier Retreating Dramatically on the Mt.Nyainqêntanglha during the Last 40 Years. *Journal of Glaciology and Geocryology*, 29(6):869-873. (In Chinese with English abstract)
22) Kang Shichang, Qin Dahe, Ren Jiawen, Zhang Yongjun, Susan Kapspari, Paul A. Mayewski, Hou Shugui. 2007b. Annual accumulation in the Mt. Nyainqentanglha ice core, southern Tibetan Plateau, China: relationships to atmospheric circulation over Asia. *Arctic, Antarctic, and Alpine Research*, 39(4).
23) Kang Shichang, Zhang Qianggong, S. Kaspari, Qin Dahe, Cong Zhiyuan, Ren Jiawen, P. A. Mayewski. 2007c. Spatial and seasonal variations of elemental composition in Mt. Everest (Qomolangma) snow/firn. *Atmospheric Environment*, 41(34): 7208-7218. DOI: 10.1016 /j.atmosenv.2007.05.024.
24) Kang Shichang, Zhang Yongjun, Qin Dahe, Ren Jiawen, Zhang Qianggong, Bjorn Grigholm, Paul A. Mayewski. 2007a. Recent temperature increase recorded in an ice core in the source region of Yangtze River. *Chinese Science Bulletin*, 52(6): 825-831.
25) Kang Shichang, Zhang Yulan, Zhang Yongjun, Bjorn Grigholm, Susan Kaspari, Qin Dahe, Ren Jiawen, Paul Mayewski. 2010. Variability of atmospheric dust loading over the central Tibetan Plateau based on ice core glaciochemistry. *Atmospheric Environment*, 44: 2980-2989.
26) Kang Shichang., P. A. Mayewski, Qin Dahe, S. A. Sneed, Ren Jiawen, Zhang Dongqi. 2004. Seasonal differences in snow chemistry from the vicinity of Mt. Everest, central Himalayas. *Atmospheric Environment*, 38(18): 2819-2829.
27) Kaspari Susan, Hooke Roger Leb, Mayewski Paul Andrew, Kang Shichang, Hou Shugui, Qin Dahe, 2008. Snow accumulation rate on Qomooangma (Mt.Everest), Himalaya: synchroneity with sites across the Tibetan Plateau on 50-100 year timescales. *Journal of Glaciology*, 54(185): 343-352.
28) Kaspari Susan, Mayewski Paul Andrew, Handley Michael, Kang Shichang, Hou Shugui, Sneed Sharon, Qin Dahe. 2009b. A high-resolution record of atmospheric dust composition and variability since AD 1650 from a Mount Everest ice core. *Journal of Climate*, 22: 3910-3925.
29) Kaspari Susan, Mayewski Paul Andrew, Handley Michael, Osterberg Erich, Kang Shichang, Sneed Sharon, Hou Shugui, Qin Dahe. 2009a. Recent increases in atmospheric concentrations of Bi, U, Cs, S and Ca from a 350-year Mount Everest ice core record. *Journal of Geophysical Research*, 114(D04302), doi: 10.1029/2008JD011088.
30) Kaspari Susan, Mayewski Paul Andrew, Kang Shichang. 2007. Reduction in northward incursions of the South Asian monsoon since ~1400 AD inferred from a Mt.Everest ice core. *Geophysical Research Letters*, 34(L16701), doi: 10.1029/2007GL030440.
31) Li Deping, Wang Liping, Liu Shiyin, Xie Zichu, Ding Liangfu, Wu Lizong. 20090 Tupu Analysis of the Spatio-Temporal Glacier Variations in the Central and Western Qangtang Plateau since the Little Ice Age. *Journal of Glaciology and Geocryology*, 32(1): 40-47. (In Chinese with English abstract)
32) Li Dongliang, Liu Yulian, Yu Hongmin, Li Yongsheng. 2009a. Spatial-temporal Variation of the Snow Cover in Heilongjiang Province in 1951-2006. *Journal of Glaciology and Geocryology*, 31 (6): 1011–1018. (In Chinese with English abstract)
33) Li Jiule, Xu Baiqing, Chappellaz J. 2010. Variations of air content in Dasuopu ice core from AD 1570-1927 and implications fore climate change. *Quaternary International*, doi: 10.1016/j.quaint.2010.05.026.
34) Li Xin, Cheng Guodong, Jin Huijun, Kang Ersi, Che Tao, Jin Rui, Wu Lizong, Nan Zhuotong, Wang Jian, Shen Yongping. 2008. Cryospheric change in China. *Global and Planetary Change*, 62 (3–4): 210–218, doi: 10.1016/j.gloplacha.2008.02.001
35) Li Xin, Cheng Guodong, Jin Huijun, Kang Ersi, Che Tao, Jin Rui, Wu Lizong, Nan Zhuotong, Wang Jian, Shen Yongping. 2008. Cryospheric change in China. *Global and Planetary Change*, 62:210-218.
36) Li Zhen, Yao Tandong, Tian Lide, et al., 2006. Atmospheric Pb variations in Central Asia since 1955 from Muztagata ice core record, eastern Pamirs. *Chinese Science Bulletin*, 51(16): 1996-2000.
37) Li Zhenkun, Wu Bingyi, Zhu Weijun. 2009b. Numerical Simulation on Effect of Spring Eurasian Snow Cover on Summer Rainfall in China. *Advances in Climate Change Research*, 5 (4): 196–201. (In Chinese with English abstract)
38) Li Zhiguo, Yao Tandong, Ye Qinhua, Tian Lide, Wang Weicai. 2010. Glaciers in the Upstream Manla Reservoir in the Nianchu River Basin, Tibet: Shrinkage and Impact. *Journal of Glaciology and Geocryology*, 32(4):650-658. (In Chinese with English abstract)
39) Li Zhongqin, Shen Yongping, Wang Feiteng, Li Huilin, Dong Zhiwen, Wang Wenbin, Wang Lin. 2007a. Response of Glacier Melting to Climate Change—Take rümqi Glacier No. 1 as an Example. *Journal of Glaciology and Geocryology*, 29(3):333-342. (In Chinese with English abstract)
40) Li Zhongqin, Shen Yongping, Wang Feiteng, Li Huilin, Dong Zhiwen, Wang Wenbin, and Wang Lin, 2007. Response of Glacier Melting to Climate Change—Take Urumqi Glacier No. 1 as an Example. *Journal of Glaciology and Geocryology*, 29: 333-342. (in Chinese with English abstract)
41) Li Zhongqin, Wang Feiteng, Zhu Guocai, Li Huilin. 2007b. Basic Features of the Miaoergou Flat-Topped Glacier in East Tianshan Mountains and Its Thickness Change over the Past 24 Years. *Journal of Glaciology and Geocryology*, 29(1):61-65. (In Chinese with English abstract)
42) Li Zongxing, He Yuanqing, Jia Wenxiong, Pang Hongxi, He Xianzhong, Wang Shijin, Zhang Ningning, Zhang Wenjing, Liu Qiao, Xin Huijuan. 2009. Changes in Hailuogou Glacier during the Recent 100 Years under Global Warming. *Journal of Glaciology and Geocryology*, 31(1):75-81. (In Chinese with English abstract)
43) Liu Jingjing, Cheng Zunlan, Li Yong, and Su Pengcheng. 2008. Characteristics of Glacier-Lake Breaks in Tibet. *Journal of Catastrophology*, 23(1):55-60.
44) Liu Shiyin, Ding Yongjian, Li Jing, Shangguan Donghui, and Zhang Yong, 2006. Glaciers in response to recent climate warming in western China. *Quaternary Sciences,* 26: 762-771 (in Chinese with English abstract).
45) Liu Shiyin, Ding Yongjian, Zhang Yong, Shangguan Donghui, Li Jing, Han Haidong, Wang Jian, Xie Changwei. 2006. Impact of the Glacial Change on Water Resources in the Tarim River Basin. *Acta Geographica Sinica*, 61(5):482-490.
46) Liu Shiyin, DingYongjian, Li Jing, Shangguan Donghui, ZhangYong. 2006. Glaciers in Response to Recent Climate Warming in Western China. *Quaternary Sciences*, 26(5):762-761. (In Chinese with English abstract)

47) Liu Shiyin, Shangguan Donghui, Ding Yongjian, Han Haidong, Zhang Yong , Wang Jian, Xie Changwei, Ding Liangf u, Li Gang. 2005. Glacier Variations since the Early 20th Century in the Gangrigabu Range, Southeast Tibetan Plateau. *Journal of Glaciology and Geocryology*, 27(1):55-63. (In Chinese with English abstract)
48) Liu Shiyin, Shangguan Donghui, Ding Yongjian, Han Haidong, Zhang Yong, Wang Jian, Xie Changwei, Ding Liangfu, Li Gang. 2005. Glacier Variations since the Early 20th Century in the Gangrigabu Range,Southeast Tibetan Plateau. *Journal of Glaciology and Geocryology*, 27(1), 55-63. (In Chinese with English abstract)
49) Liu Xingyuan, Liang Tiangang, Guo Zhenggang, Zhang Xuetong. 2008. Early warning and risk assessment of snow disaster in pastoral area of northern Xinjiang. *Chinese Journal of Applied Ecology*, 19 (1): 133–138. (In Chinese with English abstract)
50) Liu Yaping, Geng Zhixin, Hou Shugui. 2010. Spatial and seasonal variation of major ions in Himalayan snow and ice: a source consideration. *Journal of Asian Earth Sciences*, 37: 195-205.
51) Liu Yongqin, Yao Tandong, Jiao Nainzhi, Kang Shichang. 2009. Bacterial Diversity in Snow at Different Glaciers over the Tibetan Plateau. *Extremophiles*, 13(3): 411-423. Doi: 10.1007/s00792-009-0227-5.
52) Liu Yongqin, Yao Tandong, Jiao Nianzhi, Kang Shichang, Zeng Yonghui, Liu Xiaobo. 2009. Abundance and diversity of snow bacteria in two glaciers at the Tibetan Plateau. *Frontiers of Earth Science in China*, 3(1): 80-90. Doi: 10.1007/s11707-009-0016-6.
53) Liu Yongqin, Yao Tandong, Kang Shichang, Jiao Nianzhi, Zeng Yonghui, Huang Sijun, Luo Tingwei. 2007. Microbial community structure in major habitats above 6000 m on Mount Everest. *Chinese Science Bulletin*, 52(17): 2350-2357.
54) Liu Yongqin, Yao Tandong, Kang Shichang, Jiao Nianzhi, Zeng Yonghui, Shi Yang, Luo Tingwei, Jing Zhefan, Huang Sijun. 2006. Seasonal variation of snow microbial community structure in the East Rongbuk glacier, Mt. Everest. *Chinese Science Bulletin*, 51(12): 1476-1486. DOI: 10.1007/s11434-006-1476-7.
55) Lu Anxin, Wang Lihong, and YAO Tandong. 2006. The study of Yamzho lake and Chencuo lake variation using remote sensing in Tibet Plateau from 1970 to 2000. *Remote sensing technology and application*, 21(3):173-177.
56) Ma Lijuan, Qin Dahe, Bian Lingen, Xiao Cunde, Luo Yong. 2010a. Analysis of Air Temperature Sensitivity of Snow Cover Days on the Qinghai-Tibetan Plateau. *Advances in Climate Change Research*, 6 (1): 1–7.
57) Ma Lijuan, Qin Dahe, Bian Lingen, Xiao Cunde, Luo Yong. 2010b. Assessment of Snow Cover Vulnerability on the Qinghai-Tibetan Plateau. *Advances in Climate Change Research*, 6 (5): 325–331.
58) Ma Lijuan. 2008. The temporal-spatial characteristics of changes in snow cover over the Qinghai-Tibetan Plateau in the recent 50 years and its relationship with atmospheric circulation factors. Chinese Academy of Meteorological Sciences/Graduate University of Chinese Academy of Sciences, Beijing. (In Chinese with English abstract)
59) Ma Linglong, Tian Lide, Pu Jianchen, Wang Pengling. 2010. Recent Area and Ice Volume Change of Kangwure Glacier in the Middle of Himalayas. *Chinese Science Bulletin*, 55(18):1766-1774. (In Chinese)
60) Ming Jing, Cachier H, Xiao Cunde, Qin Dahe, Kang Shichang, Hou Shugui, Xu Jianzhong. 2008. Black carbon record based on a shallow Himalayan ice core and its climatic implications. *Atmospheric Chemistry and Physics*, 8: 1343-1352.
61) Nie Yong, Zhang Yili, Liu Linshan, Zhang Jiping. 2010. Glacial change in the vicinity of Mt.Qomolangma(Everest), central high Himalayas since 1976. *Journal of Geography Science*, 20(5):667-686.
62) Pang Hongxi, He Yuanqing, Zhang Ningning. 2007. Accelerating glacier retreat on Yulong mountain, Tibetan Plateau, since the late 1990s. *Journal of Glaciology*, 53(181): 317-319.
63) Pu Jianchen, Yao Tandong, Duan Keqin, SAKAI A, FUJITA K, and MATSUDA Y, 2005. Mass balance of the Qiyi Glacier in the Qilian Mountains: A New Observation. *Journal of Glaciology and Geocryology,* 27: 199-204. (in Chinese with English abstract).
64) Pu Jianchen, Yao Tandong, Duan Keqin, Sakai Akiko, Fujita Koji, Matsuda Yoshihiro. 2005. Mass Balance of the Qiyi Glacier in the Qilian Mountains: A New Observation. *Journal of Glaciology and Geocryology*, 27(2):199-204. (In Chinese with English abstract)
65) Pu Jianchen, Yao Tandong, Tian Lide. 2006. Change of the Gurenhekou Glacier in Yangbajain Area, Nyainqêntanglha Range. *Journal of Glaciology and Geocryology*, 28(6):861-864. (In Chinese with English abstract)
66) Pu Jianchen, Yao Tandong, Yang Meixue, Tian Lide, Wang Ninglian, Ageta Y, and Fujita K, 2008. Rapid decrease of mass balance observed in the Xiao (Lesser) Dongkemadi Glacier, in the central Tibetan Plateau. *Hydrological Processes,* 22: 2953-2958.
67) Pu Jianchen, Yao Tandong, Yang Meixue, Tian Lide, Wang Ninlian, Yutaka Ageta and Koji Fujita. 2008. Rapid decrease of mass balance observed in the Xiao (Lesser)Dongkemadi Glacier, in the central Tibetan Plateau. *Hydrology Process*. (22):2953-2958.
68) Qin Dahe, Liu Shiyin, Li Peiji. 2006. Snow Cover Distribution, Variability and Response to Climate Change in Western China. *Journal of Climate*, 19 (9): 1820–1833, doi: 10.1175/JCLI 3694.1.
69) Qin Dahe. Climate and Environmental Changes in China [M].Beijing: Science Press, 2006. (in Chinese)
70) Shangguan Donghui, Liu Shiyin, Ding Lian-fu, Zhang Shiqiang, Li Gang, Zhang Yong, Li Jing. 2008. Variation of Glaciers in the Western Nyainqêntanglha Range of Tibetan Plateau during 1970-2000. *Journal of Glaciology and Geocryology*, 30(2):204-210. (In Chinese with English abstract)
71) Shangguan Donghui, Liu Shiyin, Ding Yongjian, Ding Lianfu, Xu Junli, Li Jing. 2009. Glacier changes during the last forty years in the Tarim Interior River basin, northwest China. *Progress in Natural Science*, 19, 727-732.
72) Shen Yongping, Wang Guoya, Su Hongchao, Han Ping, Gao Qianzhao, Wang Shunde. 2007. Hydrological Processes Responding to Climate Warming in the Upper Reaches of Kelan River Basin with Snow-dominated of the Altay Mountains Region, Xinjiang, China. *Journal of Glaciology and Geocryology*, 29 (6): 845–853. (In Chinese with English abstract)
73) Shi Ying, Gao Xuejie, Wu Jia, Giorgi F, Dong Wenjie. 2010. Simulation of the Changes in Snow Cover over China under Global Warming by a High Resolution RCM. *Journal of Glaciology and Geocryology*, 32 (2): 215–222. (In Chinese with English abstract)
74) Song Ruiyan, Gao Xuejie, Shi Ying, Zhang Dongfeng, Zhang Xiwa. 2008. Simulation of Changes in Cold Events in Southern China under Global Warming. *Advances in Climate Change Research*, 4 (6): 352–356. (In Chinese with English abstract)
75) Khromova, T.E. G.B. Osipova, D.G. Tsvetkov, M.B. Dyurgerov, R.G. Barry. 2006. Changes in glacier extent in the eastern Pamir, Central Asia, determined from historical data and ASTER imagery. *Remote Sensing of Environment*, 102: 24-32.
76) Thompson LG, Yao Tandong, Davis ME, Mosley Thompson Ellen, Mashiotta Tracy A., Lin Pingnan, Mikhalenko Vladimir N., Zagorodnov Victor S., 2006. Holocene climate variability archived in the Puruogangri ice cap on the central Tibetan Plateau.

Annals of Glaciology, 43: 61-69.
77) Tian Lide, Yao Tandong, Li Zhen, Kenneth Macclune, Wu Guangjian, Xu Baiqing, Li Yuefang, Lu Anxin, Shen Yongping. 2006. Recent rapid warming trend revealed from the isotopic recorded in Muztagata ice core, eastern Pamirs. *Journal of Geophysical Research*, 111(D13103), doi: 10.1029/2005JD006249.
78) Tie Yongbo, Tang Chuan. 2009. Progress in glacier lake outburst assessment system. *Advances in water science*, 20(3):448-452.
79) Wang Chenghai, Wang Zhilan, Cui Yang. 2009. Snow Cover of China during the Last 40 Years: Spatial Distribution and Interannual Variation. *Journal of Glaciology and Geocryology*, 31 (2): 301–310. (In Chinese with English abstract)
80) Wang Jian, Li Shuo. 2005. Impact of climate change on snowmelt runoff in the arid region in inland China. *Science in China (Series D)-Earth Sciences,* 35 (7): 664–670. (In Chinese with English abstract)
81) Wang Lihong, Zhao Jie, Lu An-xin, Zhang Chunwen, and Zhang Huawei. 2008. The study of lake variation using remote sensing near S301 highway in Tibetan Plateau from 1970 to 2000. *Remote sensing technology and application*, 23(6):658-661.
82) Wang Ninglian, He Jianqiao, Jiang Xi, Song Gaoju, Pu Jianchen, Wu Xiaobo, and Chen Lin, 2009. Study on the Zone of Maximum Precipitation in the North Slope of the Central Qilian Mountains. *Journal of Glaciology and Geocryology,* 31: 395-403. (in Chinese with English abstract).
83) Wang Ninglian, He Jianqiao, Pu Jianchen, Jiang Xi, and Jing Zhefan, 2010. Variations in equilibrium line altitude of the Qiyi Glacier, Qilian Mountains, over the past 50 years. *Chinese Science Bulletin,* 55, doi: 10.1007/s11434-010-0000-2.
84) Wang Ninglian, Jing Zhefan, Jiao Keqin, Mikhalenko V, Li Zhen, Han Tianding, and Yang Huian, 2007. Variations of the Glacier No. 1 at the source of the Urumqi River, Tien Shan Mts., China, during the past 40 years. *Data of Glaciological Studies,* 102: 48-53.
85) Wang Ninglian, Liu Shiyin, 1997. Summer Temperature rise quantified from the change of the Glacier No.1 at the source of Urumqi River in the 20th century *Journal of Glaciology and Geocryology,* 19: 207-213. (in Chinese with English abstract).
86) Wang Ninglian, Thompson LG, Davis ME. 2006c. Variations of atmospheric dust loading in the southern and northern Tibetan Plateau over the last millennium recorded in ice cores. *Quaternary Sciences*, 26(5): 752-761.
87) Wang Ninglian, Yao Tandong, 1996. Study of the steady-state response of a glacier to climatic change. *Cryosphere,* 2: 67-74.
88) Wang Ninglian, Yao Tandong, and Pu Jianchen, 1996. Climate sensitivity of the Xiao Dongkemadi Glacier in the Tanggula Pass. *Cryosphere,* 2: 63-66.
89) Wang Ninglian, Yao Tandong, Pu Jianchen, Zhang Yongliang, Sun Weizhen. 2006. Climatic and environmental changes over the last millennium recorded in the Malan ice core from the northern Tibetan Plateau. *Science in China (Series D Earth Sciences)*, 49(10): 1079-1089.
90) Wang Ninglian, Yao Tandong, Thompson LG, Davis ME. 2006b. Strong negative correlation between dust event frequency and air temperature over the northern Tibetan Plateau reflected by the Malan ice cire record. *Annals of Glaciology*, 43: 29-33.
91) Wang Ninglian，Zhang Xiangsong. 1992. Mountain Glacier Fluctuations and Climatic Change During the Last 100 Years. *Journal of Glaciology and Geocryology*, 14(3):242-250. (In Chinese with English abstract)
92) Wang Ninglian. 2005. Decrease trend of dust event frequency over the past 200 years recorded in the Malan ice core from the northern Tibetan Plateau. *Chinese Science Bulletin*, 50(24): 2866-2871.
93) Wang Qiuxiang, Zhang Chunliang, Liu Jing, Liu Weiping. 2009. The Changing Tendency on the Depth and Days of Snow Cover in Northern Xinjiang. *Advances in Climate Change Research*, 5 (1): 39–43. (In Chinese with English abstract)
94) Wang Xiaoping, Gong Ping, Zhang Qianggong, et al., 2010. Impact of climate fluctuations on deposition of DDT and hexach; orocyclohexane in mountain glaciers: evidence from ice core records. *Environmental Pollution*, 158: 375-380.
95) Wang Xiaoping, Xu Baiqing, Kang Shichang, Cong Zhiyuan Yao Tandong. 2008. The historical residue trends of DDT, hexachlorocyclohevanes and polycyclic aromatic hydrocarbons in an ice core from Mt. Everest, central Himalayas, China. *Atmospheric Environment*, 42: 6699-6709.
96) Wang Xin, Liu Shinyin, Guo Wanqin, Yu Pengchun, and Xu Junli. 2009. Hazard assessment of moraine-dammed lake outburst floods in the Himalayas, China. *ACTA Geographica Sinica*. 64(7):782-790.
97) Wang Xin, Liu Shinyin, Yao Xiaojun, Guo Wanqin, Yu Pengchun, and Xu Junli. 2010. Glacier lake investigation and inventory in the Chinese Himalayas based on the remote sensing data. *ACTA Geographica Sinica*. 65(1):29-36.
98) Wang Yetang, He Yong, Hou Shugui. 2007. Analysis of the Temporal and Spatial Variations of Snow Cover over the Tibetan Plateau Based on MODIS. *Journal of Glaciology and Geocryology*, 29 (6): 855–861. (In Chinese with English abstract)
99) Wang Yetang, Hou Shugui, Lu Anxi, Liu Yaping. 2008. Response of glacier variations in the eastern Tianshan Mountains to climate change, during the last 40 years. *Arid Land Geography*, 31(6):813-821. (In Chinese with English abstract)
100) Wang Yiting, Chen Xiuwan, Bo Yanchen, Li Xinliang. 2010. Monitoring Glacier Volume Change Based on Multi-Source DEM and Multi-Temporal Remote Sensing Images. *Journal of Glaciology and Geocryology*, 32(1):126-132. (In Chinese with English abstract)
101) Wu Bingyi, Yang Kun, Zhang Renhe. 2009. Eurasian snow cover variability and its association with summer rainfall in China. *Advance of Atmospheric Science*, 26 (1): 31–44, doi: 10.1007/s00 376-009-0031-2.
102) Wu Guangjian, Yao Tandong, Xu Baiqing, Tian Lide, Li Zhen, Duan Keqin. 2008. Seasonal variations of dust record in the Muztagata ice cores. *Chinese Science Bulletin*, 53(16): 2506-2512.
103) Wu Guangjian, Zhang Chenglong, Gao Shaopeng, Yao Tandong ,Tian Lide, Xia Dunsheng. 2009. Element composition of dust from a shallow Dunde ice core, Northern China. *Global and Planetary Change*, 67: 186-192.
104) Wu Yanhong, Zhu Liping, Ye Qinghua, Wang Liben. 2007. The Response of Lake-Glacier Area Change to Climate Variations in Namco Basin,Central Tibetan Plateau,during the Last Three Decades. *Acta Geographica Sinica*, 62(3):301-311.
105) Xiang Shurong, Yao Tandong, An lizhe, Wu Guangjian, Xu Baiqing, Ma Xiaojun, Li Zhen, Wang Junxia, Yu Wusheng. 2005a. Vertical quantitative and dominant population distribution of the bacteria isolated from the Muztagata ice core. *Science in China (Series D-Earth Science)*, 48(10): 1728-1739.
106) Xiang Shurong, Yao Tandong, An lizhe, Xu Bingliang, Wang Junxia. 2005b. 16S rRNA sequence and differences in bacteria isolated from the Muztag Ata glacier at increasing depths. *Applied and Environmental Microbiology*, 71(8): 4619-4627.
107) Xiao Cunde, Liu Shiyin, Zhao Lin, Wu Qingbai, Li Peiji, Liu Chunzhen, Zhang Qiwen, Ding Yongjian, Yao Tandong, Li Zhongqin, Pu Jianchen. 2007. Observed changes of cryosphere in China over the second half of the 20th century: an overview. *Annals of Glaciology*, 46 (1): 382–390, doi: 10.3189/172756407782871396.
108) Xin Xiaodong, Yao Tandong, Ye Qinghua, Guo Liuping, Yang Wei. 2009. Study of the Fluctuations of Glaciers and Lakes

around the Ranwu Lake of Southeast Tibetan Plateau using Remote Sensing. *Journal of Glaciology and Geocryology*, 31(1):19-26. (In Chinese with English abstract)

109) Xu Baiqing, Cao Junji, Hansen J, Yao Tandong, Joswia Daniel, Wang Ninglian, Wu Guangjian, Wang Mo, Zhao Huabiao, Yang Wei, Liu Xianqin, He Jianqiao. 2009b. Black soot and the survival of Tibetan glaciers. *PNAS*, 105(52): 22114-22118.
110) Xu Jianzhong, Hou Shugui, Chen Fukun, et al., 2009. Trace the source of particles in the East Rongbuk ice core from Qomolangma. *Chinese Science Bulletin*, 54, doi: 10.1007/s11434 -009-0050-5.
111) Xu Jianzhong, Hou Shugui, Qin Dahe, Kang Shichang, Ren Jiawen, Ming Jing. 2007. Dust storm activity over the Tibetan Plateau recorded by a shallow ice core from the north slope of Mt.Qomolangma (Everest), Tibet-Himal region. *Geophysical Research Letters*, 34(L17504), doi: 10.1029/2007GL030 853.
112) Xu Jianzhong, Hou Shugui, Qin Dahe, Kaspari Susan, Petit Jean Robert, Delmonte Barbara, Kang Shichang, Ren Jiawen, Chappellaz Jerome, Hong Sungmin. 2010. A 108.83m ice-core record of atmospheric dust deposition at Mt.Qomolangma (Everest), Central Himalaya. *Quaternary Research*, 73: 33-38.
113) Xu Jianzhong, Kaspari Susan, Hou Shugui, Kang Shichang, Qin Dahe, Ren Jiawen, Mayewski Paul. 2009c. Records of volcanic events since AD 1800 in the East Rongbuk ice core from Mt. Qomolangma. *Chinese Science Bulletin*, 54(8): 1411-1416.
114) Yang Bao, Braeuning A, Liu Jingjing, Davis Mary, Shao Yajun. 2009. Temperature changes on the Tibetan Plateau during the past 600 years inferred from ice cores and tree rings. *Global and Planetary Change*, 69: 71-78.
115) Yang Bao, Braeuning Achim, Yao Tandong, Davis Mary. 2007. Correlation between the oxygen isotope record from Dasuopu ice core and the Asian Southwest Monsoon during the last millennium. *Quaternary Science Review*, 26: 1810-1817.
116) Yang Meixue, Yao Tandong, Wang Huijun. 2006. Microparticle content records of the Dunde ice core and dust storms in northwestern China. *Journal of Asian Earth Sciences*, 27: 223-229.
117) Yang Qing, Cui Caixia, Sun Churong, Ren Yiyong. 2007. Snow Cover Variation During 1959-2003 in Tianshan Mountains, China. *Advances in Climate Change Research*, 3 (2): 80–84. (In Chinese with English abstract)
118) Yang Wei, Yao Tandong, Xu Baiqing, Wu Guangjian, Ma Linglong, Xin Xiaodong. 2008. Ganrikapu glaciers are in intensive retreat at the southeast TP. *Science Bulletin*, 53(17): 2091-2095. (In Chinese)
119) Yang Yong, Chen Rensheng, Ji Xi-bin. 2007. Variations of Glaciers in the Yeniugou Watershed of Heihe River Basin from 1956 to 2003. *Journal of Glaciology and Geocryology*, 29(1):100-106. (In Chinese with English abstract)
120) Yao Tandong, Duan Keqin, Thompson LG, Wang Ninglian, Tian Lide, Xu Baiqing, Wang Youqing, Yu Wusheng. 2007. Temperature variations over the past millennium on the Tibetan Plateau revealed by four ice cores. *Annals of Glaciology*, 46: 362-366.
121) Yao Tandong, Duan Keqin, Xu Baiqing, Wang Ninglian, Guo Xuejun, Yang Xiaoxin. 2008. Precipitation record since AD1600 from ice cores on the central Tibetan Plateau. *Climate of the Past*, 4: 175-180.
122) Yao Tandong, Li Zexia, Thompson LG. 2006a. $\delta^{18}O$ records from Tibetan ice cores reveal differences in climatic changes. *Annals of Glaciology*, 43(1): 1-7.
123) Yao Tandong, Liu Yongqin, Kang Shichang, Jiao Nianzhi, Zeng Yonghui, Liu Xiaobo, Zhang Yongjun. 2008. Bacteria variabilities in a Tibetan ice core and their relations with climate change. *Global Biogeochemical Cycles*, 22, GB4017, doi:10.1029/2007GB003140.
124) Yao Tandong, Pu Jianchen, Lu Anxin, Wang Youqing, Yu Wusheng. 2007. Recent glacial retreat and its impact on hydrological processes on the Tibetan Plateau, China, and surrounding regions. *Arctic, Antarctic, and Alpine Research*, 39(4): 642-650.
125) Yao Tandong, Pu Jianchen, Tian Lide, Yang Wei, Duan Keqin, Ye Qinghua, Lonnie G. Thompson. 2007. Recent Rapid Retreat of the Naimona'nyi Glacier in Southwestern Tibetan Plateau. *Journal of Glaciology and Geocryology*, 29(4):503-508. (In Chinese with English abstract)
126) Yao Tandong, Wang Youqing, Liu Shiyin, Pu Jianchen, Shen Yongping, and Lu Anxin, 2004. Recent glacial retreat in High Asia in China and its impact on water resource in Northwest China. *Science in China Series D: Earth Sciences,* 47: 1065-1075.
127) Yao Tandong, Xiang Shurong, Zhang Xiaojun, Wang Ninglian, Wang Youqing. 2006b. Microorganisms in the Malan ice core and their relation to climatic and environmenta changes. *Global Biogeochemical Cycles*, 20, doi: 10.1029/2004GB002424.
128) Yao Tandong, Yang Meixue, Thompson LG. 2006c. $\delta^{18}O$ records and temperature change over the past 100 years in ice cores on the Tibetan Plateau. *Science in China (Series D Earth Sciences)*, 49(1): 1-9.
129) Ye Qinghua, Kang Shichang, Chen Feng, Wang Jinghua. 2006. Monitoring glacier variations on Geladandong Mountain, central Tibetan Plateau, from 1969 to 2002 using remote-sensing and GIS technologies. *Journal of Glaciology*, 52(179):537-544.
130) Ye Qinghua, Yao Tandong, Chen Feng, Kang Shichang, Zhang Xueqin, Wang Yi. 2008. Glacier and lake co-variations and their responses to climate change in the Mapam Yumco Basin on Tibet. *Geographical Research*, 27(5):1178-1190.
131) Ye Qinghua, Yao Tandong, Kang Shichang, Chen Feng, Wang Jinghua. 2006. Glacier variations in the Naimona'nyi region,western Himalaya, in the last three decades[J]. *Annals of Glaciology*. 43: 385-389.
132) Ye Qinghua, Zhong Zhenwei, Kang Shichang, Alfred Stein, Wei Qiufang, Liu Jingshi. 2009. Monitoring glacier and supra-glacier lakes from space in Mt. Qomolangma region of the Himalayas on the Tibetan Plateau in China. *Journal of mountain science*, 6: 101-106. (In Chinese with English abstract)
133) Ye Qinghua, Zhu Liping, Zheng Hongxing, Naruse Renji, Zhang Xueqin, Kang Shichang. 2007. Glacier and lake variations in the Yamzhog Yumco basin,southern Tibetan Plateau, from 1980 to 2000 using remote-sensing and GIS technologies. *Journal of Glaciology*, 53(183):673-676.
134) Zhang Guoliang, Pan Baotian, Wang Jie, Shangguan Donghui, Guo Wanqin. 2010. Research on the Glacier Change in the Gongga Mountain Based on Remote-Sensing and GPS from 1966 to 2008. *Journal of Glaciology and Geocryology*, 32(3):454-460. (In Chinese with English abstract)
135) Zhang Jiahua, Wu Yang, Yao Fengmei, Wei Wenshou. 2008. Analyses of Recent Xinjiang Snow Cover Feature Utilizing Satellite Remote Sensing and Surface Observation Data. *Plateau Meteorology*, 27 (3): 551–557. (In Chinese with English abstract)
136) Zhang Qianggong, Kang Shichang, Kaspari Susan, Li Chaoliu, Qin Dahe, Paul A. Mayewski, Hou Shugui. 2010. Rare earth elements in an ice core from Mt.Everest: seasonal variations and potential sources. *Atmospheric Research*, 94: 300-312.
137) Zhang Renhe, Wu Bingyi, Zhao Ping, Han Jinping. 2008. The decadal shift of the summer climate in the late 1980s over eastern China and its possible causes. *Acta. Meteorologica. Sinica.*, 22 (4): 435–445.
138) Zhang S, Hou Shugui, Ma Xiaojun, Qin Dahe, Chen Tuo. 2007. Culturable bacteria in Himalayan glacial ice in response to

atmospheric circulation. *Biogeosciences*, 4: 1-9.
139) Zhang Yong, Liu Shiyin, Ding Yongjian, Li Jing, Shangguan Donghui. 2006. Preliminary Study of Mass Balance on the Keqicar Baxi Glacier on the South Slopes of Tianshan Mountains. *Journal of Glaciology and Geocryology*, 28(4):477-484. (In Chinese with English abstract)
140) Zhang Yongjun, Kang Shichang, Qin Dahe, Bjorn Grigholm, Paul A. Mayewski. 2007a. Seasonal air temperature variations retrieved from a Geladaindong ice core, Tibetan Plateau. *Journal of Geographical Sciences*, doi: 10.1007/s11442-007-0431-0.
141) Zhang Yongjun, Kang Shichang, Qin Dahe, Bjorn Grigholm, Paul A. Mayewski. 2007b. Changes in annual accumulation retrieved from Geladaindong ice core and its relationship to atmospheric circulation over the Tibetan Plateau. *Chinese Science Bullentin*, 52(23): 3261-3266.
142) Zhao Ping, Zhou Zijiang, Liu Jiping. 2007. Variability of Tibetan spring snow and its associations with the hemispheric extratropical circulation and East Asian summer monsoon rainfall: an observational investigation. *Journal of Climate*, 20 (15): 3942–3955, doi: 10.1175/JCL I4205.1.
143) Zhao Yong, Cui Caixia, Li Hongjun. 2010. Characteristics of the Starting and Ending Dates of Snow Cover in Northern Xinjiang Region. *Journal of Glaciology and Geocryology*, 32 (2): 235–241. (In Chinese with English abstract)
144) Zheng Wei, Yao Tandong, Daniel Robert Joswiak, Xu Baiqing, Wang Ninglian, Zhao Huabiao. 2010. Major ions composition records from a shallow ice core on Mt.Tanggula in the central Qinghai-Tinetan Plateau. *Atmospheric Research*, 97: 70-79.
145) Zhou Guangpeng, Yao Tandong, Kang Shichang, Pu Jianchen, Tian Lide, Yang Wei. 2007. Mass Balance of the Zhadang Glacier in the Central Tibetan Plateau. *Journal of Glaciology and Geocryology*, 29(3):360-365. (In Chinese with English abstract)
146) Zhou Zaiming, Jing Zhefan, Zhao Shuhui, Han Tianding, Li Zhongqin. 2010. The Response of Glacier Velocity to Climate Change:A Case Study of Urumqi Glacier No.1. *Acta Geoscience Sinica*, 31(2):237-244.

Chapter 2. Frozen Ground/Permafrost

WU Qingbai and ZHAO Lin
State Key Laboratory of Cryospheric Sciences, Cold and Arid Regions Environmental and Engineering Research Institute, Chinese Academy of Sciences, Lanzhou 730000, China;

Permafrost regions occupy approximately 24% of the land area in the Northern Hemisphere, while areal extent of seasonally frozen ground (including the active layer over permafrost) covers, on average, approximately 56% of the northern hemisphere land mass. During the past several decades, studies of permafrost and global change have received great attention worldwide. These studies indicate that significant changes are occurring in permafrost and seasonally frozen ground. Such changes can have large impacts on the land surface energy and moisture balance and hence on weather and climate, surface and subsurface hydrology, carbon exchange between the land and the atmosphere, ecosystems in cold seasons/cold regions, landscape and geomorphological processes. Permafrost thaw can result in ground surface subsidence, which can disrupt infrastructure stability and operations in cold regions. As a consequence, the understanding, evaluation, and anticipation of changes in permafrost and seasonally frozen ground are of great scientific interest and bear a high relevance to society. Our study is focused on Qinghai-Tibet Railway, frozen soil mechanics, the effect of climate change on permafrost, environment change after permafrost degradation, and gas hydrate in permafrost regions during 2005 to 2010. Some results are summered:

1. *Qinghai-Tibet Railway Engineering(Tingjun Zhang)*

The Golmud–Lhasa section of the Qinghai–Tibet Railway is 1142 km in distance, of which 1118 km is being constructed. The railway covers 550 km of continuous permafrost and 82 km of island permafrost. If mean annual ground temperatures of 0 to -1.0 ^{o}C are defined as the temperature range for warm permafrost, 275 km (or 50%) of the continuous permafrost is warm permafrost and 40% is ice rich(Wu et al., 2006). Under global warming, its construction needs to take into consideration the climate changes over the next 50–100 years. Once the ice-bearing permafrost thaws, it completely loses its bearing capacity because of the strength of permafrost close to rock. Thus, the key to the success of the Qinghai-Tibet Railway is to prevent permafrost underlying the roadbed from thawing.

1.1 The design ideas adapting the impact of climate warming

For adapting the impacts caused by the climate warming and the engineering projects, a new design principle of positively protecting the permafrost, such as cooling the embankment, decreasing the permafrost temperature was proposed to deal with the stability of the embankment in warm, ice-rich permafrost regions (Cheng, 2005). Controlling the heat conduction, convection and radiation by changing the structure type of the embankment, the heat entering into the permafrost beneath the embankment were adjusted, such as decreasing the heat entering into the embankment in summer (decrease of the heat absorption) and increasing the cold into the embankment in winter (increase of the heat release), which made the heat release in winter was greater than the heat absorption in summer (Cheng, et al., 2007). Like the cooling roadbed (Fig 2.1), it effectively cooled the embankment by its special structure type (Wu et al., 2008). It decreased the permafrost temperature beneath the embankment and heaved the permafrost table which avoided the thawing of the underground ice near the permafrost table and ensured the thermal stability of the permafrost (Ma et al., 2006). This idea had been applied into the engineering design and the construction of the Qinghai-Tibet railway entirely.

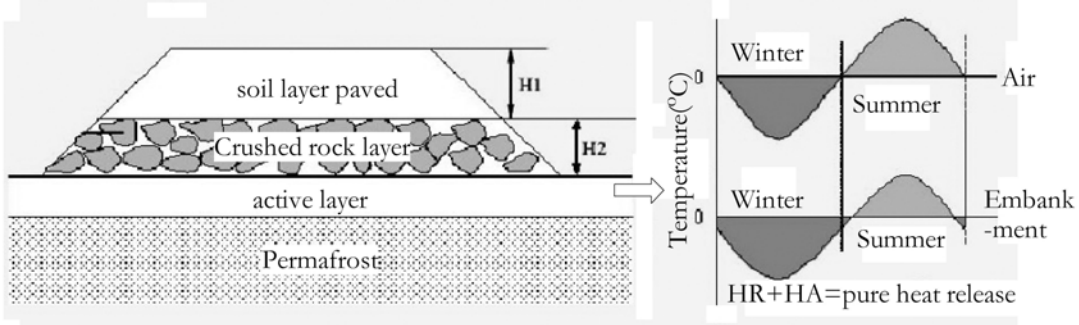

Fig 2.1 Principle of the cooling roadbed, HR is heat release, and HA is heat absorption.

1.2 Construction techniques adapting to the impact of climate warming

Heat exchange occurs through the modes such as conduction, convection and radiation between atmosphere and soil. Hence, some engineering techniques could be applied in the construction of railway to control the heat conduction, convection and radiation, i.e. to alter or decrease the heat entering into the embankment. Based on the design principle mentioned above, several techniques shown in (Cheng et al., 2009):

a. Heat conduction controlling

The construction technique of heat conduction controlling is mainly through adjusting the heat entering into the embankment to decrease the temperatures of embankment and permafrost below. For example, thermal piles (Fig 2. 2a) are mainly through the gas-liquid phase convection of the working medium inside it to bring the heat out from the permafrost beneath embankment in winter to decrease the soil temperature and to enhance the thermal stability of the embankment. The thermal pile is widely used in the Qinghai-Tibet Railway in permafrost regions to mitigate the impact of climate warming on the stability of embankment. Thermal piles in combination with heat preservation material form a complex embankment structure, which further improves the performance of thermal piles against climate warming.

b. Radiation controlling

Radiation controlling is mainly through decreasing the sunshine radiation on the side slope of embankment, hence reducing the heat entering into the embankment and the soil beneath it. The shading boards parallel with the side slope (Fig 2. 2b) reduce the sunshine radiation directly arriving at the slope, so as to enhance the thermal stability of the embankment. However, because of the paving technique and material selecting problems, this technique is still in experimental stage. The experiments of radiation controlling were conducted in some experimental fields, such as Beiluhe section of Qinghai-Tibet Railway, and parts of Qinghai-Tibet Highway and Qingkang Highway. However, the space between the shading board and the embankment slope was contributing to the aeration which reduces the heat absorbed by the shading board. Fig 2. 2 Construction techniques applied in the Qinghai-Tibet Railway in permafrost regions through the airflow in the space (Yu *et al*., 2008). Therefore, according to the fundamentals mentioned above, it was proposed to pave hollow bricks on the embankment slopes, which would be adumbral and ventilative, and could also solve the paving technique and material selecting problems (Yu, 2006).

c. Convection controlling

The convection controlling is through adjusting the thermal convection at the slope surface of and within embankment to strengthen the heat release from the embankment in winter in order to decrease the temperatures of the embankment and the soil beneath. These techniques are shown in Fig 2. 2(c, d, e). The ventiduct (Fig 2. 2c) is through the enforced convection inside to increase the release of heat from the soil within the embankment in winter. Actually, the ventiduct also increases the heat entering into the soil in summer, but the winter-time in the Qinghai-Tibet plateau is much longer than the summer-time, so the total amount of heat release is much greater than that of heat absorption annually. For better adapting to climate warming, Yu et al. (2008) proposed to install an automatic gate in each ventiduct, which closes when the air temperature is higher than 5^{o}C and opens otherwise to decrease the heat entering into the embankment in summer. The crushed rock revetment (Fig 2. 1d) is mainly through air convection to increase the release of heat from embankment in winter in order to decrease the soil temperature beneath the embankment. The crushed rock revetment has heat-insulation effect/chimney effect in summer/winter (Cheng, et al., 2007), thus reducing the heat entering into/ increasing the heat release from the embankment, respectively. The crushed rock revetment is a main construction technique to cool the embankment, and it has been widely applied in the Qinghai-Tibet Railway in permafrost regions (Wu et al., 2008).

The crushed rock-based embankment (Fig 2. 2e) is mainly through enforced air convection to enhance the heat release from embankment in winter in order to decrease the soil temperature beneath the embankment (Wu et al., 2010). Because many gaps exist in crushed rock-based embankment, different thermal activities occur in different occasions. In summer, the wind speed is relatively lower, so the heat conduction occurs in the crushed rock-based embankment dominantly. In winter, with the relatively higher wind speed, the aeration occurs, and the weak natural convection also occurs when the wind speed slows down. The crushed rock-based embankment effectively decreases the soil temperature beneath it and is proved to be very useful in adapting to the impact of climate warming (Wu et al., 2007). As the core technique for cooling embankment, the crushed rock-based embankment construction was widely applied in the Qinghai-Tibet Railway in permafrost regions.

d. Integrated controlling

The integrated controlling is a combination controlling of heat conduction, radiation and convection. Substituting a bridge for embankment is an integrated controlling (Fig 2.2f). It is adumbral and ventilative. For reducing the thermal disturbance at the foot of the slope, the thermosyphone was installed, at the same time, the crushed rock-based revetment was also applied in the Qinghai-Tibet Railway to enlarge the temperature reduction.

Fig 2.2 Construction techniques applied in the Qinghai-Tibet railway in permafrost regions

1.3 Cooling effects of the construction techniques

Because of the fundamental differences among the construction techniques, the cooling effect of each technique is different from that of the others. Fig 2.3 shows the contrastive sketches of the soil thermal regime beneath the embankment with and without the ventiduct.The soil temperature beneath the embankment with the ventiduct had been decreasing continually and the isotherm of -1℃ beneath it had been raising continually, either (Niu et al., 2006). Whereas, the isotherm of -1℃ had been declining continually beneath the embankment without the ventiduct. At the same depth, the soil temperature beneath the embankment with the ventiduct had been decreasing continually, but which had been increasing continually beneath the embankment without the ventiduct. According to the research on the forecast of the ventiduct model, if the temperature increase rate will be 2℃ per 50 years, this kind of structure with the ventiduct can work well to cool the embankment in the regions with the annual air temperature lower than -3.5℃ and also can ensure the thermal stability of the permafrost beneath it in 50 years (Zhang et al., 2005).

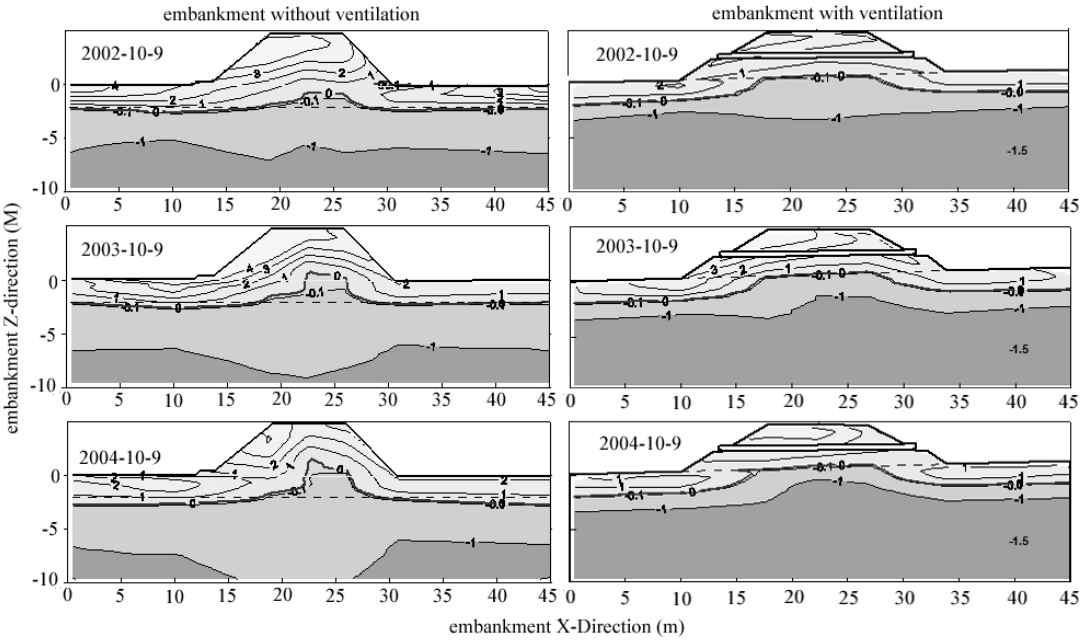

Fig 2.3 Contrastive thermal regimes of the embankment with and without the ventiduct

In Fig 2.4, it shows the variations of the soil temperature beneath the center of the crushed rock-based embankment at different depths in different places. A very remarkable trend of temperature decrease in different depths is shown in this figure and the soil temperature continually decreases year after year. Like the place in Chu-ma-er-he, beneath the center of the crushed rock-based embankment, at the depth of 0.5m the mean annual soil temperature decreased from -0.19℃ (2003) to -1.12℃ (2005), the decrease magnitude was about -1℃. In Kekexili, beneath the center of the crushed rock-based embankment, at the depth of 0.4m the mean annual soil temperature decreased from -1.0℃ (2004) to -1.85℃ (2005), the decrease magnitude was about -0.85℃ (Ma et al., 2008). Based on the forecast of the climate change (Zhang et al., 2005), with the temperature increase rate of 2.0℃ per 50 years, the crushed rock-based embankment can still work well to cool the embankment and ensure the thermal stability of the permafrost beneath the embankment.

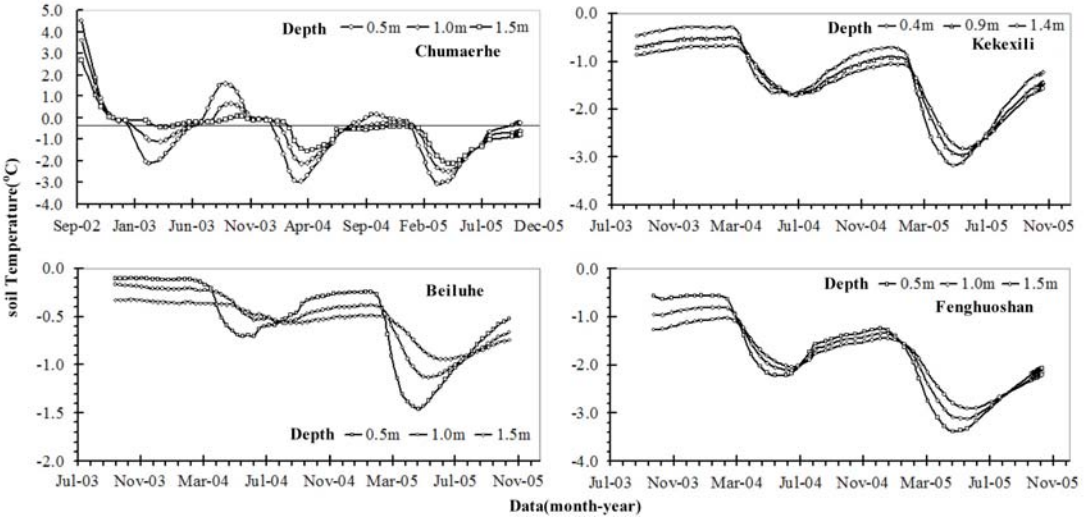

Fig 2.4 Variations of the soil temperature beneath the crushed rock-based embankment

In Fig 2.5, it shows the variations of the soil temperature at the both shoulders of the crushed rock cover (a) (b). It is shown in this figure that the soil temperatures beneath the two kinds of embankment decreased continually year after year; even the decrease magnitude was relative small but it was evident,

and the long-term effect of it could be more evident. 0.5m beneath the right shoulder, the mean annual soil temperature decreased from -0.25℃ (2005) to -0.58℃ (2006) and 1.0m beneath the right shoulder, the mean annual soil temperature decreased from -0.19℃ (2005) to -0.59℃ (2006); the temperature decrease magnitudes were -0.3℃ and -0.4℃, respectively (Wu et al., 2009).

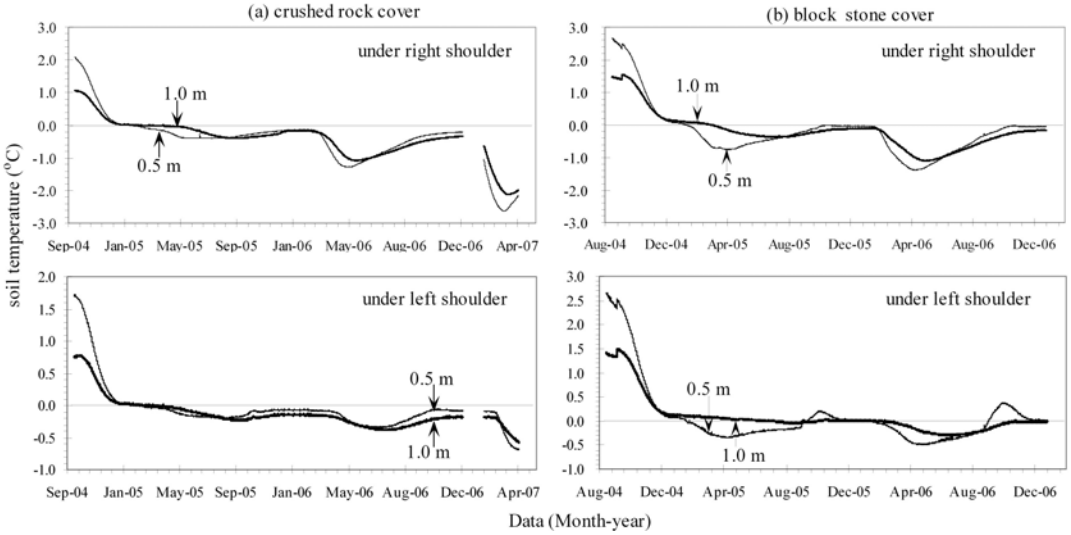

Fig 2.5 Variation of the soil temperature beneath the embankment with crushed rock-based cover

2. *Frozen Soil Strength for warm permafrost*

Due to many microdefects distributed randomly in warm frozen clay and warm ice-rich clay, the mechanical properties and behaviors of these clays display great uncertainty, so it is more reasonable to research the stress-strain relationship of them by stochastic method. Improved statistical damage constitutive model for these two types of clays is deduced on the basis of experimental data and original model, and the new model is verified by large numbers of experimental data under different temperatures. Through the study of new model, we can find that it is more definite to use the strength of soil element as random variable instead of the axial strain.

2.1 Strength distributions of warm frozen clay and its stochastic damage constitutive model

Since there are many defects such as fissures and cavities in warm frozen clay and warm ice-rich frozen clay, their strengths are distributed randomly at different temperature (-0.5 °C, -1.0 °C and -2.0 °C). Based on these experimental data, it was found that the strengths of warm frozen clay and warm ice-rich frozen clay satisfy the Weibull distribution. A stochastic damage constitutive model for warm frozen clay and warm ice-rich frozen clay was developed by applying continuous damage theory and probability, as well as probability theory (Lai, et al., 2008). Through a series of experimental data, it was found that the stress-strain relationship of warm frozen clay shows a strain softening. For the warm ice-rich frozen clay, because there is much ice, its stress-strain relationship behaves in an elastic-plastic way instead of strain softening. The discreteness of the stress – strain curves for warm frozen clay becomes larger with increasing deformation. While for the warm ice-rich frozen clay, the discreteness of the stress-strain curves almost remains the unchanged even after yielding. Among several potential probability distributions, the Weibull distribution was found to best describe the strength law for warm frozen clay and warm ice rich frozen clay (Fig 2. 6) (Lai et al., 2008). The stochastic damage constitutive model deduced in this paper could describe the stress – strain relationships for warm frozen clay, especially the warm ice-rich frozen clay well.

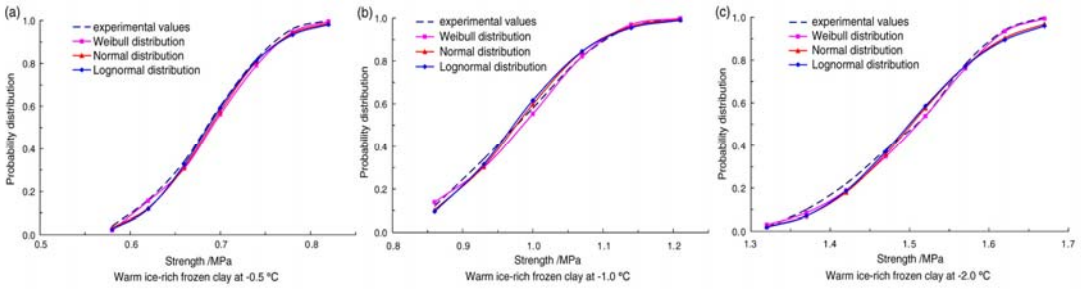

Fig 2. 6, Probability distributions of warm ice-rich frozen clay at different temperatures.

2.2 An improved statistical damage constitutive model for warm frozen clay based on Mohr – Coulomb criterion

For the warm frozen clay and warm ice-rich frozen clay, a stochastic damage constitutive model has been proposed on the foundation of a large number of experimental data, in which the axial strain is regarded as random variable. The strength of soil element is selected as random variable and an improved statistical damage constitutive model is deduced, and in this new model, the Mohr-Coulomb failure criterion is also used to judge whether the soil element is damaged. Compared with original model, the new improved model can better describe the experimental data and reflect deformation characteristics (Li et al., 2009). Especially, when the stress reaches its peak value, the experimental data and new theoretical curves overlap with each other. The improved model includes the Mohr – Coulomb failure criterion, which is very widely applied in the classical plastic theory and soil mechanics. However, when the specimen fails, there is no experimental data used to calculate some unknown parameters, thus, the improved statistical damage model can't accurately simulate stress – strain behavior of the frozen clay after its failure and the approximate analytical method is adopted. Notwithstanding its limitation at this point, this study does suggest that the improved model is more reasonable on the concept of soil mechanics.

2.3 Yield criterion and elasto-plastic damage constitutive model for frozen sandy soil

Based on the continuous damage mechanics theories, cross anisotropic damage variables are deduced and their changes are investigated. The damage strain thresholds increase linearly with increase in the confining pressures. Frozen sandy soil appears to have an obvious cross anisotropic damage in loading process and the radial damage are more serious than the axial damage. By introducing damage variables to the elasto-plastic constitutive model proposed and defining the anisotropic energy norm of stress tensor, the elasto-plastic damage constitutive model for frozen sandy soil is presented (Lai et al., 2009). Comparing the calculated results with the test results, it is found that the calculated results coincide well with the test results. This model simulates the softening phenomenon after the peak point of stress-strain curves especially well. Analyzing the results of triaxial tests on frozen sandy soil at -6 ^{o}C and drawing the streamlines and potential lines, the plastic yield surfaces are proposed according to the Drucker's postulate. Then the elasto-plastic constitutive model for frozen sandy soil was developed by selecting plastic work as a hardening parameter. Comparing with the test results, this model can exactly predict the deformation regularity of frozen soil. It describes the stress-strain process under high confining pressures when pressure melting phenomena occurs especially well.

3. Response of active layer and permafrost temperature to climate warming

Observed evidence shows that permafrost is warming, thawing, and degrading during the past few decades on the Qinghai-Tibetan Plateau and active layer thickness is increasing (Cheng and Wu, 2007). Over a period from 1995 through 2007, a systematic soil temperature measurement network of 10 sites was established along the Qinghai-Tibetan Highway. Soil temperatures were continuously measured semi-monthly and up to 12 m depth. We investigate spatial variations of active layer thickness and its change, soil temperature within active layer and permafrost temperature over the period of record.

3.1. Change of Active Layer Thickness

The primary results demonstrate that long-term and spatially averaged active layer thickness is about 2.41 m with a range from 1.32 m to 4.57 m along the Qinghai-Tibetan Highway. All monitoring sites show an increase in active layer thickness over the period of their records. The mean increasing rate of active layer thickness is about 7.5 cm/year with a range of 2.1 – 16.6 cm/year from 1995 to 2007 (Fig 2. 7) (Wu and Zhang, 2010). We estimated active layer thickness using thawing index of air temperature over a period from 1956 through 2005 near Wudaoliang meteorological station in northern Plateau. Active layer

thickness had no or very limited change from 1956 to 1983 and a sharp increase of about 39 cm from 1983 through 2005(Fig 2. 8). The magnitude of active layer thickness increase is greater in warm permafrost region than in cold permafrost region. The primary control of increase in active layer thickness is due to increase in summer air temperature, while changes in winter air temperature and snow cover condition play no or very limited role (Wu and Zhang, 2010).

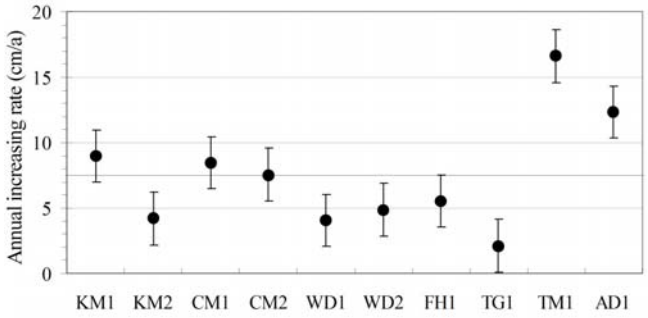

Fig 2. 7 Annual increase rate of ALT for all observed sites. Solid circle represents mean increase rate with the bar as the range at each site.

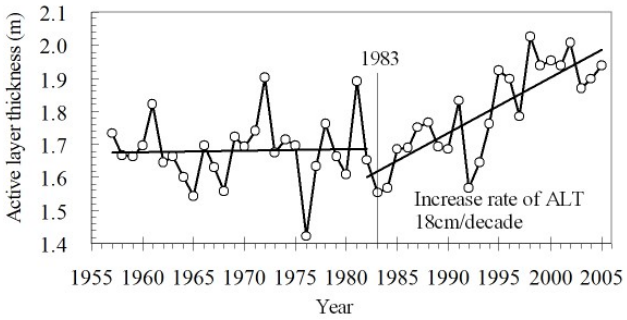

Fig 2. 8 Inter-annual variations of ALT estimated using thawing index of air temperature from the Wudaoliang Meteorological Station from 1956 to 2005.

3.2. Change of Permafrost Temperature

The long-term mean annual permafrost temperatures at 6.0 m depth vary from -0.19^{o}C at the Touerjiu Mountains (TM1) site to -3.43^{o}C at Fenghuo Mountain (FH1) site, with an average of about -1.55^{o}C from all 10 sites over the period of their records. Mean annual permafrost temperatures at 6.0 m depth have increased 0.12^{o}C to 0.67^{o}C with an average increase of about 0.43^{o}C during the past decade (Fig 2. 10) (Wu and Zhang, 2008). Over the same period, mean annual air temperatures from four National Weather Service Stations show an increase of about 0.6^{o}C to 1.6^{o}C, generally sufficient to account for the permafrost warming. Increase in summer rainfall and decrease in winter snowfall may be cooling factors to the underlying soils, offsetting less degree of permafrost warming compared with the magnitude of air temperature increase. Permafrost temperatures at 6.0 m depth increased year-around with most of the increase happened in spring and summer. Winter air temperature has increased 2.9^{o}C to 4.2^{o}C from 1995 through 2005, which may account for significant spring and summer permafrost warming at 6.0 m depth due to three to six month time lag (Wu and Zhang, 2008). However, there were no significant trends of air temperature change in other seasons. Further investigation, especially comprehensive monitoring, is needed to better comprehend the physical processes governing the thermal regime of the active layer and permafrost on the Qinghai-Tibetan Plateau.

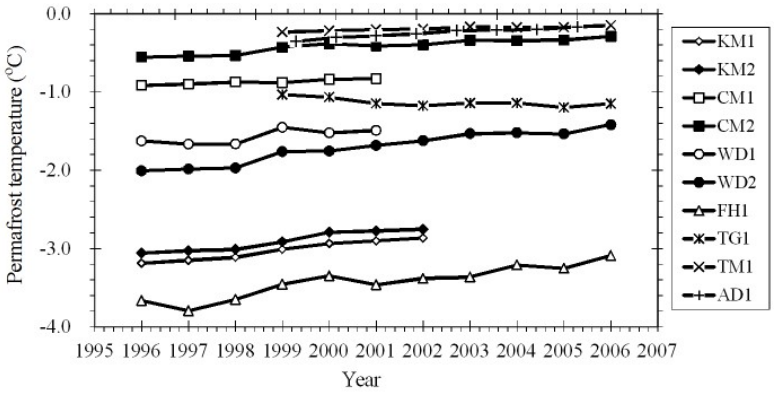

Fig 2. 8 Time series of mean annual permafrost temperatures at 6.0 m depth from 10 monitoring sites on the Qinghai-Tibetan over the period of their records.

3.3. Thermal State of permafrost and active layer in Central Asia during the International Polar Year

Measurements in boreholes in Central Asia show that much of the permafrost is currently at temperatures close to 0°C. Longer-term records, where available, demonstrate that permafrost has warmed, active layers have become thicker, and geothermal gradients have decreased over the past few decades (Zhao, et al., 2009). Permafrost in Central Asian is present in the Qinghai–Tibet Plateau in China, the Tien Shan Mountain regions in China, Kazakhstan and Kyrgyzstan, the Pamirs in Tajikistan, and in Mongolia. Monitoring of the ground thermal regime in these regions over the past several decades has shown that the permafrost has been undergoing significant changes caused by climate warming and increasing human activities. During the International Polar Year, measured mean annual ground temperature (MAGT) at a depth of 6m ranged from -3.2°C to 0.2°C on the Qinghai–Tibet Plateau and the active-layer thickness (ALT) varied between 105 and 322 cm at different sites (Zhao et al., 2010). Ground temperatures at the bottom of the active layer (TTOP) warmed on average by 0.068C yr^{-1} over the past decade. In Mongolia, MAGT at 10–15m depth increased by up to 0.02–0.038C yr^{-1} in the Hovsgol Mountain region, but by 0.01–0.028C yr^{-1} in the Hangai and Hentei Mountain regions (Zhao et al., 2010). The increase in permafrost temperatures in the northern Tien Shan from 1974 to 2009 ranged from 0.3°C to 0.6°C. At present measured permafrost temperatures vary from -0.5°C to -0.1°C. The ALT increased from 3.2 to 4m in the 1970s to a maximum of 5.2m between 1995 and 2009.

4. Ecological environment change in permafrost regions on the Qinghai-Tibetan Plateau

4.1 The influence of degradation of the swamp and alpine meadows on CH_4 and CO_2 fluxes

Studies of greenhouse gas emissions and carbon cycles in the different degraded swamp and alpine cold-meadow ecosystems of the Plateau have an important scientific and practical significance in assessing the response of the biogeochemical cycle to global changes and its feedback effect (Wang et al., 2009). CH_4 and CO_2 fluxes from a high-cold swamp meadow and an alpine meadow on the Qinghai-Tibetan Plateau, subject to different degrees of degradation, were measured over a 12-month period. For swamp meadows, the greater the degradation, the lesser the carbon efflux. CH_4 emissions at the nondegraded swamp meadow site were 1.09–3.5 and 2.5–11.27 times greater (Fig 2. 9), and CO_2 emissions 1.08–1.69 and 1.41–4.43 times greater (Fig 2. 9), respectively, than those from moderately and severely degraded sites. For alpine meadows, the greater the degradation, the greater the CH_4 consumption and CO_2 emissions. CH_4 consumption at the severely degraded alpine meadow site was 6.6–21 and 1.1–5.25 times greater (Fig 2. 9), and CO_2 emissions 1.05–78.5 and 1.04–6.28 times greater (Fig 2. 9), respectively, than those from the nondegraded and moderately degraded sites. The CH_4 and CO_2 fluxes at both sites were significantly correlated with air temperature, soil temperature, and topsoil (0–5 cm depth) moisture, indicating these to be the main environmental factors affecting such fluxes (Wang et al., 2009).

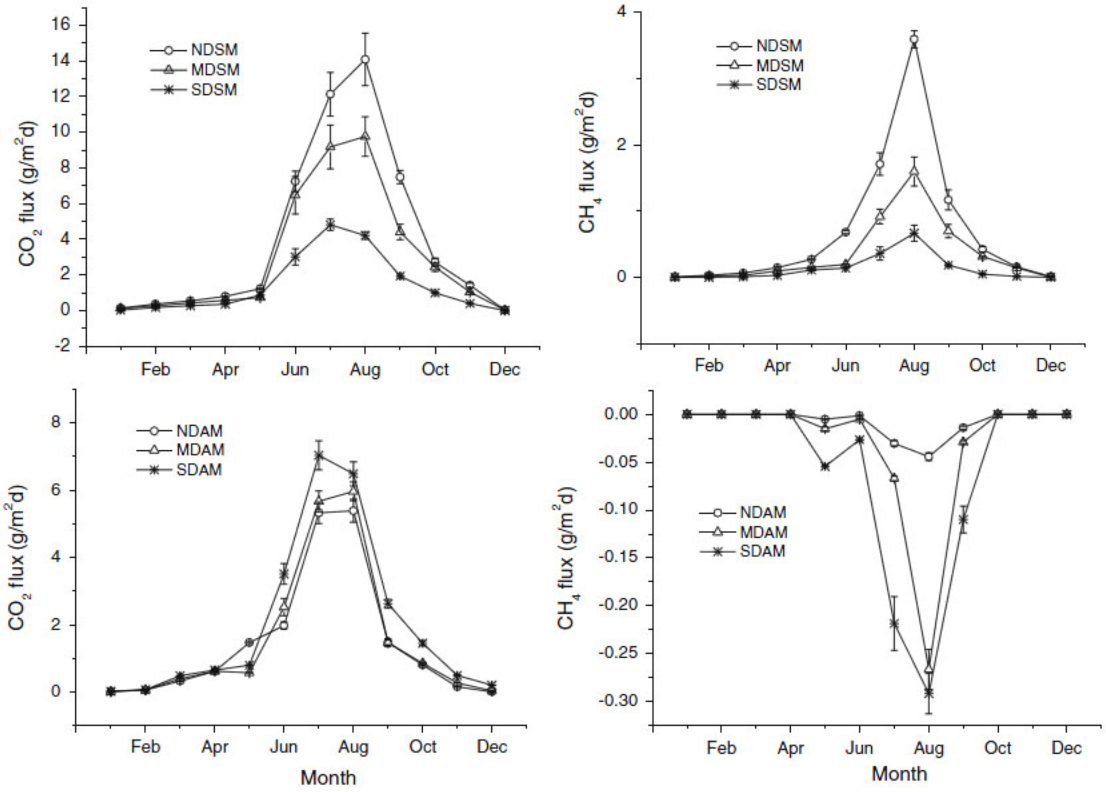

Fig 2. 9 Seasonal patterns of CO_2 and CH_4 fluxes in swamp and alpine meadows. NDSM Nondegraded swamp meadow, MDSM moderately degraded swamp meadow, SDSM severely degraded swamp meadow, NDAM nondegraded alpine meadow, MDAM moderately degraded alpine meadow, SDAM severely degraded alpine meadow.

4.2 Effects of permafrost thawing on vegetation and soil carbon pool losses

Bearing a total organic carbon (TOC) content of 9.3 – 10.7 kg C/m^2, alpine grassland soils of the Qinghai – Tibet plateau's permafrost region bear a greater organic carbon pool than do grassland soils in other regions of China or than tropical savannah soils (Wang et al., 2008). The easily released light fraction organic carbon (LFOC) accounts for 34 – 54% of the TOC and is particularly enriched in the topsoil (0 – 0.10 m). The LFOC in the organic carbon pool of alpine cold meadow and alpine cold steppe soils decreased at exponential and quadratic rates, respectively, as the vegetative cover decreased. When the vegetative cover of alpine cold meadows decreased from >80 dm^2/m^2 to 60 dm^2/m^2, the topsoil TOC and LFOC dropped by 20.4% and 38.4%, respectively. Similarly, when the vegetative cover of alpine cold meadow decreased from 50 dm^2/m^2 to 30 dm^2/m^2 and <15 dm^2/m^2, the topsoil LFOC content dropped by 60% and 86.7%, respectively (Wang et al., 2008). Under climatic warming, the degradation of permafrost and vegetation has resulted in serious soil organic carbon (SOC) loss from the carbon pool. Land cover changes that occurred between 1986 and 2000 are estimated to have resulted in a 1.8 Gg C (120 Mg C/yr) loss in SOC, and a concomitant 65% decrease in the LFOC, in the 0 – 0.30 m soil layer in the Qinghai – Tibet plateau's permafrost regions. Since the region's ecosystems are quite sensitive to global climate changes, if global warming persists, alpine cold grassland ecosystems are expected to further degrade. Hence, the influence of global climatic change on soil carbon emissions from alpine grasslands should receive more attention.

4.3 Impacts of permafrost changes on alpine ecosystem in Qinghai-Tibet Plateau

Alpine cold ecosystem with permafrost environment is quite sensitive to climatic changes and the changes in permafrost can significantly affect the alpine ecosystem. The vegetation coverage, grassland biomass and soil nutrient and texture are selected to indicate the regime of alpine cold ecosystems in the Qinghai-Tibet Plateau. The interactions between alpine ecosystem and permafrost were investigated with the depth of active layer, permafrost thickness and mean annual ground temperature (MAGTs) (Wang et al., 2006). The permafrost changes have a different influence on different alpine ecosystems. With the increase in the thickness of active layer, the vegetation cover and biomass of the alpine cold meadow exhibit a

significant conic reduction, the soil organic matter content of the alpine cold meadow ecosystem shows an exponential decrease, and the surface soil materials become coarse and gravelly. The alpine cold steppe ecosystem, however, seems to have a relatively weak relation to the permafrost environment. Those relationships resulted in the fact that the distribution area of alpine cold meadow decreased by 7.98% and alpine cold swamp decreased by 28.11% under the permafrost environment degradation during recent 15 years (Wang et al., 2006). In the future 50 years the alpine cold meadow ecosystems in different geomorphologic units may have different responses to the changes of the permafrost under different climate warming conditions, among them the alpine cold meadow and swamp ecosystem located in the low mountain and plateau area will have a relatively serious degradation (Wang et al., 2006). Furthermore, from the angles of grassland coverage and biological production the variation characteristics of high-cold ecosystems in different representative regions and different geomorphologic units under different climatic conditions were quantitatively assessed.

5. Gas hydrate research in permafrost regions

Gas hydrates are ice-like crystalline solids composed of water and gas in which water molecules trap gas molecules in a cage-like structure known as a clathrate, which can be formed when gas and water mixtures are subjected to high pressure or low temperature conditions. Gas hydrates widespread in permafrost regions and beneath the sea in sediments of outer continental margins. Although estimates of its occurrence vary widely, the carbon reserves of gas hydrate in the world may reach 2.0×10^{16} m^3, twice of explored conventional sources of energy. Gas hydrates are a new kind of potential and clean energy resource. And gas hydrates, especially methane hydrate, may easily to dissociate with variations of temperature and pressure. And the dissociation of hydrates may play a great role in climate change due to their strong greenhouse effect.

5.1 Formation conditions and distribution prediction of gas hydrate in the Qinghai-Tibet Plateau

Permafrost accounts for about 52% of the total area of the Qinghai – Tibet Plateau, and the permafrost area is about 140×10^4 km^2. The mean annual ground temperature of permafrost ranges from -0.1 to -5 ^oC, and lower than -5^oC at extreme high-mountains. Permafrost thickness ranges from 10 to 139.4 m by borehole data, and more than 200 m by geothermal gradients. The permafrost geothermal gradient ranges from 1.1^oC/100 m to 8.0^oC/100 m with an average of 2.9^oC /100 m, and the geothermal gradient of the soil beneath permafrost is about 2.8-8.5^oC /100 m with an average of 6.0^oC /100 m in the Qinghai-Tibet Plateau (Wu et al., 2010a). For a minimum of permafrost geothermal gradients of 1.1^oC /100 m, the areas of the potential occurrence of methane hydrate (sI) is approximately estimated to be about 27.5% of the total area of permafrost regions in the Qinghai-Tibet Plateau. For an average of permafrost geothermal gradients of 2.9^oC /100 m, the areas of the potential occurrence of methane hydrate (sI) is approximately estimated bout 14% of the total area of permafrost regions in the Qinghai-Tibet Plateau (Wu, et al., 2010b). For the sII hydrate, the areas of the potential occurrence of sII hydrate are more than that of sI ethane hydrate.

Based on the thickness of frozen layer and thermal gradient in Qinghai-Tibet Plateau permafrost, the occurrence and distribution of gas hydrate in the low-middle latitude and high altitude permafrost is predicted by using the thermodynamic method of natural gas hydrate stable temperature and pressure. The thermodynamic phase equilibrium of thermogenic and biogenic gas hydrate imply that gas hydrate is buried in depth from ~27 to ~2070m , and the resource potential of natural gases caged in hydrates are estimated as about 1.2×10^{11} to 2.4×10^{14} m^3 in Qinghai-Tibet Plateau permafrost (Cheng, et al., 2005). Gas hydrate is propitious to occur where the frozen layer is thicker and thermal gradient is lower in the permafrost. Seasonal change of air temperature in Qinghai-Tibet Plateau affects only the uppermost sediments 10m and does not affect gas hydrate that is buried below 30m.

5.2 Basic geological characteristics of gas hydrates in Qilian Mountain permafrost area, Qinghai Province

The gas hydrate is a new type of hydrate characterized by relatively shallow buried depth, thin permafrost zones, complex gas components, and coal-bed methane origin. The research achievement directed by Professor ZHU Youhai, Institute of Mineral Resources, Chinese Academy of Geological Sciences, ranks first among the “Top Ten Scientific and Technological Progresses of Chinese Academy of Geological Sciences in 2009”. Four scientific experimental wells were drilled in the Qilian Mountain permafrost area of Qinghai Province in the winter of 2008 and the summer of 2009. Gas hydrate was directly obtained and white ice-like gas hydrate and its burning phenomena were observed from three of the four wells (Fig 2. 10). These results were confirmed by lab-based Raman spectroscopy. In all the 4 wells,

gas hydrate related anomalous phenomena were also recorded. It is the first time for researchers to find gas hydrate in China's continent (Zhu et al., 2010). Gas hydrate and its related anomalous phenomena occur in such rocks as mudstone, oil shale, siltstone and fine-grained sandstone and are not obviously related to lithology, mainly occurring in fissures and pore space and evidently controlled by fissures. These gas hydrates are vertically discontinuously distributed and horizontally irrelatively arranged from 130 m to 400 m below the surface (Lu et al., 2010). In the study area, gas hydrate and its related anomalous phenomena are probably confined mainly to the gas hydrate stability zone based on permafrost features; individual gas hydrate occurrences are controlled jointly by fissures and gas sources. When hydrocarbon gases are generated by organic matter, they are driven by all grades of fractures to migrate upwards; when they arrive in the stability zone, they are coupled by cryogenic permafrost, leading to their preferable occurrence in fissures (Zhu et al., 2010).

Fig 2. 10 Photo of Gas hydrate in Permafrost region in Qilian Mountains

References

1) Chen D F, Wang M C, Xia B. Formation condition and distribution prediction of gas hydrate in Qinghai-
2) Cheng Guodong, Lai Yuanming, Sun Zhizhong, et al. The 'thermal semi-conductor' effect of crushed rocks. Permafrost and Periglacial Process, 2007, 18: 151-160.
3) Cheng Guodong, Wu Qingbai, Ma Wei. Engineering Effect of Proactive Roadbed- Cooling for the Qinghai-Tibet Railway, 2009, 52(2): 530-538.
4) Cheng, G. D., A roadbed cooling approach for the construction of Qinghai-Tibet Railway. Cold Regions Sci. Technol., 2005, 42, 169--176.
5) Cheng, G., and T. Wu, Responses of permafrost to climate change and their environmental significance, Qinghai-Tibet Plateau, J. Geophys. Res., 112, F02S03, doi:10.1029/2006JF000631,2007.
6) Junfeng Wang, Genxu Wang, Hongchang Hu, Qingbai Wu. The influence of degradation of the swamp and alpine meadows on CH4 and CO2 fluxes on the Qinghai-Tibetan Plateau. Environ Earth Sci, 2009, DOI 10.1007/s12665-009-0193-3.
7) Lai Yuanming, Jin Long, Chang Xiaoxiao. Yield criterion and elasto-plastic damage constitutive model for frozen sandy soil. International Journal of Plasticity, 25 (2009) 1177–1205.
8) Lin Zhao, Qingbai Wu, S.S. Marchenko, and N. Sharkhuu. Thermal State of Permafrost and Active Layer in Central Asia during the International Polar Year. Permafrost and Periglacial Processes, 2010, 21: 198–207.
9) LU Zhenquan, ZHU Youhai, ZHANG Yongqin, et al., Major Evidence for Gas Hydrate Existence in the Qilian Permafrost, Qinghai. GEOSCIENCE, 2010, 24(2): 329-336.
10) Ma, W., Shi, C.H., Wu, Q.B., Zhang. L.X., Wu, Z.J., 2006. Monitoring study on technology of the cooling roadbed in permafrost region of Qinghai-Tibet Plateau, Cold Regions Science and Technology 44(1), 1-11.
11) Niu F J, Cheng G D, Xia H M, et al. Field experiment study on effects of duct-ventilated railway embankment on protecting the underlying permafrost. Cold Reg Sci Technol, 2006, 45 (3): 178—192
12) Q. B. WU, G. D. CHENG, W. MA, F. NIU, and Z. Z. SUN, Technical approaches on permafrost thermal stability for Qinghai--Tibet Railway. Geomechanics and Geoengineering, 2006, 1(2):119—127.
13) Qingbai Wu, Liu Ge, Tingjun Zhang, Yongzhi Liu. In-situ Experimental Study of Heat Transfer Process within Crushed Rock Layer along the Qinghai-Tibet Railway. International Journal of Offshore and Polar Engineering, 2010, 20(2): 1-8.
14) Qingbai Wu, Tingjun Zhang, and Liu Yongzhi. Permafrost Temperatures and thickness along the Qinghai-Tibetan Highway. Global and Planetary Change, 2010a, 72:32-38.
15) Shuangyang Li, Yuanming Lai, Shujuan Zhang, Deren Liu An improved statistical damage constitutive model for warm frozen clay based on Mohr–Coulomb criterion. Cold Regions Science and Technology 57 (2009) 154–159.
16) Tibet Plateau permafrost. Chinese J. Geophys. (in Chinese) , 2005 , 48 (1) :165～172.
17) Wang Genxu, Li Yuanshou, Wang Yibo, Wu Qingbo. Effects of permafrost thawing on vegetation and soil carbon pool losses on the Qinghai–Tibet Plateau, China. Geoderma, 143 (2008) 143–152.
18) WANG Genxu, LI Yuanshou, WU Qingbai & WANG Yibo.Impacts of permafrost changes on alpine ecosystem in

Qinghai-Tibet Plateau. Science in China Series D: Earth Sciences, 2006, 49(11): 1156-1169.
19) Wei Ma, Guangli Feng, Qingbai Wu, Junjie Wu, 2008, Analyses of temperature fields under the embankment with crushed-rock structures along the Qinghai–Tibet Railway, Cold Regions Science and Technology,2008, 53(3): 259–270.
20) Wu Qingbai Li Mingyong Liu Yongzhi, Cool effect of crushed rock structure on permafrost under embankment. Sciences in Cold and Arid regions, 2009, 1(1): 39-50.
21) Wu Qingbai, Cheng Guodong, Ma Wei, and Liu Yongzhi. The Railway Construction Techniques Adapting the Climate Warming in Permafrost Regions, 2008, Advance in Climate change. 2008:4(Suppl.) : 60-68.
22) Wu Qingbai, Cheng Hongbin, Jiang Guanli, *et al*. Cooling mechanism of embankment with block stone interlayer in Qinghai-Xizang Railway. Science in China (Series E), 2007, 50 (3): 319-328.
23) Wu Qingbai, Jiang Guanli, Zhang Peng. Potential formation conditions of gas hydrates and permafrost in the Qinghai-Tibet Plateau, China. Energy Convers Manage, 2010b, 51:783-787.
24) Wu, Q., and T. Zhang, Changes in Active Layer Thickness over the Qinghai-Tibetan Plateau from 1995-2007, J. Geophys. Res., 115, D09107, doi:10.1029 / 2009JD01297,2010.
25) Wu, Q., and T. Zhang, Recent Permafrost Warming on the Qinghai-Tibetan Plateau, J. Geophys. Res., 113，D13108, doi:10.1029/2007JD009539, 2008.
26) Yu Q H. Study on the heat conduction process of roadbeds in permafrost region and new control methods. Dissertation of Doctoral Degree. Lanzhou: Cold and Arid Regions Environmental and Engineering Research Institute, Chinese Academy of Sciences, 2006.
27) Yu Qihao, Niu Fujun, Pan Xicai, Bai Yang, Zhang Mingyi. Investigation of embankment with temperature-controlled ventilation along the Qinghai–Tibet Railway, Cold Regions Science and Technology, 2008, 53 (2): 193–199.
28) Yu Qihao, Pan Xicai, Cheng Guodong, *et al*. An experimental study on the cooling mechanism of a shading board in permafrost engineering. Cold Regions Science and Technology, 2008,53(3): 298–304.
29) Yuanming Lai, Shuangyang Li, Jilin Qi, Zhihua Gao, Xiaoxiao Chang. Strength distributions of warm frozen clay and its stochastic damage constitutive model. Cold Regions Science and Technology 53 (2008) 200–215.
30) Zhang M Y, Lai Y M, Liu Z Q, et al. Nonlinear analysis for the cooling effect of Qinghai-Tibet Railway embankments with different structures in permafrost regions. Cold Regions Science and Technology, 2005, 42: 237—249
31) Zhao L, Marchenko SS, Sharkhuu N, et al. 2008. Regional changes of permafrost in Central Asia. In Extended Abstracts, Proceedings Ninth International Conference on Permafrost, Vol. 2, Kane DL, Hinkel KM (eds). Institute of Northern Engineering, University of Alaska: Fairbanks; 2061–2069.
32) ZHU You-hai, ZHANG Yong-qin, WEN Huai-jun, LU Zhen-quan, WANG Ping-kang. Gas Hydrates in the Qilian Mountain Permafrost and Their Basic Characteristics. Acta Geoscientica Sinica, 2010,31(1):7-16.

Chapter 3. Hydrology in Cold Regions

YE Baisheng
State Key Laboratory of Cryospheric Sciences, Cold and Arid Regions Environmental and Engineering Research Institute, Chinese Academy of Sciences, Lanzhou 730000, China

Cryosphere is one of the most sensitivity to climate change in the earth, and also closely related to the hydrology. The effect of cryosphere change on hydrological process is one of the challenges in the global change research. Large and widely distributed glaciers are an important component of surface water resources and glacier runoff provides precious freshwater for arid and semi-arid regions in western China(Jansson and Hock, 2003; Yang, 1991) . Glacier runoff significantly affects catchment hydrology by temporarily storing and releasing water on various time scales(Braithwaite and Zhang, 2000;Liuet al., 1998). The permafrost, as an impermeable substrate, affects hydrological processes and leads directly to large surface streamflow and less groundwater(Kane and Yang, 2004). Permafrost degradation has been caused by regional climate warming over the last several decades, and has enhanced winter river discharge. Investigations on the hydrological effect of the permafrost degradation are therefore important for predicting future streamflow changes in these cold regions.
The earlier snow melting occurred and results in increase discharge in spring in most rivers with snow cover. Our research are mostly focused on the effect of glacier, permafrost and snow cover change on the hydrology during 2005-2010. Some results are summered:

1． Glacier runoff

All observed and modeling result show that the glacier runoff has been increased obvious in west China in past decades due to glacier shrinking caused by climate warming. The glacier increased enhanced river discharge increase or weaken the discharge decrease.

1.1 Observed results

a. The Urumqi River source Glacier No. 1 in Tianshan
The long-term observed results over the past 45 years (1959-2004) in Urumqi River source region, the Tianshan Mountains of China show that summer temperature and annual precipitation near the glacier increased by 0.8℃ and 87 mm (19%), respectively. The glacier continuously retreated from 1962 to 2003, with the cumulated mass balance being -10,032 mm, or 20% of the glacier volume. Annual basin runoff has significantly increased by 413 mm or 62% during 1980–2003 due to precipitation increase and enhanced glacier melt caused by summer climate warming. Both summer precipitation and temperate are negatively correlated with mass balance and positively associated with runoff. Relative to precipitation mass balance relation, the regression between temperature and mass balance is much stronger, indicating that summer temperature controls glacier mass balance and runoff changes. A 1℃ increase in summer temperature leads to an increase of 486 mm glacier mass loss (Fig 3.1) (Ye et al., 2005). The annual glacial runoff calculated at the Urumqi glacier No. 1 hydrometeorological station has increased by 145.5×10^4 m^3 a^{-1}, a factor of 2, over the 48-year span from 1959 to 2006. A significant increase in runoff occurred after 1985, particularly after 1995 due to an increase in both temperature and precipitation in the area (Li et al., 2010).

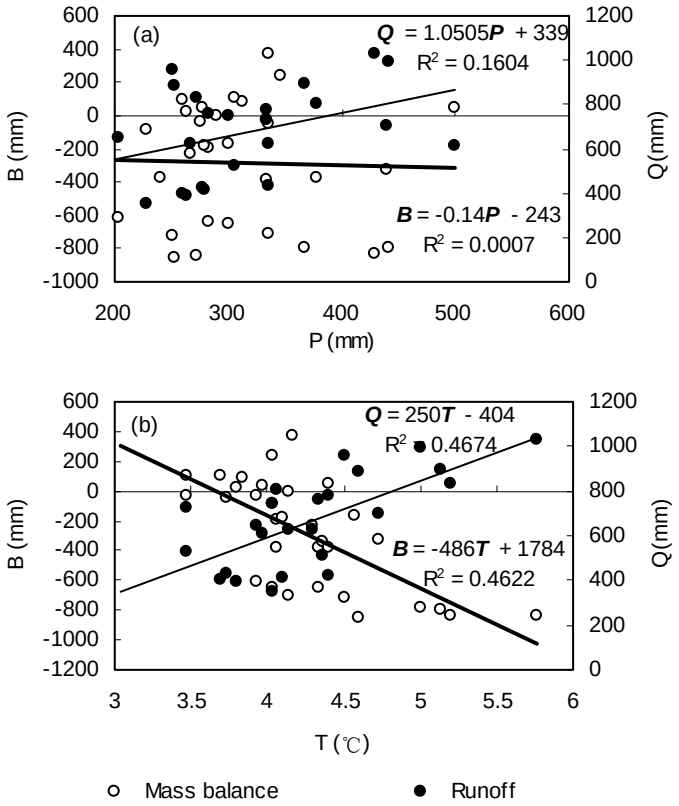

Fig 3.1. Regression relationships of summer temperature (T) and precipitation (P) vs. mass balance (B) and runoff (Q) during 1959–1966 and 1980–2003 (Ye et al., 2005)

b. The Glaciers in on Mt. Hengduan and Baishui glacier No.1 on Yulong

Ablation is heavy in the glacier tongue areas, and the mean ablation water equivalent in Hailuogou glacier in Sichuan during 1990/91–1997/98 was 876 mm more than that in 1982/83. Ablation depth on the exposed ice area increased by 1.4 m/a over the period 1983/84–1990/91. Mass balance records also show that glaciers suffered a constant mass loss of snow and ice, and the accumulated mass balance in Hailuogou basin and Baishui glacier No.1 was -10.83 mwater equivalent in the past 45 years, and -11.38 m in the past 52 years. Local hydrological and climatic data demonstrated that, in Yanggong basin during 1979–2003 and Hailuogou basin during 1988–2004, runoff from the glacier areas has been increasing both seasonally and annually. Overall, it is clear that China's monsoonal temperate glaciers are losing mass and are retreating under the background of climate warming (Li et al., 2010). The Hailuogou glacier area subject to melting has increased and the ablation season **has become longer due to the warming, the ablation of glacier enhanced, leading to increasing contribution of meltwater to annual river discharge (Pang et al., 2010).**

c. Rongbuk Glacier in Mt. Qomolangma Region

The discharge of the Rongbuk Glacier catchment from 8 April to 11 October in 2005 shows a time lag ranging from 8 to 14 hours between daily discharge peaks and maximum melting (maximum temperature). Compared with the discharge data in 1959, the runoff in 2005 was much more, and the runoff in June, July and August increased by 69%, 35% and 14%, respectively. The rising of temperature is a major factor causing the increase in runoff. The discharge induced by precipitation accounts for about 20% of the total runoff, while snow and ice melting for about 80% (Liu, et al., 2010).

d. Keqikaer glacier, south slope of Tuomuer mountain

There is large lag time in the lag time in Keqikaer glacier, south slope of Tuomuer mountain. The lag time is exceeds 1 day in May and September but falls short of 1 day in other months, and it decreases from May to August, but increases in September (Xie et al., 2006). The degree-day model results show that under the warming and wetting scenario, the primary supply for the runoff in Keqikaer basin is glacier meltwater, with precipitation being the dominant secondary source; 84% and 8% of total runoff, respectively (Zhang et al., 20061). Also, the artificial neural networks has been used to simulate meltwater runoff of Keqikaer

Glacier (Chen and Ding 2009). The effect of change in temperature is much more noticeable than that for change in precipitation (Zhang et al., 2007a)

e. Zhadang Glacier in Nyainqêntanglha Rang

2007/2008 observation in the Zhadang Glacier located on the northern slope of e, Tibet, indicates precipitation increased by 17.9% in summer months of 2008 compared with the same period in 2007, drainage basin runoff decreased by 33.3%, and glacial meltwater decreased by 53.8%. Change in positive accumulated air temperature explained approximately half of the inter-annual difference in glacial meltwater using a degree-day model. This suggests that the glacier is extremely sensitive to changes in air temperature. Energy balance analysis showed that change in glacier surface albedo, considered to be caused by difference in precipitation form, resulted in the large inter-annual difference in glacial meltwater. It was shown statistically that precipitation form in the summer months of 2007 was mainly rainfall which comprised 71.5% of total precipitation, while during the same period in 2008 rainfall accounted for 30.7%, with the majority of precipitation falling as snow. Precipitation form should be considered an independent factor when analyzing glacier sensitivity to climate change or forecasting the runoff from certain glaciers.

1.2 Glacier runoff change in typical basins

The degree-day model is widely used for glacier ablation. The degree-day factor (DDF) is an important parameter for the degree-day model, which is a widely used method for ice- and snowmelt computation. The spatial variations of the DDF varied among 2.6 and 13.8 mm/d/℃ with mean of 7.113.8 mm/d/℃ for ice and between 3.1-5.9 mm/d/℃ with 4.1 mm/d/℃ for snow over China. the DDF for a single glacier is subject to significant small-scale variations, and the factor for maritime glaciers is higher than that for subcontinental and extremely continental glaciers (Zhang et al. 2006b). The model has been used to calculate the glacier runoff for basin scale in China.

.a. the Yangtze River source

Most of the glaciers in the Tuotuo River basin, western China has retreated in the period from 1968/1971 to 2001/2002, and their shrinkage area is 3.2% of the total area in the late 1960s. As a result, glacier runoff has increased in the last 44 years, especially in the 1990s when a twothirds increase in river runoff was derived from the increase in glacier runoff caused by loss of ice mass in the entire Tuotuo River basin. (Zhang et al., 2007b). Glacier runoff from the Yangtze River source region ()at Zhimenda gauge station (YRSR), China, is estimated for the period 1961–2000 using a degree-day approach. In the investigation area, glacier runoff accounts for 11.0% of the total river runoff during the period 1961–2000. In the 1990s its contribution to river runoff rises to 17.0%. Due to the current rate of glacier decline, the impact of glacier runoff on river runoff has recently increased in the source region (Fig 3.2). The glacier runoff also has been projected using the GCM scenario output (Liu, et al., 2009).

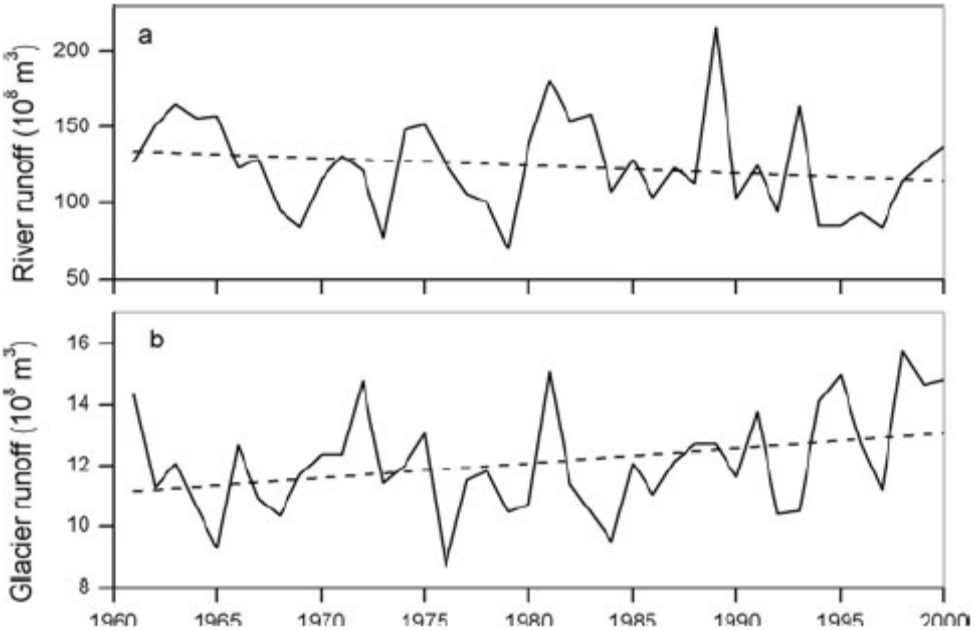

Fig 3.2. Variation in annual river runoff (a) and glacier runoff (b) of the YRSR for the climatic normal period 1961–2000. Dashed

lines are regression lines indicating trend(Liu et al., 2009).

b. the Tarim River Basin (TRB)

The degree-day model simulated the glacier ablation and runoff over Tarim River basin. The result shows mean annual glacier mass balance during 1961–2006 was −139.2 mm per year and the cumulative mass balance over the 46 year period was −6.4 m in the TRB. The average annual glacier runoff in the TRB was 144.16×10^8 m^3 for 1961–2006. The results also show that glacier runoff has increased in the last 46 years, especially since the 1990s with 85.7% of the increased river flow being derived from the increased glacier runoff caused by loss of ice mass. Over the entire TRB, glacier runoff accounts for 41.5% of the total river flow during 1961–2006. The impact of glacier runoff on river flow has increased in the TRB as a result of glacier shrinkage (Fig 3.3) (Gao et al., 2010).

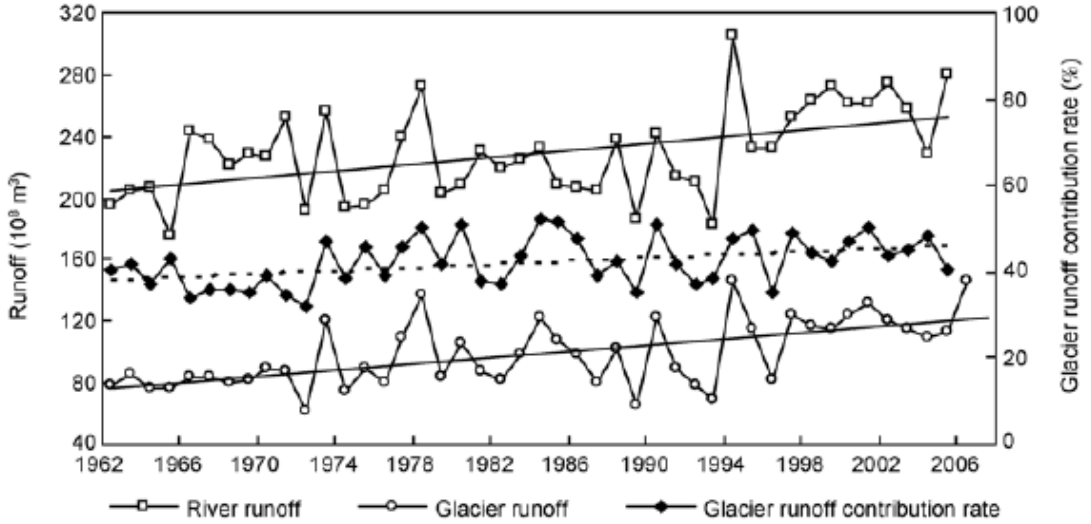

Fig 3.3 Variations in annual river flow, glacier runoff and the contribution of glacier runoff to river flow at four source rivers in the TRB during 1961–2006. The solid lines are the linear trend in river flow and glacier runoff, and the dotted line is the linear trend in the contribution of glacier runoff to river flow (Gao et al., 2010).

2． Snowmelting

2.1 variation of snow depth and runoff

Spatio-temporal variation of snow depth in the Tarim River basin has been studied by the empirical orthogonal function (EOF) based on the data collected by special sensor microwave/imager (SSM/I) and scanning multichannel microwave radiometer (SMMR) during the period from 1979 to 2005. The long-term trend of snow depth was significant in the northwestern, western and southern parts of the basin, whereas the long-term trend of runoff was significant in the northwestern and northeastern parts. The regression analysis revealed that the runoff of the rivers replenished by snow melt water and rainfall was related primarily to the summer precipitation, followed by the summer temperature or the maximum snow depth in the cold season. Our results suggest that snow is not the principal factor that contributes to the runoff increase in headstreams, although there was a slow increase in snow depth. It is the climatic factors that are responsible for the steady and continuous water increase in the headstreams (2009).

2.1 Snowmetling forecast

The Weather Research and Forecasting (WRF) modelling system and the Distributed Hydrology Soil Vegetation Model (DHSVM) to forecast snowmelt runoff has been coupled and used to forecast the snowmelt runoff. In this study, a limited-region 24-h Numeric Weather Forecasting System was formulated using the new generation atmospheric model system WRF with the initial fields and lateral boundaries forced by Chinese T213L31 model. Using the WRF forecasts, the DHSVM hydrological model was used to predict 24 h snowmelt runoff at the outlet of the Juntanghu watershed. Forecasted results showed a good similarity to the observed data, and the average relative error of maximum runoff simulation was less than 15%. The results demonstrate the potential of using a meso-microscale snowmelt runoff forecasting model for forecasting floods. The model provides a longer forecast period compared with traditional models such as those based on rain gauges or statistical forecasting (Zhao et al., 2009).

3．Hydrology in Permafrost regions

3.1 hydrological regime and permafrost coverage in basin

The ratios of monthly maximum/minimum flows directly reflect discharge regimes. There is a significant positive relationship between the ratio and basin permafrost coverage. This relationship indicates that permafrost condition does not significantly affect streamflow regime over the low permafrost (less than 40%) regions, and it strongly affects discharge regime for regions with high permafrost (Fig 3.4) (greater than 60%) (Ye et al., 2009).

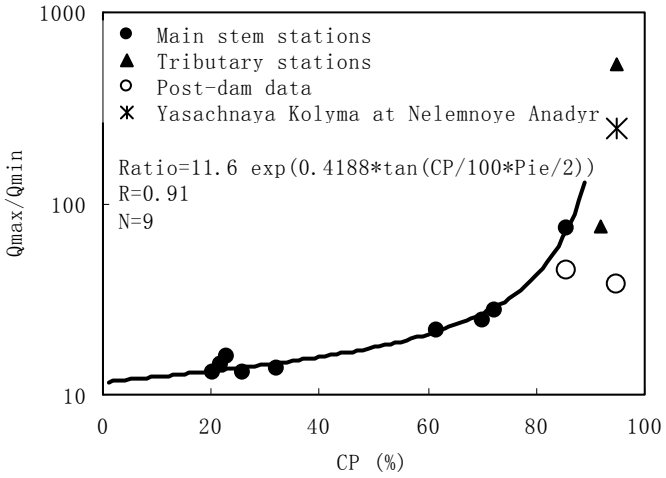

Fig 3.4. The ratios of Qmax/Qmin versus coverage of permafrost (CP) at the nine stations from the upper Lena to basin outlet without reservoir regulation. Two additional stations (the Aldan and Vilui subbasins in Lena basin) and one additional basin (the Yasachnaya Kolyma River) in East Siberian are also shown. The ratios of Qmax/Qmin are showed at the Vilui subbasin and Kusur at Lena basin outlet with reservoir regulation since 1967. Note: the Y axis is in logarithm scale.

3.2 Hydrological parameters change in basin with permafrost

The hydrological process in typical basins with various permafrost coverage (between 33%- 73%) in northwestern China shows that the monthly recession coefficient (RC) in winter has increased obviously for the Shule and Heihe rivers to 73% and 58% permafrost coverage, respectively, but did not increase for the Shiyang River, and decreased insignificantly for the upper Yellow River, which had less permafrost coverage. There is a distinct positive relationship between RC and annual negative degree-day temperature (NDDT) at the meteorological stations in the basins with high permafrost coverage. These results imply that permafrost degradation due to climate warming affects hydrological processes in winter. The effect is obvious in the basins with high permafrost coverage but negligible in those with low permafrost coverage. Permafrost degradation increases infiltration, enlarges the groundwater reservoir, and leads to slow discharge recession. The result means that hydrological processes are affected strongly by permafrost degradation in river basins with high permafrost coverage, but less in river basins with less permafrost coverage (Niu, 2010). Also, The statistically significant trends in basin hydrological regime has been detected in northwest China for the period 1957–2004 included strong increases in winter air temperatures and winter monthly flows (December to March) (Liu et al., 2007). A monthly-scale spatial-distributed hydrological model with consideration of snow and permafrost has been developed. The simulated result in upper Yangtze River (Zhang et al., 2006).

4．Bias-correction of precipitation over China

Ye et al (2004) carried out bias corrections of Chinese standard precipitation gauge (CSPG) measurements for wind-induced undercatch, a trace amount of precipitation, and wetting loss for the long-term daily data of precipitation, temperature, and wind speed during 1951–98 at 710 meteorological stations in China. They reported that wind-induced gauge undercatch is the greatest error in most regions, and wetting loss and a trace amount of precipitation are important in the low-precipitation regions in northwest China. Monthly correction factors ratio of corrected amount to measured amount of precipitation differ by location and by type of precipitation. Considerable

interannual variation of the corrections exists in China due to the fluctuations of wind speed and frequency of precipitation. More importantly, annual precipitation has been increased by 8 to 740 mm with an overall mean of 130 mm at the 710 stations over China because of the bias corrections for the study period. This corresponds to 6%–62% increases (overall mean of 19% at the 710 stations over China) in gauge-measured yearly total precipitation over China. This important finding clearly suggests that annual precipitation in China is much higher than previously reported. The results of their study are useful to hydrological and climatic research and application in China.

To determine the impact of bias corrections on monthly and yearly precipitation trends, Ding et al., (2007) analysed long–term monthly climatic data during 1951-1998 at 627 meteorological stations over China. Their analyses show that bias corrections have changed monthly and yearly precipitation trend direction from positive to negative over some regions in China. The trend changes are large enough to affect regional climate and hydrology analyses, particularly over cold regions. They recommend more efforts to quantify the impact of bias corrections on precipitation change analyses over other large countries and regions.

5. Glacier lake

5.1 Lake with glacier supply

The all lake area in Nam Co catchments has been extended in Nam Co Catchment from 1070s-2000s, meanwhile the glacier are in retreating (Fig 3.5). This indicate the lakes supplied by glacier have been extended during last 40a due to glacier retreat/mass losses caused by the climate warming(Yao et al., 2010)

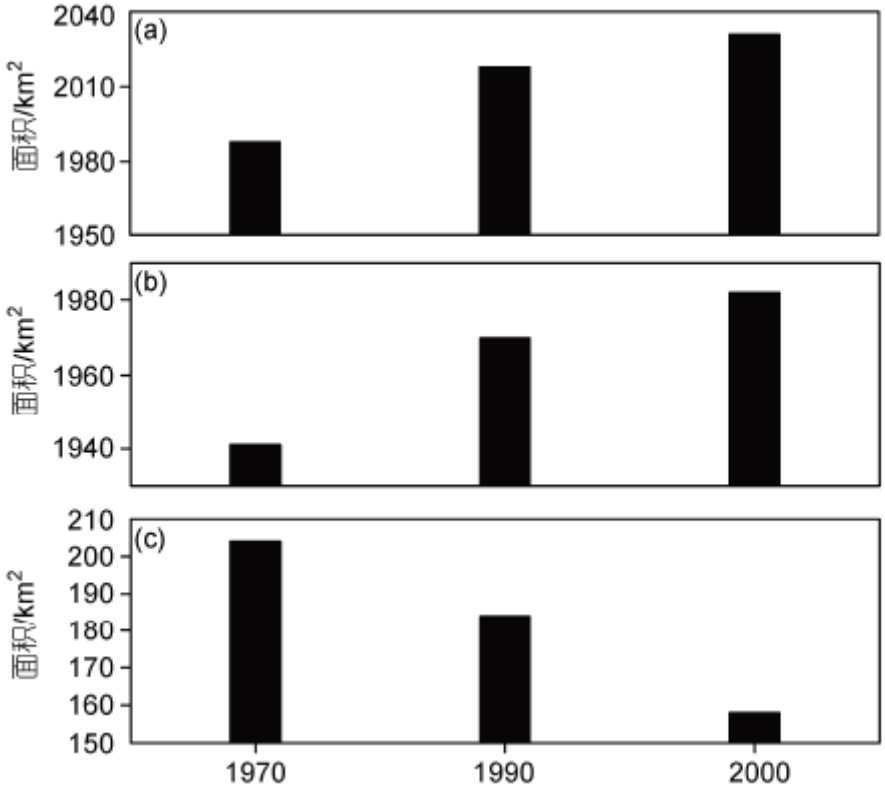

Fig. 5 The areas of (a) all lakes, (b) Nam Co Catchment and (c) Glacier area in different decades in Nam Co Catchment from 1070s-2000s (Yao et al., 2010)

5.2 Outburst floods of glacier lake

The thermo-mechanical modelling has been successfully used to interpret a 40-year flood record from Merzbacher Lake in the Tian Shan. We show that the mean air temperature during each flood modulates its peak discharge, by influencing both the rate of meltwater input to the lake as it drains, and the lake-water temperature. The flood devastation potential thus depends sensitively on weather,

and this dependence explains how regional climatic warming drives the rising trend of peak discharges in our dataset. For other subaerial ice-dammed lakes worldwide, regional warming will also promote higher-impact of subglacial outburst floods by raising the likelihood of warm weather during their occurrence, unless other factors reduce lake volumes at flood initiation to outweigh this effect (Fig 3.6) (Ng et al., 2007).

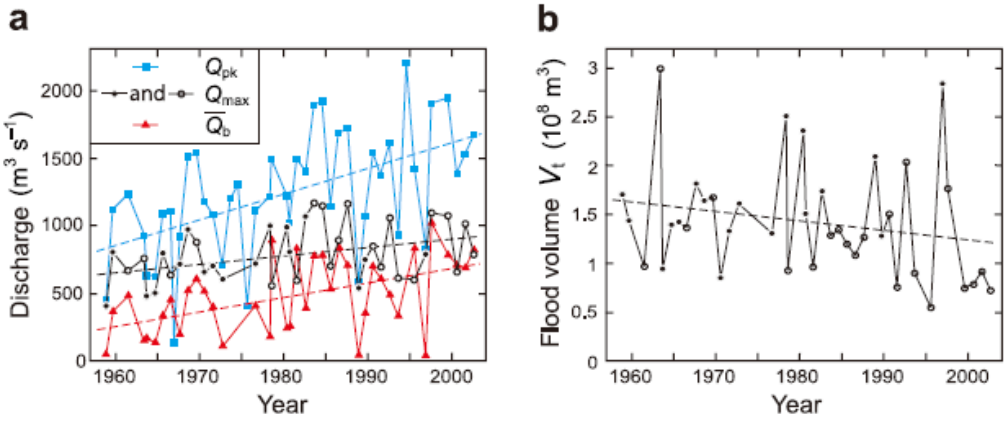

Fig 3.6. Merzbacher flood characteristics from 1958 to 2002. (a) Xiehela peak discharge Q_{pk}, mean Xiehela base flow Q_b, and flood peak discharge Q_{max}. Linear trends for Q_{pk}, Q_b, Qmax are +19.0, +10.5, +6.2 m^3/s/yr, respectively. (b) Flood volume V_t; linear trend -1.0×10^6 m^3/yr (Ng et al., 2007).

1) Braithwaite R J, Zhang Y. Sensitivity of mass balance of five Swiss glaciers to temperature changes assessed by tuning a degree-day model. J Glaciol, 2000, 46: 7–14
2) Ding Y, Yang D, Ye B, Wang N, 2007. Effects of bias correction on precipitation trend over China. J. Geophys. Res., 112: D13116. doi:10.1029/2006JD007938.
3) Gao X, Ye B S, Zhang S Q, et al. Glacier runoff variation and its influence on river runoff during 1961–2006 in the Tarim River Basin, China. Sci China Earth Sci, 2010, 53: 880–891, doi: 10.1007/s11430-010-0073-4
4) He Yuanqing, Pu Tao, 138 Li Zongxing, Zhu Guofeng, Wang Shijin, Zhang Ningning, Wang Shuxin, Xin Huijuan, et al., 2010, Climate Change and Its Effect on Annual Runoff in Lijiang Basin-Mt. Yulong Region, China, Journal of Earth Science, 21(2):137–147, DOI: 10.1007/s12583-010-0012-5
5) Jansson P, Hock R, Schneider T. The concept of glacier storage: A review. J Hydrol, 2003, 282: 116–129
6) Kane, D. L., and D. Yang (2004), Overview for Water Balance Determinations for High Latitude Watersheds. In Northern Research Basins Water Balance (Edited by Douglas L. Kane and Daqing Yang), Int. Assoc. of Hydrological Sciences Publication 290. 1-12.
7) Laumann T, Reeh N. Sensitivity to climate change of the mass balance of glaciers in southern Norway. J Glaciol, 1993, 39: 635–665
8) Li Z., W. Wang, M. Zhang, F. Wang and H. Li, 2010, Observed changes in streamflow at the headwaters of the Urumqi River, eastern Tianshan, central Asia, HYDROLOGICAL PROCESSES Hydrol. Process. 24, 217–224.
9) Li, Zongxing, He Yuanqing, Pu Tao, Jia Wenxiong, He Xianzhong, Pang Hongxi, Zhang Ningning, Liu Qiao, Wang Shijing, Zhu Guofeng, Wang Shuxin, Chang Li, Du Jiankuo, Xin Huijuan，2010，Changes of climate, glaciers and runoff in China’s monsoonal temperate glacier region during the last several decades，Quaternary International， 218 13–28
10) Liu Jingshi, Siyuan Wang, and Yuying Huang, 2007, Effect of Climate Change on Runoff in a Basin with Mountain Permafrost, Northwest China, Permafrost and Periglac. Process. 18: 369–377
11) Liu S Y, Ding Y J, Wang N L et al. Mass balance sensitivity to climate change of the Glacier No. 1 at the Urumqi River Head, Tianshan Mts. (in Chinese). J Glaciol Geocryol, 1998, 20: 9–13
12) Liu, SY; Zhang, Y; Zhang, YS, et al., 2009, Estimation of glacier runoff and future trends in the Yangtze River source region, China, Journal of Glaciology, 55(190): 353-362
13) LIU, Weigang, REN Jiawen, QIN Xiang, LIU Jingshi, LIU Qiang, CUI Xiaoqing and WANG Yetang，2010，Hydrological Characteristics of the Rongbuk Glacier Catchment in Mt. Qomolangma Region in the Central Himalayas, China，J. Mt. Sci. ，7: 146–156
14) Ng, F., S. Liu, B. Mavlyudov, and Y. Wang (2007), Climatic control on the peak discharge of glacier outburst floods, Geophys. Res. Lett., 34, L21503, doi:10.1029/ 2007GL031426.
15) Niu L, Ye B S, Li J, et al. Effect of permafrost degradation on hydrological processes in typical basins with varying permafrost coverage in Western China. Sci China Earth Sci, 2010, 53: 1–10, doi: 10.1007/s11430-010-4073-1
16) Pang, Hongxi, He Yuanqing, Zhang Ningning, Li Zongxing, Wilfred H Theakstone, 2010, Observed Glaciohydrological Changes in China’s Typical Monsoonal Temperate Glacier Region since 1980s Journal of Earth Science, 21(2): 179–188
17) Xie Changwei, Yongjian Ding, Shiyin Liu, Response of meltwater runoff to air-temperature fluctuations on Keqikaer glacier, south slope of Tuomuer mountain, western China, Annals of Glaciogy, 2006, 43(1): 275-279.
18) Xu, CC; Chen, YN; Hamid, Y, et al., 2009, Long-term change of seasonal snow cover and its effects on river runoff in the Tarim River basin, northwestern China, Hydrol. Process. 23, 2045–2055

19) Yao T., Z. Li, W. Yang, X. Guo, L Zhu, S. Kang, H Wu., and W Wu, 2010, the glacier distribution, mass balance characteristics and their on the lakes in Yaluzangbu River Basin, Chinese Science Bulletin, (in Press)
20) Ye, B., D. Yang, K. Jiao, T. Han, Z. Jin, H. Yang, and Z. Li (2005), The Urumqi River source Glacier No. 1, Tianshan, China: Changes over the past 45 years, Geophys. Res. Lett., 32, L21504, doi:10.1029/2005GL024178.
21) Ye, B., D. Yang, Z. Zhang, and D. L. Kane (2009), Variation of hydrological regime with permafrost coverage over Lena Basin in Siberia, J. Geophys. Res., 114, D07102, doi:10.1029/2008JD010537.
22) Ye B, Yang D, Ding Y, Han TD, Toshio Koike, 2004. A bias-corrected precipitation climatology for China. J. of Hydrometeorology, 5(6): 1147–1160.
23) Zhang Yong, Liu Shiyin, Xie Changwei, Ding Yongjian, 2006a，Application of a degree-day model for the determination of contributions to glacier meltwater and runoff near Keqicar Baqi Glacier, southwest Tianshan Mountains. Annals of Glaciology, 43:280-284
24) Zhang Yong, Shiyin Liu, Yongjian Ding, 2006b, Observed degree-day factors and their spatial variation on glaciers in western China, Annals of Glaciology, 43: 301-306
25) Zhang Yong , Shiyin Liu, Junli Xu, Donghui Shangguan, 2007b, Glacier change and glacier runoff variation in the Tuotuo River basin, the source region of Yangtze River in western China, Environ Geol (2008) 56:59–68 DOI 10.1007/s00254-007-1139-2
26) ZHANG Yong, LIU Shiyin, DING Yongjian, 2007a,Glacier meltwater and runoff modelling, Keqicar Baqi glacier, southwestern Tien Shan, China, Journal of Glaciology, 53(180):91-98.
27) Zhang shiqiang, Ding yongjian, Ye Baisheng, 2006, The monthly discharge simulation/construction on upper Yangtze River with absent or poor data Coverage, Liu Zhiyu & Yang Dawen edit, Proceedings of the international symposium on flood forecasting and water resources assessment for IAHS-PUB,324-333Chen Caiping and Ding Yongjian, The application of artificial neural networks to simulate meltwater runoff of Keqikaer Glacier, south slope of Mt. Tuomuer, western China, Environ Geol (2009) 57:1839–1845, DOI 10.1007/s00254-008-1471-1
28) Zhao Q., Z. Liu, B. Ye, Y. Qin, Z.Wei and S. Fang, 2009, snowmelt runoff forecasting model coupling WRF and DHSVM, Hydrol. Earth Syst. Sci., 13, 1897–1906.
29) Zhou S Q, Kang S C, Gao T G, et al. 2010, Response of Zhadang Glacier runoff in Nam Co Basin, Tibet, to changes in air temperature and precipitation form. Chinese Sci Bull, 55: 2103−2110, doi: 10.1007/s11434-010-3290-5

Chapter 4. Ecology in Cold Regions

WANG Genxu[1] and ZHAO Xinquan[2]

1. Institute of Mountain Hazards and Environment, Chinese Academy of Sciences, Chengdu, 610041, China;

2. Northwest Institute of Plateau Biology, Chinese Academy of Sciences, Xining, 810008, China

Abstract: During 2008-2010, Professional working group of cold area ecology undertook the research works including the experiment for alpine ecosystems response to climate changes and snow pack changes, the soil seed banks and the rehabilitation of engineering area in permafrost region, the ecosystem evolution processes and its mechanism in proglacier region, and water-thermal coupling processes in the air-vegetation-permafrost system and the water cycle in frozen soil-ecosystem. The advancing results of variation in vegetation forms and root systems, the changes of vegetation community coverage and biomass, and the variation in carbon and nitrogen pools of alpine ecosystems under effects of temperature enhancement have improved the understanding in alpine ecosystems' response to climate change. We also obtained some new advances in the impacts of snowpack changes on alpine ecosystems, the interactions between soil thermal and hydrological dynamics in the response of alpine meadow to vegetation cover changes, the effects of grazing on alpine grassland production and community construction, the features of alpine ecosystem distribution in permafrost region and the assessment on vegetation restoration capacity of several grassland ecosystems under destroyed disturbance in permafrost regions. Some results are summered.

1. Responses of High-cold ecosystem to global change

1.1 Changes in the distribution pattern of High-cold ecosystem

It was about 642 pieces of literatures related that could be retrieved since 1990, and 92% of which were focused on the source areas of The Yellow River and the Yangtze River. So the advances and current state of the research are summarized mainly in the source region of the two rivers.

（1）Distribution pattern process of the High-cold ecosystem

As is shown in Fig 4.1, the areas of high covering meadows (the coverage is bigger than 70) in the source areas of The Yangtze River has been decreased by 16.4% in 40 years since 1967, especially by 11.3% between 1986 and 2000; whereas low covering meadows has been increased by 12.6%. Especially by 21.2% between 1986 and 2000; yet, low covering meadows has been increased by 39.3%. The whole area of the alpine meadow grassland has been decreased by 19.5%, whereas low covering meadows has been increased by 17.4%. The areas of high covering grasslands in the source areas of The Yellow River has been decreased by 7.9%,including 5.5% between 1986 and 2000,and the areas of low covering grassland increased by 2.0%. In the meantime, The areas of high covering grasslands in the source areas of The Yellow River has also been decreased by 6.8%,including 3.5% between 1986 and 2000,and the areas of low covering grassland increased by 1.63% also. To sum up, the areas of high covering grasslands in the Yangtze-Yellow rivers source region has been decreased by 8.6%, whereas the areas of low covering grassland has been increased by 3.2%.

Swampy meadow in headwater area is one kind of the most serious degenerate ecosystem, for its area sharply decreased by 32.1%. The areas of swampy meadow in the headwater region of The Yangtze River have been sharply decreased by 37.3%, especially 27.3% between 1986 and 2000.meanwhile, the areas in the headwater region of The Yellow River have been decreased by 18.6%, and 13.1% for years between 1986 and 2000.

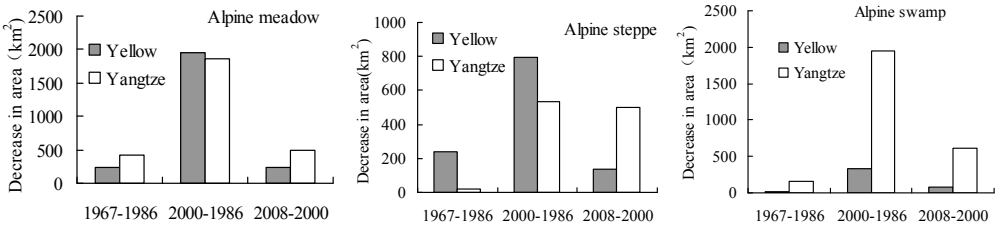

Fig 4.1 The spatial distribution area changes of the alpine ecosystems in the source regions of Yangtze and Yellow river

The continued degradation of the high-cold ecosystems is a urgent issue in the headwater areas, and the basic tendency are: alpine marsh→alpine Meadows→low covering meadows→alpine steppe meadow or the "black barren"; high covering alpine grasslands →low covering grasslands→desertification grassland or sandy land.

1.2 Changes in composition of high-cold ecosystem

The degenerations of meadows and grasslands in typical alpine regions are also characterized by its changes in community composition structure. After the seriously deterioration of alpine meadow and grassland, Communities with grassy vegetation as its dominant and constructive species were developed, accompanying with the gradually disappearance of kobresia species. Among the processes from alpine grassland to desertification grassland, there is an important tendency that is Carex moorcroftii (C.moorcroftii Falc.ex Boott) grasslands are usually developed from former Stipa purpurea grasslands, with coenotype also changed. The decrease of good herbages and Biodiversity Characteristics is one of the direct results of the variations of the community structure which is mentioned above.

1.3 The response mechanism of alpine ecosystems to climate change

(1) The response mechanism and adaption of alpine meadow vegetation to ultraviolet radiation increase and intense light

Ultraviolet radiation addition could significantly increase leaf thickness of the alpine meadow vegetation and change the foliage phenology, but photosynthetic pigments and photosynthetic rate are not changed significantly. Therefore plant photosynthesis and matter production shall not be affected (Shi et al.2004).

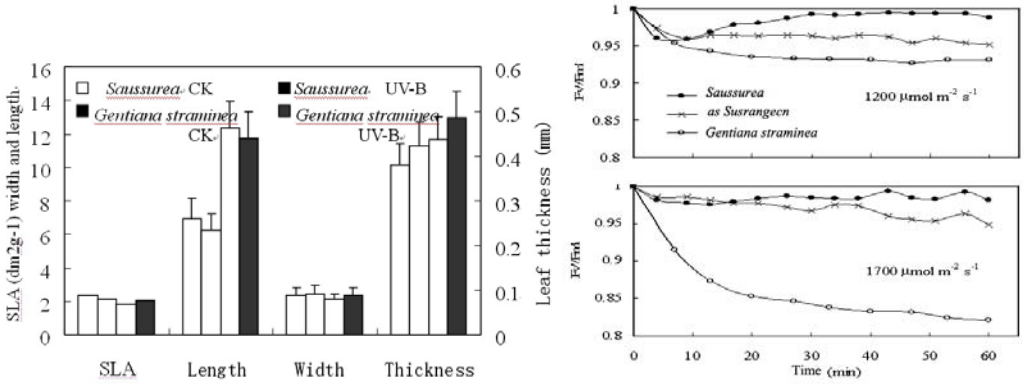

Fig 4.2 Response of alpine ecosystems to dynamic light and long-term enhancement of UV-B radiation in Qinghai-Tibet Plateau

With higher light saturation point, alpine meadow vegetation would better adapt to intense light stress. in strong light, low plants with flat leaves would rely on its higher photochemical properties to enhance its photorespiration rate and prevent photic injury under hard light, however it would reduce net carbon fixation of leaves; plants with upright leaves prevent photic injury by heat dissipation.

(2) The effect of warming on biodiversity of alpine meadow

Experimental warming would cause the biodiversity decrease quickly, and moderated grazing could cushion the negative impact of warming. There has a consistency among different vegetation in high-cold areas. Plants with deep roots have better adaptability for experimental warming. On the contrary, plants with shallow root lost much of its species in warming experiment.

The biomass is greater in warming experiment than in the control plot in early years, but somewhat decreased after the 5th year. Graminaceous plants species increased under warming conditions, but weeds species decreased. On the surface, warming can prolong growth period of plants and be helpful to biomass increase. Unfortunately it was not as seemed. In fact , The growing speed of a plant was accelerated under warming, and mature period moved up, so the growth period shortened and the effect of the daily range of temperature to dry matter yield was weakened, and vegetation biomass decreased insteadly (Klein et al. 2004,2007).

2. Energy-water cycle of alpine ecosystem and its impacts

2.1 The influence of vegetation coverage change on surface energy budgets in alpine meadow

The results show that the surface energy budgets are affected prominently by the land cover change in

alpine meadow. The higher coverage in alpine meadow, the bigger latent heat flux in rainy season could be observed, and also the bigger sensible heat flux in dry season; the higher coverage in alpine meadow, the bigger geothermal heat flow upward in winter. Owing to some reasons just like the land cover change in alpine meadow, geothermal heat flow upward presented a consistently decline trend in the past 15 years(Wang et al., 2008; Hu et al., 2008).

2.2 Influence of Vegetation Coverage change on Water and Heat Processes of the Active Layer

The dates of seasonally frozen soil beginning to freeze and permafrost beginning to thaw have become significantly earlier than as usual with the reduction of vegetation coverage, and the frozen and freeze durations shorten obviously. The maximum invasion depth and duration of minus isotherm in the freezing period and positive isotherm in non-freezing period increased with the decrease of the vegetation coverage(Wang et al., 2008; Hu et al., 2008).

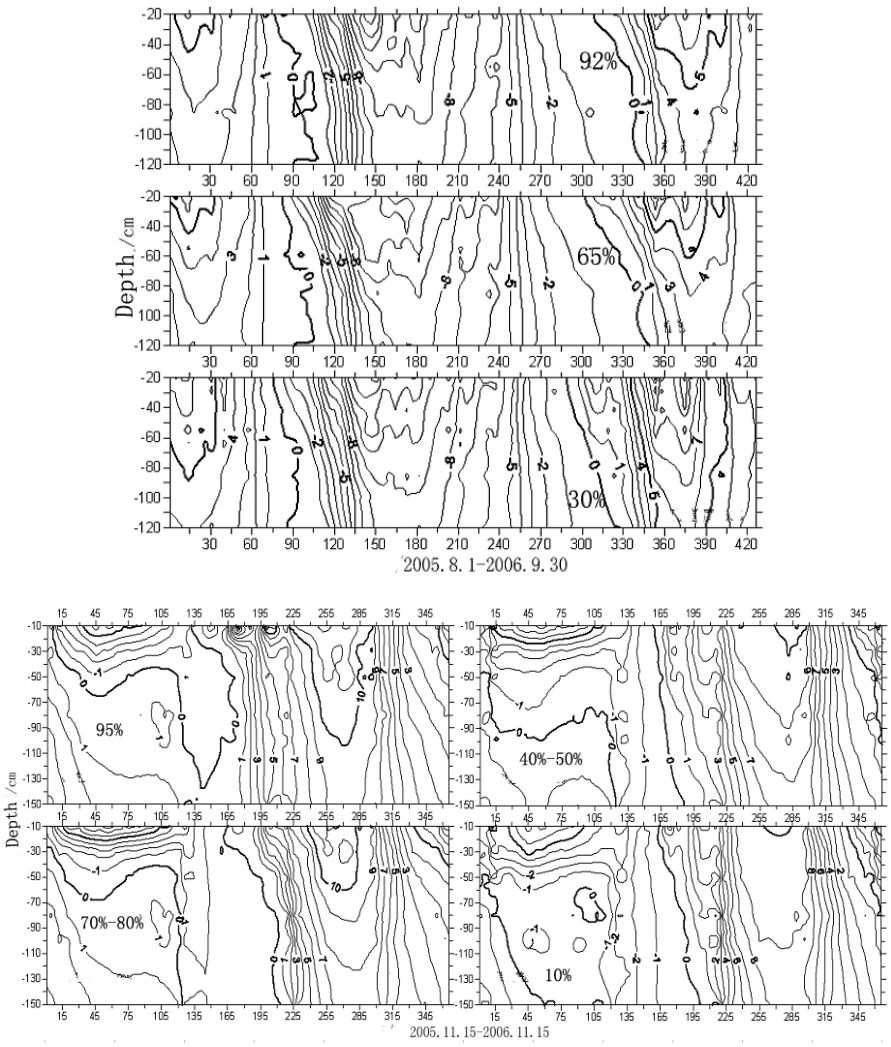

Fig 4.3 Impacts of vegetation cover variation on soil temperature in permafrost and season freezing regions

With the decrease of vegetation coverage, the response of soil moisture to temperature became stronger, and response time started earlier than before, and also the variation rate of soil moisture increased in entire active layer(0—1.2m) with the increase of variations of thawing and uplift rate among different layers. “dry layer” phenomena was detected in active layer of alpine meadow, which was significantly drying with the increase of vegetation coverage, and its drying degree was also changed along with the rainfall.

The ground temperature and time of soil moisture s’ freeze and thawing are different if the vegetation

coverage of alpine meadow is different; along with the increase of vegetation coverage, thawing temperature of soil water dropped but freeze temperature raised.

2.3 Coupled heat-moisture mode of soil under different vegetation coverage in alpine meadow

Soil freeze process: $T_s = ST_c + A_c \Big/ \left[1 + \exp\left(\theta_0 - \theta_v\right) \Big/ B_c\right]$

Coupled heat-moisture mode of soil is similar among grasslands with different coverage, only the parameters may be different.

Soil thawing process:

(1) If the coverage is equal or greater than 65%:

$$T_s = ST_c + \left[A_c \times Ln\left(\theta_v - \theta_0\right)\right]$$

This formula is in accordance with the mode acquired by Xuezu Xu in laboratory experiment.

(2) if the coverage is equal or smaller than 30%:

$$T_s = ST_c + A_c\theta_v \Big/ \left(\theta_v + \theta_0\right)$$

3. Engineering activity & conservation and reconstruction of degraded ecosystem

3.1 Ecological process and capacities of natural recovery of vegetation in engineering slash (Chen et al.,2008; Wang et al.,2007)

Ecological processes of natural recovery of alpine steppe vegetation in the engineering destroy sites is shown in Fig 4.4, from that we can concluded that indexes such as composition structure of community, coverage and biodiversity are almost the same to or even greater than natural control plot in the engineering destroy sites in 1980s and 1070s.

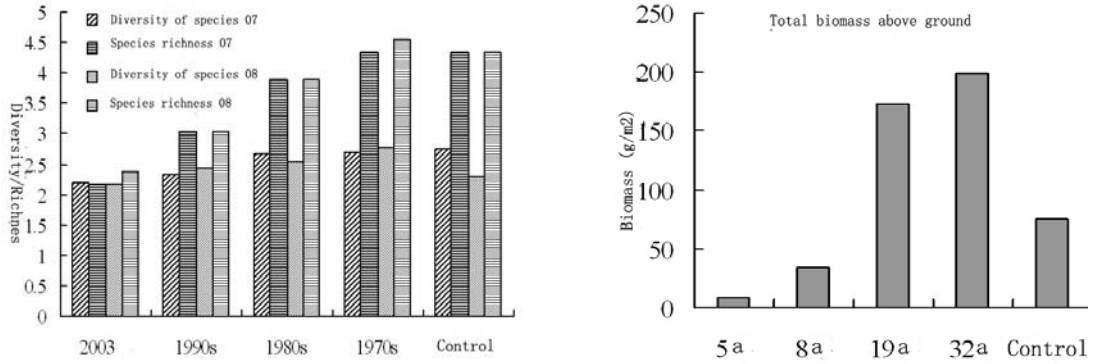

Fig 4.4 Compare on ecological processes under different resume time of alpine steppe in the engineering destroy sites

In addition, recovered community biomass of the engineering destroy sites is significantly greater than natural control plots in 1980s and 1970s, but the biomass of Gramineae (Poaceae) plants and leguminous plants is significantly smaller than control plot, which have stabilized colonization significance. Although vegetation recovery witnessed some favourable trends in 20-30 years afterwards, community structure and community composition have not yet reached its original standards.

As to alpine meadow, the vegetation recovery process in engineering slash is slower than alpine grasslands, whether from the point of coverage, biomass, biodiversity or community composition and structure. The difference between vegetation community in engineering slash and control plots is obvious relatively, reflecting natural recovering capacities of alpine meadow is lower than alpine grassland.

3.2 The evolutionary process of soil seed bank in degraded ecosystem (Chen et al. 2008; Zhou, et al. 2010)

Soil seed bank is the potential vegetation community, and also the basis of community ecesis, survivorship, population reproduction and dispersion. So the research on this problem is helpful to describe the mechanism of vegetation succession and biodiversity in depth. The research is also important in practice because the conclusion can provide decision-making basis for vegetation recovery.

The study found that the mean density of germinated seed of soil seed bank in engineering slash with a recovering time of 4,7,18 and 31 years are 270,620,1410 and 2150 grain/m^2 respectively, comparing with 1310 grain/m^2 in control natural plot.

It indicates that the density of soil seed bank increased along with the prolonging of time, although much smaller than the density in Qinghai Lake zone.

In the term of diversity and abundance of soil deed bank, their variations are similar to the laws of aboveground vegetation, with the diversity and abundance is close to control grassland plot after 18 years of recovering and the diversity significantly exceeded after 31 years.

3.3 Restored and re-established of degraded ecosystem (Chen et al. 2006, 208; Zhou et al. 2010)

Borrow sites in alpine grassland in the some areas such as Tuotuo river basin ware chosen to be carried out experimental study of vegetation recovery in 2001 and 2002. Kengyilia thoroldiana and Elymus nutans Griseb were selected as the recovering plant, and some related results were obtained:

(1) The change of community coverage: the coverage degree increased consistently from the 1th year to the 4^{th} year and peaked at the 4^{th} year, and instead reached its trough in 5^{th} year followed by another consistent increase from the 6^{th} year. Whether the change of vegetation coverage is in relation to the years' climate needs to be further observation and analysis.

(2) Diversity of community species: the abundance of species index in artificial restoration areas, R0 and R1, both of them are increased with the growth year, and the same tendency can also apply to Shannon-winner index（H'）, Hill index(D) and abundance index.

(3)Aboveground biomass of engineering slash was consistently increased from the 1th year to the 4^{th} year and reached its peak in the 4^{th} year, and then decreased gradually in the years afterwards. The biomass of engineering slash surpassed the biomass of native grasses in the 2th year, which was about 63.12±54.96 g/m^2.

Some conclusions:

(1) The natural Restoration of vegetation is a slow and complex process in disturbed area with human activities of large-scale and high strength.

(2) The seeds of Kengyilia thoroldiana and Elymus nutans Griseb could germinated normally and live through the winter safely. Because of the germination and overwintering of the plant seed, the growth and development of plant individual and the characteristics of community, the conclusion could induced that vegetation has some adaptive function for borrow sites in the plateau.

(3) Planting Kengyilia thoroldiana and Elymus nutans Griseb in bare land in Qinghai-Tibet Plateau through some procedure measure, such as flat ground surface, plough up the soil of surface layer, trenching the fields for draining, sowing and covering, it would accelerates the recovering of vegetation in engineering destroyed sites and is a effective measure for vegetation recovery.

4.1 The response of alpine meadow ecosystem to climate change

(1) The change of plant morphology and root

CK represents control experimental plot, and T1 and T2 represent OTC1 and OTC2 of warming plots, respectively (Table 4.1). We can draw the conclusion that with the rise of temperature, the leaves of dominant species of alpine meadow became thinning and even longer, while the tightness of inner epidermal cells reduced. The height, base diameter and leaf length of key species during the growing season will all increase, while the thickness of leaf decreased significantly.

To alpine meadow, the root activity would increased of *Kobresia pygmaea* with short-term warming effects (Fig 4.5), however, with the temperature increased, root activity was limited, which demonstrated that appropriate warming can promote cycling and utilizing of nutrients by roots, but when the temperature beyond a certain value, warming will represent prohibitive effect. The reason may be that more warming may result in soil water stress.

Table 4.1 Two representative studied species of alpine meadow

Type	Height (mm)	Base diameter (mm)	Leaf length (mm)	Thickness of leaf epidermal cells (mm)	Leaf lower epidermis thickness (mm)	Total leaf thickness (mm)
CK	55.65	1.34	36.24	19.47	23.04	223.97
T1	65.66	1.47	50.45	19.33	17.93	206.61
T2	59.48	1.47	51.72	17.88	12.35	181.05
T-K					11.73	114.85

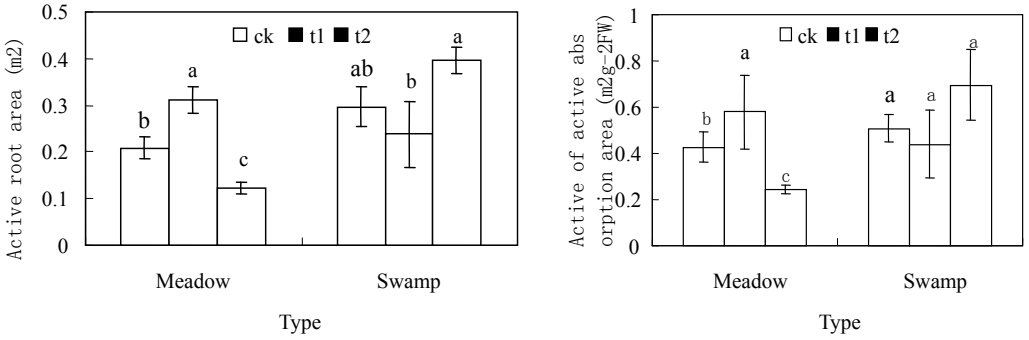

Fig 4.5 The variation of root active absorption area and unit root absorption area under different warming effect

(2) The change of plant coverage fraction and biomass

The observational results were shown in Table 4.2. With the increasing of temperature, the coverage of dominant grass communities among alpine meadow tended to decreased, however, weeds communities tended to increased. While the swamp meadow showed the reverse result. The soil water content of alpine meadow decreased with temperature increased, the widely distributional *Kobresia pygmaea* reduced coverage and enhanced water use efficiency to adapt warming and water stress. However, the swamp meadow, because of adequate moisture conditions, the larger leaf area after warming effect, and distributed in the upper of community, augmented photosynthetic rate and tillering ability. Thereby, the coverage of grass communities of swamp meadow increased.

The vegetation would grow and the biomass will accumulate with short-term warming (Table 4.2). Because of accumulated effect of warming and drought, the biomass of alpine meadow diverted to deeper soil, which made the increasing extent of biomass in ground and root front becoming even more. While the biomass of swamp meadow increased significantly aboard and below ground because of adequate moisture conditions and more proper temperature conditions, the biomass tended to distributed on the soil surface. Additionally, the biomass of standing dead and litter decreased in the end of growing season for both two type of meadow.

Table 4.2 The change of vegetation coverage of alpine meadow and swamp meadow

	Type	Coverage (%)		
		Bare ground	Grasses	Forbs
Alpine meadow	Control	21.7±3.2a	79.6±4.2a	13.2±2.2a
	OTC1	19.2±2.6a	68.2±3.3a	19.3±3.1a
	OTC2	18.5±2.8a	70.1±4.2a	17.9±2.9a
Swamp meadow	Control	7.9±2.1a	82.5±5.2a	11.6±2.1c
	OTC1	5.8±2.8b	90.6±4.5b	7.3±2.6b
	OTC2	5.0±1.9b	93.2±5.5b	5.6±1.3a

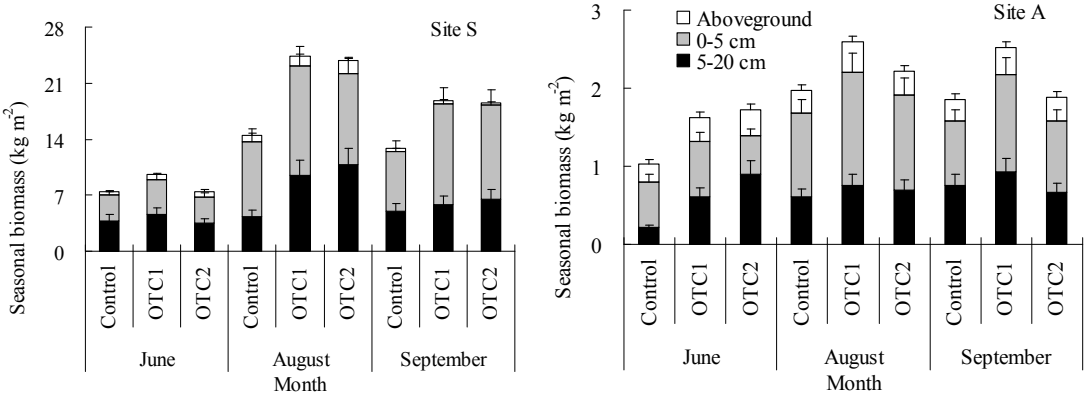

Fig 4.6 The aboveground and root biomass in the control, OTC1 and OTC2 plots at site S and site A with warming treatments. The values are means (+S.E.) of three replicate plots. Where swamp meadow S represented swamp meadow, and A represented alpine meadow.

(3) The distribution of C, N and seasonal change of alpine ecosystem under warming effect

1) Variation of C, N content in soil

The organic carbon and total nitrogen content in soil of alpine meadow decreased with the temperature increased, while the organic carbon and total nitrogen in soil of swamp meadow increased significantly (Fig 4.7). We can draw the conclusion that the decomposition rate of swamp meadow increased due to warming effect, which decomposed more roots and litters, and transfer more carbon and nitrogen to soil.

2) Variation of C, N content in plant

The organic carbon and total nitrogen content in plant of alpine meadow decreased with the temperature increased significantly, especially for shallow root system (Fig 4.8). The carbon and nitrogen content in alpine meadow aboard and below ground increased with minor warming, while decreased with major warming (Site A). In September, plant carbon content decreased with the temperature increased. Hence, we summarized that the alpine meadow ecosystem became carbon source, and swamp meadow ecosystem became carbon sink.

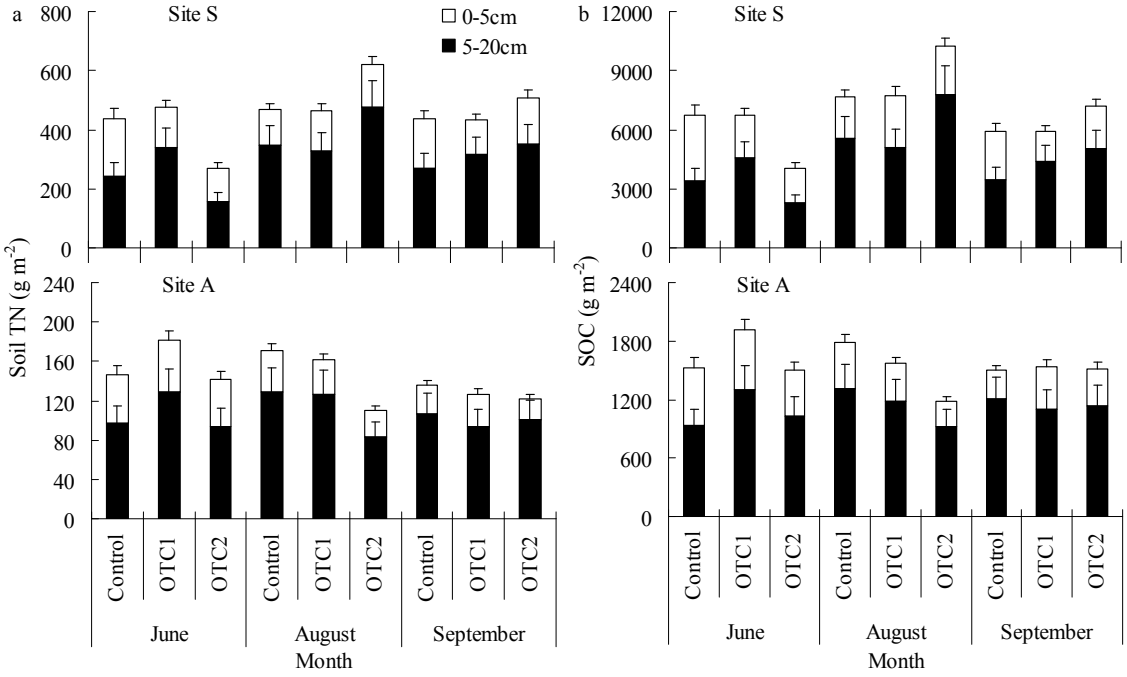

Fig 4.7 Seasonal change of soil TN and OC contents in the control, OTC1, and OTC2 plots after 2 years of warming treatments.

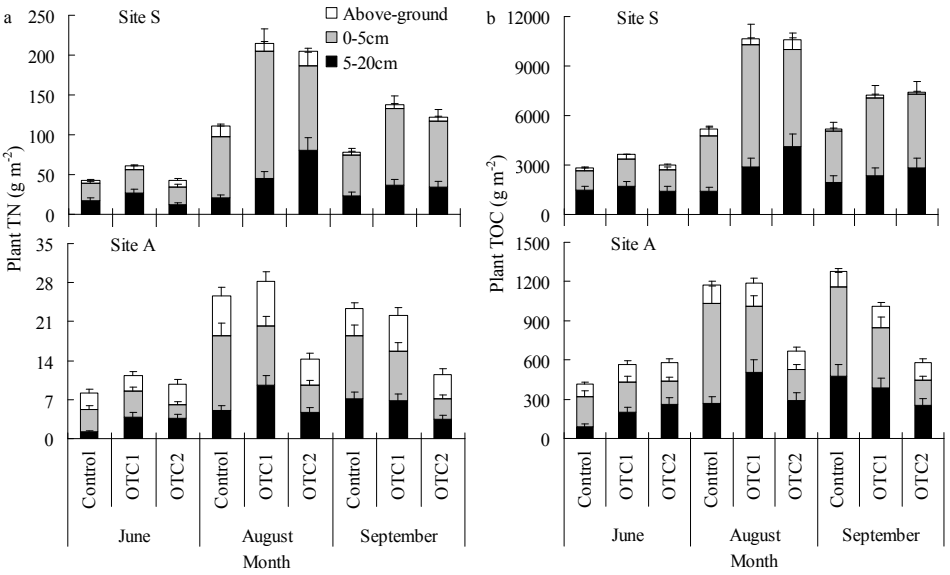

Fig 4.8 Seasonal change of plant TN and OC in above-ground and roots in the control, OTC1, and OTC2 plots after 2 years of warming treatments

5 Interactions between soil thermal and hydrological dynamics in the response of alpine meadow to vegetation cover changes

1) Variation in the relationship between soil and air temperature

Under different vegetation cover in alpine swamp grassland, there were significant liner relationships between air temperature and soil temperature. However, there were remarkable variations in gradient and intercept of liner regression models between alpine meadow and swamp meadow. As shown in Fig 4.9, in the thawing process, the gradient and intercept of linear regression models decreased with the coverage increased in alpine meadow, however, the swamp meadow showed the reverse result.

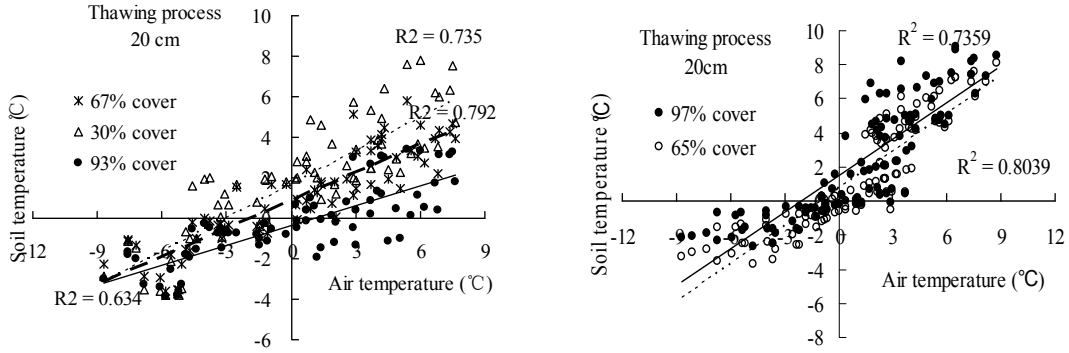

Fig 4.9 The influence of vegetation coverage to relationship of soil-air temperature

2) Seasonal variation of soil temperature dynamics in profile distribution with vegetation cover changes

As shown in Fig 4.10, no matter alpine meadow or swamp meadow, the variation of vegetation coverage had significant influence on the profile distribution and seasonal vary process of soil temperature. During freezing periods, the greater the vegetation cover, the higher the soil temperature, and the later the onset of change in soil temperature thaw-freezing transformation during freezing period. In thawing periods, the alpine meadow showed different rules compared with swamp meadow on ground temperature distribution and dynamics with vegetation cover changes, the more vegetation cover, the higher temperature in the same depth of alpine meadow.

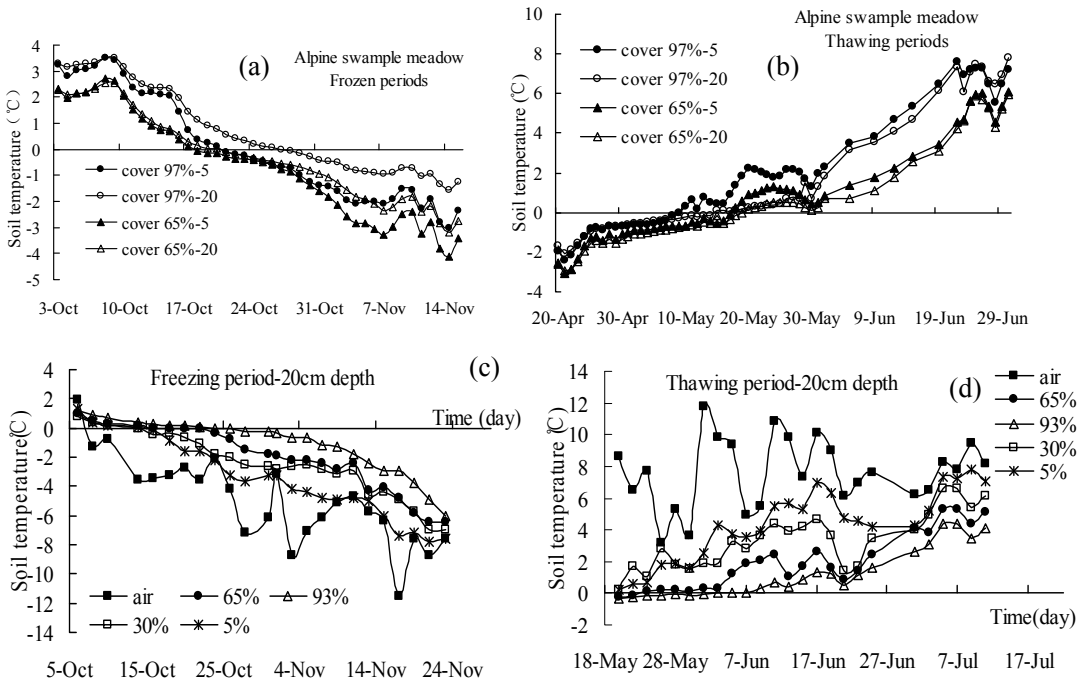

Fig 4.10 The variation process and profile distribution of ground temperature of alpine meadow to vegetation coverage

3) Seasonal variation of soil water content dynamics in profile distribution with vegetation cover changes

As shown in Fig 4.11, in swamp meadow grassland, the greater the vegetation cover, the higher the soil water content during thawing period and more ahead of time in freeze-thawing transformation during thawing period. The greater the vegetation cover, the more ahead of time in thaw-freezing transformation during freezing period and the more soil water content. The phenomenon was different in alpine meadow grassland, the lower the vegetation cover, the more intense response of soil water content to temperature, the earlier response time, the more extent of moisture and less duration of soil water content, the larger variation rate of moisture in the whole layer (0 – 1.2m) and the higher speed of thawing and freezing between different layers.

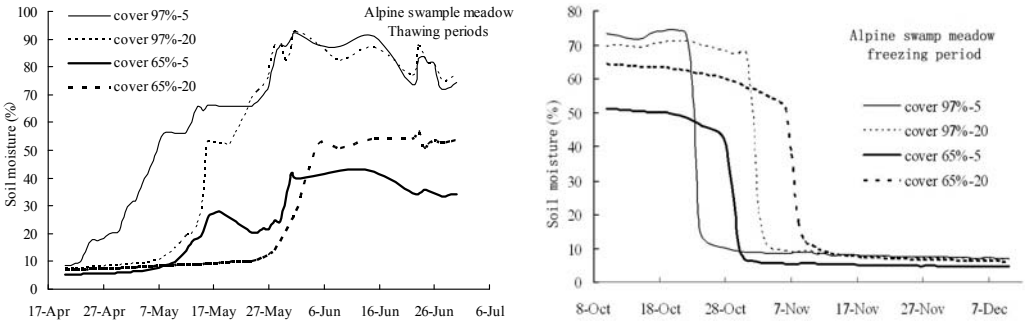

Fig 4.11 The soil water content distribution and dynamics of swamp meadow to vegetation coverage

References:

1) Chen QC, Zhou GY, Sun J, Chen ZG, Han YJ, Lu XF. Application of Kengyilia thoroldiana to vegetation restoration in gravel-soil-taken field along the Qinghai-Tibet railway. Journal of Glaciology and Geocryology. 2006, 28 (4): 506-511

2) Chen QC, Zhou GY, Sun J, Chen ZG, Lu XF. Test study on the application of Elymus Nutans to the vegetation restoration in the gravel-soil-taken field along Qinghai-Tibet railway. China Railway Science, 2008, 29(5):134-137

3) Hu QW, Wu Q, Cao GM, Li D, Long RJ, Wang YS. Growing season ecosystem respirations and associated component fluxes in two alpine meadows on the Tibetan Plateau. Journal of Integrative Plant Biology, 2008, 50(3): 271-279

4) Klein JA, Harte J, Zhao XQ. Experimental warming causes large and rapid species loss, dampened by simulated grazing, on the Tibetan plateau. Ecology letters, 2004, 7(12):1170-1179

5) Klein JA, Harte J, Zhao XQ. Experimental warming, not grazing, decreases rangeland quality on the Tibetan plateau. Ecological Applications, 2007, 17(2):541-557
6) Li DM, Guo ZG, An LZ. 2008. Assessment on vegetation restoration capacity of several grassland ecosystems under destroyed disturbance in permafrost regions of Qinghai-Tibet Plateau. Chinese Journal of Applied Ecology, 19(10)：2182—218
7) Li N, Wang GX, GaoYH, Wang JF. Effects of experimental warming on plant growth, soil nutrients, microbial biomass, and soil enzyme activities of two alpine meadows in Qinghai-Tibet Plateau. Polish Journal of Ecology. In press, 2011.3.
8) Li N, Wang GX, Yang Y, GaoYH. Short-term effects of temperature enhancement on plant production and carbon and nitrogen pools of alpine ecosystems in Qinghai-Tibet Plateau. Soil Biology and Biochemistry. In press, 2011.
9) Shi SB, Zhu WY, Li HM, Zhou DW, Han F, Zhao XQ, Tang YH. Photosynthesis of *Saussurea superba* and *gentiana straminea* is not reduced after long-term enhanced of UV-B radiation. Environmental and Experimental Botany. 2004, 51(1):75-83
10) Sun J, Li XZ, Wang XW et al., Ecological characteristics and areal types of permafrost wetland plants in Great Hing'an Mountains. Chinese Journal of Ecology. 2010,29(6):1061-1067
11) Wang GX, Li YS, Hu HC, Wang YB. Synergistic effect of vegetation and air temperature changes on soil water content in alpine frost meadow soil in the permafrost region of Qinghai-Tibet. Hydrological Processes. 2008, 22(17):3310-3320
12) Wang GX, Wang YB, Li YS, Cheng HY. Influences of alpine ecosystem responses to climatic change on soil properties on the Qinghai-Tibet Plateau, China. Catena, 2007, 70:506-514
13) Wang GX，Yao JZ，Guo ZG，et a1．Changes in permafrost ecosystem under the influences of human engineering activities and its enlightenment to railway construction．Chinese Science Bulletin，2004，49：1741—1750
14) Zhou GY, Yang LC, Xu WH, Sun J, Chen GC. Response of Soil Seed Bank to the Process of Restoring Succession of Vegetation of Permafrost Land for Construction on the Qinghai-Tibet Plateau. 2010, in press.

Chapter 5. Cryosphere and Climate

Wu Bingyi[1], Luo Yong[2], Li Weiping[2], Li Zhenkun[1], Shi Xueli[2], Zuo Zhiyan[1], and Xin Yufei[1]

1. Chinese Academy of Meteorological Sciences, Beijing 100081; 2.National Climate Center, Beijing 100081

Abstract

This chapter briefly reviews some progresses in the cryosphere and climate fields in 2010 emphasizing on the feedback of cryosphere, including comparative studies of parameterization schemes of snow cover fractions, effects of improved soil freezing process on East Asia, initial snow and soil moisture effects on summer precipitation over China, Eurasian snow cover variability and its impacts on Chinese spring rainfall, and high-resolution simulations over Antarctica. These results indicate that the impacts mechanisms of cryosphere processes on atmospheric circulation variability deserve further investigations in the future using observations and simulations.

1. A Comparative Study of Parameterization Schemes for Snow Cover Fraction in Climate Models

Many comprehensive physical-based snow schemes have been developed to capture the seasonal evolution of accumulation and melting of snow, but relatively less attention has been paid to the snow cover fraction (SCF, the percentage of a GCM grid cell that is covered by snow) in General Circulation Models (GCMs). Forced by NCEP reanalysis-based and Global Land Data Assimilation System (GLDAS) land surface data, offline NCAR CLM3 was run with 6 parameterization schemes (CLM3 default, Douville1995, Roesch2001, Wu2004, Yang1997, Niu2007) for calculation of SCF to investigate the performance of these SCF schemes in simulating the seasonal and inter-annual variation of snow cover in the northern Hemisphere.

In comparison with the observations derived from NOAA Advanced Very High Resolution Radiometer (AVHRR) and Moderate Resolution Imaging Spectroradiometer (MODIS), under the framework of NCAR CLM3, SCF schemes like CLM3 default, Douville1995, and Roesch2001 underestimate SCF over vast areas, snow covered areas simulated in these three schemes are smaller and located to the north of that in the observation, especially in autumn when snow pack begins to establish; Wu2004 scheme which is almost a linear enlargement of CLM3 default scheme also underestimates SCF in the Eurasian continent in autumn; Those schemes taking SCF as the tangent function of snow depth (e.g., Yang1997, Niu2007) improves the SCF simulation along the southern border of snow covered area (snow line) where snow pack is relatively shallow. Yang1997 scheme slightly overestimates SCF, especially along the southern border of the snow covered area; Niu2007 scheme which accounts for the seasonal variation of snow density overcomes the positive bias of SCF simulated by Yang1997 scheme to some extent. Douville1995 and Roesch2001 schemes underestimate SCF over mountainous areas, but Yang1997 and Niu2007 overestimate SCF in

those areas where the variability of sub-grid topography is large. At the end of spring, snow lines simulated by all the aforementioned 6 schemes are located to the north of the AVHRR observation over both North American and Eurasian Continents. Over most land areas with relatively small variation of topography, Niu2007 scheme performs the best.

Table 1 Formulations of the 6 SCF parameterization schemes analyzed in this study

Yang1997	$f_{sno} = \tanh(\frac{h_{sno}}{2.5 z_{0,g}})$
Niu2007	$f_{sno} = \tanh(\frac{h_{sno}}{2.5 z_{0g} (\rho_{sno} / \rho_{new})^m})$
Roesch2001	$f_{sno} = 0.95 \tanh(0.1 \cdot s_n) \sqrt{\frac{s_n}{s_n + \varepsilon + 0.15\sigma_z}}$
Douville1995	$f_{sno} = \frac{s_n}{s_n + 10} \cdot \sqrt{\frac{s_n}{s_n + \max(1, 0.15\sigma_z)}}$
Wu2004	$f_{sno} = \min(1, \frac{a \cdot h_{sno}}{10.6 + 100 h_{sno}})$
CLM3	$f_{sno} = \frac{h_{sno}}{10 z_{0g} + h_{sno}}$

Where h_{sno} is snow depth（m），Z_{0g} is roughness length of bare soil，ρ_{sno} is bulk snow density（kg m^{-3}），ρ_{new} is newly fallen snow density（100 kg m^{-3}），m is an adjustable constant，a is dependent on grid scale，s_n is snow water equivalent（mm），ε is a small constant，σ_z is the standard deviation of sub-grid topography（m）。

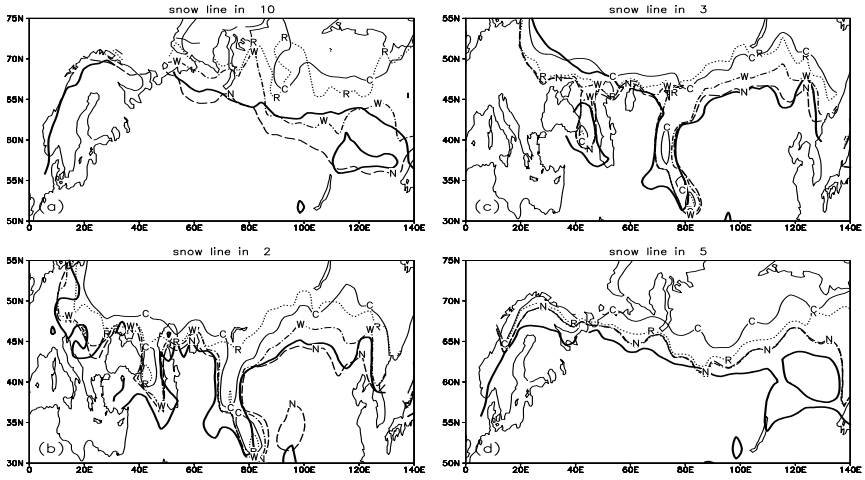

Fig 5. 1 Seasonal movement of snow line in the Eurasian continent simulated by different SCF schemes (thin solid: C, CLM3; dot: R, Roesch2001; dot-dash: W, Wu2004; dash: N, Niu2007) and that derived from NOAA AVHRR (thick solid). (a) October; (b) February; (c) March; (d) May.

Since snow depth is calculated by snow water equivalent and bulk snow density, no additional information is provided by accounting for snow density in Niu2007 scheme. Considering the surface heterogeneity of a GCM grid greatly influence the spatial distribution of snowfall and therefore affect the snow cover fraction in the GCM grid, on the basis of the previous SCF schemes, a new parameterization scheme which accounts for snow depth and the variability of sub-grid topography is proposed and evaluated by running CLM3 in an offline way. This modified scheme alleviates the overestimation of SCF simulated by Niu2007 scheme over the Tibetan Plateau and the Mongolian Plateau to some extent. Further studies are needed to validate this SCF scheme.

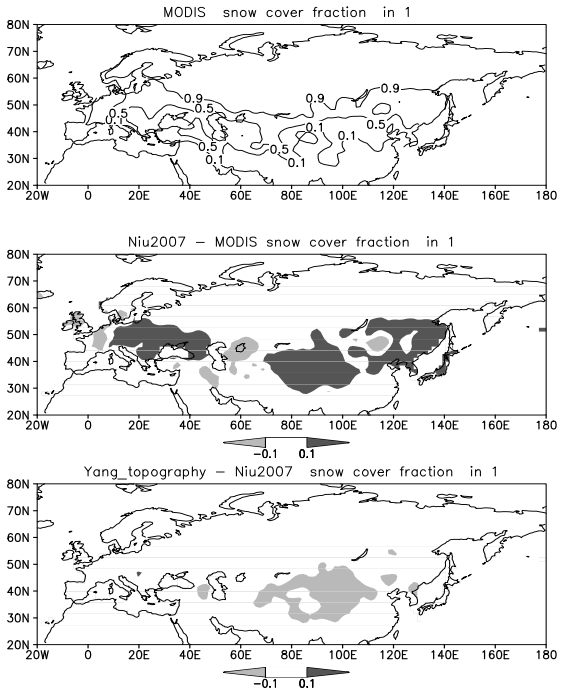

Fig 5.2 January mean snow cover fraction over Eurasian continent. (top) Observation derived from MODIS, (middle) simulated by Niu2007 scheme, (bottom) the difference between simulation by modified Yang1997 scheme which account for sub-grid topography and that of Niu2007 scheme. Light and dark shadings indicate magnitudes less than -0.1 and more than 0.1 respectively.

2. Effects of Improved Soil Freezing Process on Climate of East Asia Using NCAR CAM

The importance of land surface processes in climate systems has been widely recognized. Soil moisture not only affects the precipitation, temperature and humidity at regional scales (Shukla, 1982), it also can affect the atmospheric circulation at global scales (Simmonds, 1992). Frozen ground is another phase of soil moisture. When the soil temperature drops below the freezing point, moisture content within the soil becomes frozen and latent heat is released, vice versa. Due to the latent energy of freezing or thawing and impermeability when frozen, Soil freezing could therefore greatly affect thermal and

hydrological land surface conditions both in magnitude and on a spatial scale, thus playing an important role in energy and water cycles on a continental scale (Takata, 2000; Poutou, 2004).

Many investigators have studied the freezing-thawing process in land-surface modeling (Cherkauer, 1999; Koren, 1999). However, the linkages between frozen grounds and climate remain insufficiently studied and their effects on climate still poorly represented in land surface schemes. In this study, an improved soil freezing process parameterization is introduced and its impacts on East Asia climate are evaluated by NCAR CAM (Community Atmospheric Model).

The NCAR CAM has been already coupled with a matured land surface model CLM3 (Community Land Model). CLM3 has considered the exchange processes of energy and matter among snow, soil, vegetation and boundary layer air in detail. It is one of the most promising land surface models in the world. The thermal and hydraulic properties of frozen soil of CLM3.0 are described in detail in Oleson (2004).

When ice is present, soil water potential remains in equilibrium with the vapor pressure over pure ice. The soil water matric potential ψ for each soil layer is

$$\psi = 10^3 \frac{L_f (T - T_{frz})}{gT} \qquad (1)$$

Where L_f is latent heat of fusion, T_{frz} freezing point, and g the acceleration of gravity. The matric potential in frozen soil should also be a function of both liquid water and ice content in soil:

$$\psi = \psi_{sat} (\frac{\theta_{liq}}{\theta_{sat}})^{-b} (1 + 8\theta_{ice})^2 \quad (2)$$

where ψ_{sat} and θ_{sat} are porosity and the partial volume of liquid water. By equating ψ in equation (1) to ψ in equation (2), we can obtain

$$\theta_{liq\max} = \theta_{sat} \left[\frac{10^3 L_f (T - T_{frz})}{gT\psi_{sat}} (1 + c_k \theta_{ice})^{-2} \right]^{-1/b} \qquad (3)$$

Where $\theta_{liq\max}$ is the maximum liquid water when the soil temperature is below the freezing point. Thus, in modified CLM3, soil water freezing occurs $\theta_{liq} > \theta_{liq\max}$ and $T^{N+1} < T_{frz}$.

We run CAM3.1 coupled with original CLM3 (CAM experiment, hereafter) and improved CLM3 (NCAM experiment, hereafter) with prescribed climatology SST for 20 years respectively. Only the last 5-year monthly averaged data is used for analysis. Fig 5.1a shows the 500 hPa geopotential height differences between NCAM and CAM experiments in JJA. It is apparent that there is a marked negative anomaly near Baikal Lake. At the same time, the west Pacific Ocean subtropical high is enhanced and westward. The anomaly pattern at 500 hPa will be beneficial to the converge of cold air from the high latitudes and warm air from low latitudes, which may cause the increased precipitation in the northern part of west Pacific Ocean subtropical high.

Surface pressure and 850 hPa wind anomaly between the two runs is displayed in Fig 5.3.

Corresponding with Fig 5.3a, the southwesterly wind is obviously intensified in east part of China. It may carry more warm and moist air from the ocean into north China, resulting in increased precipitation in the region. In addition, due to the increased surface temperature in Fig 5.3b, the surface pressure in East Asian land is reinforced, whereas pressure in west Pacific Ocean is weakened (Fig 5.3b). Thus there is an intensive trend for the pressure gradient force from ocean to land, which implies the East Asian summer monsoon is intensified.

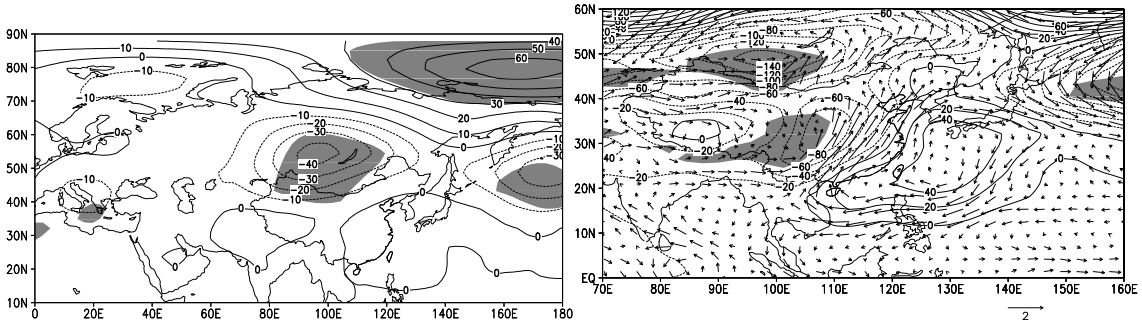

Fig 5.3 The differences of (a) 500 hPa height (gpm) and (b) 850 hPa wind (m/s) and surface pressure (Pa) in JJA between NCAM and CAM experiments. (Shaded areas are statistically significant at the 0.05 level)

We also analyze the difference of precipitation between NCAM and CAM experiments (Fig 5.4). A large positive anomaly is observed in north and northeast China. The most increased area locates at Yangtze-Huaihe River Basin, and the maximum of positive anomaly reaches 1.5 mm/d. Meanwhile, the precipitation in South China is slightly decreased. As a whole, the precipitation in northern China and the middle and lower reaches of the Yangtze River is intensive, whereas in south China it is descending. Precipitation in East Asia is mainly influenced by Asian summer monsoon. Precipitation in study region occurs during summer and its distribution is strongly correlated with the activities of the summer monsoon and the location and the strength of the subtropical high over the western Pacific. The results show that the climate of East Asia is very sensitive to the modified parameterization scheme of freezing process. However, further studies are needed to validate the new scheme.

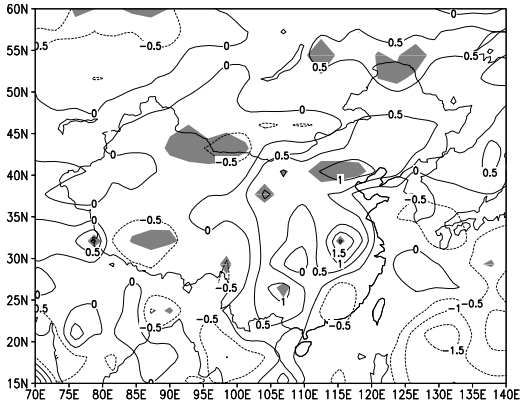

Fig 5.4 Same as Fig 5.3, but for JJA precipitation (mm/d)

3. Investigations of initial snow and soil moisture effects on summer precipitation over China

The study mainly focused on the effects of initial snow depth and related surface conditions on the subsequent climate with regional climate model simulations. The interest area is the Tibetan Plateau (areas where the height > 3000 m in the Western China, noted as TP). Additionally, the relationships between three mass snow cover areas and observed rainfall are also analyzed.

Initial snow depth effects

The initial preceding winter TP snow depth impacts on the following summer rainfall were made by the regional climate model (RegCM_NCC). By keeping all the other configurations unchanged, the snow depth is changed from zero to 20 cm (averaged observed depth). The simulation results are consistent with the relation of (by) observed snow depth and rainfall, namely, more rainfall occurs in the Yangtze River valley, less rainfall in South China and North China. This implies that more snow in TP in winter is one important reason causing "southern flood and northern drought" in summer in China.

The possible physical mechanism is as followed, the more snow over TP weakened the sensible heat source, which results in stronger winter monsoon in winter, and its effect can reach south China, south-west China and the Bay of Bengal. Additionally, weaker TP heat source can last to summer, which is a reason for the weakening of East and South Asian summer monsoon. The simulation results show that the distinct affect time of snow over TP can persist to June, but the dominant factor is the snow albedo increase in winter and the moistening of soil due to snow melting in spring to prolonging the influence process of snow on weather and climate. (Zhu Yuxiang, Ding Yihui, Liu Haiwen. 2009. The simulation research of the influence of snow depth over Tibetan Plateau in winter on rainfall in summer in China. *Chinese Journal of Atmospheric Sciences* (in Chinese), 33(5), 903-915).

Spring soil moisture of TP

The effects of "initial" soil moisture (SM) in arid and semi-arid Northwestern China on subsequent climate were investigated with the RegCM_NCC. Besides the control simulations (denoted as CTL), a series of sensitivity experiments were conducted, including the DRY and WET experiments, in which the simulated "initial" SM over TP was only 5% and 50%, and up to 150% and 200% of the simulated value in the CTL, respectively.

The results show that SM change can modify the subsequent climate in not only the SM-change region proper but also the far downstream regions in Eastern and Northeastern China. The SM-change effects are generally more prominent in WET than in DRY experiments. After SM is initially increased, the latent (sensible) heat flux there increases (decreases), and the surface air temperature decreases. Spatially, the most prominent changes in the WET experiments are surface air temperature decrease, geopotential height decrease and corresponding abnormal changes of cyclonic wind vectors at the mid-upper troposphere levels. Generally opposite effects exist in the DRY experiments but with much weaker intensity. Additionally, the variations of rainfall is not consistently changes as temperature in the WET and DRY

experiments. This might imply that SM is only one of the factors that impact the subsequent climate, and its effect is involved in complex processes within the atmosphere, which needs further investigation. (Shi Xueli, 2009: 'Initial' soil moisture effects on the climate in China – a regional climate model study. *J. Ocean Univ. China*, 8(2), 111-120. DOI 10.1007/s11802-009-0111-z.）

Observed relations between rainfall and three snow cover areas

According to the stationary observations, the largest snow cover regions in winter and spring locate at the Tibetan Plateau (TP), the northern Xinjiang (XJ, 74°~96 °E, 40°~50 °N) and the North-Eastern China (including the Inner Mongolia region (NE, 114°~134 °E, 40°~54 °N). The monthly rainfall of 160 stations are used for the SVD analysis with the snow cover of the above three areas.

The first mode shows different patterns at the three regions. For the TP, the previous winter-spring snow cover is consistent and significant positive related to the summer precipitation at the Yangtze River Valley. The spatial patterns of snow cover at NE are not consistent in winter and spring, but they are generally negative related to the summer rainfall of the NE and the lowest part of Yangtze River Valley, and positive related at the South China (especially with the winter snow cover). A distinct positive related area to the spring snow cover is located at the North China. As for the XJ, correlation patterns of the summer rainfall at East China are generally opposite to the winter and spring snow cover. It is negative (positive) related at regions north to the 35 °N, but positive (negative) related at regions along and south to the Yangtze River Valley to the XJ winter (spring) snow cover.

4. Decadal Variability in Springtime Snow over Eurasia: Relation with Circulation and Possible Influence on Springtime Rainfall over China

During winter, more than 60% of the Eurasian continent is covered with snow (Morinaga *et al.*, 2003), which affects local and large-scale atmospheric circulation and hydrological processes by changing the process of energy and water transfer between the land and atmosphere. The relationship between Eurasian wintertime snow cover and summertime rainfall in southern and northern China was strongly in-phase, whereas an inverse relationship was found between Eurasian wintertime snow cover and summertime rainfall in western, central, and northeastern China (Yang and Xu, 1994). Wu and Kirtman (2007) investigated the relationship between East Asian rainfall in spring–summer and Eurasian snow in winter–spring, and found that excessive springtime snow cover in western Siberia was accompanied by above-normal springtime rainfall in southern China. In addition, Wu *et al.* (2009) showed that reduced springtime snow throughout most of Eurasia was associated with increased summertime rainfall in South and Southeast China, but decreased summertime rainfall in the upper reaches of the Yellow River.

The influence of snow on the land–sea thermal contrast was generally considered to be the process that links Eurasian snow cover to the Asian monsoon (Douville and Royer, 1996; Bamzai and Shukal, 1999). anomalously extensive snow cover in autumn within Eurasia can cause a negative AO in the following winter via the influence of upward-propagating stationary Rossby waves (Saito *et al.*, 2001) .Given that the connection between Eurasian snow cover and Asian monsoon rainfall is complicated and that the associated

physical process remains unclear, it is more relevant to study the relationship between Eurasian snow cover and synchronous rainfall. Based on the above studies, the present study focuses on the relationship between Eurasian snow water equivalent (SWE) data derived from satellite observations and observed springtime rainfall in China. Wu *et al.* (2009) showed a clear decadal shift in springtime Eurasian SWE. Thus, the present study focuses on the relationship in the decadal time scale, with the aim of determining the relationship between springtime Eurasian snow and springtime rainfall in China, as well as relevant physical processes.

The relationship between decadal variability in springtime (March–May) snow water equivalent (SWE) over Eurasia and springtime rainfall over China is investigated for 1979–2004 using satellite-observed SWE, rainfall observations from 595 stations, and NCEP/NCAR reanalysis data. Variation in springtime (March–May) SWE in the leading EOF mode is homogeneous over large parts of Eurasia, with a maximum value of 20 mm in western and central Siberia, whereas the opposite variation is found over small areas such as the region south of Lake Balkhash and the eastern TP. Springtime Eurasian snow showed a decreasing trend from 1979 to 2004. Strong positive SWE anomalies appeared in 1979–1987, whereas frequent negative anomalies occurred in 1988–2004 (Fig 5.5). Based on decadal variations in springtime snow, the period 1979–1987 was selected as a high-snow index episode (hereafter referred to as the HSWI case) and 1988–2004 was selected as a low-snow index episode (hereafter referred to as the LSWI case) in conducting composite analyses.

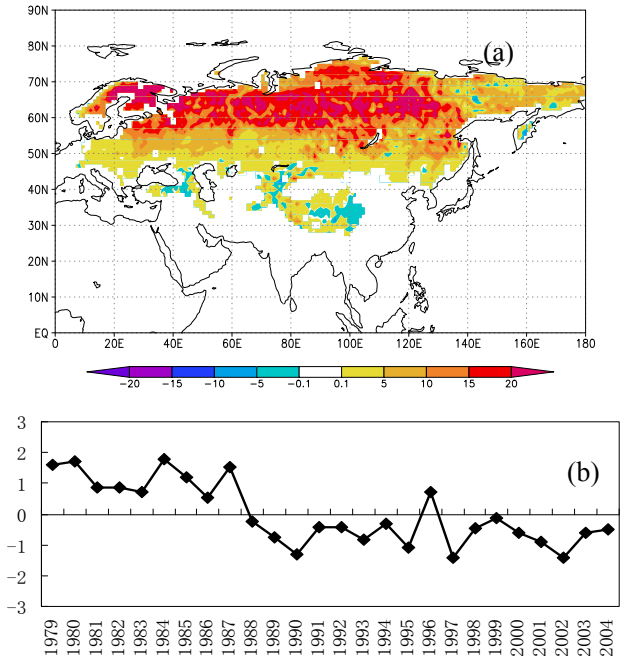

FIG 5. 5 (a) Spatial pattern of springtime SWE anomalies of the leading mode for the period 1979–2004, and (b) the corresponding time series.

This decadal variability of Eurasian spring SWE showed a statistically significant correlation with

springtime rainfall over China. With decreasing springtime SWE over Eurasia, negative anomalies in springtime rainfall appeared over southeastern and Northeast China, and enhanced precipitation occurs over southwestern and northwestern China (Figures 6a and 6b). The first EOF mode of springtime rainfall over China is similar to the composite difference between LSWI and HSWI (Fig 5.6c). Note that the variance percentage explained by the mode is 23.5%, demonstrating that the bulk of rainfall variability is explained by decadal variations in Eurasian springtime SWE. Here we can see that the primary variability in springtime rainfall over China is accounted for by the change in springtime snow over Eurasia. Given this result, it is now important to investigate the background atmospheric circulation associated with this relationship.

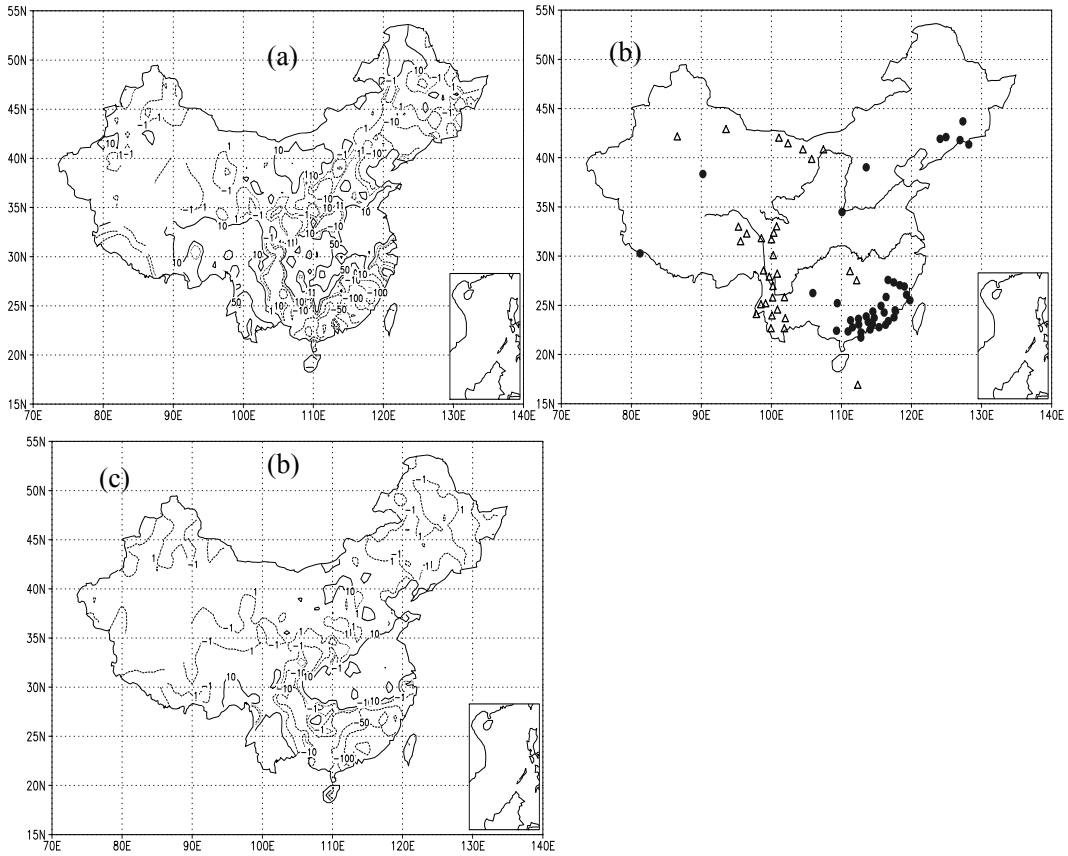

FIG 5.6 (a) Composite difference the low SWE and high SWE cases, (b) distribution of stations for which the composite difference exceeds the 0.1 level of significance [triangles (dots) indicate significant positive (negative) difference], and (c) the spatial pattern of springtime rainfall anomalies of the leading EOF mode for the period 1979–2004.

Decreasing springtime SWE in Eurasia corresponded to reduced springtime rainfall over southeastern and Northeast China, and more rainfall over southwestern and northwestern China. This relationship was supported by the feedback effect of snow in high-latitude areas to changes in background atmospheric circulation. The reduction in Eurasian SWE resulted in reduced upward surface heat flux to the atmosphere. In other words, reduced Eurasian springtime snow acts as a heat sink for the atmosphere, and thereby

higher boundary layer height (Fig 5.7).

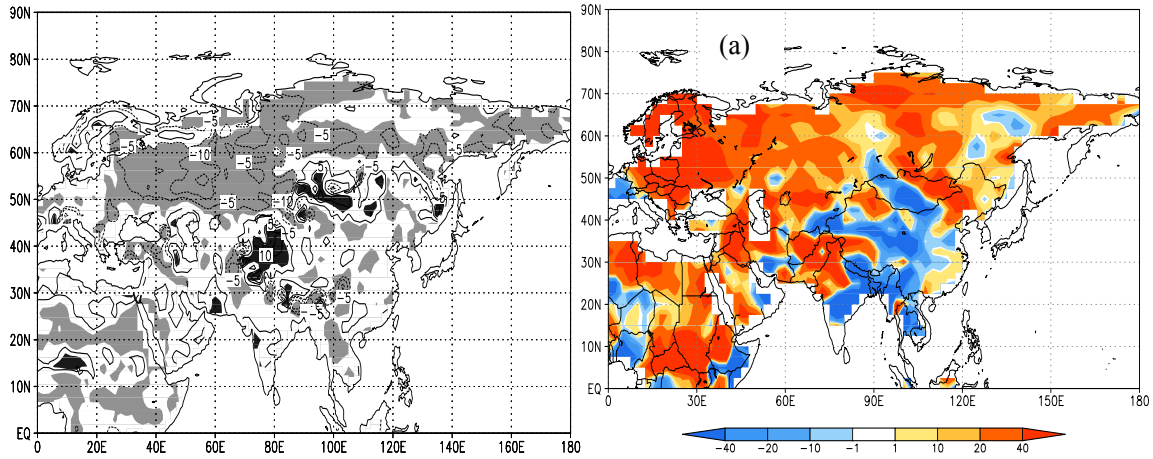

FIG 5. 7 (a) Composite difference of the net heat flux (W m^{-2}) be (b) e LSWI and HSWI cases. Shaded areas exceed the 0.1 level of significance [dark (light) shading represents significant positive (negative) difference], and (b) Composite difference of BLH (m) for the periods 1988–2002 and 1979–1987

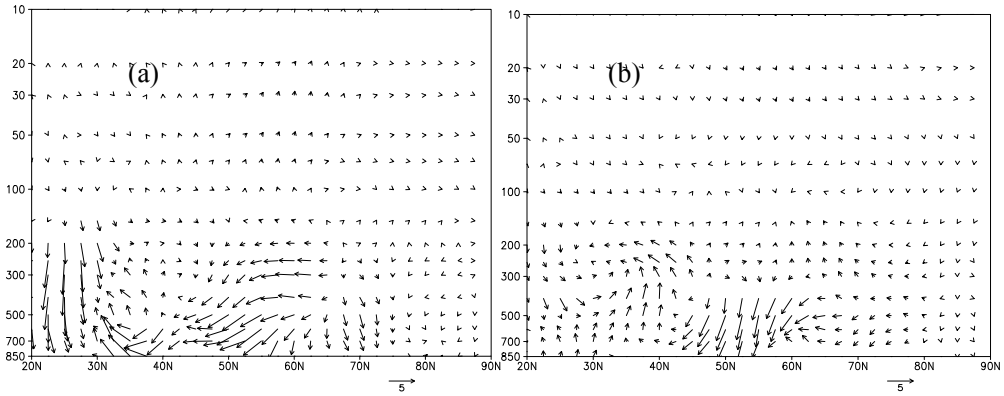

FIG 5. 8 (a) Composite difference of vertical (×10) wave activity flux (m^2 s^{-2}) at 90°E, and (b) the zonal-mean vertical (×10) wave between the low SWE and high SWE cases

As is well known, the stationary wave is a response to topographical and thermal forcing. The reduced upward heat flux from the land to the atmosphere, combined with the higher boundary layer, acted to weaken the upward and poleward wave activity flux in the troposphere over Siberia. The zonal-mean wave activity flux was also strongly weakened due to reduced snow in Eurasia (Fig 5.8), which corresponded to anomalous negative heights/pressures in the Arctic and anomalous positive heights/pressures in mid-latitude regions from the upper-level troposphere to the surface (Fig 5.9). In fact, Eurasian snow show a strong correlation with the leading EOF mode of SLP (–0.42 for the period 1979–2004, exceeding the 0.05 level of significance).

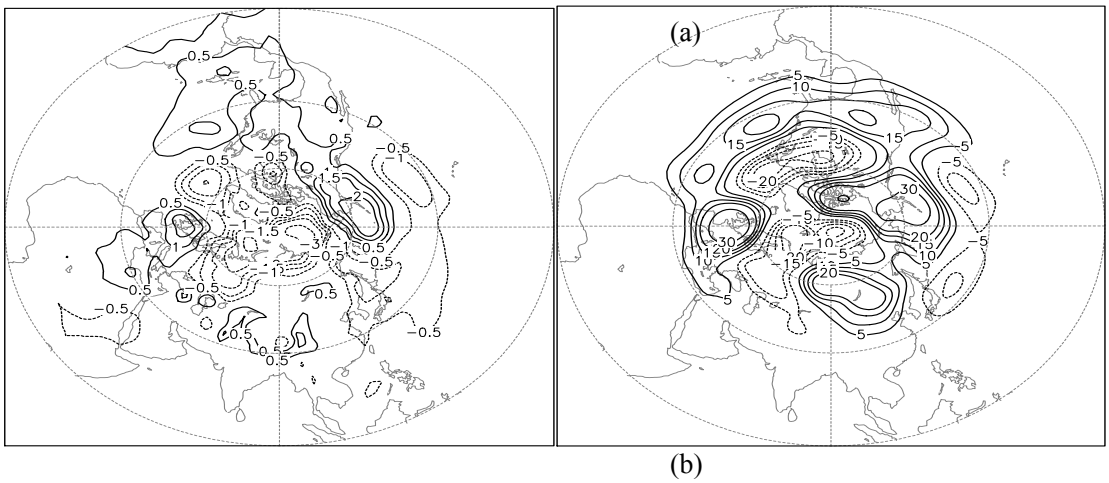

FIG 5. 9 (a) Composite difference of (a) SLP (mb) and (b) geopotential height at 500 hPa (gpm) between the LSWI and HSWI cases

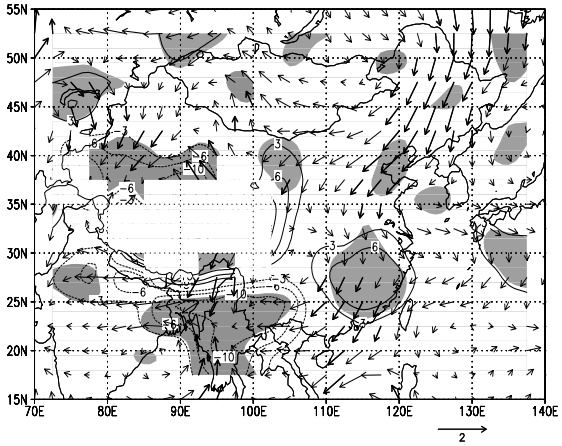

FIG 5. 10 (a) Composite difference of the horizontal wind field (vectors, m s–1) and horizontal moisture flux divergence (contours and shading, g × (s × cm × mb)–1 × 10–7) at 850 hPa between LSWI and HSWI cases. Shaded areas in (b) indicate composite difference exceeding the 0.1 level of significance

With a persistent decrease in Eurasian snow, the positive AO phase is associated with anomalous anti-cyclonic circulation over Siberia and a weakened WPSH, resulting in turn in robust northerly anomalies over all of eastern China, with maxima in Northeast and southeastern China (Fig 5.10). Consequently, the warm and moist southerly is weakened, resulting in divergence anomalies over Northeast and southeastern China and reduced regional rainfall. In contrast, the northerly anomaly corresponds to greater amounts of water vapor being blocked in southwestern China, resulting in enhanced rainfall. Moreover, the westerly anomaly due to the anomalous anti-cyclone over Siberian is associated with enhanced water vapor convergence over northwestern China, resulting in a positive precipitation anomaly. Thus, the anomalous northerly resulted in reduced water vapor convergence in southeastern and Northeast China, and reduced water vapor export for southwestern and northwestern China. As a result, negative

rainfall anomalies developed over southeastern and Northeast China, and positive rainfall anomalies appeared over southwestern and northwestern China.

5 Climate and Forecast Mode Simulations for Antarctica: Implications for Temperature and Wind

High-resolution simulations over Antarctica are important for regional real-time mesoscale forecasting, the modelling of atmospheric processes over Antarctica, and the simulation of the mass balance of the Antarctic Ice Sheet. Several regional climate models (RCMs) have been applied over pan-Antarctic domains for these purposes (e.g. van de Berg et al., 2006; Parish and Bromwich, 2007; Gallée and Gorodetskaya, 2010). In order to investigate the uncertainty in RCM simulations over a pan-Antarctic domain, the differences between 'usual' climate mode simulations (continuous integration with a single initialization at the beginning of the run) and forecast mode simulations (frequent re-initialization during the run) are investigated, with the analysis focused specifically on the temperature and wind fields. The uncertainty of the initial conditions is examined in the climate mode simulations.

Data and Model

The primary set of observations used for the analysis are the radiosonde data from the year 2007 obtained from the Australian Antarctic station Davis (68°S, 78°E; 10 m above sea level), Mawson (67°S, 62°E) and Casey (66°S, 110°E). the model in this study is HIRHAM. HIRHAM is based on the limited area model HIRLAM (High Resolution Limited Area Model; Machenhauer,1988) and uses the physical parameterization package of the general circulation model ECHAM4 (Roeckner et al., 1996).The ECHAM GCM has its original roots in global forecast models developed at ECMWF and has been modified for climate research at the Max Planck Institute for Meteorology, Hamburg, Germany.

Result

vertical temperature structure

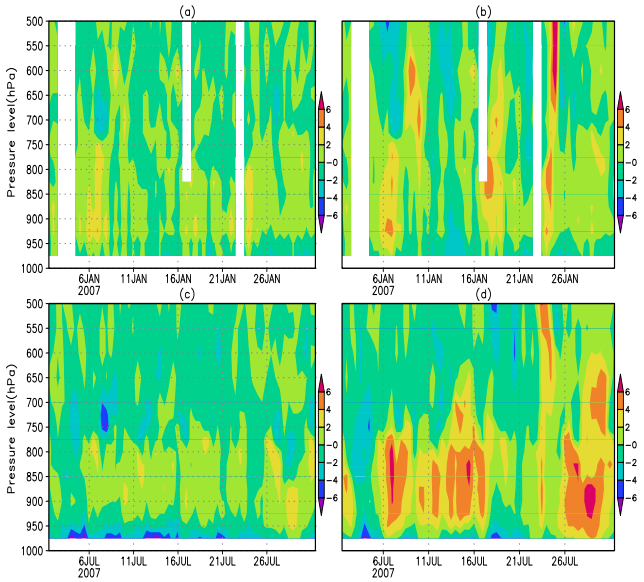

Fig 5. 11 Height-time cross sections of the temperature bias “forecast minus observation” (°C) at Davis for (a) January and (b) July 2007; height-time cross sections of the temperature bias “climate minus observation” (°C) at Davis for (b) January and (d) July 2007.

Fig 5.11 shows height–time cross sections of the temperature bias (“simulation minus observation”). Generally, the bias of the forecast mode simulation is in both seasons smaller than that of the ensemble mean of the climate mode simulation. As expected, the frequent re-initialization in the forecast mode simulation maintains the observed meteorological evolution in the model. In contrast, the model develops its own internal variability in the climate mode, which can cause deviations in the development and path of cyclones, and thus in the timing of synoptic events. Consequently, the Fig 5.shows larger biases in the ensemble mean of the climate mode on days associated with main synoptic events. Fig 5.11 further shows that the bias has different characteristics in the two seasons. In January, the forecast mode bias is generally within ±2°C, while the ensemble mean bias of the climate mode is larger (between -4°C and +6°C) for specific days. The biases are larger in July. Here, generally, the simulated temperature at the near surface is colder than observed, by 2°C–6°C. Furthermore, the climate mode shows an additional large positive bias of up to 8°C in the lower troposphere (950–800hPa), i.e. the climate mode simulation at these levels is warmer than the observations.

vertical wind field

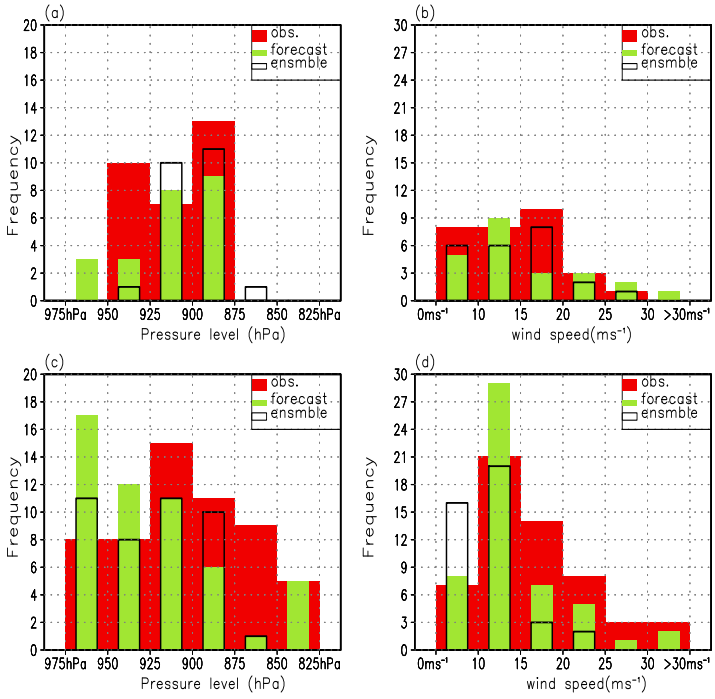

Fig 5. 12 Frequency distributions of the main jet core height at Davis for (a) January and (c) July 2007; frequency distributions of the main jet core speed at Davis for (b) January and (d) July 2007. Red: observation; green: forecast run; black: ensemble mean of climate mode runs.

Most regions of Antarctica are characterized by a stable planetary boundary layer (PBL), where low level jets (LLJs) often occur, characterized by a wind speed maximum in the PBL (e.g. Andreas et al., 2000). Fig 5.12 explain the statistics of the simulated jet characteristics. The most striking difference is that the model tends to generate the LLJ less often and at lower altitudes and with a reduced core wind speed compared to what is observed. The model (both modes) simulates 77% of the observed jets in January, while the forecast (climate) mode represents 93% (73%) of the observed LLJs in July. Particularly in July, the simulated jet heights are lower than in the observations. The statistics of the jet core wind speed show that the model covers the total range of the observed wind speeds, but underestimates the occurrence of high-speed jets in July. This may arise from the model cold biases at the near surface and the associated damping of the turbulent mixing of higher momentum air from the jet to the surface when the colder surface temperature increases the near-surface stability (Guo et al., 2003). Additionally, the relatively coarse model resolution of ca. 50 km and the so reduced orographic slopes around Davis as well as the relatively few vertical levels may also be partly responsible for the model under-representativeness of the LLJ. Also, smaller mesoscale systems are not going to be captured by the model, and Prydz Bay near the Davis station does generate a significant number of small-scale systems that will be reflected in the radiosonde data.

Spatial patterns of temperature, wind, and geopotential height

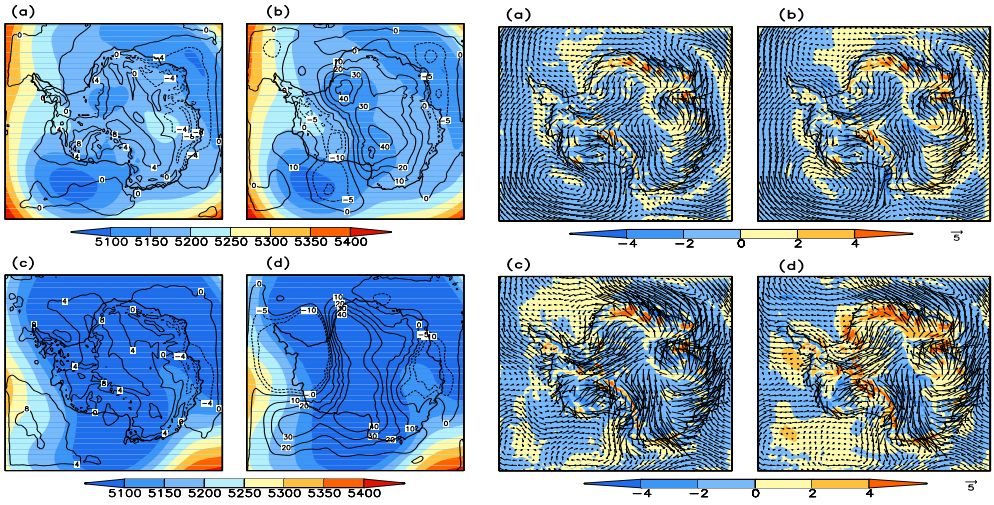

Fig 5. 13 Left: Patterns of 500 hPa geopotential height (z500) of forecast run for (a) January and (c) July, 2007; pattern of 500hPa geopotential height (z500) of ensemble mean for (b) January and (d) July, 2007. Color: z500 [m], isolines: z500 bias "ECMWF minus simulation" [m]; Right: Patterns of 10 m wind of forecast run for (a) January and (c) July, 2007; patterns of 10m wind of ensemble mean for (b) January and (d) July, 2007. Arrows: 10m wind vector, color: 10m wind speed bias "ECMWF minus simulation" [ms^{-1}].

Fig 5.13 shows that the largest biases of the geopotential height occur over the ice sheet, and not along the coast. Over the ice sheet, the biases of the climate mode simulation ranges from -10–60 m at the 500hPa

level, and are comparable with other simulations (e.g. Genthon et al., 2002). However, it is obvious that the forecast mode calculates much smaller biases (of less than 10 m) compared to the climate mode. The biases over the region of interest (along the East Antarctic coast) are generally small and range from -10–0 m; thus the tropospheric circulation is reproduced with great accuracy. Fig 5.13 also demonstrates that the simulated near-surface wind vectors (direction and speed) around the Antarctic coasts and over the continent reproduce the ECMWF pattern. The HIRHAM mesoscale simulations clearly produce the continental-scale drainage flow over East Antarctica. The flow is deflected to the left by the Coriolis force producing a net easterly flow. The biases show that HIRHAM simulates weakened wind speeds (up to 4 m s^{-1}) over the East Antarctic coastline, compared to ECMWF.

REFERENCES

1) Armstrong RL, Brodzik MJ. 2005. Northern Hemisphere EASE-grid weekly snow cover and sea ice extent version3. National Snow and Ice Data Center, Boulder, CO, digital media.
2) Bamzai AS, Shukla J. 1999. Relation between Eurasian snow cover, snow depth, and the Indian summer monsoon: An observational study. *Journal of Climate* 12: 3117–3132.
3) Cherkauer K. A. andLettenmaier D. P.. Hydrologic effects of frozen soils in the upper Mississippi river basin, J. Geophys. Res., 1999, 104: 19599–19610.
4) Dethloff, K., A. Rinke, R. Lehmann, J. H. Christensen, M. Botzet, and B. Machenhauer, 1996: Regional climate model of the Arctic atmosphere. *J. Geophys. Res.*, **101**, 23401--23422.
5) Dethloff, K., K. Glushak, and A. Rinke, 2010: Antarctic 20th century accumulation changes based on regional climate model simulations. *Adv. Meteorol.*, in press
6) Douville H., J. F. Royer, J. F. Mahfouf. A new snow parameterization for the Meteo-France climate model. Climate Dynamics, 1995, 12: 37-52.
7) Douville H, Royer JF. 1996. Sensitivity of the Asian summer monsoon to an anomalous Eurasian snow cover within the Meteo-France GCM. *Climate Dynamics* 12: 449–466.
8) Gallée, H., and I. V. Gorodetskaya, 2010: Validation of a limited area model over Dome C, Antarctic Plateau, during winter. *Clim. Dyn.*, **34**, 61--72, doi: 10.1007/s00382-008-0499-y
9) Genthon, C., G. Krinner, and E. Cosme, 2002: Free and laterally nudged Antarctic climate of an atmospheric general circulation model. *Mon. Wea. Rev.*, **130**, 1601--1616.
10) Glushak, K., 2008: Atmospheric circulation and the surface mass balance in a regional climate model of Antarctica. PhD dissertation, University of Potsdam, Germany, 143pp.
11) Gong, D., and S. Wang, 1999: Definition of Antarctic Oscillation Index. *Geophys. Res. Lett.*, **26**, 1601--1604.
12) Koren V., Schaake J., et al. A parameterization of snowpack and frozen ground intended for NCEP weather and climate models, J. Geophys. Res., 1999, 104: 19569–19586.
13) Liu X, Yanai M. 2002. Influence of Eurasian spring snow cover on Asian summer rainfall. *International Journal of Climatol*ogy 22: 1075–1089. DOI: 10.1002/joc.784.
14) Morinaga Y, Tian S-F, Shinoda M. 2003. Winter snow anomaly and atmospheric circulation in Mongolia. *International Journal of Climatology* 23: 1627–1636. DOI: 10.1002j/joc.961.
15) Niu Guo-Yue, Yang Zong-Liang. An observation-based formulation of snow cover fraction and its evaluation over large North American river basins. Journal of Geophysical Research, 112, D21101, doi:10.1029/2007JD008674.
16) Oleson, K. W., Yongjiu Dai, G. Bonan et al. Technical description of the Community Land Model. NCAR Tech. Note NCAR/TN-461+STR, 2004, 174pp.

17) Parish, T. R., and D. H. Bromwich, 2007: Re-examination of the near-surface air flow over the Antarctic continent and implications on atmospheric circulations at high southern latitudes. *Mon. Wea. Rev.*, **135**, 1961--1973.

18) Poutou E., Krinner G., et al. Role of soil freezing in future boreal climate change, Climate Dyn., 2004, 23: 621-639.

19) Rinke, A., and K. Dethloff, 2000: On the sensitivity of a regional Arctic climate model to initial and boundary conditions. *Climate Res*., **14**, 101--113.

20) Roeckner, E., and Coauthors, 1996: The atmospheric general circulation model ECHAM4: Model description and simulation of present-day climate. MPI Rept., 218, Max Planck Institute for Meteorology, Hamburg, Germany, 90pp.

21) Roeckner, E., and Coauthors, 2003: The atmospheric general circulation model ECHAM5. Part I: Model description. MPI Rept., 349, Max Planck Institute for Meteorology, Hamburg, Germany, 127pp.

22) Roesch, A., M. Wild, H. Gilgen, A. Ohmura. A new snow cover fraction parameterization for the ECHAM4 GCM. Climate Dynamics, 2001, 17: 933-946.

23) Saito K, Cohen J, Entekhabi D. 2001. Evolution of atmospheric response to early-season Eurasian snow cover anomalies. *Monthly Weather Review* 129: 2746–2760.

24) Shukla J. and Mintz Y.. Influence of land-surface evapotranspiration on the Earth's climate, Scince. 1982, 215: 1498-1501.

25) Simmonds I. and Lynch A.H.. The influence of pre-existing soil moisture content on Australian winter climate, Int. J. Climatology, 1992, 12: 33-54.

26) Stull, R. B., 1988: An introduction to boundary layer meteorology. Springer Netherland, 670pp.

27) Takata K. and Kimoto M.. A numerical study on the impact of soil freezing on the continental-scale seasonal cycle, J. Meteor. Soc. Japan, 2000, 78: 199-221.

28) Uppala, S. M., and Coauthors, 2005: The ERA-40 re-analysis, *Quart. J. Roy. Meteor. Soc.*, **130**, 2961--3012.

29) Van de Berg, W. J., M. R. van den Broeke, E. van Meijgaard, and C. H. Reijmer, 2006: Reassessment of the Antarctic surface mass balance using calibrated output of a regional atmospheric climate model. *J. Geophys. Res.*, **111**, D11104, doi: 10.1029/2005JD006495.

30) Van den Broeke, M. R., and N. P .M. van Lipzig, 2003: Factors controlling the near-surface wind fields in Antarctica. *Mon. Wea. Rev.*, **131**, 733--743.

31) Wu BY, Yang K, Zhang RH. 2009a. Eurasian snow cover variability and its association with summer rainfall in China. *Advances in Atmospheric Sciences* 90: 31–44.

32) Wu R, Kirtman BP. 2007. Observed relationship of spring and summer East Asian rainfall with winter and spring Eurasian snow. *Journal of Climate* 20(1): 1285–1304.

33) Wu Tongwen, Wu Guoxiong. An empirical formula to compute snow cover fraction in GCMs. Advances in Atmospheric Sciences. 2004, 21(4): 529-535.

34) Yang, Z.-L., R. E. Dickinson, A. Robock, and K. Y. Vinikov, Validation of the snow sub-model of the biosphere-atmosphere transfer scheme with Russian snow cover and meteorological observation data. Journal of Climate, 1997, 10:353-373.

Chapter 6. Advances on In-Situ and Remote Sensing Observation, Establishment of Cryospheric Data Base

LI Xin and LI Zhongqin
State Key Laboratory of Cryospheric Sciences, Cold and Arid Regions Environmental and Engineering Research Institute, Chinese Academy of Sciences, Lanzhou 730000, China

1. Glacier Change Observations

1.1 In the north slop rivers of Tianshan

Junggar Basin, North Slop Rivers of Tianshan Mountain contains a total of 3399 glaciers, an area of 2251 km^2, the volume of 137.35 km^3, the annual flow of glacial melt water about16.8 $\times 10^8$ m^3, accounting for13.5% of river runoff 125×10^8 m^3. River area can be divided into two categories by the amount of glacier melt water, one category main is small glaciers within 1 km^2, individual glaciers reach within 2-5 km^2, glacial melt water runoff accounted for 6-20 %, including rivers in north slope of Bogda, Urumqi River, Toutun river, Santun River, taxi river, Jinghe, etc.; and others for Manas River, Horgos River, Anjihaihe, etc. Glacier Basin is area over 200 km^2, glacial melt water, and accounts for 35-53 % of river runoff (Shi Yafeng, 2005; LZIGG, CAS,1986; Xie Zichu et al, 2006; Yang Zhenniang,1991).

There are two located observation glaciers in the area, Glacier No. 1 at headwater of Urumqi River (Glacier No. 1), and Glacier No. 51 Kuitun River Haxilegen. Glacier No. 1 has been retreating since 1959, since the1980s, showing a trend of decrease. Glacier area had a decrease of 14% in 1962-2006, from 1.95 km^2 reduced to 1.68 km^2, an average reduction rate of 0.0061 km^2/a. Because of glaciers retreat, so that the original one glacier separated into East and West two glaciers in 1993.The terminal average rate of glacier retreat was 4.5 m/a in 1959-1993, the East branch of 3.5 m/a, west branch of 5.8 m/a in 1994-2004. The glacier thickness of eastern branch of the mainstream online average thinned 0-30m in 1981-2006. Correspond with the glacial retreat, the glacial melt water runoff had substantial increase, the Glacier No. 1 average glacier melt water runoff reached 508.4 mm/a, while 936.6 mm/a in 1986-2001, an increase of 84.2 %(Zhongqin et al, 2009; 2003; 2007). By inference, the rapid warming has led to glacier melt water runoff to river runoff increased significantly since 1980s.

Glacier No. 51 Kuitun River Haxilegen Glacier started to observe from 1998, and the ablation extent was less than glacier No. 1, but the ablation trend is clearly accelerating. Glacier area has been reduced from 1.558km^2 in 1964 to 1.356km^2 in 2004, shrinking 0.202km^2 or 13%, the glacier terminal rate was 3.9m/a. The average annual retreat rate was 2m/a in 1964-2006 at the glacier terminal, while in 1999-2006, reached 5.1m a^{-1}, an increase of 1.5 times. The glacier surface velocity is also reduced, indicating the thickness of the thinning. The inspection discovered that the neighboring glacier No. 48, is quite close in the glacier terminal flinching speed with the glacier No.51, but the area change is relatively small, as a result of glacier No. 48 area is relatively big possibly. In the low 10m firn of the glacier accumulation area, also exists massively unfrozen the glacier melt water in October, indicated that the glacier cold reserves is low, is weak to climate warming resistance, occupies in the rapid ablation. According to the Jiangjunmiao hydrological stations data of downstream, glacial melt water runoff increased significantly since 1990s.

In 1962-2006, the fan-shaped shunt glaciers and Glacier No.4 Sigonghe in the north slope of Bogda, with an area were reduced by 7.1 % and 10.6 %, respectively, the terminal of the average retreat rate of 8.7 m/a and 7.5 m/a. Compared to the inspection in 1981, the study found that glaciers terminal show a large number of glacial lakes, and melting is increasing.

There are 588 glaciers through remote sensing and ground verification method, distributed four regions: Urumqi River basin, Toutun River, Kuitun River basin Kuitun River basin and Bogda Peak. Urumqi River Basin, a total of 150 glaciers with a total area of 48.667 km^2 in 1964 reduced to 41.965km^2 in 1992, a decrease of 13.8 % (Chen Jianming, etc, 1996), glacier area has reduced to 32.052 km^2 by 2005, compared with 1964, decreased by 34.2 %, and the average glacier narrowed 0.111 km^2, the terminal retreated 5.0m/a. Due to ablation, there were 11 glaciers completely disappear. The glaciers of Toutun river basin are close to the Urumqi River Basin, small glaciers dominated. There are 172 glaciers in the study area in 1964, by 2005 had five small glaciers disappear. The glacier area loss of 31.5 % in the past 41 years, the average glacier shrink 0.092 km^2, the terminal retreated 4.8ma^{-1}. Kuitun River Basin study area contains 167 glaciers in 1964, by 2004, there were 11 glaciers disappeared, an area of loss of 15.4 %, the average

glacier shrink 0.095 km^2, the glacier terminal retreat average rate 3.5m/a. The study area of Bogda Peak contains 99 glaciers in 1962. In 1962-2006 periods, glacier area loss was 16.9 %, average glacier shrink 0.107 km^2, the glacier terminal retreat 3.6 m/a.

According to Glacier No. 1 glacier dynamics model simulation prediction results, the Glacier No. 1 has 50 years of observational data; glacier changes study the dynamics model recently, estimates the future changes in the Glacier No. 1 and its impact on water resources. The results show that, even if the current climate conditions remain unchanged, for the fit with the current climate, glacier No. 1 will continue to retreat, until 2180, while the glacial melt water runoff steady decline in the next century, weakened to the present half that level around 2075. In the IPCC report, several climate change scenarios, glacier No. 1, will disappear in the next 70-90 years, and disappear in 50 years in extreme temperature conditions. Glacial runoff remained relatively stable in the next 40 years, then the rapid decline occurred, this downward trend has continued into the glaciers disappear. If adopting the weather station near glacier measured data based on to predicate the climate scenarios, the glacial melt water runoff will increase in the next 30 years, by a rate of up to about 21% of current levels, and then falling sharply, until the glaciers disappear. This estimate implementation on the 150 glaciers in the Urumqi River, found the melt-water runoff has a slight increasing trend in the next 20 to 30 years, then a sharp weakening, until all the glaciers disappear of the Urumqi River. The Urumqi River basin runoff changes in glacial melt water is faster than the Glacier No. 1, due to Glacier No. 1 area is one of the largest glaciers in basin.

Through the model sensitivity analysis, we found a total of 7250 glaciers in the Tianshan Mountains is likely to faster than the Glacier No. 1 in change and disappear. The glaciers quantity, area (2133 km^2) and volume (60.27 km^3) accounted for 80 % 23 % and 6 % of all glaciers respectively. The factors causing these glaciers melting is stronger than the Glacier No. 1, for example, glacier size is smaller than the glacier No. 1, altitude of less than Glacier No.1 and so on, even if more stringent parameter sensitivity analysis, changing faster than the Glacier No. 1, the number of glaciers will be less, but the credibility will increase.

Despite glacier relative changes have some difference in the north slop of Tianshan, but a single glacier average change has almost the same, for about 0.1 km^2. According to the findings of Glacier No. 1, we speculate that within the next 30-40 years, the northern rivers of Tianshan glaciers tend to disappear, with area less than 2 km^2, more than 5 km^2 glaciers ablation violent. Therefore, climate change is relatively large differences on glacial water resources in different basins in this region; for small glaciers, such as Urumqi River and the Toutun River Basin, the glacial melt water runoff will become insignificant, for coverage of a large glaciers, glacial melt water run-off will continue to maintain a certain share.

1.2 Tarim River

Tarim Basin is China's largest internal area, surrounded by high mountains，there are 11665 glaciers, area of 19878 km^2, the ivolume about 2313 km^3 in China. Kyrgyzstan has 613 glaciers with area of 2120 km^2, the volume of 260 km^3. Estimate the total amount of glacial melt Water Rivers covered 40% of the total runoff, in which Yarkant River, Yulong Kashgar River and Kumalik River glacial water runoff was as much as 50-80 % in the headwater of Tarim River (Shi Yafeng, 2005; LZIGG, CAS,1986; Xie Zichu et al, 2006; Yang Zhenniang,1991; Kang Ersi et al 2000).

The location observed glacier for Glacier No. 72 Qingbingtan of Tuomur peak, located in the upper of Aksu River. Aksu River is the main tributary of the Tarim River, water supply accounts for over 70 % of surface runoff in Tarim River. According to observations, glacier No. 72 area decreased 22.7 %, from 7.27 km^2 reduced to 5.62 km^2 in 1964-2008. The terminal retreat rate reached 41.0 m/a, compared with Glacier No.1 at the headwater Urumuqi River, glacier retreat and ablation speed is larger ,and more part of the mainstream line of valley glaciers is relatively thin thickness, glacier temperatures are high, close to 0 ℃, weak ability to hedge against future warming; Moraine thickness at bottom of glacier has relationship with ablation closely. However, glacier movement supply is relatively strong, glacier surface velocities are up to a 70m/a, and domical effects can not be ignored. Compared to Glacier No. 1, the glacier melting and sports supplies should be much stronger, with some characteristics of the marine-based glacier, are very sensitive to climate change.

The recent study of glaciers in this region, there are three glaciers: Glacier No. 74 Qingbingtan (9.55 km^2), Keqikuzibayi Glacier (42.83 km^2), and tuomur Glacier (310.14 km^2) , The glacier area change rates were 14.7 %, 4.1 % and 0.3 % in period 1964-2009 years, the glacier terminal retreat rate 30.0 m/a, 22.9 m/a, 3.0 m/a. Field thickness measurement found that glaciers became intense ablation in this region, glacier thickness has become very thin, glacial area - the thickness of empirical formula has been impossible to apply in other basins created.

Through remote sensing and ground verification method of 740 glaciers in this region, located in two

areas: Tuomuer of the upper of the Aksu River area and Yarkant River Basin. Tuomur region examined a total of 483 glaciers, located in north-south slope Haerketawu Mountain, glaciers scale is very different, the largest in more than 300 km^2. The total area of glaciers from 2267.708 km^2 in 1964 reduced to 2067.412 km^2 in 2003, a decrease of 8.8 %. Glacier shrinks an average of each of 0.382 km², the terminal retreat 6.8ma-1. The upper of Yarkand River study area includes 257 glaciers, with a total area of 768.633 km² in 1967, reduced to 670.328 km² in 2002, narrowed by 12.8%, with an average per Glacier shrink 0.383 km², the terminal retreat 10.5m/a.

Field observations indicate that glaciers response to climate change in Tuomur peak formed four characteristics: 1) ablation strong, despite the shrinking glaciers area was relative small, but the each glaciers loss was absolute large; 2) the large glacier become thinning and ablation rapidly. Glaciers usually follow "thinning back" laws, because of moraine glacier coverage of the terminal, delayed the glaciers retreat, thus rapid melting in thinning, which can be confirmed by the thinning of glacier thickness. 3) The relatively high temperatures have a significant impact on the low altitude of duplex valley glaciers, analysis shows that this type of glacier ice tongue covered 70% of the total glacier volume. Low latitudes, are very sensitive to climate change, is the main body of glacial melt water runoff. According to Qingbingtan Glacier No.72 glacier dynamics simulation, the glacier ice tongue-scale ablation exhausted about 10 years, which is very like y to lead to a runoff greatly reduced. While the remaining small amount of ice distributed at high altitudes, although it can be a long time, but the glacial melt water is limited; 4) the glacial moraine decreased the glaciers ablation of limited. Generally believed that glaciers are "tuomuer type" glaciers in the area, moraine widely distributed and has a strong protection to glacier. The adoption of remote sensing methods analysis moraine covered 14.9 % of glacier area. Field observations found that only a small part of the moraine thickness are more than 6-10 cm, this inhibited glacier ablation, and most of the moraine thickness is very thin, plays a facilitating role on the glacier ablation. Above characteristics show that the glaciers are rapidly melting, its melting speed is much faster than expected in Tuomuer area.

Yarkand River basin, due to lack of field trips, is not yet right to make accurate judgments for glacier ablation characteristics. Remote sensing analysis shows that a single glacier area reduction was \ slightly larger than Tuomur, indicating a glacier melting is also very strong. With tomur area is different is that the area covered by glacial moraine at the glacier terminal, which may lead to large glaciers shrinking.

According to the distribution characteristics and glacier melting changes, combined with the typical pattern of glacier forecast, we speculated that, if continued warming, the glaciers melt water runoff will continue to maintain a certain level, but at low temperatures year, low water level increased in the next 30-50 years in the Tarim River. After this, because most glaciers melting solid-state resources exhausted, which lead to sharp drop in glacial runoff and eventually at a lower level. As lack of the systemic observational data, shorter time series, there is uncertainty to the process and time scales of prediction, need to continue observation and research. In short, the glacial water resources play a pivotal role in the Tarim Basin, at present ablation intense. Once the glaciers ablation exhausted, water resources will have disastrous effects in the region.

1.3 The Eastern River Basin of Xinjiang,

Eastern Xinjiang Tulufan - Hami Basin is a water resource shortage area. glaciers distribution include the southern slope of Harkeli mountain, the southern slope of Balikun mountain, the southern slope of Bogda Mountain, and the southern slope of Tianger mountain, where has a total of 446 glaciers, an area of 252.7 km^2, ice volume of 11.4 km^3. Over the past 40 years, the glacier area decreased 11% in the region. It is estimated that annual glacier melt water runoff is over 25%of above river runoff.

Located in the southern slope of Bogda Glacier belongs to Turpan Basin water. we conducted field visits to glacier No.8 Heigou in the southern slope of Bogda in August 2009, compared to previously drawn topographic maps and examination of data in 1981, found that the glacier area decreased by 5.71 km² to 5.63 km² since 1962, with a decrease of 1.3%. The terminal average retreat rate is 11.0ma-1. The mainstream line average thickness reduces 10m in1981-2009 (Wang Zongtai, 1991).

Through remote sensing and ground verification methods, studied 104 glaciers in the southern slope of Bogda. The results show, in 1962-2006, the total area reduced by 25.3%, with an average per glaciers shrink 0.198 km², the terminal retreat 4.5 m/a. Bogda Peak North Slope glacier change is smaller than the south slope during the same period, a total of 12 glaciers disappear in north-south slope.

In water system of Hami basin, the location observed glacier is Miaoergou flat-topped glacier since 2004 (Li Zhongqin et al, 2007). Observational studies have shown that the glaciers area reduced from 3.64 km² to 3.28 km², narrowing the 0.360 km², or 9.9% in 1972-2005. The largest average retreat rate was 2.3m/a at the terminal of ice cap. The largest average retreat rate increased 2.7ma-1 at the terminal of ice

cap since 2005. Mass balance shown melting weak at the top. The ice core data showed that glaciers melting speed up in the recent 20-30 years. The thickness of ice caps thinned 0-20 m in 1981-2007, mainly in the lower part of the ice caps, the top of the thinning is not obvious. The glacier temperature was relatively low, at the bottom of 60 m of ice cap, glacier temperature was -8℃

Through remote sensing and ground verification method, there are a total of 75 glaciers examined in Miaoergou area, which belonged to south and north slope of Harlik Mountain, of which 50 glaciers in the southern slope, the northern slope of 25 glaciers, the south slope of average area is slightly larger than he north slope. The 75 glaciers area decreased by from 98.252 km^2 to 87.964 km^2 in 1972-2005, an area loss of 10.5%, Glacier shrink an average of each of 0.137 km², the terminal retreat 5.0 m/a. While there are four glaciers disappeared.

Relatively speaking, Miaoergou region glacier change is small in Xinjiang, at the present, because relatively high altitude glaciers may be preserved, the average size is relatively large. However, the district water system is vulnerability. Glacial melt water is the highly dependent. Rapid changes in the past 20 years indicated that glaciers were rapid melting. According to Hami Hydrographic Office of the observational data, temperatures increased and a slight increase of precipitation in recent years, without glaciers melt water supply of rivers, such as Toudaogou river, there has been decrease in runoff, which may indicate that precipitation increment can not compensate for increased evaporation; for less glacial melt water supply rivers, such as Guxiang river, runoff kept increasing before 2000, and after showed the slow emergence of the trend of decrease and increase, but the runoff percentage changes increased. Water change is large in flood or dry season, extended the dry season, these are likely to the weakening of the glaciers regulatory role; glacial melt water larger supply rivers, such as Yushugou river etc, although runoff continues to maintain an upward, the growth rate has begun to decrease. The runoff process reflected the glacier change impact on hydrology, water resources and the different stages.

In short, in the water systems of Tulufan Basin, the Bogda Peak region's glaciers, regardless of the southern slope and the northern slope are in rapid retreat, exerting a significant impact on water resources to the downstream of Urumqi and Tulufan basin. The Hami basin glaciers ablation was increasing; annual distribution of water resources has resulted in a significant impact. Overall, in the East River basin of Xinjiang, the glacier accelerated melting, has led to water resources deteriorating.

1.4 Ili River and Ertix River

Ili River is one of the largest rivers in Xinjiang. A total of 2373 glaciers in the basin, with area of 2022.66 km^2, the volume of 142.18 km^3, Ili river runoff is 193.0 × 10^8 m^3, in which glacial runoff is about 37.14 × 10^8 m^3, accounting for 19.2% of the total runoff. The average glacier area is 0.85 km^2 in Ili river basin, is a medium-sized, more sensitive response to climate.

Using remote sensing methods, studied 293 glaciers in the upstream of Akesu River basin. The results showed that the total glacier area of 265.812 km² reduced to 215.510 km² in 1963-2004, with a loss of 18.9%, on average each glaciers shrink 0.172 km², the terminal retreat 7.0 m/a. There are 11 glaciers disappeared. While this finding verified the lack of field trips, it demonstrates that glacier change is at the middle level in Xinjiang, glaciers impact on runoff, can not be ignored.

Ertix River lies the southern foot of Altai, Xinjiang, a total of 403 glaciers, glacier area of 289.29 km^2. Ertix River runoff is about 100.0 × 10^8 m^3, where glacial melt water runoff was about 7.73 × 10^8 m^3, the proportion of the total runoff of 7.7%. The average glacier area of 0.72 km^2 is the lowest in the distribution of glacial valley snow line.

The glaciers distribution Focused on around the main peak of Youyi peak of the Altai Mountains. We carried out glaciological study to the largest glacier- Kanas glaciers near Youyi peak in 1981 (Wang Lilun, 1983), a second inspection in August 2009. Study found that the glacier altitude is relatively low; response to climate warming is also very sensitive. Kanas glaciers have taken place great changes since 1981, glacier snow accumulation area is significant thinning, the snow line up at least 30m. The lower part of glacier forms the surface ablation caves, glaciers terminal appear a huge hole and the melting water surging out. Contrast to the previous topographic maps found that the glacier area reduced from 30.13km² in 1959 to 28.74 km² in 2009, a loss of 4.6%, glaciers terminal retreated 16.4 m/a.

Although a substantial proportion of glacial melt water supply in the rivers, the mountain precipitation and snow runoff play the leading role. Observational data show that Crane River basin in Ertix River main is snowmelt runoff. Temperature rise makes the biggest run-off moth from in June 1950s-1960s in advance of the present in May, an increase in spring runoff, summer runoff reduction, especially in the July-August run-off reduction, which have a great impact on downstream agricultural production, fisheries, etc.

1.5 West Kunlun Shan

Recent studies have indicated that widespread wastage of glaciers in western China has occurred since the late 1970s. By using digitized glacier outlines derived from the 1970 inventory and Landsat satellite data from 1990/91 to 2001, we obtained area changes of about 278 glaciers with a total area of 2711.57 km^2 in the heavily glaciated west Kunlun Shan (WKS) in the northern Tibetan Plateau(TP). Results indicate that the prevailing characteristic of glacier variation is ice wastage, and glacier area decreased by 10 km^2 (0.4% of the total 1970 area) between 1970 and 2001. Both the south and north slopes of the WKS presented shrinkage during 1970–2001, but whereas on the north slope a slight enlargement of ice extent during 1970-90 was followed by a reduction of 0.2 % during 1990–2001, on the south slope the glacier area decreased by 1.2% during 1970–91, with a small increment of 0.6 % during 1991–2001. Comparisons with other glaciated mountainous regions in western China show that glaciers in the research area have experienced less retreat. Based on records from the Guliya ice core, we believe that an increase in air temperature was the main forcing factor for glacier shrinkage during 1970–2001.

1.6 Gangrigabu mountains, southeast Qinghai–Xizang (Tibetan) Plateau,

The present research focuses on glacier changes in the southeast of the Qinghai–Xizang (Tibetan) Plateau, where most of the temperate glaciers in China are located. Our results show that the 102 measured glaciers in the region have all retreated between 1915 and 1980, with total area and volume decreases of 47.9 km^2 and 6.95 km^3, respectively. The extrapolated mass loss of all glaciers in the Gangrigabu mountains amounted to 2 7 km^3, 9.8% of the ice mass in 1915. Between 1980 and 2001, glaciers in the region have also experienced a general retreat; however, up to 40% of the glaciers were advancing. Our analysis demonstrates that precipitation in the studied area has increased substantially since the mid-1980 s. This precipitation increase is likely to bring about a positive mass balance for glaciers in the region, so that the retreat of retreating glaciers might slow down or even turn into advance. Considering the sensitivity of the temperate glaciers in the region and the uncertainty in climate projections, more attention must be paid to glacier changes in the southeast Tibetan Plateau region.

1.7 The Su-lo Mountain in Northeastern Tibetan Plateau

The total glacier area in the Su-lo Mountain decreased by about 7% during 1966~1999. The majority of glaciers in this region are thinning, and the global volume loss is about 1.4 km^3 from 1966 to 2000. The summer temperature increased dramatically in the last 30 years, which is possibly a direct driver of glacier recession over the same period in this region. In addition, the local variables such as the orientation of each glacier, its altitude, slope and initial size seem to exert a considerable influence on the spatial differences in the magnitude of the losses.

1.8 Central Himalaya

Glacier variation is one of many indicators of climate change. Repeat measurements of the glacier terminus positions for selected glaciers in the central Himalaya document that they have been in a state of continuous retreat over the past few decades. Since the 1960s the average retreat rate on the north slope of Qomolangma (Mount Everest) is 5.5-9.5ma^{-1} and on Xixiabangma it is 4.0-5.2ma^{-1}. Many glaciers on the south slope of the central Himalaya have been in retreat, and recently their retreat rate has accelerated. Ice-core studies show that the annual accumulation on these glaciers has fluctuated, but over the last century it has declined. It decreased rapidly in the 1960s and has remained consistently below the long-term mean thereafter. Meteorological station records indicate that the annual mean temperature in the region has slowly increased, particularly during the summer months. The strongest warming has occurred in the last 30 years. These data suggest that the current glacier retreat is due to the combined effect of reduced precipitation and warmer temperatures, and, if these conditions continue, the glaciers in the region will continue to shrink.

1.9 Tuotuo River basin, the source region of Yangtze River

Glaciers in the Tuotuo River basin, western China, have been monitored in recent decades by applying topographical maps and high-resolution satellite images. Results indicate that most of glaciers in the Tuotuo River basin have retreated in the period from 1968/1971 to 2001/2002, and their shrinkage area is 3.2% of the total area in the late 1960s. To assess the influence of glacier runoff on river runoff, a modified degree–day model including potential clear-sky direct solar radiation has been applied to the glaciated regions of the river basin over the period 1961–2004. It was found that glacier runoff has increased in the last 44 years, especially in the 1990s when a twothirds increase in river runoff was derived from the increase in glacier runoff caused by loss of ice mass in the entire Tuotuo River basin.

1.10 Monsoonal Temperate Glaciers

Based on various data, it can be concluded that eight monsoonal temperate glaciers in China were in

stationary or ad-vancing between 1900s~1930s and 1960s~1980s, and were in retreating during 1930s~1960s and 1980s~present under the background of climate warming. The total glacier area has reduced by 3.11 km^2 with a mean front altitude rise of 3.2 m/yr and 4 glaciers have disappeared in Mt. Yulong during 1957~1999. Mass balance records indicated that glaciers had suf-fered a constant mass loss of snow and ice during the last several decades, and the accumulated mass balance in Hailuo-gou basin in Mt. Gongga was -10.83 m water equivalent in the past 45 years with a annual mean value of -0.24 m, and the value at Baishui glacier No.1 was -11.38 m water equivalent in the past 52 years with -0.22 m/yr. The inverse variation between mass balance and temperature in China and the Northern Hemisphere reflected that climate warming is mainly corresponding to constant ice and snow mass loss in the past 50 years. The change of the glaciers' surface morphology has occurred since the 1980s, such as enlargement of glacier-lake and ice falls, resulted from the accelrative climate warming.

2. Snow-Firn Pack Stratigraphy Changes Observations

The snow stratigraphy of an alpine glacier reflects processes of snow metamorphism and melt at specific locations on the glacier (Shumskii, 1964). Alteration of these characteristics over long time periods can be a direct result of climate change.

2.1 Snow pack stratigraphy

In the period 1961-1962 the proportion of coarse-grained, medium-grained and fine-grained firn, fresh snow and other layers (such as ice layers, dust layers and depth hoar etc.) accounted for 40%, 25%, 22%, 6% and 7% of the snow pack respectively. In 1981-1983, the proportion of the coarse-grained firn layer and medium-grained firn layer increased to 55% and 22% while the proportion of fine-grained firn decreased from 25% to 12%. By 2002-2005 the coarse-grained firn layer had increased to 65% and the proportion of fine-grained firn had continued to decrease going from 12% to 7% between the 1980s to 2000s.

To summarize, from 1961 to 2005 stratigraphic profiles of the snow-firn pack become less complex; ice layers and ice lenses almost or completely disappeared and coarse-grained firn became the dominant firn type (increasing from 40% to 65%). All of these changes in the snow-firn pack correspond to a warming trend in regional climate, which became more pronounced between 1985 and 2005. The changes in the composition of the snow pack also reflect changes in the distribution of the glacier zones.

2.2 Changes in the number of annual layers, percolation and density

Dust and ice layers occur in specific seasons (for instance, spring and summer). This seasonality permits identification of annual layers and hence can be used to date the snow layers. At Glacier no. 1, Wang et al. (2006) found that one dust layer is preserved in the snow-firn pack per year as the result of two dust layers merging because of percolation during the summer. Annual layers were thus identified and measured based on single dust layers. Ice layers in the snow pack indicate the presence of small amounts of liquid water. Observations showed that ice layers usually form in spring and summer. In spring, the day-time surface temperature exceeds 0℃, leading to a partial melting of the snow, the water refreezes at night forming an ice layer. In summer, ice layers form when melt water penetrates downward and refreezes above an impermeable layer such as a layer of glacier ice, or even coarse firn.

Long-term changes in stratigraphy from the three time periods were investigated using historical data collected in 1961-1962, 1980-1983 and new data collected in 2002-2005. In general the data suggests that the time required to transform snow into ice has decreased, and the volume of water percolating in the snow pack and the bulk density have increased substantially. For example, between 1961 and 1962 an average of 5.2 dust layers were found in the West branch snow pack (Table 1), suggesting that 5 years of snow accumulation was present above the ice. However during 1980-1983 and 2002-2005 the average number of dust layers above the ice (and hence the number of annual layers) were 4.6 and 2.5 respectively. During the same time periods the average number of dust layers on the east branch decreased from 4.5 to 3.3. The declining number of annual layers identified by the dust suggests that the time required to transform the snow-firn pact into ice has been steadily decreasing.

As well as the decrease in the number of dust layers in the snow pack over the three periods a decrease was also observed in the number of ice layers. In 1961-1962, the West branch contained 7 ice layers, but this decreased to 3.6 and 2 in 1980-1983 and 2002-2005 respectively. On the East branch, the number of the ice layers decreased from 9 to 2.9 over the same period. The decrease in ice layers can be explained by an increase in the percolation of melt water which destroys the ice layers.

Corresponding to these changes the average bulk density of the snow-firn pack increased by 20% on the west branch and 28% on the east branch between 1961 to 1962 and 2001 and 2005.

2.3 Snow pack ablation

Four long-term stratigraphic observation sites above the ELA were selected to investigate the snow pack

response to climate change during spring and summer. Snow-firn stratigraphy was recorded every 10 days between May to September in 1962 and 1980 on the West branch and 1980 and 2004 on the East branch.

Snow depth and mean ablation rates for the different time periods are shown in Table 3. The mean ablation rate over the melt season increased at the west branch site by ~26% from 1962 to 1980 and by ~75% at from 1980 to 2004 at the east branch site.

The slopes of the linear regression lines reflect the mean ablation rate of the snow pack during the melt season. We observe that ablation at the West branch site increased between 1962 and 1980, with the regression slope increasing from 0.3 to 0.51. From 1980 to 2004 at the East branch site, ablation can divided into two periods: 1 May-4 July (days: 1-65) (period 1), and 5 July-31August (days: 66-123) (period 2). For period 1, the ablation is remarkably similar from 1980 to 2004 however during period 2 the ablation rate increased significantly, the regression slope increasing from 0.27 to 1.25.

Differences in the absorption of solar radiation, determined by slope, surface albedo, aspect and shading affect glacier ablation rates. In the period for which there is data for both branches (1980) the slope of the regression line, and hence the ablation rate for the West branch is higher than the East branch. The difference is explained by the lower surface slope and shading of the West branch compared to the East branch.

2.4 Spatial changes in the glacier zones

The distribution of the glacier's zones have changed over the past 45years. Xie Zichu (1965) found that in 1962 the glacier consisted of four zones from terminus to summit: an ablation zone, an infiltration-congelation zone, an infiltration zone, and a recrystallization-infiltration zone. By 1989, the recrystallization-infiltration zone had disappeared, being taken over by the infiltration zone. Meanwhile, the boundaries of all zones moved upward and the accumulation area shrank considerably. By 2004, in addition to the continued change and upward march of the zone boundaries, a small meltwater pool (approximately 30 m^2) emerged at the upper end of the east branch (4224 m asl), evidently as a result of air temperature rise and absorption of solar radiation from increasingly exposed rocks (Li et al., 2005). The appearance of the meltwater pool suggests the melting of Glacier No. 1 is ongoing at both ends.

3. Glacier Processes Investigation Observations

3.1 Characteristics of atmospheric dust deposition in snow on the glaciers of the eastern Tien Shan, China

Wind-blown mineral aerosol dust derived from the crustal surface is an important atmospheric component affecting the Earth's radiation budget. Deposition of water-insoluble dust was determined in snow deposited on Urumqi glacier No. 1, Haxilegen glacier No. 51 and Miaoergou glacier, eastern Tien Shan, China. Analysis of the horizontal distribution of snow depth and concentration, and flux of dust particles in the snow cover suggests that dust deposition differs on each of these glaciers as the atmospheric environment changes from west to east. Mean mass concentrations of micro-particles in the size range 0.57-26 mm diameter at the three locations are respectively 969, 1442 and 3690 mg kg^{-1}, with an increasing trend from west to east. Dust layers in the snow cover contain Na- and Ca-rich materials typically found in central Asian dust particles. Volume size distributions of dust particles in the snow showed single-modal structures having volume median diameters of 3-22 mm. Dust profiles in the snow cover over the past 4 years reveal frequent, sporadic high dust concentrations with a large year-to-year variability, implying that dust deposition in the eastern Tien Shan is very sensitive to atmospheric environment change.

3.2 Characteristics of Surface Dust on Urumqi Glacier No. 1 in the Tien Shan Mountains, China

Monitoring studies show that many mountain glaciers worldwide are decreasing in mass. An important component of the process of ice mass loss is the effect of dust on albedo and its effect on glacier mass balance. The characteristics of surface dust were investigated in August 2006 on the Urumqi Glacier No. 1 in the Tien Shan Mountains, China. The bare ice surface of the glacier was mostly covered by brown dust. The amounts of surface dust on the ice surface (dry weight) ranged from 86 to 1113 g m^{-2} (mean: 335 g m^{-2}, standard deviation: =211), which is within the normal range for Asian glaciers, but significantly greater than those on glaciers in other regions such as Alaska, Patagonia, and the Canadian Arctic. An analysis of organic matter and microscopy of the surface dust revealed that the dust contained high levels of organic matter, including living cyanobacteria. This suggests that it is comprised not only of deposits of wind-blown desert dust, but is also a product of microbial activity on the glacier itself. Spectral albedo of the glacial surface showed spectrum curves typical of those of snow and ice contaminated with dust. The integrated surface albedo ranged from 0.09 to 0.24 (mean: 0.14) in the ice area, from 0.50 to 0.64 (mean: 0.56) in the snow area. The lower albedo on the glacial surface compared with that of clean bare ice or snow surface suggests that the albedo was significantly reduced by the surface dust on this glacier. Results suggest that the mineral and organic dust on the glacial surface substantially accounts for the recent

shrinkage of the glacier.

3.3 Characteristics of ionic concentration and$\delta^{18}O$ and their variability in dry-season and wet-season snow on Urumqi glacier No. 1, eastern Tien Shan, central Asia

To investigate the environmental and climatic significance of the ice-core records from the Tien Shan, central Asia, the characteristics of ionic concentration and oxygen isotopic ratio ($\delta^{18}O$) as well as their variability are assessed from surface-snow samples as well as old-snow samples collected year-round at weekly intervals from November 2002 to October 2005 onUrumqi glacier No. 1, eastern Tien Shan. The results indicate that the$\delta^{18}O$ in surface-snow samples is reversely coincident with air temperature and insignificantly affected by post-depositional processes. Ionic concentrations in the wetseason (1 November to 31 March) snow are overall higher than those in dry-season (1 April to 31 October) snow, while the variability of relative ionic composition between dry seasons is slightly less than that between wet seasons. During dry seasons, surface-snow chemistry was mostly controlled by the chemical content entrained in some sporadic precipitations. When precipitation is absent, the effect of all post-depositional processes together elevated the ionic concentrations in surface snow. During wet seasons, the snow chemistry is determined mainly by the input of aerosols entrained in precipitation and the elution process from percolation of meltwater.

3.4 Depositional characteristics of NH_4^+ on Urumqi glacier No. 1, eastern Tien Shan, China

Investigation into the depositional and post-depositional processes of atmospheric NH_4^+ on Urumqi glacier No. 1 (UG1), China, was implemented within the Program for Glacier Processes Investigation (PGPI) campaign. Aerosol and surface snow samples were collected concurrently on a weekly basis from March 2004 to March 2005 in the UG1 accumulation zone at the headwaters of the Urumqi river, eastern Tien Shan. All samples were analyzed for NH_4^+ and other chemical species. This paper investigates the seasonal variations of NH_4^+. A significant linear relationship (R^2=0.70, N=21, $P < 0.01$) between NH_4^+ concentrations in surface snow and aerosol was found during spring and summer, indicating that the warm–wet condition facilitates the air-snow exchange of NH_4^+. Humidity was found to be a significant meteorological factor influencing NH_4^+ in deposition in autumn and winter. The NH_4^+ concentration in aerosol clearly shows a trend similar to that in surface snow, suggesting that the variation of atmospheric NH_4^+ might have been preserved in the surface snow.

3.5 Development of depth hoar and its effect on stable oxygen isotopic content in snow-firn stratigraphy on Urumqi glacier No. 1, Eastern Tianshan, China

Long term data were used to determine the development of depth hoar and its relation to stable oxygen isotopic content in snow-firn stratigraphy on UG1 in the eastern Tianshan. Direct observations show that a depth hoar formed during mid-October and early June at the observation site. The depth hoar begins to form as the temperature gradient reached a maximum value of 13.0 $^oC\ m^-1$ on mid-October. From February to the end of March, the depth hoar is fully developed and account for 25 % of the total snow-firn pack depth. After April, as the weather becomes warm and meltwater percolates downward, the depth hoar rapidly turns into coarse-grained firn. Fractional condensation of water vapor (produced by sublimation of the snow) on growing snow crystals as the vapor moves vertically through the snow-firn pack results in isotopic fractionation. The bottom 15cm of the depth hoar show an increase in $\delta^{18}O$ associated with mass loss, and the upper part shows decrease associated with mass gain.

3.6 Seasonal variations of pH and electrical conductivity in a snow-firn pack on Glacier No. 1, eastern Tianshan, China

Analyses of pH and electrical conductivity (EC) in surface snow and snow-firn pack samples collected successively in a weekly basis during September 2002 to September 2004 on the east branch of Glacier No. 1, eastern Tianshan, China is presented. pH and EC in surface snow show obvious seasonal variations. pH and EC values are high in spring and early summer, and they are low in late summer; moreover, pH value indicates more and less alkalinity in spring and winter, respectively. In addition, both pH and EC peaks strongly coincide with the corresponding period of greatest NE and ENE wind velocity. After deposition, pH and EC in snow-firn pack display diverse features and seasonal trends, which correlate with snow compaction, dry deposition, precipitation and temperature, and so on. Furthermore, both pH and EC peaks occur above dust layers, and are adjacent to dust layers in some snow-firn packs. This implies that dust layers may have an influence on the elution process of soluble ions. In addition, linear correlation analyses among major chemical species (Na^+, K^+, Ca^{2+}, Mg^{2+}, NH_4^+, Cl^-, SO_4^{2-}, NO_3^-, pH and EC) in surface snow indicate that Ca^{2+} is the key ion determining pH and EC in the study area.

3.7 Atmosphere-to-snow-to-firn transfer of NO_3^- on Glacier No. 1, eastern Tien Shan, China

A two-year study of aerosol, surface snow, and snow pit NO_3^- was conducted to determine the depositional and post-depositional processes that occur on Glacier No.1 in the eastern Tien Shan Mountains. The concentrations of NO_3^- in both surface snow and aerosol display ambiguous seasonal changes. Low values are commonly observed during winter, and relatively high concentrations during autumn. Extremely high NO_3^- (> 4000 ng/g) concentrations were found in surface snow during September and October 2002. These concentrations are high enough to have a significant impact on the aquatic ecosystems of the eastern Tien Shan. Atmospheric back trajectories suggest that this event may have been the result of large late season fires in Kazakhstan. Other possible sources of the NO_3^- include local-to-regional anthropogenic emissions, which may be enhanced by transport in dust storms. Further research is required to assess whether such events are impacting the aquatic ecosystems of the region. A significant correlation between aerosol and surface snow NO_3^- concentrations was found for the dry season from December 2003 to mid-February 2004. The dominance of dry deposition during this season is believed to be the primary cause of the high correlation. While there was no significant correlation during the other seasons, a similar trend in the aerosol and surface snow NO_3^- was found suggesting that long term variations in atmospheric NO_3^- may be preserved in the surface snow. From the analysis of snow pack NO_3^- profiles it was determined that the NO_3^- stratigraphy at the site is formed by different processes during winter and summer. During winter the NO_3^- stratigraphy is due to the dry deposition of ambient aerosol followed by snow compaction and sublimation. During summer NO_3^- is deposited primarily by wet deposition and then eluted downward through the snow pack by meltwater. The percolation of meltwater was found to attenuate the NO_3^- stratigraphy, but still preserved some of its temporal variability in superimposed ice at the bottom of the snow pack. However, co-registration of NO_3^- with other soluble chemical species within the superimposed ice is probably lost due different elution characteristics. This has many implications for the interpretation of chemical records in similar alpine glaciers.

3.8 Preliminary results from measurements of selected trace metals in the snow–firn pack on Urumqi glacier No. 1

We present preliminary results on the occurrence of Pb, Cd, Zn, Al and Fe in dated samples collected from snow-firn packs at an altitude of 4130m on Urumqi glacier No. 1, eastern Tien Shan. Extreme precautions for avoiding contamination were taken throughout the sampling, processing, transportation and analysis procedures. The concentrations of trace metals were determined by a double-focusing inductively coupled plasma mass spectrometer in an ultra-clean room. The average concentrations for these metals in surface snow are (in ng g^{-1}): Pb, 2.4; Cd, 0.05; Zn, 10.0; Al, 100.0; and Fe, 130.0. These are higher concentrations (especially for Pb and Zn) than those in the polar and/or lowlatitude remote areas. The data show that the input of trace metals to the snow has a clear seasonal change. Lower concentrations in surface snow can be found in July through September and higher concentrations from October to March, with an exception for January. The mean concentrations of the elements in the snow-firn pack also indicate seasonal variations and show a marked inverse relationship with temperature, possibly a result of meltwater percolation in the snow-firn pack.

4. Streamflow Observations

4.1 Urumqi glacier No. 1 hydrometeorological station

The catchment area is 3.34 km^2 for the gauging station, of which approximately 54 % is covered by Urumqi glacier No. 1. The runoff at the gauging station demonstrates a significant amplification and an increase of 165.1×10^4 m^3 or 1.5 times on average from 1959 to 2006. Compared with the period 1959 to 1984, the average runoff during 1985 to 2006 has increased by 66 %. The temporal variation during the period 1959 to 2006 is inversely correlated with the glacier mass balance of Urumqi glacier No. 1 (R^2 = 0.53; N = 48; P $<$ 0.01), as shown in Fig 6.1, which suggests that the escalating runoff largely originates from the increased meltwater production as a result of the mass loss of the glacier.

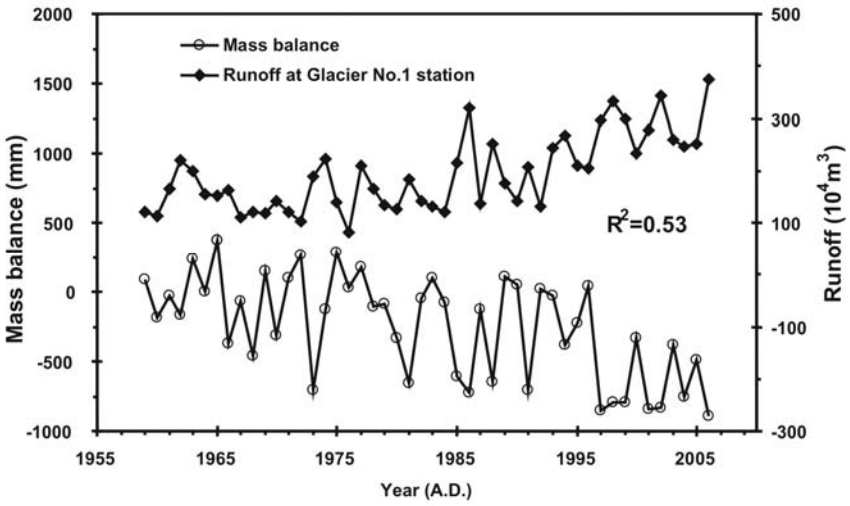

Fig 6.1. Comparison of runoff at Urumqi glacier No. 1 hydrometeorological station together with the annual mass balance of Urumqi glacier No. 1, illustrating that they have an explicit inverse correlation.

Fig 6.1 also shows that the negative mass-balance year increases modestly from 1959 to 1985 and rapidly from 1986 to 2006. Prior to 1985, the mass balance was determined by both precipitation and temperature, whereas after 1986, it is mainly controlled by the temperature, even under a high-precipitation regime (Li *et al*., 2007). Several previous studies (Li *et al*., 2003, 2007; Han *et al*., 2006; Jing *et al*., 2006) have indicated that the recession of Urumqi glacier No. 1 resulting from climate warming prevails throughout the entire period of observation and has shown an accelerated tendency since the mid-1980s, particularly after 1995. The area of the glacier has reduced a total of 0.27 km^2 or 14.0 % from 1962 to 2006, especially in the last 14 years from 1992 to 2006 , whereby the reduction totaled 0.16 km^2, an amount greater than the area reduction from the last 30 years during 1962 to 1992. The terminus has undergone a constant recession since 1958, which has accelerated ever since the mid 1990s from 4.5 to 5 m/a. The continuous mass reduction led to the separation of the two glacier tributaries in 1993, which increased the terminus area of the glacier and in turn enhanced glacial melting. Furthermore, the radar sounding measurements demonstrated that ice thinning occurred from 1980 to 2001, and became more remarkable from 2001 to 2006. Consistent with glacier thinning, the maximum surface velocity has exhibited a decreasing trend since the 1980s.

In contrast to a steep temperature rise during 1997 to 2006, the runoff demonstrates a gradual increase since 1986. This is not only produced by enhanced melt due to warming, but also by an increase in precipitation from 1986, which has a dual effect: direct increase in runoff and enhanced ice melt due to heat transfer by liquid precipitation.

4.2 Zongkong hydrometeorological station.

The runoff at Zongkong hydrometeorological station shows a similar annual fluctuation compared to the precipitation trend (Fig 6.2), indicating a major contribution from precipitation. With an approximate 18.5 % glacierized-area in the catchment, glacial melt is considered an important component of the runoff, which is revealed by the observed runoff ratio (runoff / precipitation) average value of 1.1 at the station, a value much higher than in the nearby non-glacierized catchment of Empty Cirque where it is approximately 0.7. The annual runoff at the station demonstrates an overall ascending trend and increased approximately 355.4×10^4 m^3 or 29.6 % on average from 1983 to 2006. Nevertheless, considering the 34.7 % increase in precipitation and escalating glacial melting during the same period, the runoff did not rise to a higher-than-expected level, especially after 2000. Further analysis shows that the average runoff ratio actually reduced by 3 %, indicating the inefficient tendency of precipitation in contributing to runoff and (or) the reduction of glacial melting. Similar cases have been observed in other areas of Tianshan during the last decade, where the increase of precipitation and temperature did not lead to an apparent increase of surface runoff.

A possible explanation of the smaller predicted runoff is that the increased precipitation is lost predominantly as enhanced evaporation resulting from temperature rise, or is percolated to the groundwater system. The enhanced ecological development, perhaps mainly the plant colonization resulting from

temperature rise may also raise the water consumption as well in the catchment. In addition, despite the increase of meltwater from Urumqi glacier No. 1, the glacial runoff from the other six small glaciers (0.61 km^2 for each glacier on average) in the catchment may have started to decline in recent years as a result of decreased glacierized-area and corresponding reduction in glacial melting.

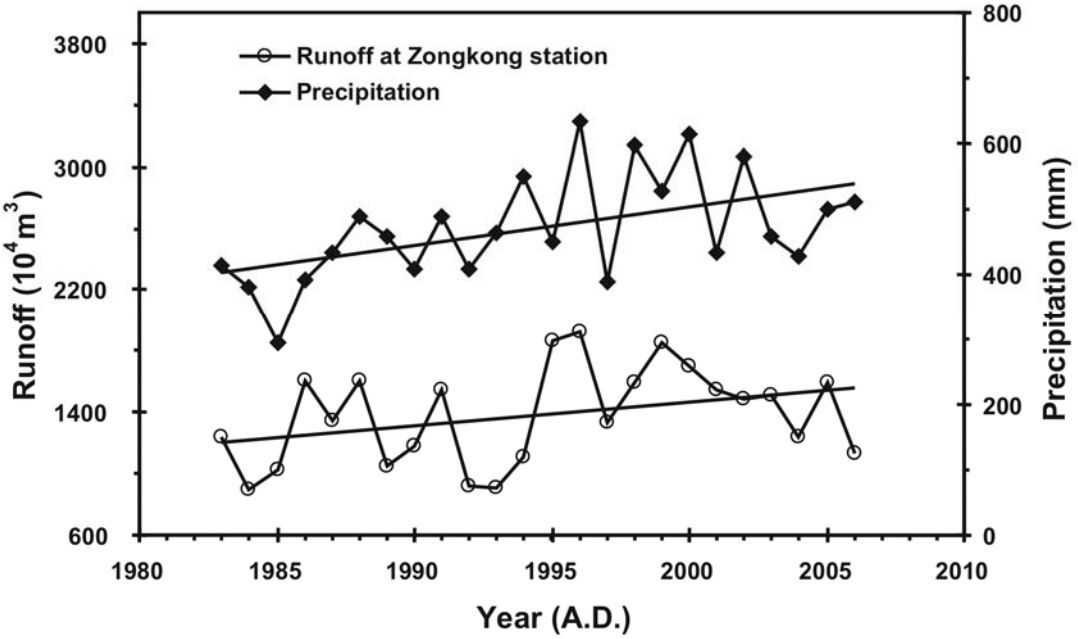

Fig 6.2. Runoff records at Zongkong hydrometeorological station and precipitation observed at Daxigou meteorological station from 1983 to 2006 with corresponding linear regressions.

4.3 Empty Cirque hydrometeorological station.

Due to the absence of glacier cover in the catchment, the major water source for this station is seasonal snowmelt. The annual snowfall in the catchment after applying a wind correction averages approximately 560 mm a^{-1} (Wang and Zhang, 1985; Yang *et al*., 1988), which is about 33% higher than at the Daxigou meteorological station. The annual runoff (see Fig 6.3) is found to be well correlated to the precipitation (R^2 = 0.53; N = 12; P = 0.07) and associated with the temperature from 1982 to 1993. The water balance at the gauging station can be simply described by the following equation:

$$R = P - E - \Delta S \quad (1)$$

where R is runoff at the station, P is precipitation, E is evaporation (including sublimation), and ΔS is the change in the storage of snow, ground ice, and soil moisture in the catchment (Woo *et al*., 1994). The coarse materials of the catchment ground facilitate rapid infiltration and exfiltration rendering a large ΔS. Compared to P and ΔS, the magnitude of E is insignificant. Under normal air temperatures, the runoff ratio R/P is calculated as 0.75 indicating a very efficient P to R transit. At abnormally low or high temperatures, the meltwater from the snow cover enables ground ice formation or ice storage release, respectively. This case was found during the period 1984 to 1987. The runoff in 1985 was a record low, inexplicable because of the low precipitation. Note that the air temperature in the previous year (1984) was extremely low, which might have possibly contributed to the transformation of meltwater infiltration to ground ice, effectively storing water in the active layer of the catchment ground. As the temperature rose in subsequent years, the stored water from previous years was released due to the melting of ground ice and resulted in a subsequent increase in runoff. Therefore, the record high of annual runoff in 1987 is considered to be a combined result of high precipitation and groundwater exfiltration.

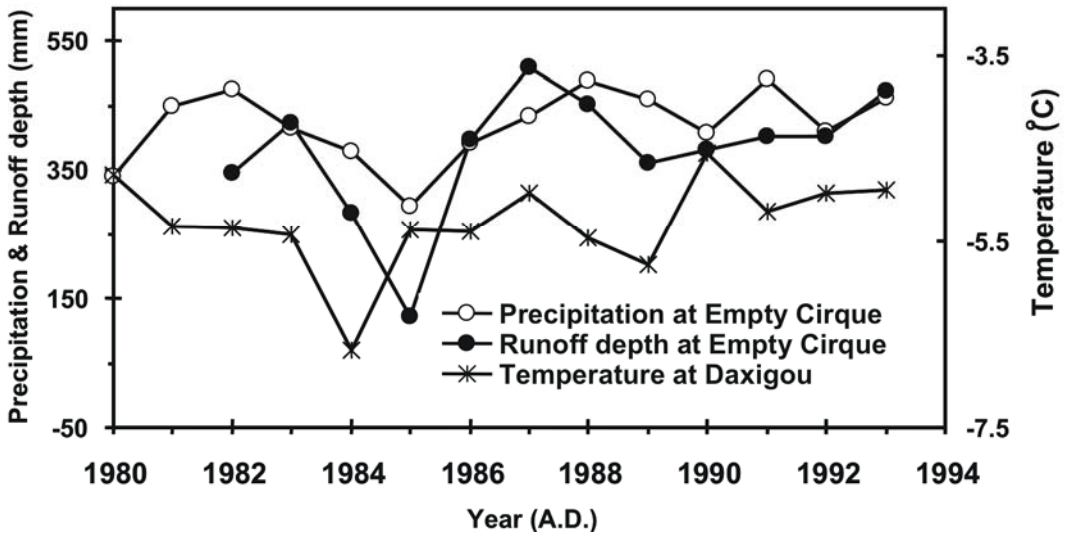

Fig 6.3. Runoff depth and the precipitation records at Empty Cirque hydrometeorological station, and air temperature observed at Daxigou meteorological station from 1980 to 1993.

Reference

1) Chen Jianming, Liu Chaohai, Jin Mmgme, 1996. Application of therepeated aerial photogrammetrY to monitoring glacier variation in the drainage area of the Uriimqi River. Journal of Glaciology and Geocryology, 18(4), 331-336
2) Dong Zhiwen, Li Zhongqin, Wang Feiteng and Zhang Mingjun. 2009. Characteristics of atmospheric dust deposition in snow on the glaciers of the eastern TienShan, China. Journal of Glaciology, 55(193), 797-804
3) Dong Zhiwen, Zhang Mingjun, Li Zhongqin, Wang Feiteng.2009.The pH value and electrical conductivity of atmospheric environment from ice cores in the Tianshan Mountains. Journal of Geographical Sciences, 4, 416-426
4) Jiawen Ren, Zhefan Jing, Jianchen Pu, Glacier variations and climate change in the central Himalaya over the past few decades, Annals of Glaciology, 2006, 43, 218-222
5) Kang Ersi,Yang Zhenniang, Lai Zuming et al, 2000. Runoff of snow and ice meltwater and mountainous rivers. In: Shia Yafeng ed Glaciers and Their Environments in China ---The Present, Past and Future. Beijing; Science Press, 190-233
6) Lanzhou Institute of Glaciology and Geocryology, Chinese Academy of Sciences, 1986. Glacier Inventory of China (III); Tianshan Mountains (Ili Biver Drainage Basin).Beijing; Science Press, 1-158
7) Lanzhou Institute of Glaciology and Geocryology, Chinese Academy of Sciences, 1986. Glacier Inventory of China (III); Tianshan Mountains (Interior Drainage Area of Scattered Flow in East).Beijing: Science Press, 1 1-83
8) Lanzhou Institute of Glaciology and Geocryology, Chinese Academy of Sciences, 1986. Glacier Inventory of China (III); Tianshan Mountains (Interior Drainage Area of Tarim Basin in Southwest. Beijing:Science Press, 1-187
9) Lanzhou Institute of Glaciology and Geocryology, Chinese Academy of Sciences, 1986. Glacier Inventory of China (III); Tianshan Mountains (Interior Drainage Area of Junggar Basin in Northwest).Beijing: Science Press, 1-206
10) Li Baolin, Zhu A-xing, Zhang Yichi et al, 2006. Glacier change over the past four decades in the middle Chinese Tien Shan. Journal of Glaciology and Geocryology, 52(178), 425-432
11) Li Huilin, Li Zhongqin, Shen Yongping, Wang Feiteng, Wang Wenbin. 2007. Summarization and perspective of Dynamic models for mountain glaciers. Journal of Glaciology and Geocryology, 29(2), 201-208
12) Li Huilin, Li Zhongqin, Wang Wenbin, Wang Feiteng.2008. Deposition characteristic of the NH_4^+ on Urumqi glacier No.1, eastern Tien shan,China. Annals of glaciology, 49, 161-165
13) Li Huilin,Li Zbongqin,Qin Dahe eds, 2009. Basic Principles of Glacial Dynamic Models and Observation Guide for Corresponding Parameters. Beijing: China Meteorologlical Press, 1-56
14) Li Zhnngqin, Han Tianding, Jing Zhefan et al, 2003. A summary of 40-yearobserved variation facts of climate and glacier No.1 at headwater of Urumqi River, Tianshan, China. Journal of Glaciology andGeocryology, 25 (2), 117-123
15) Li Zhnngqin, Wang Wenbin,Zhang Mingjun et al, 2009. Observed changes in streamflnw at the headwaters of the Uriimqi River, Eastern Tianshan, Central Asia. Hydrological Processes, doi: 10.1002/hyp.7431
16) Li Zhongqin, Li Chuanjin, Li Yuefang, Wang Feiteng. 2007. Preliminary results from measurements of selected trace metals in the snow-firn pack on Urumqi glacier No.1, eastern Tien Shan, China. Journal of Glaciology, 53(182), 368-373
17) Li Zhongqin, Ross Edwards, E. Mosley-Thompson, Wang Feiteng, et al. 2006. Seasonal variabilities of ionic concentrations in surface snow and elution process in snow-firn packs at PGPI site on Glacier No.1, in eastern Tianshan, China. Annals of glaciology, 43, 250-256
18) Li Zhongqin, Shen Yongping, Wang Feiteng et al, 2007. Response of glacier melting to climate change---Take Uriimqi glacier No.1 as an example. Journal of Glaciology and Geocryology, 29(3), 333-342
19) Li Zhongqin, Wang Feiteng, Zhu Guocai et al, 2007. Basic features of the Miaoergou flat-topped glacier in East Tianshan Mountains and its thickness change over the past 24 pears. Journal of Glaciology and Geocryology, 29(1), 61-65
20) Li Zhongqin, Wang Wenbin, Zhang Mingjun, Wang Feiteng. 2009. Observed changes in streamflow at the headwaters of the UrumqiRiver, eastern Tianshan, central Asia. Hydrological Processes, DOI:10.1002/hyp.7431

21) Li Zhongqin, Wenbin Wang, Feiteng Wang, Huilin Li. 2008.Characteristics of ionic concentration and $\delta^{18}O$ and their variability in dry season and wet season snow on Urumqi Glacier No. 1 in eastern Tianshan, China.Annals of glaciology, 49, 217-223
22) Liu Shiyin, Ding Ynngjian, Shangguan Dnnghui et al, 2006. Glaeier repeat as a result of climate wanning, and increaed precipitation in the Tarim River basin, North West China.Annals of GLacioLogy, 43, 91-96
23) Mountaineering and Expedition Term of Chinese Academy of Sciences, 1985. Glacial and Weather in Mt. Tuomuer District, Tianshan. Uriimqi; Xinjiang People's Publishing House, 32-98
24) Oerlemans J,Anderson B, Hubhard A et al, 1998. Modeling the response of glaciers to climate warming. Climate Dynamics, 14(4), 267-274
25) Shangguan Donghui, Liu Shiyin, Ding Yongjian. Glacier changes in the West Kunlun Shan from 1970 to 2001 derived from Landsat TM/ETM+ and Chinese glacier inventory data. Annals of Glaciology, 2007, 46, 204-208
26) Shen Yongping, Liu Shipin, Ding Yongjian et al, 2003. Glacier mass balance change in Tailanhe River watersheds on the Tianshan Mountains and its impact on water resources. Journal of Glaciology and Geocryology, 25 (2), 124-129
27) Shi Yafeng, 2005. Concise Chinese GLacier Inventory. Shanghai;Shanghai Scientific Popularization Press, 17-188
28) Su Zhen, 1998. Glaciers and Environment of the Karakorum-Kunlun Mountains.Beijing: Science Press, 10-123
29) Wang Feiteng, Li Zhongqin, R. Edwards, Li Huilin. 2007. Long term changes in the Snow-Firn pack Stratigraphy on Glacier No. 1, Eastern Tianshan Mountains. Annals of glaciology, 46, 331-334
30) Wang Feiteng, Li Zhongqin, You Xiaoni et al. 2006. Seasonal evolution of aerosol stratigraphy in Glacier No. 1 percolation zone, eastern Tianshan, China. Annals of glaciology, 43, 245-249
31) Wang Feiteng, Li Zhongqin, Li Huilin, Zhang Mingjun, Wang Wenbin, Wang Lin. 2008.Development of depth hoar and its effect on stable isotopic content in snow-firn stratigraphy on Urumqi glacier No.1, eastern Tien shan ,China. Annals of glaciology, 49, 135-138
32) Wang Lilun, Liu Chaohai, Kang Xingcheng et al, 1983. Fundamental features of modern glaciers in the Altay Shan of China. Journal of Glaciology and Geocryology, 5 (4), 27-38
33) Wang Zongtai, 1991. A discussion on the questions of development of Heigou Glacier No.8 at Bogda-peak region. Journal of Glaciology and Geocryology, 13(2), 141-158
34) Wu Guanghe, Zhang Shunping, Wang Zhongxiang, 1983. Retreat and advance of modern glaciers in Bogda, Tianshan. Journal of Glaciology and GeocryoLogy, 5 (3), 143-152
35) Xie Changwei,Ding Yongjian,Liu Shiyin et al, 2006. Variation of Keqikaer glacier terminus in Tomur peak during last 30 years. Journal of Glaciology and Geocryology, 28(5), 672-677
36) Xie Zichu, Wang Xin, Kang Ersi et al, 2006. Glacier runoff in China:An evaluation and prediction for the future 50 years. Journal of Glaciology and Geocryology, 28(4), 457-466
37) Yang Zhenniang, 1991. Glacier Water Resources in China. Lanzhou Gansu Science and Technology Press, 81-150
38) Ye Baisheng, Daqing Yang, Keqin Jiao, et al. The Urumqi River Source Glacier No. 1, Tianshan, China: Changes over the Past 45. Geophysical Research Letters, 2005, 32(21), doi:10.1029/2005GL024178
39) Zhang Yong, Liu Shiyin Xu Junli. Glacier change and glacier runoff variation in the Tuotuo River basin, the source region of Yangtze River in western China. Environ Geol, 2008, 68(56), 56-59
40) Zhao Zhongping; Li Zhongqin, Ross Edwards, Wang Feiteng, et al. 2006. Atmosphere-to-snow-to-firn transfer of NO_3^- on Glacier No. 1, eastern Tien Shan, China. Annals of glaciology, 43, 239-244

Chapter 7. Cryospheric Science in Polar Regions

XIAO Cunde[1, 2] LI Yuansheng[3]， Ding Minghu[1,2]

1. State Key Laboratory of Cryospheric Sciences, Cold and Arid Regions Environmental and Engineering Research Institute, Chinese Academy of Sciences, Lanzhou 730000, China; 2. Chinese Academy of Meteorological Sciences, 46 Zhongguancun South Avenue, Beijing 100081, China; 3. Polar Research Institute of China, 451 Jinqiao Road, Pudong, Shanghai, 200136, China.

3． Glaciological and climatological studies along the traverse route from Zhongshan to Dome A, Antarctica

1.3 Snow accumulation rate, snow/ice chemistry and ice flow

Stake measurements of surface snow accumulation have been made at 2-km intervals since January 1997 along a 1248-km traverse route from Zhongshan Station, Antarctica, to the Dome A summit *(Fig 7.1)*. The surface snow density was measured to convert the stake height to surface mass balance. According to topographical parameters, meteorological features and the records of ~650 stakes and 6 stake arrays, the route is divided into and discussed as 5 sectors. They find that although the altitude increases from the coast to Dome A, the average annual accumulation rate in the region 524-800 km from the coast for 1999-2008 (52.3 kg m^{-2} a^{-1}) is lower than that in the region 800-1128 km from the coast (71.8 kg m^{-2} a^{-1}). These two sections exhibit the highest standard deviations in accumulation due to wind-driven processes and/or topography. The Dome A area (1128-1248 km) has the lowest accumulation rate (34.7 kg m^{-2} a^{-1}, 2005-2008) along the traverse route due to its higher elevation and distance from the coast. The accumulation rate in the region 202-1128 km from the coast exhibits little change from 65.52 kg m^{-2} a^{-1} (1999-2005) to 65.55 kg m^{-2} a^{-1} (2005-2008), but the accumulation rate at 524-1128 km has increased from 59.38 kg m^{-2} a^{-1} (1999-2005) to 64.85 kg m^{-2} a^{-1} (2005-2008). Inland snow accumulation has increased over the past 11 years *(Fig 7.2)* (Ding et al., 2010).

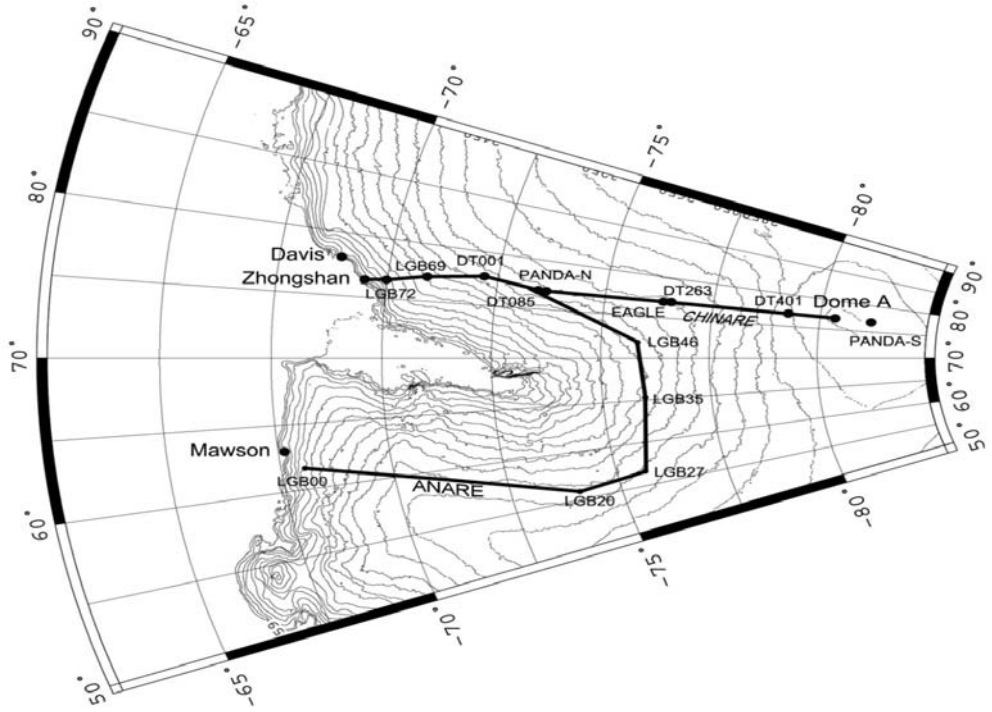

Fig 7.1 Map of the traverse area and location of stake arrays, firn cores and automatic weather stations. (ANARE is the Australian National Antarctic Research Expedition).

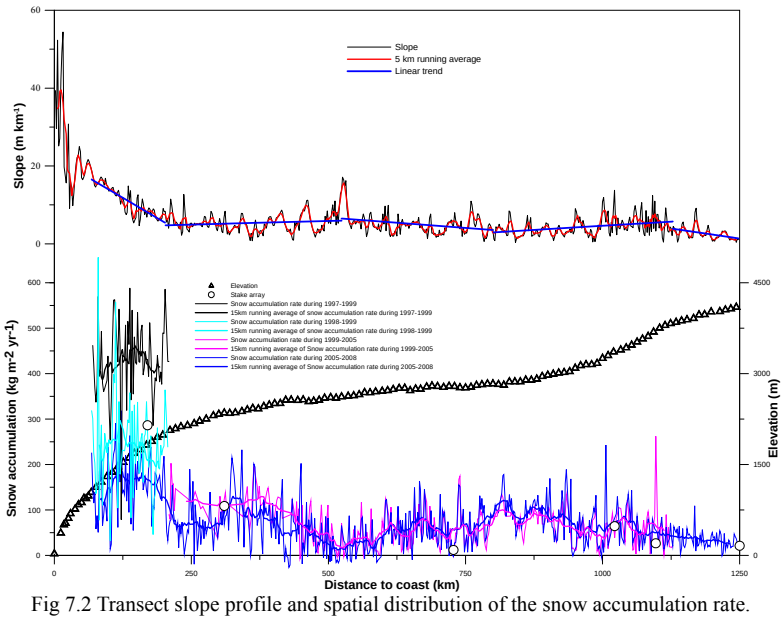

Fig 7.2 Transect slope profile and spatial distribution of the snow accumulation rate.

The stable isotope ratios of the surface snow were measured to investigate their relationships with temperature and geographical parameters (latitude, longitude, altitude and distance from the coast; (Fig 7.3). The results reveal a strong positive correlation (R=0.945) between δ^{18}O and annual mean temperature, with a gradient of 0.84‰ ℃$^{-1}$, which is a little higher than in Terre Adelie Land. Regression analyses also show that the δ^{18}O of surface snow is strongly correlated with distance to the coast (R=0.942), latitude (R=0.942), and altitude (R=0.941). But no significant correlation was found between δ^{18}O and longitude in the study area. Altitude should be the most important factor influencing the δ^{18}O distribution because of distinctive topography. The δ^{18}O-altitude and T-altitude gradients along this transect are determined to be -1.1‰/100m and 1.31°C/100m, respectively. The δD is similar to δ^{18}O, with a gradient of 6.412‰ ℃$^{-1}$ to annual mean temperature (Ding et al., 2010).

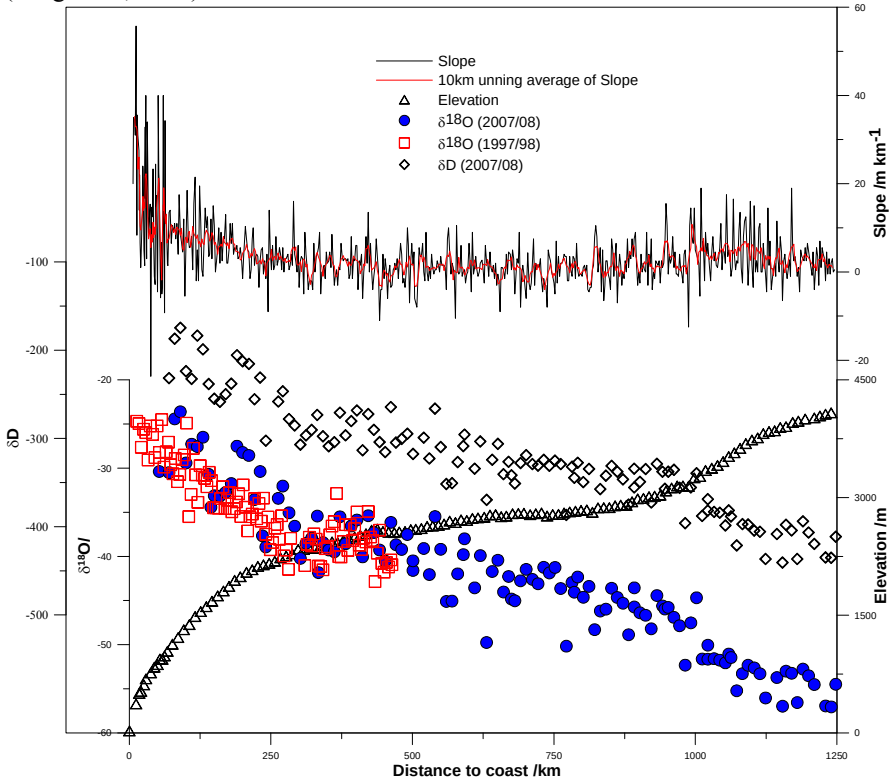

Fig 7.3. The Variability of $\delta^{18}O$ and δD along Zhongshan Station to Dome A route.

During the 21st CHINARE, more than 20 global positioning system (GPS) sites were established at approximately 50 km intervals along the 1228km traverse route, to monitor the surface ice velocity, which will be reported elsewhere. Here, we present the surface topography of the summit of Dome A (Fig 7.4) measured by real-time kinematic (RTK) GPS, a tool that is well suited to surface topography measurements in the interior of the Antarctic as it allows high-precision measurements to be made relatively quickly and with minimum logistical support (Zhang et al., 2007).

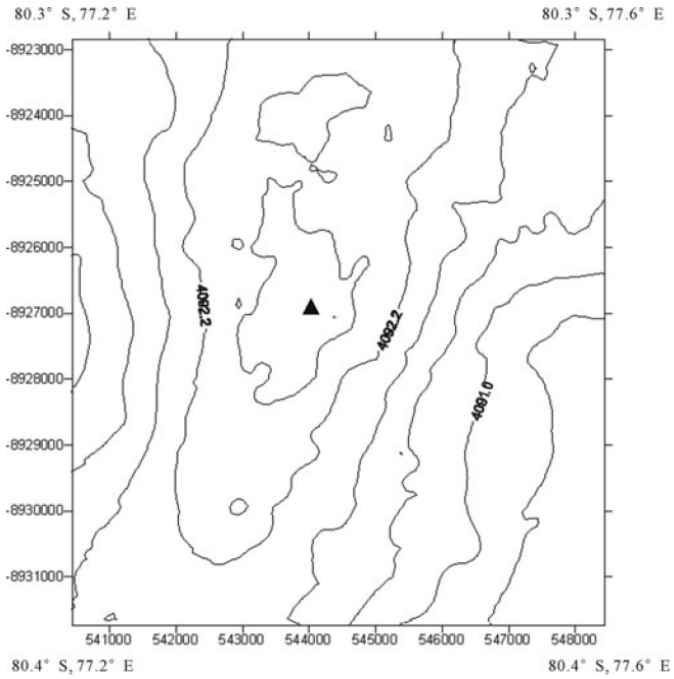

Fig 7.4 Dome A surface topographic map based on GPS data from the 21st CHINARE. Heights are relative to the WGS84 ellipsoid. Contour interval is 0.40 m. The black triangle indicates the position of the summit of Dome A.

Based on an estimate of the summit position from the topography around Dome A, obtained from the RADARSAT-1 Antarctic Mapping Project (RAMP) digital elevation model (Liu et al., 1999), a survey was carried out during 9–11 January 2005 using a total station to obtain a second estimate of the summit position. A camp was set up at this new position which was established as a reference station, initially occupied by a GPS receiver for 36 hours. The location of the reference station was calculated using Leica Geo Office (LGO) V1.0 point positioning software. The World Geodetic System 1984 (WGS84) ellipsoid coordinates were 80 22 01.62888 S, 77 22 22.90269 E, 4092.457 m.

Repeat GPS measurements provided ice velocities along Zhongshan to Dome A traverse line (Zhang et al., 2008). The horizontal surface ice velocities increase from the summit of the ice sheet to the coast. In the Dome A area, the velocities are <10m a^{-1}; in the plateau area, velocities range from 8 to 24m a^{-1} and reach about 98.2m a^{-1} at a site (LT980) near the coast. The flow directions are roughly perpendicular to the ice-sheet surface elevation contours, primarily toward the Lambert Glacier basin *(Fig 7.5).*

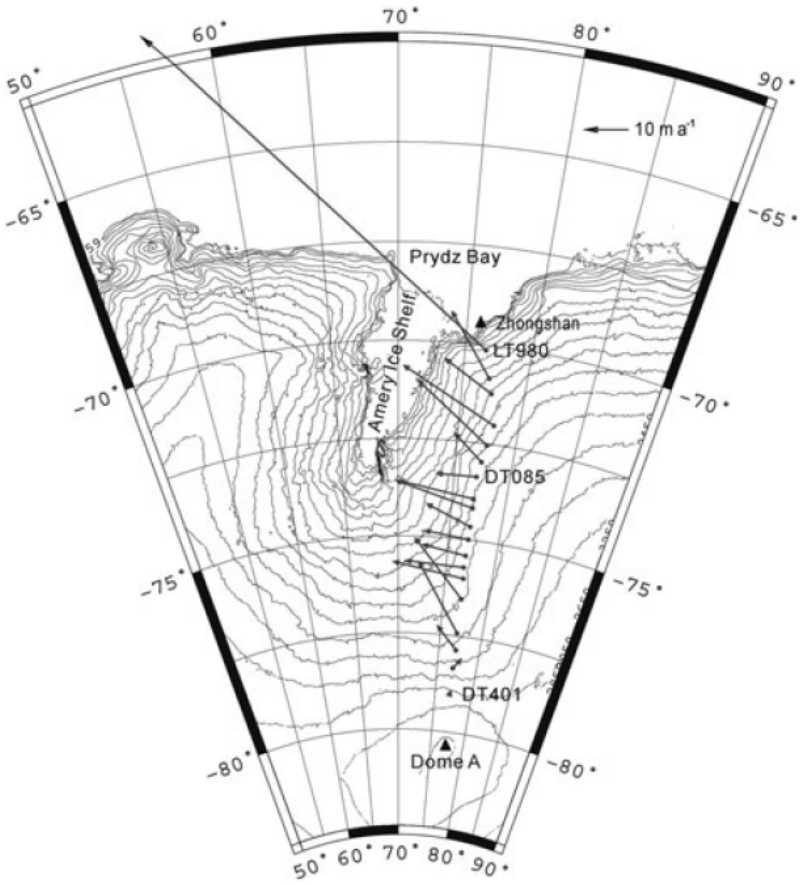

Fig 7.5 Vector map of surface ice flow along the traverse from Zhongshan station to Dome A. (Elevation contours derived from the RAMP DEM.)

Present measurements of surface topography of the summit area of Dome A (Fig 7.6), based on post-processing of differential GPS data. Fast-static differential GPS is a useful tool in measuring surface topography in the Antarctic interior, because it allows high-precision measurements to be made relatively quickly with minimal logistical support. The post-processing fast-static differential technique was chosen, as the distance maximum (14 km) between the rover and the base station exceeds the communication limit of the radio of the GPS system (Cheng et al., 2009).

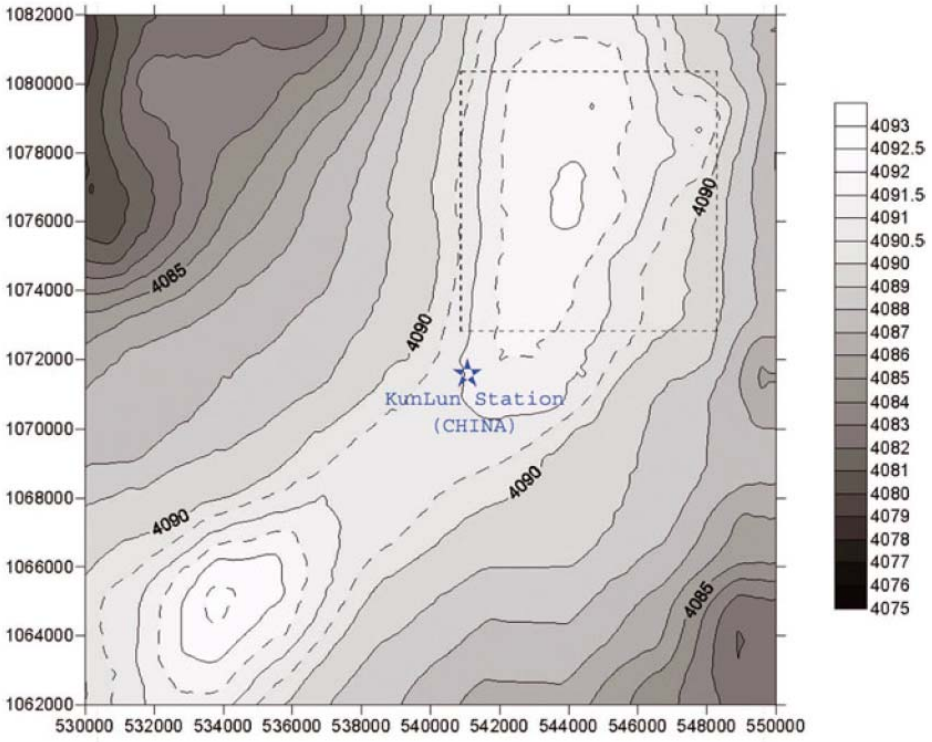

Fig 7.6 Map of surface topography over the Dome A region surveyed by the 24th Chinese Antarctic National Research Expedition (CHINARE) in January 2008. Heights are with respect to the WGS84 system. The map is projected into the Universal Transverse Mercator (UTM) 43S zone. Contour interval is 1m (with dashed contours at 0.5 m). The dashed rectangle covering the northern peak is the 64km2 area surveyed in early 2005 (Zhang et al., 2007).

1.4 Meteorology and Climatology

The first multiyear surface meteorological observations over Dome A, the highest ice feature in the entire Antarctica continent, are analyzed to understand the surface wind, temperature, and stability climatology over Dome A and how it differs from the surface climatology at two lower-latitude/lower-elevation sites along similar longitude in East Antarctica. The climatology is also compared with that over Dome C. In contrast to the surface winds at lower sites, where moderate to strong northeasterly winds prevail with a distinct diurnal oscillation in wind speed in response to the diurnal change in katabatic forcing, summertime surface winds over Dome A are very weak, are variable in direction, and show little diurnal variation. Although both temperature and temperature gradient oscillate diurnally, the gradient over Dome A remained positive all day long, indicating a persistent surface inversion, while at the two lower sites, as well as over Dome C, sufficient insolation leads to the breakup of inversion and the development of a convective boundary layer in the afternoon. Wavelet analysis of near-surface stability revealed that besides the strong diurnal signal, the near-surface stability also exhibits annual, semiannual, and interseasonal (period _50 days) oscillations at all locations. These oscillations in near-surface stability are linked to the same peaks in the 500-hPa geopotential height spectra and therefore are believed to be caused by variations of synoptic conditions (Zhou et al., 2009).

Seasonal variation of temperature, pressure, snow accumulation, winds, and their harmonic analysis are presented by using the data from Zhongshan Station and three Automatic Weather Stations deployed between the East Antarctic coast and the summit of the ice sheet at Dome A for the period 2005–07 (Fig 7.1). Results show that: 1) temperature, snow accumulation and specific humidity decrease with increasing elevation and distance from the coast, with snow accumulation decreasing from 199 mm water equivalent (w.e.) yr^{-1} at LGB69 (180 km from the coast) to 31 mm w.e. yr^{-1} at Dome A, 2) Dome A experiences an extremely low minimum temperature of -82.5°C with the monthly mean temperature below -50°C for eight months in contrast to Zhongshan Station which does not show any monthly mean temperatures below -20°C, 3) mean surface wind speed increases from the coast to the escarpment region, and then reduces rapidly towards the interior plateau with the strongest winds occurring at katabatic sites with the greatest surface slopes (Fig 7.7), 4) temperature and pressure all shows a distinct biannual oscillation with a main

minimum in spring and a secondary minimum in autumn, differing slightly from station to station, and 5) winter temperature corelessness increases as a function of elevation and distance from the coast, from 0.260 at the coastal Zhongshan Station to 0.433 at Dome A (Ma et al., 2010).

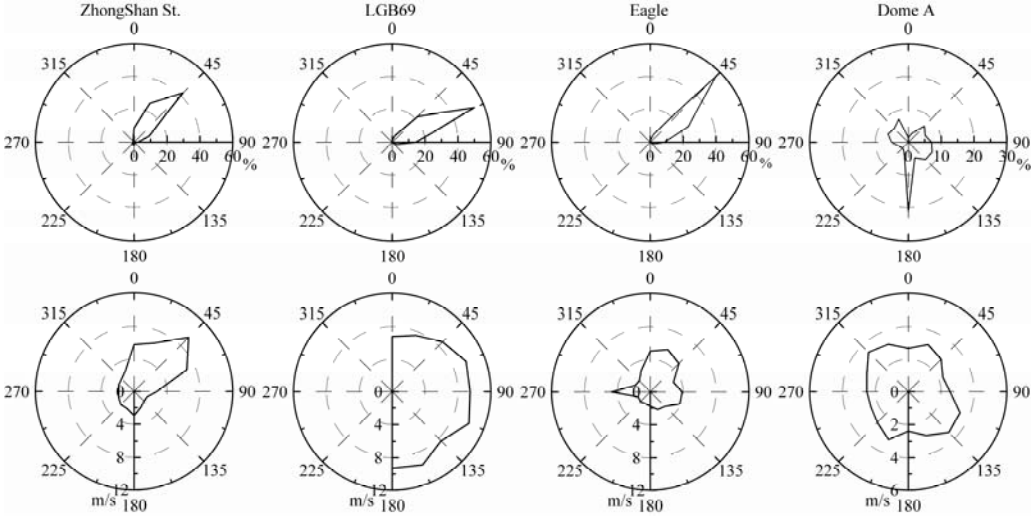

Fig 7.7. Wind direction/speed rose charts for all stations along the ZS–Dome A section.

1.5 Ice core record

Volcanic signals recorded in the Antarctic and Greenland ice cores can provide useful information on past explosive volcanism and its impact. In this study, we carried out a continuous sulfate analysis of a 102.65 m East Antarctic ice core (DT－401, dated as 2682 years) and identified 36 extensive volcanic eruption signals using Cole－Dai's method, which gives an average of 1.4 eruptions per century, consistent with the results from the Plateau Remote (PR－B) ice core (Fig 7.8). When the record is divided into three parts, the latest millennium (1999–1000 A.D.), the middle millennium (999–1 A.D.), and the earliest 682 years (0 A.D. to 682 B.C.), it is found that there were more volcanic eruptions that occurred during the latest millennium (19 eruptions) than during the middle millennium (10 eruptions) of the record and that the intensities of the eruptions in the latest millennium are markedly larger than those in the middle one. There were only seven events recorded in the earliest 682 years, but their intensities were greater, and nearly half of the eruptions had a similar intensity to Tambora's (1815 A.D.), which differs from the PR－B record. It is also found that volcanism and its average accumulation rate were lower during the "Little Ice Age" than during the "Medieval Warm Period." Comparison of volcanic records between DT－401 and other Antarctica ice cores (PR－B, Dome C, DT－263, and Byrd) show that in the East Antarctica area with its lower accumulation rates, postdepositional effects may play an important role in the deposition of the sulfate (Ren J. etc. 2010).

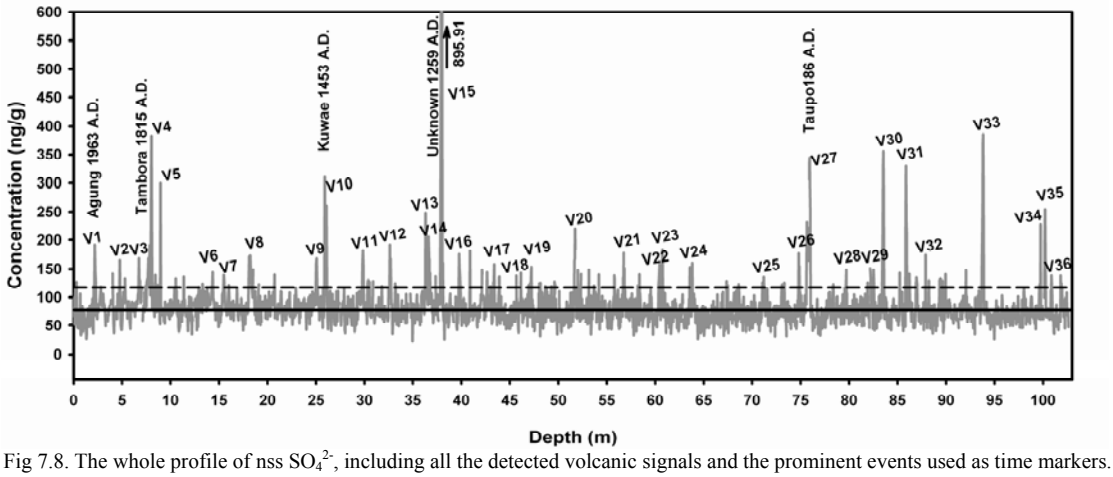

Fig 7.8. The whole profile of nss SO_4^{2-}, including all the detected volcanic signals and the prominent events used as time markers. The

solid straight line shows the mean value of the nss SO_4^{2-} after subtraction of the prominent volcanic signals. The dashed straight line shows the threshold value for the volcanic signals (background mean + 2σ), and the solid curve shows the 20 year running mean values of the nssSO_4^{2-}.

Chemical analysis of a shallow (82.5 m) ice core from a location (DT263) in the essentially unexplored area of Princess Elizabeth Land, East Antarctica, has been used to construct a continuous, high-resolution 780-year (AD 1207–1996) glaciochemical record. During the twentieth century, snow accumulation rates and concentrations of chemical species in snow appear to be stable with short-term variations, indicating relatively stable and warm climatic conditions. The period of AD 1450–1850 in this record is characterized by sharply reduced snow accumulation rates and decreased concentrations of several chemical species that suffer postdepositional losses linked to very low accumulation rates (Fig 7.9). These characteristics are consistent with colder climatic conditions and suggest that this is likely a neoglacial episode. The timing of this episode coincides with the Little Ice Age (LIA), a relatively cold period in the Northern Hemisphere between the beginning of the fifteenth century and the end of the nineteenth century. Evidence in ice core and sedimentary records also indicates neoglacial conditions in some Southern Hemisphere locations during the general time frame of LIA. The DT263 record, along with a few published ice core records, points to the existence of an LIA-type climatic episode in Antarctica between the fifteenth century and the twentieth century. However, other Antarctic ice core records show no such evidence. Together, these records highlight the regional differences in Holocene climate variations in Antarctica. The DT263 record suggests that colder and drier conditions prevailed during the LIA time period at the eastern Indian Ocean sector of East Antarctica (Li Yuansheng etc. 2009).

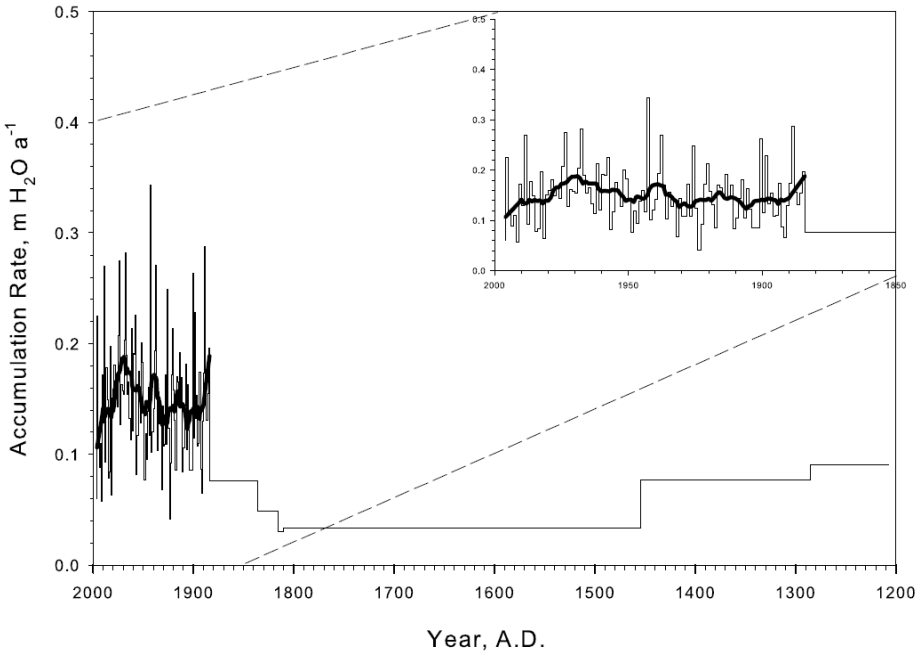

Fig 7.9 Snow accumulation rates over the last 780 years as recorded in the DT263 ice core. Accumulation rates for the period of 1884–1996 (inert) are based on measured annual layer thickness, and the data prior to 1884 are averages between volcanic time stratigraphic markers. Heavy lines represent smoothed data.

4. Interaction between snow and atmosphere and preliminary results of deep ice core drilling at Dome A region

2.1 Interaction between snow and atmosphere at Dome A region

Based on the horizon of β activity and the density profiles, recent accumulation rate at Dome A, Antarctica is calculated to be 0.023 m water equivalent per year (Fig 7.10). This value is comparative to the accumulation rates deduced from the other inland sites of Antarctica. Clear-sky precipitation (or diamond dust) dominates the total precipitation at Dome A region. We speculate Dome A as a potential site to discover the oldest ice in Antarctica due to its tremendous ice thickness (>3000 m), extremely low accumulation rate, and low ice velocity (Hou et al., 2007).

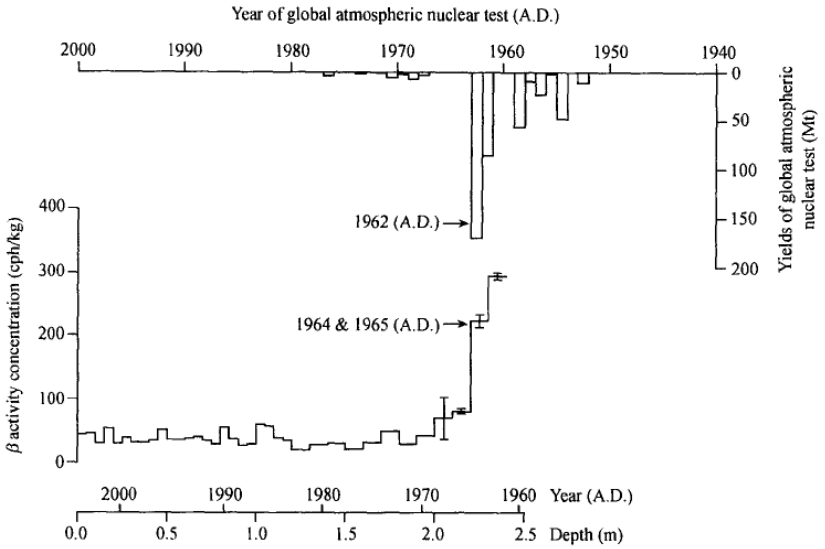

Fig 7.10 The β activity profile at Dome A in comparison to the yields of the global atmospheric nuclear tests. The results of the bottom 4 samples are the averages of three independent measurements and ± one standard deviation.

An assessment of the glaciological and meteorological characteristics of Dome A, the summit of the East Antarctic ice sheet, is made based on field investigations during the austral summer of 2004/05. Knowledge of these characteristics is critical for future international studies such as deep icecore drilling. The assessment shows that: (1) Dome A is characterized by a very low 10m depth firn temperature, –58.38℃ (nearly 38℃ lower than at EPICA Dome C and 18℃ lower than at Vostok). (2) Automatic weather station (AWS) measurements of snow surface height and reference layers in a snow pit indicate the present-day snow accumulation rate at Dome A is within the range 1–3cm w.e. a^{-1}. Densification models suggest a range of 1–2cm w.e. a^{-1}. This is lower than at other sites along the ice divide of East Antarctica (IDEA). Annual layers at Dome A are thus potentially thinner than at other sites, so that a longer record is preserved in a given ice thickness. (3) The average wind speed observed at Dome A (<4 m s^{-1}) is lower than at other sites along IDEA. Together, these parameters, combined with radio-echo sounding data and information on the subglacial drainage distribution beneath Dome A, suggest Dome A as a candidate site for obtaining the oldest ice core (Xiao et al., 2008; Xiao et al., 2008).

As the summit of the Antarctic Plateau, Dome A has been received international attentions. In this paper, observational data of an automatic weather station (AWS) at Dome A in 2005–2007 were used to analyze the seasonal variations of air temperatures near the ground and snow temperatures within a depth of 10 m. Analyses on the air temperatures show a typical feature of the coreless winter, and strong inversion maintains during the long winter. Accordingly the stratification near the ground is dominated by the near-neutral stable states. Seasonal fluctuations of the snow temperature decrease in amplitude and lag in phase with depth increasing, which leads to distinct seasonal temperature profiles within the depth of 10 m. Measurements show the mean annual air temperature near ground is about 5°C higher than the 10 m firn temperature due to the strong inversion near the ground. However, our estimation of the annual mean of air temperature at the ground based on the boundary layer theory is close to the mean 10 m firn temperature. The lowest air temperature (−82.7°C) currently measured at the Dome A is not the lowest one ever recorded in Antarctica, but the extremely low mean 10 m firn temperature (−58.2°C) indicates very low ground temperature. Given the prominent inversion near the ground, it is expected that Dome A might house the lowest ground temperature on the planet (Chen, 2010).

A vertical one-dimensional numerical model for heat transferring within the near-surface snow layer of the Antarctic Ice Sheet was developed based on simplified parameterizations of associated physical processes for the atmosphere, radiation, and snow/ice systems. Using the meteorological data of an automatic weather station (AWS) at Dome A (80°22′S, 70°22′E), we applied the model to simulate the seasonal temperature variation within a depth of 20 m. Comparison of modeled results with observed snow temperatures at 4 measurement depths (0.1, 1, 3, 10 m) shows good agreement and consistent seasonal variations. The model

results reveal the vertical temperature structure within the near-surface snow layer and its seasonal variance with more details than those by limited measurements. Analyses on the model outputs of the surface energy fluxes show that: 1) the surface energy balance at Dome A is characterized by the compensation between negative net radiation and the positive sensible fluxes, and 2) the sensible heat is on average transported from the atmosphere to the snow, and has an evident increase in spring. The results are considered well representative for the highest interior Antarctic Plateau (Chen, 2010).

2.2 P*reliminary results of deep ice core drilling at Dome A region*

A 109.91 m ice core was recovered from Dome A (or Dome Argus), the highest ice feature in Antarctica, during the 2004/05 austral summer by the 21st Chinese National Antarctic Research Expedition (CHINARE-21). Both methane profile along the core and firn densification model calculation suggest that the close-off depth is at about 102.0 m with an ice age about 4200 a (Fig 7.11). Stable isotopes (δ^{18}O and δD) of the chips samples produced during each run of ice core drilling at Dome A, together with those of the other cores recovered from the eastern inland Antarctica, suggest a relative stable climate with a temperature fluctuation amplitude about ±0.6℃ at the eastern inland Antarctica during the late Holocene. The average *d*-excess (or $d = \delta D - 8\delta^{18}O$) of 17.1‰ along the Dome A core is probably the highest among the Antarctic inland ice cores, which may be resulted from the kinetic fractionation during the snow formation under an oversaturation condition. Moreover, the increasing trend of *d*-excess during the late Holocene reflects mainly the migration of the water source area for precipitation at Dome A towards low latitudes. This paper presents the first results of a shallow ice core recovered from the unexplored highest area of the Antarctic ice sheet, providing a background for the proposing deep ice core drilling at Dome A (Hou et al., 2009).

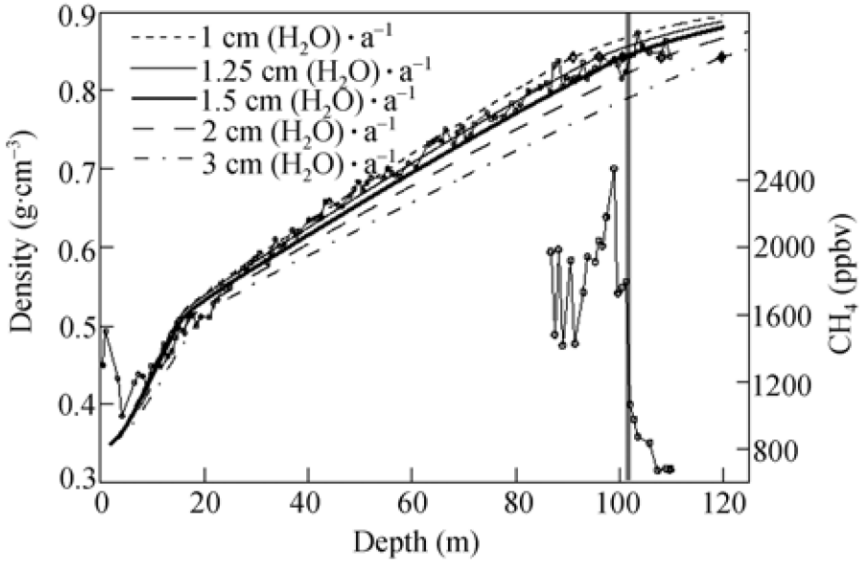

Fig 7.11 Upper curve, the measured density profile of the Dome A ice core (continuous line with circles); and the simulated density profiles by the LGGE firn densification model forced with an annual mean surface temperature of −58.5℃ and with annual mean accumulation rates of 1 (short dashed line), 1.25 (continuous line), 1.5 (thick continuous line), 2 (long dashed line), and 3 (dashed dotted line) cm $(H_2O)\cdot a^{-1}$. The diamonds on each curve indicate the simulated close-off depth. Bottom curve, the CH_4 concentrations measured between the depth range 87.00—109.91 m. The high values (>1400 ppbv) above 101.2 m indicated a partly closed porosity. The progressively decreasing values below 102.0 m correspond to the completely trapped atmospheric CH_4 concentrations before the industrial period. The abrupt transition between the two groups of CH_4 data indicates the position of the close-off depth (101.6±0.4 m, grey vertical bar), which fits well with the simulated result of the densification model forced by an accumulation rate of 1.5 cm $(H_2O)\cdot a^{-1}$.

3．Subglacial topography and early evolution of the Antarctic ice sheet

Ice-sheet development in Antarctica was a result of significant and rapid global climate change about 34 million years ago. Ice-sheet and climate modelling suggest reductions in atmospheric carbon dioxide (less than three times the pre-industrial level of 280 parts per million by volume) that, in conjunction with the development of the Antarctic Circumpolar Current, led to cooling and glaciation paced by changes in Earth's orbit. Based on the present subglacial topography, numerical models point to ice-sheet genesis on mountain massifs of Antarctica, including the Gamburtsev mountains at Dome A, the centre of the present ice sheet. Our lack of knowledge of the present-day topography of the Gamburtsev mountains means, however, that the nature of early glaciation and subsequent development of a continental-sized ice sheet are

uncertain. Here we present radar information about the base of the ice at Dome A (Fig 7.12; Fig 7.13), revealing classic Alpine topography with pre-existing river valleys overdeepened by valley glaciers formed when the mean summer surface temperature was around 3 °C. This landscape is likely to have developed during the initial phases of Antarctic glaciation. According to Antarctic climate history (estimated from offshore sediment records) the Gamburtsev mountains are probably older than 34 million years and were the main centre for ice-sheet growth. Moreover, the landscape has most probably been preserved beneath the present ice sheet for around 14 million years (Sun et al., 2009).

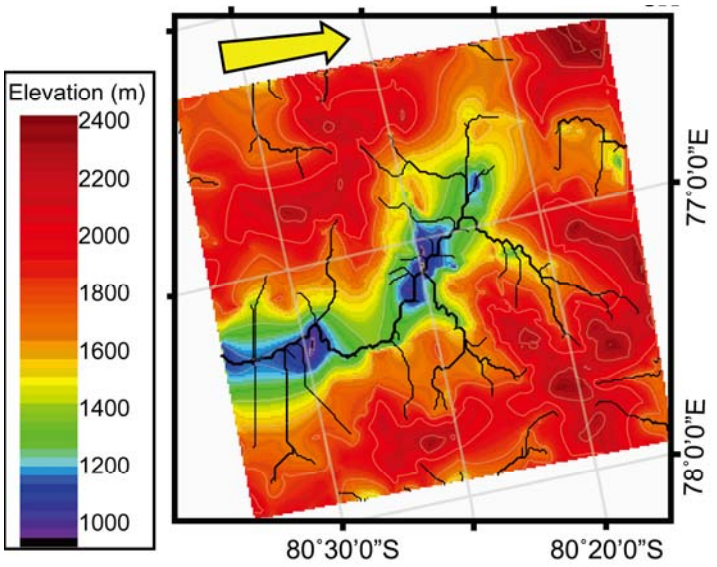

Fig 7.12 Topography of the surveyed section of the Gamburtsev mountains. Topographic contours (spaced at 200 m, lowest contour at 1,000 m) in grey; extracted valley network in black. Local elevation minima are those which lie more than 150m below the nearest down-valley saddle; this elevation change is well in excess of the vertical error.

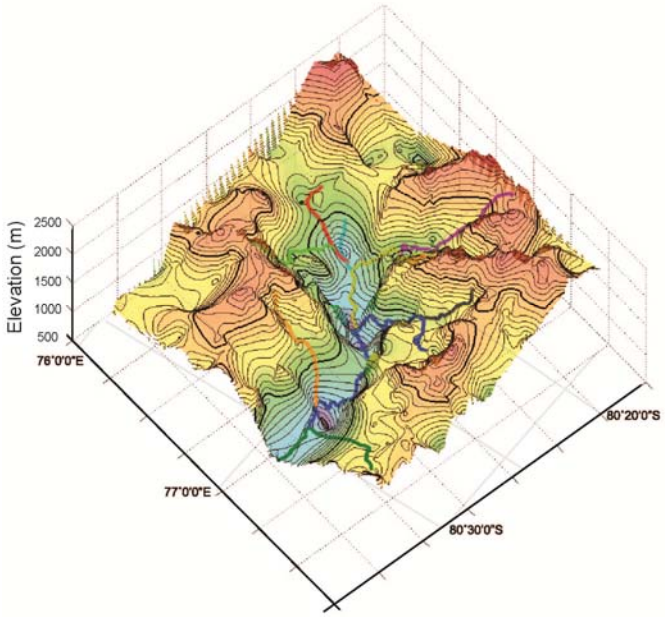

Fig 7.13. 3D Subglacial topography at Dome A region

Dome A, located in the central East Antarctic ice sheet (EAIS), is the highest summit of the Antarctic ice sheet. From ice-sheet evolution modeling results, Dome A is likely to preserve over one million years of

the Earth's paleo-climatic and -environmental records, and considered an ideal deep ice core drilling site. Ice thickness and subglacial topography are critical factors for ice-sheet models to determine the timescale and location of a deep ice core. During the 21st and 24th Chinese National Antarctic Research Expedition (CHINARE 21, 2004/05; CHINARE 24, 2007/08), ground-based ice radar systems were used to a three-dimensional investigation in the central 30 km×30 km region at Dome A. The successfully obtained high resolution and accuracy data of ice thickness and subglacial topography were then interpolated into the ice thickness distribution and subglacial topography digital elevation model (DEM) with a regular grid resolution of 140.5 m×140.5 m (Fig 7.14). The results of the ice radar investigation indicate that the average ice thickness in the Dome A central 30 km×30 km region is 2233 m, with a minimal ice thickness of 1618 m and a maximal ice thickness of 3139 m at Kunlun Station. The subglacial topography is relatively sharp, with an elevation range of 949–2445 m. The typical, clear mountain glaciation morphology is likely to reflect the early evolution of the Antarctic ice sheet. Based on the ice thickness distribution and subglacial topography characteristics, the location of Kunlun Station was suggested to carry out the first high-resolution, long time-scale deep ice core drilling. However, the internal structure and basal environments at Kunlun Station still need further research to determine (Cui et al., 2010).

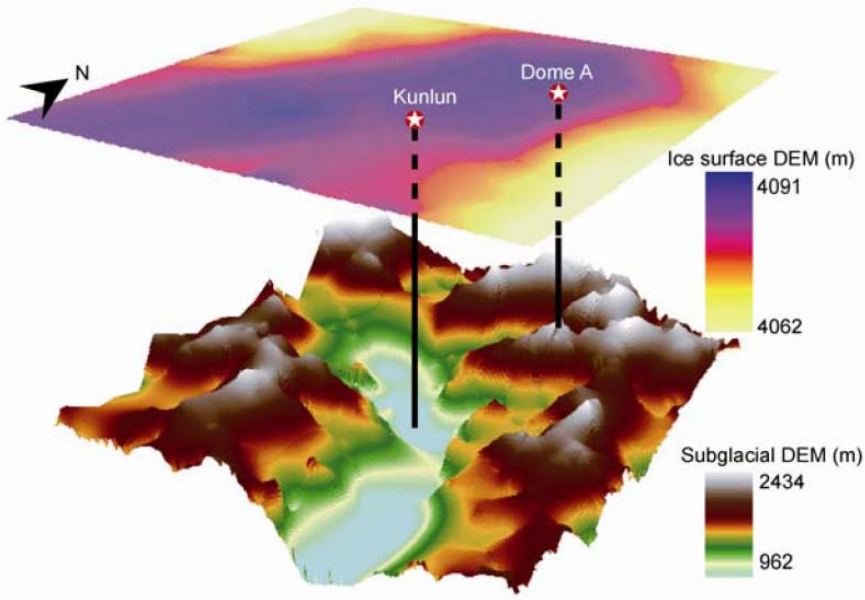

Fig 7.14. Three-dimensional ice surface and subglacial topography in the central 30 km×30 km region at Dome A. Ice surface elevation data from the field measurements by GPS.

4. Biogeology of sediment around Antarctic ice sheet

During the summertime of 2005/2006 net methane (CH4) fluxes and environmental variables were investigated in two tundra wetlands Wolong Marsh and Tuanjie Marsh of eastern Antarctica, using the closed chamber technique. At Wolong Marsh, the measurements were made at four wet tundra sites, four mesic tundra sites, and two dry sites. CH4 flux for wet tundra sites averaged $163.4\mu g\,m^{-2}\,h^{-1}$ and for the mesic sites $132.4\mu g\,m^{-2}\,h^{-1}$. For the dry sites, all the CH4 fluxes showed the negative values with an average of $-99.9\,\mu g\,m^{-2}\,h^{-1}$. At Tuanjie Marsh, flux measurements were made at two open ponds, two shallow fens and two dry sites. The average CH4 flux for the pond sites was $170.4\mu g\,m^{-2}\,h^{-1}$ and for the fen sites $134.7\mu g\,m^{-2}\,h^{-1}$. For the dry sites CH4 fluxes were approximately one order of magnitude lower than those for pond and fen sites and averaged $18.4\mu g\,m^{-2}\,h^{-1}$. Spatial variations in CH4 flux were primarily driven by the water table position at two tundra wetlands, whereas temporal variations in CH4 flux from wet and mesic sites were related with the thermal regime of tundra soil layers. The fluxes from six observation sites showed a consistent diurnal cycle with the peak at 14:00 and the lowest at 2:00 (local time), which was correlated with ground temperature at the depth of 0–10 cm (Fig 7.15). The CH4 emissions from coastal wetlands could constitute an important part of the annual CH4 budget for Antarctic tundra ecosystems (Zhu et al., 2007).

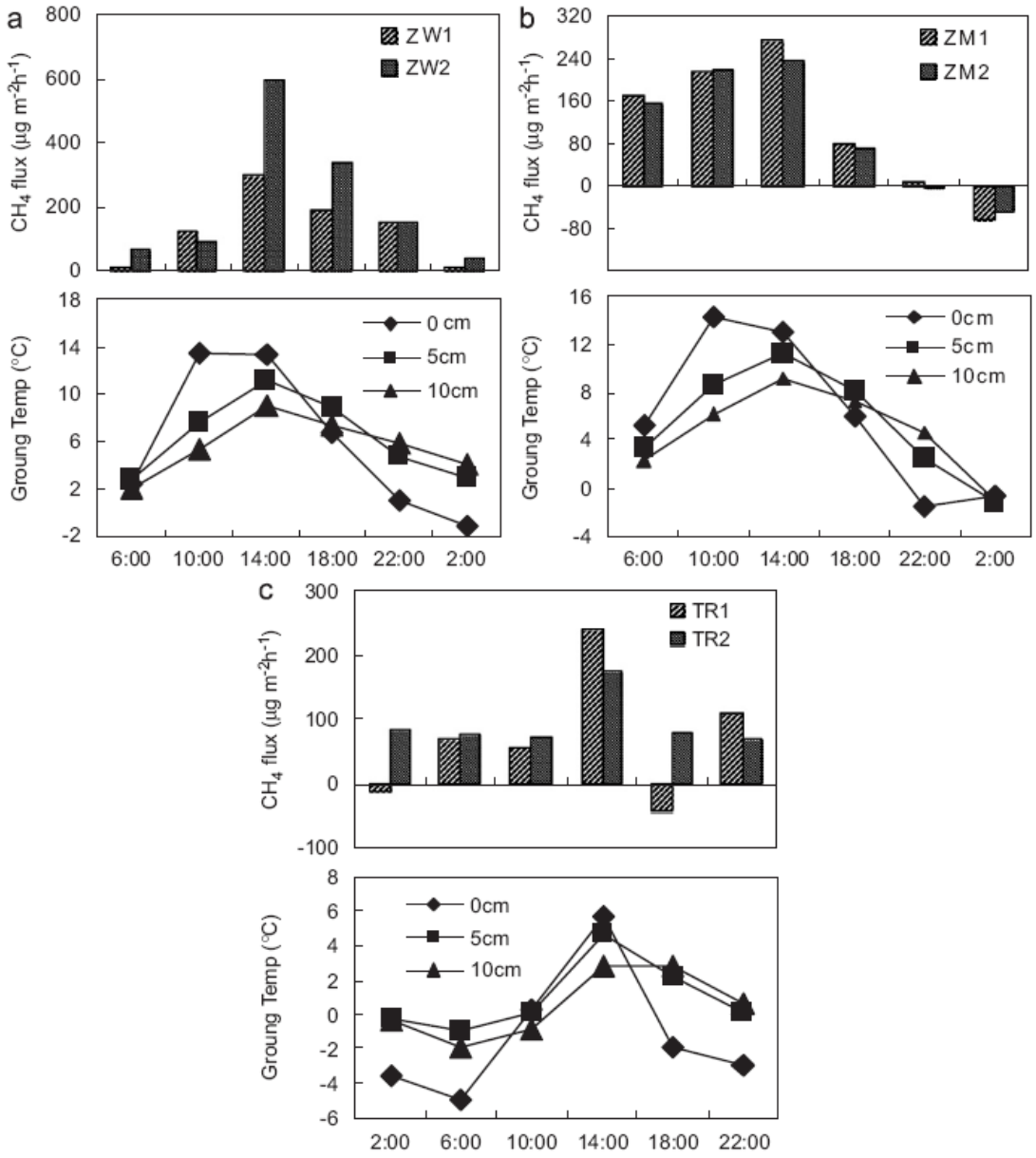

Fig 7.15 Daily variations of CH_4 fluxes from six obseravtion sites ZW1, ZW2, ZM1, ZM2, TR1, and TR2 in Wolong Marsh and Tuanjie Marsh. (a) December 30–31, 2005; (b) December 30–31, 2005; (c) February 5, 2006.

In order to reconstruct past changes in penguin populations we performed geochemical analyses on a penguin ornithogenic sediment core DG4 retrieved from a lake catchment on Gardner Island, Vestfold Hills. P, Se, F, S, As, Sr and Cu in DG4 were identified as the bio-element assemblage by R-clustering analyses on the elemental concentrations and comparisons with those in bedrock and fresh penguin guano. Factor analysis on the levels of these bio-elements in the core permitted a reconstruction of variations in historical penguin populations at Gardner Island spanning the past 8500 years. The penguin population showed significant fluctuations, reaching its highest density between 4700–2400 calibrated years before present. This coincides with evidence for a late Holocene warm period in the Vestfold Hills, similar to that associated with the late Holocene penguin optimum recorded in the Ross Sea and Antarctic Peninsula regions (Huang et al., 2009).

A 118-cm-long and well-preserved sediment profile in a paleo-notch, which was formed by ocean wave action before rising to the terrace, was collected from the first terrace of Ny-Ålesund, Svalbard, Arctic. The bottom of this profile was dated as 9,400 years B.P. based on two radiocarbon dates of fossil mollusc shell

fragments. The organic material in the sediment was identified by $\delta^{13}C_{org}$–C/N plot and $\delta^{15}N_{org}$ characteristics to be predominantly composed of seabird guano, which was transported from the ocean via preying and excreting by seabirds. These results indicate that seabirds have inhabited Ny-Ålesund since 9,400 years B.P. after Kongsfjorden was completely deglaciated. This is the first report on Holocene seabird occupation on Ny-Ålesund and it provides the foundation for understanding the ecological history of seabirds in Svalbard in Holocene (Yuan et al., 2010).

The total gaseous mercury (TGM) measurements were performed using an automatic Mercury Vapor Analyze (model 2537B) aboard the Chinese research vessel (R/V) *XueLong* during the 24th China Antarctic Research Expedition from Shanghai, China to Prydz Bay, Antarctica in 2007. TGM ranged between 0.302 and 4.496 ng m^{-3} with an average of 1.536 ± 0.785 ng m^{-3} over the entire period. Geographically, TGM in the Northern Hemisphere and the Southern Hemisphere along the cruise path were 1.746 ± 0.513 and 1.471 ± 0.842 ng m^{-3} in average, respectively (Fig 7.16). Higher TGM concentrations were observed in the coastal regions outside the polar region due primarily to air masses transported from the adjacent mainland reflecting the contribution from anthropogenic sources. The pronounced episode was recorded when ship passed through Sunda straits, which should be ascribed to the volcano plume and/or biomass burning contamination. In the maritime Antarctic TGM level was in agreement with the values by land-based observation, presenting a diurnal cycle with the maximum around midday and minimum at night. Atmospheric mercury destruction events dominated by the oxidation of atmospheric Hg^0 were apparently observed in this region (Xia et al., 2010).

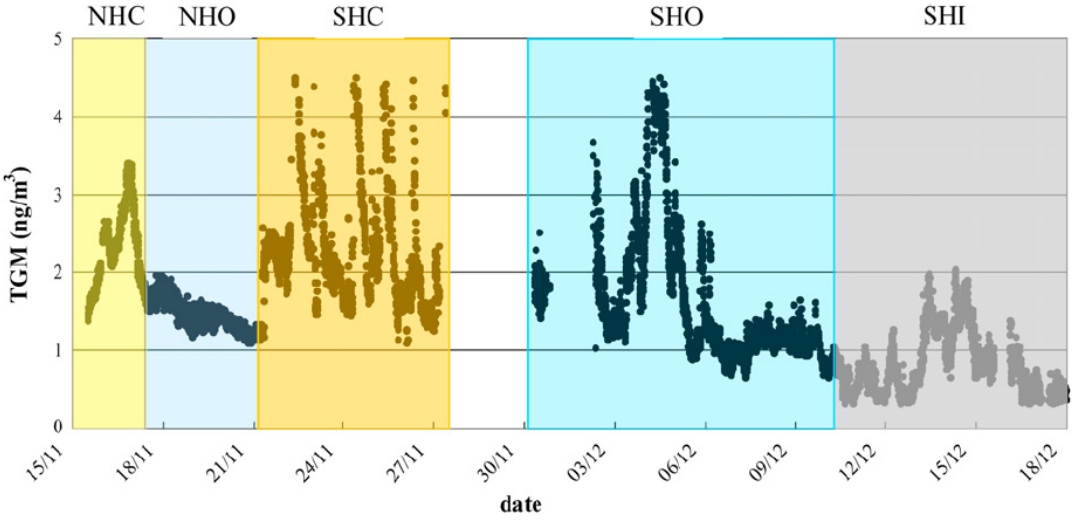

Fig 7.16. Record of TGM concentration during the cruise.

Zhu2010AE: In coastal Antarctica, freezing and thawing influence many physical, chemical and biological processes for ice-free tundra ecosystems, including the production of greenhouse gases (GHGs). In this study, penguin guanos and ornithogenic soil cores were collected from four penguin colonies and one seal colony in coastal Antarctica, and experimentally subjected to three freezing–thawing cycles (FTCs) under ambient air and under N_2. We investigated the effects of FTCs on the emissions of three GHGs including nitrous oxide (N_2O), carbon dioxide (CO_2) and methane (CH_4). The GHG emission rates were extremely low in frozen penguin guanos or ornithogenic soils. However, there was a fast increase in the emission rates of three GHGs following thawing. During FTCs, cumulative N_2O emissions from ornithogenic soils were greatly higher than those from penguin guanos under ambient air or under N_2. The highest N_2O cumulative emission of 138.24 μg N_2O–N kg^{-1} was observed from seal colony soils. Cumulative CO_2 and CH_4 emissions from penguin guanos were one to three orders of magnitude higher than those from ornithogenic soils. The highest cumulative CO_2 (433.0 mg CO_2–C kg^{-1}) and CH_4 (2.9 mg CH_4–C kg^{-1}) emissions occurred in emperor penguin guanos. Penguin guano was a stronger emitter for CH_4 and CO_2 while ornithogenic soil was a stronger emitter for N_2O during FTCs. CO_2 and CH_4 fluxes had a correlation with total organic carbon (TOC) and soil/guano moisture (M_c) in penguin guanos and ornithogenic soils. The specific CO_2–C production rate (CO_2–C/TOC) indicated that the bioavailability of TOC was markedly larger in penguin guanos than in ornithogenic soils during FTCs. This study showed that FTC-released organic C and N from sea animal excreta may play a significant role in FTC-related

GHG emissions, which may account for a large proportion of annual fluxes from tundra ecosystems in coastal Antarctica.

5. ***Simulation of Arctic sea ice and its association with climate in East Asia***

The interannual atmosphere-ocean-sea ice interaction (AOSI) in high northern latitudes is studied with a global atmosphere-ocean-sea ice coupled model system, in which the model components of atmosphere and land surface are from China National Climate Center and that of ocean and sea ice are from LASG,Institute of Atmospheric Physics, Chinese Academy of Sciences. A daily flux anomaly correction scheme is employed to couple the atmosphere model and the ocean model with the effect of inhomogenity of sea ice in high latitudes is considered. The coupled model system has been run for 50 yr and the results of the last 30 years are analyzed. After the sea level pressure (SLP), surface air temperature (SAT), sea surface temperature (SST), sea ice concentration (SIC), and sea surface sensible heat flux (SHF) are filtered with adigital filter firstly, their normalized anomalies are used to perform the decomposition of combined complex empirical orthogonal function (CCEOF) and then they are reconstructed with the leading mode. The atmosphere-ocean-sea ice interactions in high northern latitudes during a periodical cycle (approximately4 yr) are analyzed. It is shown that: (1) When the North Atlantic Oscillation (NAO) is in its positive phase, the southerly anomaly appears in the Greenland Sea, SAT increases, the sea loses less SHF, SST increases and SIC decreases accordingly; when the NAO is in its negative phase, the northerly anomaly appears in the Greenland Sea, SAT decreases, the sea loses more SHF, SST decreases and SIC increases accordingly. There are similar features in the Barents Sea, but the phase of evolution in the Barents Sea is different from that in the Greenland Sea. (2) For an average of multi-years, there is a cold center in the inner part of the Arctic Ocean near the North Pole. When there is an anomaly of low pressure, which is closer to the Pacific Ocean, in the inner part of the Arctic Ocean, anomalies of warm advection appear in the region near the Pacific Ocean and anomalies of cold advection appear in the region near the Atlantic Ocean. Accompanying with these anomalies of warm and cold advection in these two regions, warm and cold anomalies appear respectively. Accordingly, SHF sent to the atmosphere from the sea surface decreases and increases, and SST increases and decreases, SIC decreases and increases in these two regions. When there is an anomaly of high pressure in the inner part of the Arctic Ocean, the former relationships reverse.From these results, it can be deduced that, during the interannual cycle of the coupled atmosphere-ocean system, the variability of large-scale atmospheric circulation plays a dominant role and variations of SST and SIC are mainly responding to that of atmospheric circulation (Liu et al., 2008).

A statistical relationship between spring Arctic sea ice concentration (SIC) and Chinese summer rainfall is identified using singular value decomposition (SVD) (Fig 7.17). Results show that decreased (increased) spring SIC in the Arctic Ocean and the Greenland Sea corresponds to increased (decreased) summer rainfall in northeast China and central China between the Yangtze River and the Yellow River (28°–36°N); and decreased (increased) rainfall in south China. Corresponding summer 500 hPa height anomalies show a Eurasian wave train structure, which originates in northern Europe and extends southeastwards to northeast China, and a south-north dipole structure over East Asia south to Lake Baikal. Such a spatial distribution of 500 hPa height anomalies and corresponding summer rainfall anomalies cannot be entirely attributed to the impact of East Asian summer monsoon (EASM) variability. The spring Arctic SIC provides a complementary precursor for Chinese summer rainfall variability. The combined impacts of both spring Arctic SIC and Eurasian snow cover on the Eurasian wave train may explain their statistical linkage (Wu et al., 2009).

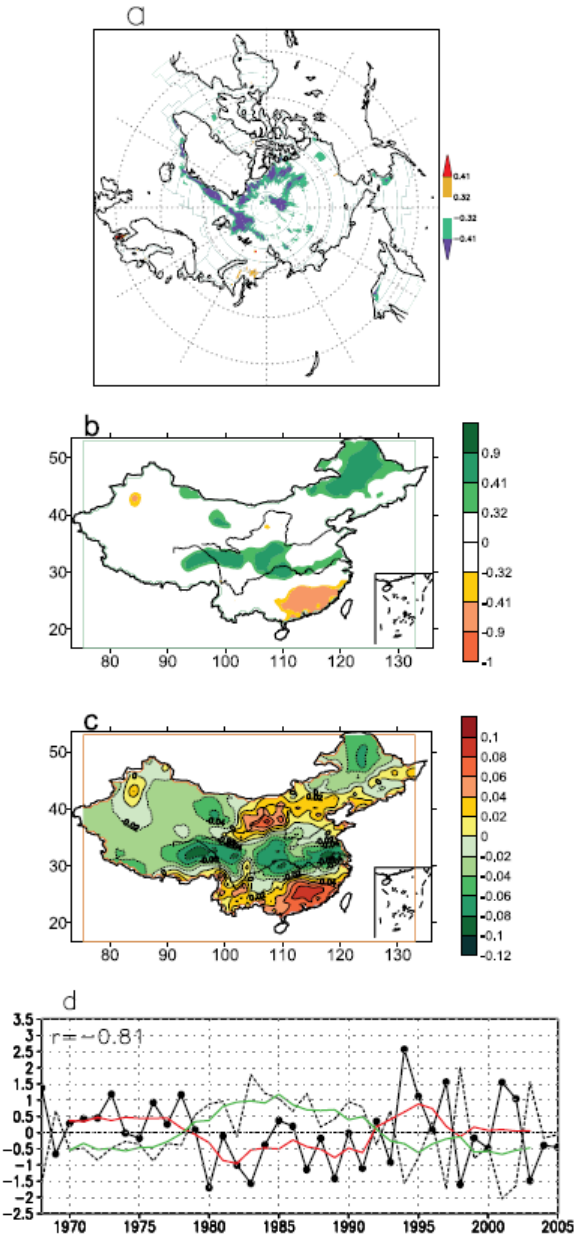

Fig 7.17. (a) The spatial distribution of spring Arctic SIC heterogeneous correlations, the shading areas denote correlations at the 0.05 and 0.01 significance levels, respectively, (b) same as in Fig 7.a but for Chinese summer rainfall, (c) the spatial distribution of the leading EOF of Chinese summer rainfall (Units: arbitrary), (d) normalized time series of both the leading EOF of summer rainfall (solid line) and summer rainfall variations in the leading SVD (dashed line), the red and green lines denote their 5-year running means, respectively.

In our previous study, a statistical linkage between the spring Arctic sea ice concentration (SIC) and the succeeding Chinese summer rainfall during the period 1968{2005 was identied. This linkage is demonstrated by the leading singular value decomposition (SVD) that accounts for 19% of the co-variance. Both spring SIC and Chinese summer rainfall exhibit a coherent interannual variability and two apparent interdecadal variations that occurred in the late 1970s and the early 1990s. The combined impacts of both spring Arctic SIC and Eurasian snow cover on the summer Eurasian wave train may explain their statistical linkage. In this study, we show that evolution of atmospheric circulation anomalies from spring to summer, to a great extent, may explain the spatial distribution of spring and summer Arctic SIC anomalies, and is dynamically consistent with Chinese summer rainfall anomalies in recent decades. The association between spring Arctic SIC and Chinese summer rainfall on interannual time scales is more important relative to interdecadal time scales. The summer Arctic dipole anomaly may serve as the bridge linking the spring

Arctic SIC and Chinese summer rainfall, and their coherent interdecadal variations may re°ect the feedback of spring SIC variability on the atmosphere. The summer Arctic dipole anomaly shows a closer relationship with the Chinese summer rainfall relative to the Arctic Oscillation (Wu et al., 2009).

This paper identified an atmospheric circulation anomaly–dipole structure anomaly in the Arctic atmosphere and its relationship with winter sea ice motion, based on the International Arctic Buoy Program (IABP) dataset (1979–98) and datasets from the National Centers for Environmental Prediction (NCEP) and the National Center for Atmospheric Research (NCAR) for the period 1960–2002. The dipole anomaly corresponds to the second-leading mode of EOF of monthly mean sea level pressure (SLP) north of 70°N during the winter season (October–March) and accounts for 13% of the variance. One of its two anomalous centers is stably occupied between the Kara Sea and Laptev Sea; the other is situated from the Canadian Archipelago through Greenland extending southeastward to the Nordic seas. The dipole anomaly differs from one described in other papers that can be attributed to an eastward shift of the center of action of the North Atlantic Oscillation. The finding shows that the dipole anomaly also differs from the "Barents Oscillation" revealed in a study by Skeie. Since the dipole anomaly shows a strong meridionality, it becomes an important mechanism to drive both anomalous sea ice exports out of the Arctic Basin and cold air outbreaks into the Barents Sea, the Nordic seas, and northern Europe (Wu et al., 2006).

When the dipole anomaly remains in its positive phase, that is, negative SLP anomalies appear between the Kara Sea and the Laptev Sea with concurrent positive SLP over from the Canadian Archipelago extending southeastward to Greenland, there are large-scale changes in the intensity and character of sea ice transport in the Arctic basin. The significant changes include a weakening of the Beaufort gyre, an increase in sea ice export out of the Arctic basin through Fram Strait and the northern Barents Sea, and enhanced sea ice import from the Laptev Sea and the East Siberian Sea into the Arctic basin. Consequently, more sea ice appears in the Greenland and the Barents Seas during the positive phase of the dipole anomaly. During the negative phase of the dipole anomaly, SLP anomalies show an opposite scenario in the Arctic Ocean and its marginal seas when compared to the positive phase, with the center of negative SLP anomalies over the Nordic seas (Fig 7.18). Correspondingly, sea ice exports decrease from the Arctic basin flowing into the Nordic seas and the northern Barents Sea because of the strengthened Beaufort gyre (Wu et al., 2006).

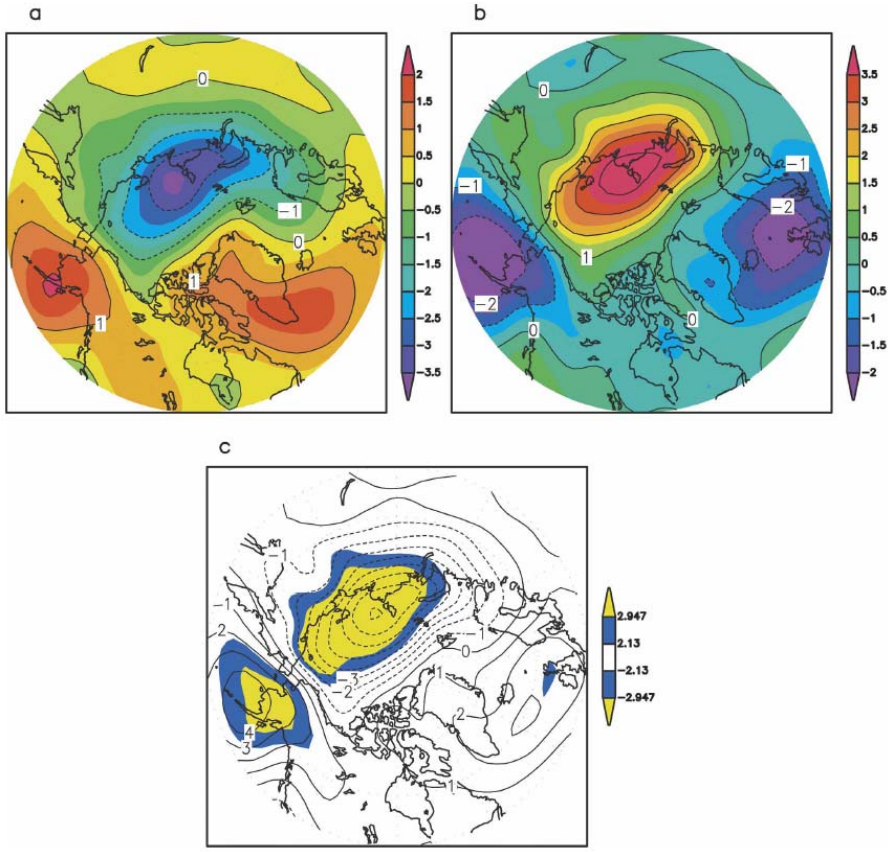

Fig 7.18. Composites of SLP anomalies: (a) the positive phase, (b) the negative phase, and (c) differences between (a) and (b). The blue and yellow areas in (c) represent differences exceeding the 0.05 and 0.01 significance levels, respectively. Contour interval: 1 hPa.

The finding indicates that influences of the dipole anomaly on winter sea ice motion are greater than that of the winter AO, particularly in the central Arctic basin and northward to Fram Strait, implying that effects of the dipole anomaly on sea ice export out of the Arctic basin become robust. The dipole anomaly is closely related to atmosphere–ice–ocean interactions that influence the Barents Sea sector (Wu et al., 2006).

6．*Eurasian cryospheric variability and its effect on East Asia*

Two distinct modes of the East Asian winter monsoon (EAWM) have been identified, and they correspond to real and imaginary parts of the leading mode of EAWM, respectively (Fig 7.19). Analyses of these modes used the National Centers for Environment Prediction (NCEP) and National Center for Atmospheric Research (NCAR) monthly mean reanalysis datasets for the period 1968-2003, as well as the Southern Oscillation index (SOI), North Atlantic Oscillation (NAO) index and eastern equatorial Pacific sea surface temperature (SST) data. Results were obtained by resolving a complex Hermit matrix derived from 850 hPa anomalous wind fields, and determining the resulting modes' associations with several climate variables. The first distinct mode (M1) is characterized by an anomalous meridional wind pattern over East Asia and the western North Pacific. M1 is closely related to several features of the atmospheric circulation, including the Siberian High, East Asian trough, East Asian upper-tropospheric jet and local Hadley circulation over East Asia. Thus, M1 reflects the traditional EAWM pattern revealed in previous studies. The second distinct EAWM mode (M2), which was not identified previously, displays dominant zonal wind anomalies over the same area. M2 exhibits a closer relation than M1 to sea level pressure (SLP) anomalies over the northwestern Pacific southeast of Japan, and with the SOI and equatorial eastern Pacific SST. Unlike M1, M2 does not show coherent relationships with the Siberian High, East Asian trough, East Asian upper-tropospheric jet. Since atmospheric circulation anomalies relevant to M2 exhibit a quasi-barotropic structure, its existence cannot simply be attributed to differential land-sea heating. El Niño events tend to occur in the negative phase of M1 and the positive phase of M2, both corresponding to a weakened EAWM. The Arctic Oscillation (AO) does not appear to impact the EAWM on interannual time scales. Although the spatial patterns for the two modes are very different, the two distinct modes are complementary, with the leading EAWM mode being a linear combination of the two. Our results therefore demonstrate that a single EAWM index may be inappropriate for investigating and predicting the EAWM (Wu et al., 2006).

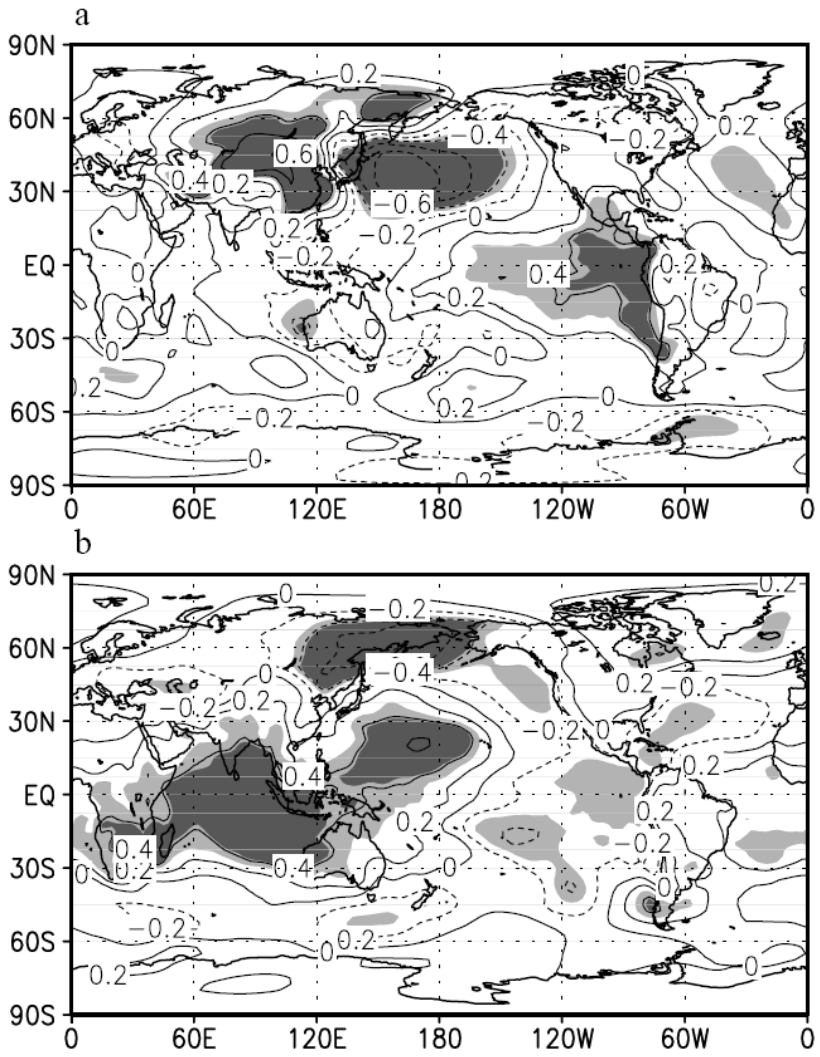

Fig 7..19 Correlation coefficients of winter SLP with (a) the real part and (b) the imaginary part of the leading complex principal component. The gray and dark areas denote correlations that exceed the 0.05 and 0.01 significance levels, respectively.

This study investigates the statistical linkage between summer rainfall in China and the preceding spring Eurasian snow water equivalent (SWE), using the datasets of summer rainfall observations from 513 stations, satellite-observed snow water equivalent, and atmospheric circulation variables in the NCEP/NCAR reanalysis during the period from 1979 to 2004. The first two coupled modes are identified by using the singular value decomposition (SVD) method. The leading SVD mode of the spring SWE variability shows a coherent negative anomaly in most of Eurasia with the opposite anomaly in some small areas of the Tibetan Plateau and East Asia. The mode displays strong interannual variability, superposed on an interdecadal variation that occurred in the late 1980s, with persistent negative phases in 1979–1987 and frequent positive phases afterwards. When the leading mode is in its positive phase, it corresponds to less SWE in spring throughout most of Eurasia. Meanwhile, excessive SWE in some small areas of the Tibetan Plateau and East Asia, summer rainfall in South and Southeast China tends to be increased, whereas it would be decreased in the up-reaches of the Yellow River. In recent two decades, the decreased spring SWE in Eurasia may be one of reasons for severe droughts in North and Northeast China and much more significant rainfall events in South and Southeast China. The second SVD mode of the spring SWE variability shows opposite spatial variations in western and eastern Eurasia, while most of the Tibetan Plateau and East Asia are in phase. This mode significantly correlates with the succeeding summer rainfall in North and Northeast China, that is, less spring SWE in western Eurasia and excessive SWE in

eastern Eurasia and the Tibetan Plateau tend to be associated with decreased summer rainfall in North and Northeast China (Wu et al., 2009).

The relationship between decadal variability in springtime (March–May) snow water equivalent (SWE) over Eurasia and springtime rainfall over China is investigated for 1979–2004 using satellite-observed SWE, rainfall observations from 595 stations, and NCEP/NCAR reanalysis data. Decreasing springtime SWE in Eurasia corresponded to reduced springtime rainfall over southeastern and Northeast China, and more rainfall over southwestern and northwestern China. This relationship was supported by the feedback effect of snow in high-latitude areas to changes in background atmospheric circulation.

A decadal shift in springtime Eurasian SWE occurred in the late 1980s, marked by a change from persistent positive phases in 1979–1987 to frequent negative phases. The reduction in Eurasian SWE resulted in reduced upward surface heat flux to the atmosphere and thereby a higher boundary layer height due to increased downward heat flux into subsurface soil. These changes resulted in reduced upward and poleward wave flux activity, which corresponded to anomalous negative heights/pressures in the Arctic and anomalous positive heights/pressures in mid-latitude regions from the upper-level troposphere to the surface. There was an anomalous anti-cyclonic circulation over Siberia and the western Pacific subtropical high was weakened, accompanied by an anomalous northerly in eastern China and westerly in northwestern China. The anomalous northerly resulted in reduced water vapor convergence in southeastern and Northeast China, and reduced water vapor export for southwestern and northwestern China (Fig 7.). Thus, negative rainfall anomalies developed over southeastern and Northeast China, and positive rainfall anomalies appeared over southwestern and northwestern China （Zuo et al., submitted）.

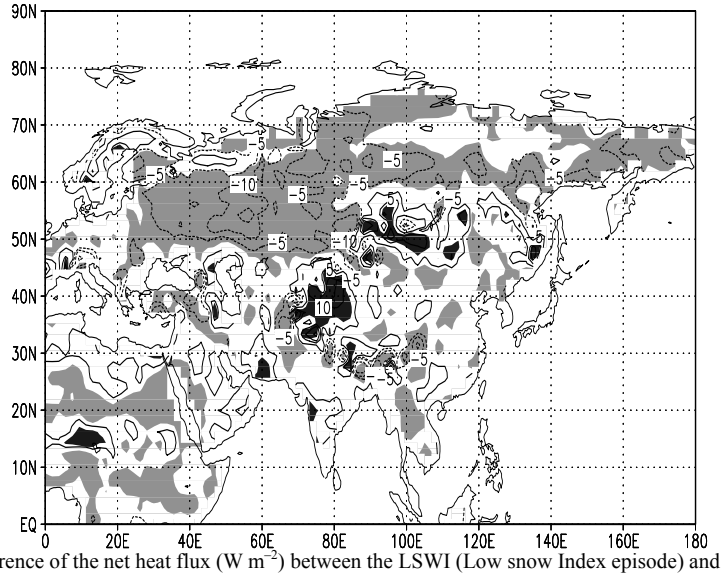

Fig 7.20. Composite difference of the net heat flux (W m^{-2}) between the LSWI (Low snow Index episode) and HSWI (High snow Index episode) cases. Shaded areas exceed the 0.1 level of significance [dark (light) shading represents significant positive (negative) difference].

Using Russian historical data such as air temperature, precipitation, snow cover and soil temperatures at various depths from more than 700 stations across Siberia, we documented changes in permafrost conditions and their causes. Our preliminary results indicate that permafrost temperature has increased about 2 to 3°C since the early 1960s; active layer thickness has increased about 25 cm over the same time period. It is highly possible that there is widespread talik development in central Siberia. Permafrost temperature increase may be mainly due to the early snow cover establishment in autumn and thicker snow depth in winter. We strongly believe that talik development is mainly due to less soil freeze in winter due to stronger snow insulation effect with slightly increase in active layer thickness in summer. However, changes in snow conditions need further comprehensive investigation (Personal communication with Zhang Tingtun).

Changes in active layer thickness (ALT) over northern high-latitude permafrost regions have important impacts on the surface energy balance, hydrologic cycle, carbon exchange between the atmosphere and the land surface, plant growth, and ecosystems as a whole. This study examines the 20th century variations of ALT for the Ob, Yenisey, and Lena River basins. ALT is estimated from historical soil

temperature measurements from 17 stations (1956–1990, Lena basin only), an annual thawing index based on both surface air temperature data (1901–2002) and numerical modeling (1980–2002). The latter two provide spatial fields. Based on the thawing index, the long-term average (1961–1990) ALT is about 1.87 m in the Ob, 1.67 in the Yenisey, and 1.69 m in the Lena basin (Fig 7.21). Over the past several decades, ALT over the three basins shows positive trends, but with different magnitudes. Based on the 17 stations, ALT increased about 0.32 m between 1956 and 1990 in the Lena. To the extent that results based on the soil temperatures represent ground "truth," ALT obtained from both the thawing index and numerical modeling is underestimated. It is widely believed that ALT will increase with global warming. However, this hypothesis needs further refinement since ALT responds primarily to summer air temperature while observed warming has occurred mainly in winter and spring. It is also shown that ALT exhibits complex and inconsistent responses to variations in snow cover (Zhang et al., 2005).

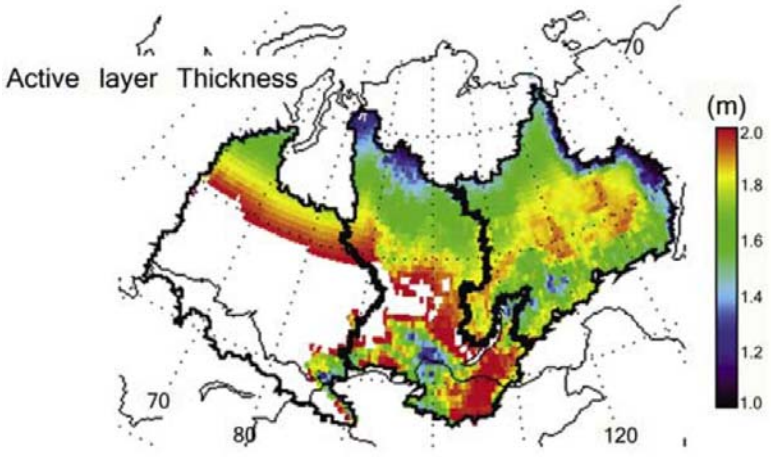

Fig 7.21. The 1961–1990 climatology of active layer thickness estimated from the annual thawing index over the Ob (left), Yenisey (middle), and Lena (right) basins.

The recently published digital version of the International Permafrost Association (IPA) Circum-Arctic Map of Permafrost and Ground Ice Conditions (the IPA map), together with ancillary data sets of the global land cover characteristics data base and the Global Land One-kilometer Base Elevation data base, are used to investigate the distribution of permafrost and ground ice in the Northern Hemisphere. Our study indicates that permafrost underlies approximately 22.79×10^6 km^2 or 23.9% of the exposed land area of the Northern Hemisphere. Permafrost extends from 26°N in the Himalayas to 84°N in northern Greenland. Approximately 70% of the permafrost is distributed between 45 and 67°N. Generally, permafrost with high ice content (>20% by volume) and relatively thick overburden cover (>5 to 10 m) is found at high latitudes, representing approximately 8.57% of the total permafrost area, or 2.02% of the exposed land area of the Northern Hemisphere. Permafrost with low ice content (<10% by volume with either thick or thin overburden cover) occurs mainly in mountainous regions and high plateaus, representing approximately 66.5% of the total permafrost area or 15.8% of the exposed land area. Approximately 62% of the permafrost of the Northern Hemisphere is found below 500 m a.s.l. and about 10% occurs above 3000 m a.s.l. Based on the IPA map categories, the estimated volume of ground ice in the Northern Hemisphere is between 5.63 and 15.12×10^3 km^3, corresponding to 2-4 cm sea level equivalent. Based on alternative assumptions, the volume of ground ice may be between 11.37 and 36.55×10^3 km^3, which corresponds to 3-10 cm sea-level equivalent (Zhang et al., 2008).

References:

1) Cheng, X., P. Gong, Y. Zhang, Z. Sun, and F. Wei, 2009, Surface topography of Dome A, Antarctica, from differential GPS measurements: Journal of Glaciology, v. 55, p. 185-187.
2) Cui, X. B., B. Sun, G. Tian, X. Y. Tang, X. P. Zhang, Y. Y. Jiang, J. X. Guo, and X. Li, 2010, Ice radar investigation at Dome A, East Antarctica: Ice thickness and subglacial topography: Chinese Science Bulletin, v. 55, p. 425-431.
3) Ding, M. H., C. D. Xiao, B. Jin, J. W. Ren, D. H. Qin, and W. Z. Sun, 2010, Distribution of δ 18 O in surface snow along a transect from Zhongshan Station to Dome A, East Antarctica: Chinese Science Bulletin, v. 55, p. 2709-2714.
4) Ding, M., C. Xiao, Y. Li, J. Ren, S. Hou, B. Jin, and B. Sun, 2010, Spatial variability of snow accumulation along a travers route from Zhongshan Station to Dome A, Antarctica: Journal of Glaiciology. In press.
5) Hou, S. G., Y. S. Li, C. D. Xiao, H. X. Pang, and J. Z. Xu, 2009, Preliminary results of the close-off depth and the stable isotopic records along a 109.91 m ice core from Dome A, Antarctica: Science in China Series D: Earth Sciences, v. 52, p.

1502-1509.
6) Hou, S. G., Y. S. Li, C. D. Xiao, and J. W. Ren, 2007, Recent accumulation rate at Dome A, Antarctica: Chinese Science Bulletin, v. 52, p. 428-431.
7) Huang, T., L. Sun, Y. Wang, X. Liu, and R. Zhu, 2009, Penguin population dynamics for the past 8500 years at Gardner Island, Vestfold Hills: Antarctic Science, v. 21, p. 571-578.
8) Liu, H., K. C. Jezek, and B. Li, 1999, Development of an Antarctic digital elevation model by integrating cartographic and remotely sensed data: A geographic information system based approach: Journal of Geophysical Research, v. 104, p. 23199-23213.
9) Liu, X., H. Liu, W. Li, X. Zhang, R. Yu, and Y. Yu, 2008, Numerical Simulation of Atmosphere-Ocean-Sea Ice Interaction During Interannual Cycle in High Northern Latitudes: Acta Meteorological Sinica, v. 22.
10) Ma, Y., L. Bian, C. Xiao, I. Allison, and X. Zhou, 2010, Near surface climate of the traverse route from Zhongshan Station to Dome A, East Antarctica: Antarctic Science, p. 1-17.
11) Sun, B., M. J. Siegert, S. M. Mudd, D. Sugden, S. Fujita, X. Cui, Y. Jiang, X. Tang, and Y. Li, 2009, The Gamburtsev mountains and the origin and early evolution of the Antarctic Ice Sheet: Nature, v. 459, p. 690-693.
12) Wu, B., J. Wang, and J. E. Walsh, 2006, Dipole anomaly in the winter Arctic atmosphere and its association with sea ice motion: Journal of Climate, v. 19, p. 210-225.
13) Wu, B., K. Yang, and R. Zhang, 2009, Eurasian snow cover variability and its association with summer rainfall in China: Advances in Atmospheric Sciences, v. 26, p. 31-44.
14) Wu, B., R. Zhang, B. Wang, and R. D'Arrigo, 2009, On the association between spring Arctic sea ice concentration and Chinese summer rainfall: Geophys. Res. Lett, v. 36.
15) Wu, B., R. Zhang, and B. Wang, 2009, On the association between spring Arctic sea ice concentration and Chinese summer rainfall: A further study: Advances in Atmospheric Sciences, v. 26, p. 666-678.
16) Wu, B., R. Zhang, and R. D'Arrigo, 2006, Distinct Modes of the East Asian Winter Monsoon: Monthly Weather Review, v. 134, p. 2165-2179.
17) Xia, C., Z. Xie, and L. Sun, 2010, Atmospheric mercury in the marine boundary layer along a cruise path from Shanghai, China to Prydz Bay, Antarctica: Atmospheric Environment, v. 44, p. 1815-1821.
18) Xiao, C. D., Y. Li, S. Hou, I. Allison, L. Bian, and J. Ren, 2008, Preliminary evidence indicating Dome A (Antarctica) satisfying preconditions for drilling the oldest ice core: Chinese Science Bulletin, v. 53, p. 102-106.
19) Xiao, C., Y. Li, I. Allison, S. Hou, G. Dreyfus, J. M. Barnola, J. Ren, L. Bian, S. Zhang, and T. Kameda, 2008, Surface characteristics at Dome A, Antarctica: first measurements and a guide to future ice-coring sites: Annals of Glaciology, v. 48, p. 82-87.
20) Yuan, L., L. Sun, N. Long, Z. Xie, Y. Wang, and X. Liu, 2010, Seabirds colonized Ny- lesund, Svalbard, Arctic~ 9,400 years ago: Polar biology, v. 33, p. 683-691.
21) Zhang, S., D. E, Z. Wang, C. Zhou, and Q. Shen, 2007, Surface topography around the summit of Dome A, Antarctica, from real-time kinematic GPS: Journal of Glaciology, v. 53.
22) Zhang, S., D. E, Z. Wang, Y. Li, B. Jin, and C. Zhou, 2008, Ice velocity from static GPS observations along the transect from Zhongshan station to Dome A, East Antarctica: Annals of Glaciology, v. 48, p. 113-118.
23) Zhang, T., O. W. Frauenfeld, M. C. Serreze, A. Etringer, C. Oelke, J. McCreight, R. G. Barry, D. Gilichinsky, D. Yang, and H. Ye, 2005, Spatial and temporal variability in active layer thickness over the Russian Arctic drainage basin: Journal of Geophysical Research, v. 110, p. D16101.
24) Zhang, T., R. G. Barry, K. Knowles, J. A. Heginbottom, and J. Brown, 2008, Statistics and characteristics of permafrost and ground-ice distribution in the Northern Hemisphere: Polar Geography, v. 31, p. 47-68.
25) Zhou, M., Z. Zhang, S. Zhong, D. Lenschow, H. M. Hsu, B. Sun, Z. Gao, S. Li, X. Bian, and L. Yu, 2009, Observations of near-surface wind and temperature structures and their variations with topography and latitude in East Antarctica: Journal of Geophysical Research, v. 114, p. D17115.
26) Zhu, R., Y. Liu, L. Sun, and H. Xu, 2007, Methane emissions from two tundra wetlands in eastern Antarctica: Atmospheric Environment, v. 41, p. 4711-4722.
27) Zuo Z, Zhang R, Wu B, and Rong X;Decadal Variability in Springtime Snow over Eurasia: Relation with Circulation and Possible Influence on Springtime Rainfall over China, Journal of Climate (Submitted)

Chapter 8. Research Advances on Cryospheric Change and Regional Sustainable Development in China

ZHANG Yili[1] and FANG Yiping[2]

1. Institute of Geographic Sciences and Natural Resources Research, Chinese Academy of Sciences,Beijing, 100101, China; 2. Institute of Mountain Hazards and Environment, Chinese Academy of Sciences, Chengdu, 610041, China

On the basis of analyses of the importance of cryospheric researches in China and the current status of cryospheric sciences over the world, Qin and Ding (2009) addressed some key issues and main contents that must be handled at present. Generally, the impacts of cryospheric changes on climate, sea level and physical environments receive worldwide concerns, whereas in China, cryospheric changes are of great importance in ecology, fresh water, physical environments and climate since China has a most developed cryosphere among countries in mid- and low-latitudes. The key issues that should be currently addressed are: i) fluctuation mechanisms of different types of glaciers in responses to climate changes and the scale-conversion in water resources assessments of glaciers; ii) modeling of water and heat exchanges between frozen soil and vegetation; iii) parameterization of physical processes in the cryosphere as well as their coupling with climate models. Towards full solution of these key issues, works in following three aspects should be highlighted, i.e. cyrospheric processes and their responses to climate changes, influences of cryospheric changes, and adaptation strategies for cryospheric changes. By this, more special progresses of cryospheric change and sustainable development research in China during 2005-2020 are described below:

1. Cryospheric change and disasters

Glacial lakes and glaciers are sensitive indicators of recent climate change. Chen et al.,(2007) presented the post-1986 changes in the size and distribution of both glacial lakes and glacier in the Poiqu River basin of southern Tibet, 60-100 km NW of Mt. Everest. Trends indicate that the total area of glaciers will continue to decrease and that both the numbers and areas of glacial lakes will continue to increase. Accompanying these trends will be an increased risk of debris flows, formed by entrainment of sediment in glacial-outburst floods and in surges from both failure and avalanche- and landslide-induced overtopping of moraine dams. Based on both the local and world-wide history of catastrophes from flows of these origins, disaster mitigation must be planned and appropriate engineering countermeasures put in place as soon as possible (Chen et al.,2007) .

Glacier lake outburst floods (GLOFs) have been a source of many local and some regional disasters and cause serious hazard. Hydrological records at the downstream gauging station on the Yarkant River in the Karakoram Mountains show that GLOFs now frequently repeat from the glacier lakes 500 km upstream, after an inactive phase of 10 years (1987-1996) (Wang et al., 2009). Wang et al.,(2009) investigated the abnormal GLOF and a glacier dammed lake using Landsat7 ETM + imagery in 2002. It is found that the dammed lake is clearly visible a long the Shaksgam valley at 4 700 m to 4 860 m in summer, with a maximum length of 6102 km and an area of 3101 km^2. Wang et al., (2009) argue that the GLOFs frequently occurrence caused by glacier advances at the lake basins results from the ice dam rise. In the recent decades, a decrease in both summer air temperature and meltwater and an increase in winter precipitation due to the increasing Indian Monsoon resulted in glacier advancing, glacier lake expanding, which also cause GLOFs occurrence more frequent and more intensive. Based on the glacial flood events and climate change in the Yarkant River basin during the past 50 years, Chen et al., (2010) investigated the long-term change of temperature and precipitation, the characteristics of glacial floods, the origin of sudden flood release, the suggested flood mechanism of glacial lakes and the relationship between glacial floods and climate change. Results showed that there was an obvious increase in the temperature of the basin since 1987. Specifically in the mountainous area, the significantly increasing temperature in the summer and autumn seasons accelerated the melting rate of glaciers and caused glacial-lake burst. Sudden flood release occurred frequently. The frequency of glacial lake outburst floods was 0.4 times/a during the period 1959-1986 and increased to 0.7 times/a during 1997-2006. Peak discharge also increased. There were seven floods with peak discharge over 4000 m3/s from 1959-2006, and three occurred after 1997. The increasing

frequency and magnitude of glacial outburst floods mirrored the effect of climate warming on glaciers.

2. The impacts of cryospheric change

2.1 The impacts of glacial change on water resource

Glacier is a kind of "solid reservoir" build by nature, which occupies an important status in the composing of water resources. The impact of cryospheric change on water resource has become a major concern attraction broad attention in China. In this context, numerous studies have been made.

The Tarim River Basin, a river system converged by nine source tributaries, is the mostly glacierised watershed in the arid northwest China, where there are 11665 glaciers with a total area of 19878 km^2 and a volume of 2313 km^3. Glaciers in the basin play a significant role in the water resource formation and variations. An estimation indicated that glaciers provide meltwater of about 133×108 m^3 every year, taking 39% of the total river runoff. With the influence of global warming, northwest China has experienced a general warming and drying change of climate since the mid-19th century (Liu et al., 2006). Liu et al., (2006) analyzed the variations of more than 3000 glaciers since the 1960s by applying topographical maps, high resolution satellite images and aerial photos for the river basin. Results indicate that glaciers in the basin has been mostly in retreat in recent 40 years, and the ice wastage have significantly influenced the variations of water resources in the Tarim River Basin. Similar study conducted by Lan et al., (2007) in Xinjiang Uigur Autonomous Region. The changes of the glaciers and the melting runoff from the glaciers in Xinjian, especially in the Tianshan Mountain since 1960 were analyzed based on Chinese Glacier Catalogue and some others observation data of glaciers (Lan et al., 2007). The results showed that the changes of the glaciers in Tianshan Mountain presented basically a cancrizans trend because of the impact of global warming since 1960. The glacier areas reduced averagely for 12% during the period from 1963 to 2000 (Lan et al., 2007). The runoff in most rivers which are supplied by melting runoff from glacier in the Tianshan Mountain presented an increasing trend along with the increase of melting runoff from glacier resulting by glacier in intense moving back (Lan et al., 2007). Li et al.,(2008) summarized the progress in the research on the impact of glacial change on water resources, and put forward the big gap between native research and foreign ones in scope and depth. Especially, the impact of west glacier change on socio-economy and ecological environment must be taken into consideration in the process of Western Development. Shen et al., (2009) studied the contribution and dynamic trend of glacier meltwater to runoff in Sary Jaz -Kumarik River Basin of Tianshan Mountains, Xinjiang. Shen et al., (2009) revealed that ice melt contributed about 58.65% of the total runoff in the Shehel hydrological Station, so the effects of changes in glacier meltwater on water resources is very vital. As a result of a large number of glacier ice melting which were accumulated in the past, by preliminary calculations, mass balance wastages supply additionally 309.47×$10^8$$m^3$, an increase of 6.19×$10^8$ m^3, about 13 % of annual runoff to the river due to climate warming in the past 50 years. The supply additionally of glacier melt is 5.3×10^8 m3, and occupies 11% of the mean annual river runoff in 1957 -1993, and is 8.8×10^8 m3 and 18% in 1994 -2006. With climate warming, although precipitation increasing, glaciers is more sensitive to temperature, the glacial meltwater will be increasing continually. Sun et al., (2010) also examined the relationship between runoff and glacial change in the Bosten Lake valley, Xinjiang Uygur Autonomous Region. Results reveal that proportion shift between runoff depth and precipitation contributes mainly to this fluctuation, and the change in glacier-melt up stream plays a crucial role in this process. Glacier melt makes valley water resources concentrate to the lower reach (terminal lake), which has resulted in the ample runoff period (1987~2002). Small and middle sized glaciers are more sensitive to temperature rising, with the gradual diminishing of these scale glaciers situated in a relative low altitude position the water supply from melting glaciers lessened. As a result, runoff depth fell back to a normal level under the mean precipitation, which also reflects the fact of rising falling curve in glacier-melt runoff during climate warming.

The other important region of this field is the Qinghai-Tibet Plateau. Wu and Zhu (2008) artificially interpreted boundaries of lake and glaciers in Nam Co Catchment, and quantified lake-glacier area variations in different stages by "integrated method" with the support of GIS. Results show that from 1970 to 2000, lake area increased from 1942.34 km^2 to 1979.79 km^2 at a rate of 1.27 km^2/a, while glacier area decreased from 167.62 km^2 to 141.88 km^2 at a rate of 0.86 km^2/a. The result suggests that lake expansion is mainly induced by the increase of the glacier melting water, increase of precipitation and obvious decrease of potential evapotranspiration. Zhang et al., (2009) discussed the Himalayan glaciers fluctuation over the latest decades and its impact on water resources. As Zhang et al., (2009) concluded, widely air temperature rising, precipitation decreasing, glaciers retreating and glacier lakes enlarging are the main features of Himalayan climate change and glacier fluctuations. In the middle section the Himalayas, among 23 glaciers,

an average of -7.0 m/a change were observed for the last several decades. The south slope of west Himalayas shows even fast retreating, for example, Gangotri Glacier has shown a recession of 28m/a during 1935-1996 and 34 m/a during1971-1996, meaning accelerate of melting in recent decades. Retreating glaciers result in the increase of glacial disasters and can impact regional river flow and long-term water resources in the Himalaya region. Based topographic map, TM, ETM and CBERS satellite images taken in the year of 1980, 1988, 2001 and 2005, the spatial variations of glaciers and lakes in the Ranwu Lake valley, southeast Tibetan Plateau, are analyzed using remote sensing and GIS technology (Xin et al., 2009). The results suggest that the increased runoff from glaciers contributed to the extending of lakes (Xin et al., 2009). Yao and Yao (2010) analyzed the impacts of glacial reretreat on runoff on Tibetan Plateau. Results indicate that with the climate warming since the 20th century, particularly the rapid warming since the 1980s, most glaciers are retreating. The runoffs of the seven rivers (the Yongtze River, Yellow River, Ganges River, Indus River, Yarlung Zangbo River, Nujiang River) have shown an unstable changing with the retreat of the glaciers. They tend to increase, particularly in the winter half year because of more glacial meltwater supply. As glaciers continuously retreat, the amount of glacial meltwater would decrease at some stage; this would be especially true in the middle and small reaches.

2.2 The impacts of frozen soil change on socio-economy

The land cryosphere, mostly underlain by permanently or seasonally frozen ground, is projected to experience a largest increase of near-surface temperatures under the Global Warming at the end of this century. Changes in hydro-thermal regimes in those regions, such as degradation of permafrost, or changes in the active layer depths and seasonally-frozen layers, are anticipated to exert a large impact both on the local socio-economy and eco-climate system.

In the past decades, the impact of frozen soil change on construction project has become a major concern attracting broad attentions in China. Bases on the elasto-plasticity theory and creep theory, by simulation of the variation of water content and temperature distribution and soil property, Wang et al., (2005) establishes a two-dimensional model to calculate the stress and deformation of highway embankment in permafrost area. In this model the creep deformation, the self-deformation in volume and the instantaneous deformation are considered. Especially the creep and instantaneous deformation behaviors under the changing process of soil property with time are studied. The sensitive permafrost environments along the Qinghai-Tibet Engineering Corridor (QTEC) from Golmud to Lhasa are controlled by periglacial processes, geography, geocryology and the local climate. During the past 50 years, permafrost has been degrading at a rapid rate due to the combined influences of steadily increasing human activities and persistent climatic warming, and extensive accelerated degradation has been observed along the QTEC (Jin et al., 2008). Jin et al., (2008) concluded that the environmental management and protection along the QTEC are urgent and important for the long-term stability of engineering foundations, and for the sustainable development on the Qinghai-Tibet Plateau (QTP). The development of a non-interference plan and acceleration in the enactment and enforcement of environmental protection (laws, regulations and stipulations) was highlighted based on an extensive and thorough understanding and practical rehabilitation techniques for disturbed or damaged permafrost environments (Jin et al., 2008). On the other hand, Jin et al., (2009) also discussed the principles and criteria for the zonation and assessment of the frozen-ground environments and conditions of engineering geology for the design, construction, and operation of the pipeline system based on an extensive and in-depth summary and analysis of the survey and exploration data. And the zonation, assessment principles and criteria have been applied in the design of the China-Russia Crude Oil Pipeline Route. They have also been used as the scientific bases for the construction, environmental management, operation and maintenance/contingency plans.

There is closely relationship between permafrost and ecosystem productivity. Permafrost play a significant role on vegetation production in the alpine grassland ecosystem in permafrost region due to that permafrost as semi-permeable could prevent soil moisture infiltrating and supply an ample water resource for plant growth, in the meanwhile, permafrost is beneficial for plant survivor and organism remaining in soil and played an important role on nutrients cycling. Therefore, the degradation of permafrost would alter vegetation pattern and change ecosystem productivity. Wang et al. (2006) reports results of a study of the correlation between permafrost changes and alpine ecosystem, finding that with the increase in the thickness of active layer, the vegetation cover and biomass of the alpine cold meadow exhibit a significant conic reduction, the soil organic matter content of the alpine cold meadow ecosystem shows an exponential decrease, and the surface soil material become coarse and gravelly. Those relationships resulted in the fact that the distribution area of alpine cold meadow decreased by 7.98% and alpine cold swamp decreased by 28.11% under the permafrost environment degradation during recent 15 years in Qinghai-Tibet plateau.

Guo et al. (2007) revealed that primary productivity of grassland decreased gradually during permafrost degradation: plant biomass lowed 60% when alpine marsh meadow changed into alpine meadow and alpine desert steppe had the lowest plant biomass, only about 500 kg/hm^2. However, there were not significantly different in plant biomass between alpine meadow and alpine steppe meadow. The main cause being responsible for permafrost degradation led to the decrease of ecosystem productivity was that ecological water level and groundwater level lowered due to increased depth of seasonal thawing layer, and soil moisture was not restricted in the surface soil reducing the available water to plant growth, causing the root withered and resulting in the decrease of primary productivity of alpine ecosystem (Yang et al., 2010). An anthropological study reported that the theory carrying capacity of livestock descended by 11% in the source regions of the Yangtze and Yellow Rivers due to mainly spatial change of frozen soil (ground temperature change) during 1980s~2000s (Fang et al., 2010b).

3. Cryospheric change and vulnerability

Social systems include personal, family, community subsystems and regions impacted by the considerations: cosmology, relations with 'the other' and changes in relationships to space and place-of which cryospheric change is the concern of this field. The extent to which individuals, families and communities are vulnerable is perhaps best understood in terms of concerns for security.

Based on the scientific evaluation guidelines and modes, by means of GIS and decision-supported systems, and comprehensive studies, an integrated analysis and vulnerability assessment system on cryospheric changes should be constructed to enhance adaptation measures on cryospheric changes in China (Qin and Ding, 2010).

3.1 Assessment index of vulnerability

The dominant elements of the cryosphere are glaciers, snow and permafrost. Using the framework defined vulnerability as a function of exposure, sensitivity, and adaptive or coping capacity (Fussel, 2007), Yang (2009) and Fang (2009) establish the assessment index of cryospheric vulnerability, and ecosystem vulnerability of the source regions of the Yangtze and Yellow Rivers respectively (see Fig 8.1 and Table 8.1).

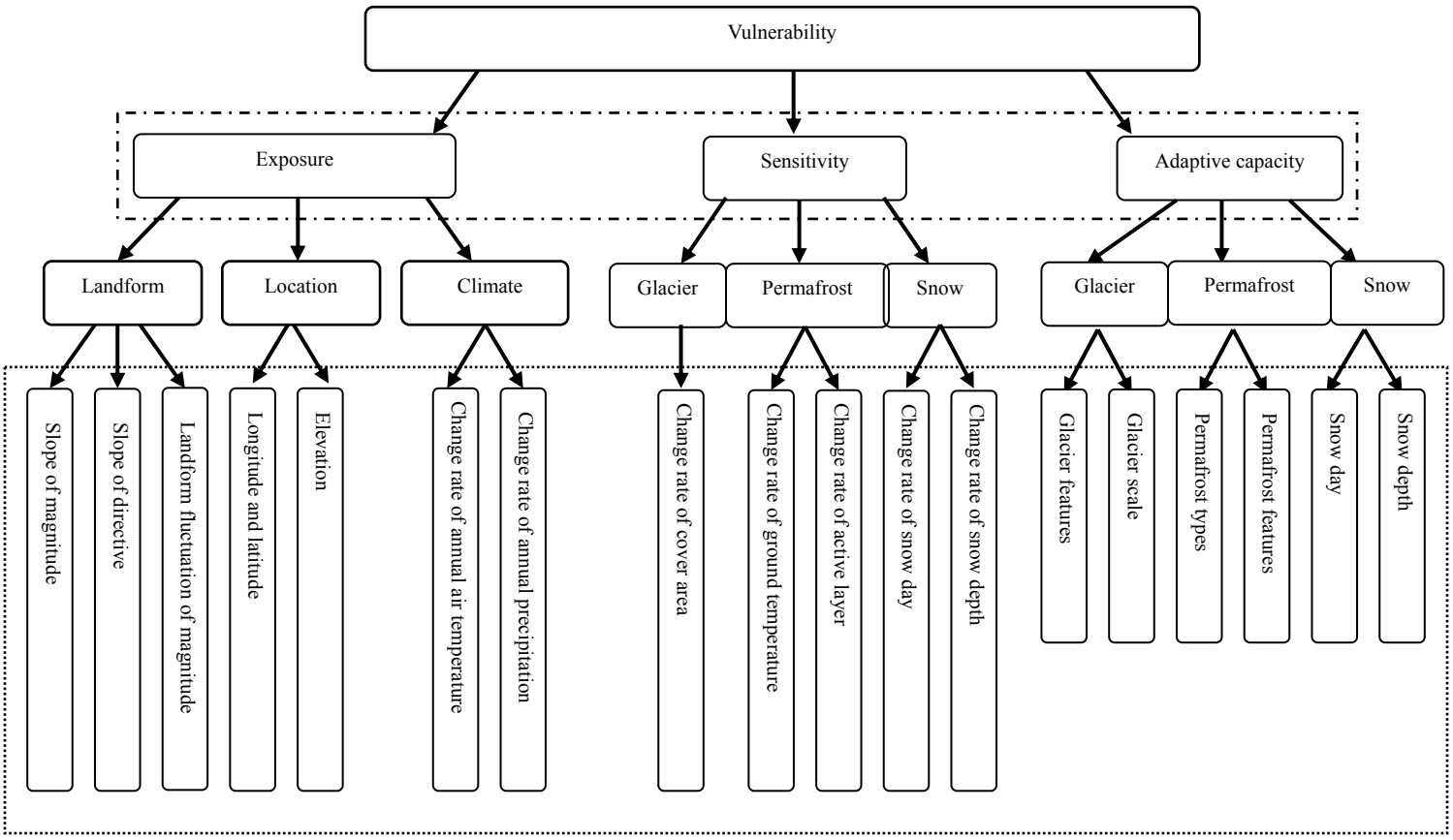

Fig 8.1 Assessment index of cryosphere in China

Table 8.1 Assessment index of ecosystem vulnerability for the source regions of the Yangtze and Yellow Rivers based on cryospheric change

First level	Second level	Detailed indicators
Exposure	Exposure of cryospheric chanhe	The number of glacier
		Distribution of glacier
		Days of snow cover
		Intensity of population
		Intensity of livestock
		Frequency of disaster
Sensitivity	Sensitivity of cryospheric chanhe	Change rate of water resource
		Variation coefficient of annual precipitation
		Change rate of 0cmground temperature
		Change rate of NPP
		Rate of vegetation degeneration
		Change rate of population intensity
		Change rate of livestock
Adaptive capacity	Adaptive capacity of cryospheric chanhe	Per capita area of grassland
		Per capita water resource
		Diversity index of ecosystem
		Fragmentation index of ecosystem
		Separation index of ecosystem
		Capacity of disaster prevention
		Living index
		The index of industrial sussession
		The index of public security
		Accessibility index of information
		The level of science and education

3.2 Vulnerability Assessment

Vulnerabilities are the gateways by which threats are manifested. In other words, a system compromise can occur through a weakness found in a system. A vulnerability assessment is a search for these weaknesses/exposures in order to apply a patch or fix to prevent a compromise. Decision-makers today face increasingly complex problems of cryospheric change that require integrative and innovative approaches for analyzing, modeling, and interpreting various types of information. Therefore, Fang (2009) develop the assessment index of vulnerability (especially in sensitive regions of cryospheric change, fragile ecosystem), and assess the vulnerability of ecosystem for the source regions of the Yangtze and Yellow Rivers according to the assessment index listed in Table1. And vulnerability is categorized into slightly, slightly strong, middle strong, strong and highly strong regimes. Results indicate that the source region of the Yangtze and Yellow rivers is characterized by middle strong vulnerability. The area of middle strong vulnerability occupies 41.26% of the whole areas. In spatial perspective, vulnerability magnitude is lower in western region than that of eastern region, and higher in southern region than that of northern region in the source region of the Yangtze and Yellow rivers. It is in consistence with permafrost sensitivity and spatial pattern.

Shen (2009) use vulnerability index approach of river basin, integrated resource stresses, development pressures, ecological insecurity and management challenges dimensions. And evaluate the vulnerability of Tarim river basin in Xinjiang Uigur Autonomous Region. Table 8.2 illustrates that the share of glacial meltwater is higher, vulnerability of river basin imposed by changing glacier is higher. This study highlights starkly the important of glacial meltwater to arid region of China. It also underscores the complex security concerns and water justice issues so pervasive in Xxinjian and whole arid regions of China politics.

Table 8.2 Vulnerability index of Tarim river basin based on cryospheric change

River basin	Share of glacier meltwater	Sensitivity of cryosphere	Vulnerability index
Yarkand-Kashgar River	0.64	0.36	0.20
Hetian River	0.45	0.55	0.41

Alksu-Weigan Rive	0.65	0.35	0.24
Kaidu-Kongque River	0.13	0.87	0.71
Easter Kunlun-North Aerjin River	0.40	0.60	0.34

4. Cryospheric change and adaptation

The changes in the cryosphere highlighted here interact in many ways. The interactions affect people in cryosphere and beyond, along with local, regional, and national environments. Understanding the results of these interactions is a major scientific challenge. Some of progresses under study in China are:

4.1 Himalaya north region

Although artificially inducing the retreat of glaciers may not be ecologically or climatologically wise, the Himalayan region nonetheless has an interest in storing glacial meltwater that represents the amount of glacial melt in excess of historic level. In many mountain regions, the quantity, variability, and timing of runoff from snowmelt and glaciers can directly and indirectly affect the incidence and prevalence of water-related disasters. Successful adaptation must be accomplished through actions that reduce vulnerabilities of poor people, as they dependent on ecosystem goods and services for their livelihoods. There is a need to restore a balance between economic interests and ecological imperatives. An integrated approach is needed to identify multi-stakeholders and participatory processes for the selection, implementation and appraisal of adaptation strategies. In this context, according to questionnaire survey, Yang et al., (2009) discussed the demands of adapting glacier retreating and adapting climate change for different social and economic sectors in Tingri County in the central Himalayas. In order to build the adaptation capacity of cryospheric change. Yang et al.,(2009) suggested that the local governments should firstly boost infrastructure construction against climate hazards, including infrastructures for preventing or controlling flood and drought. Energy construction can quicken local socio-economic development and facilitate an increase of adaptation capacity. Various types of professional and technical talents are necessary for adapting cryospheric change.

4.2 The source regions of the Yangtze and Yellow rivers

Taking the source regions of the Yangtze and the Yellow River as a case study, Fang et al., (2009) presents a conceptual framework for an adaptive management of mountain tourism services according to technical, policy, social and economic dimensions based on a vulnerability assessment of mountain ecosystems. Xu et al., (2010) establish the evaluation model of disaster adaptive capacity, and evaluate the response capacity in source Regions of the Yangtze and Yellow Rivers, in order to strengthen the disaster adaptive capacity of this region, suggested approaches include promoting the agglomeration of population, deepening ecological migration project and constructing new cities and towns; strengthening the road network and other transport infrastructure construction; improving policies to enhance the protection capacity of disaster relief etc. At the same time, Fang et al., (2010a) select pasture fence, livestock shed, pasture deratization, and artificial pasture construction as the intervention indictors of grassland ecosystem, and GDP per capita, herdsman income of per capita, the output of meat per capita as the indictors of economic welfare. Fang et al., (2010a) analyzed the relationship between intervention indictors of grassland ecosystem and indictors of economic welfare in the source region of Yellow river. The results show that there are close relationship between selected intervention indictors and economic welfare indictors. It means further that positive intervention approaches is critical to strengthen the adaptive capacity of grassland ecosystem under frozen soil change context in the source region of Yellow river.

Based on the evidence of frozen soil change, Fang et al., (2010b) establish the framework of adaptation of animal husbandry according to national, regional, and community scales, and release the detail instruments of cryospheric change adaptation, including adaptive capacity of policies, adaptive capacity of people, and adaptive capacity of the environment/key project. Fang et al., (2010b) suggest that further support to mainstream cryospheric change concerns in adaptation policies of animal husbandry must include a focus on support to knowledge management and social learning processes across multiple levels with a view to promoting the development of adaptation plans and support policies that reflect the needs of diverse stakeholders in sustainable utilization of the rivers source region's grasslands. And the attention to community capacity building is also very important. It is necessary to keep a constant iterative science policy dialogue among stakeholders in the region.

4.3 Northeastern China

Sun et al., (2009) select six typical counties in northeast China to investigate permafrost degradation and adaptation with some questionnaires. Sun et al., (2009) present the current situations, the reasons and strategies of the local adaptive permafrost degradation. The situations include: the local residents pay great attention to the climate changes, the effect of the ecologic protection policy is quite prominent, the adjustment of the industry structure has great potentials, but the management system of forestry has its deficiencies. The capability of adapting to the permafrost degradation in these areas is quite weak. The reasons are: the bad natural conditions and the vulnerable ecology, the low income of local people and their vulnerable adaptive capability, the difficult to employ forestry workers, the graze oriented lifestyle of pastoralists in grassland areas and t he lack of correspondingly alternative plans. The countermeasures are: First, relying on their high prestige, the local authority should reinforce the guide to deal with the permafrost degradation. Secondly, establish the reasonable ecological compensatory policy. Thirdly, strictly implement all kinds of measures and protect the farmers' deserved benefits. Fourthly, due to the high rate of forest fire which may be caused by the global warming, the prevention work should be made against fire. Finally, intensify the publicity of education as well as encourage people to build up a high sense of responsibility.

4.4 National scale

Questionnaire is designed facing experts in climate change and cryosphere science fields, some conclusions are drawn based on questionnaires statistical analysis: (1) the cryospheric change impacts on ecosystem significantly; changing of the cryosphere threats to human survival, and human being should can be not adaptable if the cryospheric change surpasses the threshold value; (2) governments should reinforce law related and increase investment in science and technology; Enterprises should promote clean production and energy reduction, adjustment of enterprise development strategies; Public awareness should be enhanced; especially to improve the breadth and depth public participation (Wang et al., 2009).

Zhou et al., (2010) distinguish the difference and relationship between climate change and cryospheric change, the impacts between on the natural ecosystem and human society in space and time by effective mechanisms and processes. And then correct policies and measures can be made against these changes.

References

1) CHEN Xiaoqing, CUI Peng, LI Yong, YANG Zhong, QI Yongqing. Changes in glacial lakes and glaciers of post-1986 in the Poiqu River basin, Nyalam, Xizang (Tibet).Geomorphology 2007,88(3-4):298-311
2) CHEN Yaning, XU Changchun, CHEN Yapeng, LI Weihong, LIU Jingshi. Response of glacial-lake outburst floods to climate change in the Yarkant River basin on northern slope of Karakoram Mountains, China. Quaternary International, In Press, Corrected Proof, Available online 15 January 2010
3) FANG Yiping. Research advance report of ecosystem vulnerability in the source regions of the Yangtze and Yellow Rivers, Annual meeting on Cryospheric progresses in China and their climatic, hydrologic and ecological effects and adaptation, 2009, Lanzhou, China.
4) FANG Yiping, QIN Dahe, DING Yongjian, YANG Jianping. Adaptation management of mountain tourism service: the case of the source regions of the Yangtze and Yellow rivers. Journal of Mountain Science, 2009,6(3):299-310.
5) FANG Yiping, QIN Dahe, DING Yongjian. The influence of grassland ecosystem manual intervention to economic welfare: a case of the source region of Yellow River. Resources and Environment in the Yangtze Basin 2010a,19(9):1009-1105.
6) FANG Yingping, QIN Dahe, DING Yongjian. The influence of spatio-temporal pattern of permafrost on NPP and policy adaptation implications: a case of the source regions of Yangtze and Yellow Rivers, International Joint Conference by the CliC and IACS, Cryospheric change and its influences-cryospheric issues in regional sustainable development, 12-14 August, 2010b, Lijiang, China.
7) FÜSSEL, H.M. Vulnerability: A generally applicable conceptual framework for climate change research. Global Environmental Change 2007, 17(2):155–167
8) GUO Zhenggang, NIU Fujun, ZHAN Hu, WU Baiqing. Changes of grassland ecosystem due to degradation of permafrost frozen soil in the Qinghai-Tibet Plateau. Acta Ecologica Sinica 2007, 27 (8) :3294-3301
9) JIN Huijun, HAO Jiaqian, CHANG Xiaoli, ZHANG Jianming, YU Qi'hao, QI Jilin, LU Lanzhi, WANG Shaoling. Zonation and assessment of frozen-ground conditions for engineering geology along the China-Russia crude oil pipeline route from Mo'he to Daqing, Northeastern China. Cold Regions Science and Technology, In Press, Corrected Proof, Available online 28 December 2009
10) JIN Huijun, YU Qihao, WANG Shaoling, LU Lanzhi. Changes in permafrost environments along the Qinghai-Tibet engineering corridor induced by anthropogenic activities and climate warming. Cold Regions Science and Technology 2008,53(3): 317-333
11) LAN Yougchao, SHEN Yongp ing, WU Sufen, ZHONG Yinjun, WEN Jun, MA Xiaobo, Hu Zeyong. Changes of the glaciers and the glacier water resources in the typical river basins on the north and south slopes of the Tianshan Mountains since 1960s. Journal of Arid Land Resources and Environment 2007,21(11):1-8
12) LI Zhiguo, YAO Tandong, TIAN Lide. Progress in the research on the impact of glacial change on water resources. Journal of

natural Resources 2008,23(1):1-8
13) LIU Shiyin, DING Yongjian, ZHANG Yong, SHANGGUAN Donghui, LI Jing, HAN Haidong, WANG Jian, XIE Changwei. Impact of the Glacial Change on Water Resour ces in the Tar im River Basin. ACTA GEOGRAPHICA SINICA 2006,61(5):482-489.
14) QIN Dahe, DING Yongjian. Cryospheric changes and their impacts: present, trends and key issues. Advances in Climate Change Research 2009,5(4):187-195.
15) QIN Dahe, DING Yongjian. Key issues on cryospheric changes, trends and their impacts. Advances in Climate Change Research 2010,1(1):1-10.
16) SHEN Yongping. Research advance report of typical river basin vulnerability, Annual meeting on Cryospheric progresses in China and their climatic, hydrologic and ecological effects and adaptation, 2009, Lanzhou, China.
17) SHEN Yongping, WANG Guoya, DING Yongjian, MAO Weiyi, L IU Shiyin, WANG Shunde, Duishen M Mamat kanov. Changes in glacier mass balance in watershed of Sary Jaz-Kumarik Rivers of Tianshan Mountains in 1957-2006 and their impact on water resources and trend to end of the 21th century. Journal of Glaciology and Geocryology 2009, 31(5):792-800.
18) SUN Xike, ZHOU Lihua, MA Yonghuan, ZHU Yanling, XIE Xia. The adaptive countermeasures against permafrost degradation in Northeast China. Journal of Glaciology and Geocryology 2009, 31(3):532-539.
19) SUN Zhandong, Christian Opp, WANG Run, GAO Qianzhao. Response of land surface flow to climate change in the mountain regions of Bosten ake Valley, Xingjiang, China. Journal of Mountain Science 2010,28(2):206-211
20) WANG Di, LIU Jingshi, HU Linjin, ZHANG Mingxuan. Monitoring and analyzing the glacier lake outburst floods and glacier variation in the upper Yarkant River, Karakoram. Journal of Glaciology and Geocryology 2009, 31(5):808-814.
21) WANG Gengxu, LI Yuanshou, WU Qinbai, WANG Yibo. Impacts of permafrost changes on alpine ecosystem in Qinghai-Tibet Plateau. Science in China-Series D (Earth Sciences) 2006, 49(11):1156-1169.
22) WANG Mingjie, FANG Yiping, YANG Jianping, ZHOU Lihua. Analysis of questionnaire survey cryospheric change and adaptation measures in China. Environment and Ecology in the Three Gorges 2009,2(1):1-4,9
23) WANG Tiehang, HU Changshun, LI Ning. Simulation method for calculating stress and deformation of highway embankment on frozen soil area. Cold Regions Science and Technology, 2005,42(2): 89-95
24) WU Yanhong, ZHU Liping. The response of lake-glacier variations to climate change in Nam Co Catchment, central Tibetan Plateau, during 1970–2000. Journal of Geographical Sciences 2008,18(2):177-189
25) XIN Xiaodong, YAO Tandong, YE Qinghua, GUO Liuping, YAN Wei. Study of the fluctuations of glaciers and lakes around the Ranwu Lake of Southeast Tibetan Plateau using remote sensing. Journal of Glaciology and Geocryology 2009, 31(1):19-26.
26) XU Keyan, FANG Yiping, BAO Wen. Resistance disaster ability evaluation based on 3S technology in the source regions of Yangtze and Yellow Rivers. Environment and Ecology in the Three Gorges 2010,32(2):29-31,34.
27) YANG Jianping. Research advance report of cryospheric change vulnerability, Annual meeting on Cryospheric progresses in China and their climatic, hydrologic and ecological effects and adaptation, 2009, Lanzhou, China.
28) YANG Jianping, TAN Chunping, LIU Junfeng, HAN Chuntan. Building up the capacity of adapting to the climate change in the Himalayas of China: demand investigation and analysis. Journal of Glaciology and Geocryology 2009, 31(3):510-517.
29) YANG Zhaoping, OU Yang Hua, XU Xingliang, ZHAO Lin, SONG Minghua, ZHOU Caiping. Effects of permafrost degradation on ecosystems. Acta Ecologica Sinica, 2010,30(1): 33-39
30) YAO Tandong, YAO Zhijun. Impacts of glacial reretreat on runoff on Tibetan Plateau. Chinese Journal of Nature 2010,32(1): 3-8.
31) ZHANG Dongqi, XIAO Cunde, QIN Dahe. Himalayan glaciers fluctuation over the latest decades and its impact on water resources. Journal of Glaciology and Geocryology 2009, 31(5):885-895.
32) ZHOU LiHua, ZHU YanLing, SUN XiKe. Distinguishing the effects of cryosphere change in the background of climate change in China. Sciences in Cold and Arid Regions 2010, 2(1): 0087–0092.

Appendex: Committee of CNC-IACS

Scientific Advisor Group: (in alphabetical order)

Chen Yiyu Cheng Guodong Cui Zhijiu Ding Yihui Dong Zhaoqian Hu Dunxin
Jiang Youxu Li Jijun Liu Changming Shi Yafeng Sun Shufen Wu Guoxiong Zhou Xiuji

Chair: Qin Dahe

Vice- Chair: Yao Tandong Ding Yongjian Dong Wenjie Luo Yong Yang Huigen Ma Wei

Committee: (in alphabetical order)

Bian Lingen	Chen Yaning	Chen Zhenlin	Deng Mingjiang
Ding Yongjian	Dong Wenjie	Fu Bojie	Guo Yaxi
He Daming	He Yuanqing	Jin Huijun	Kang Shichang
Li Xin	Li Yaoqing	Li Yuansheng	Li Zhen
Li Zhongqin	Liu Shiyin	Luo Yong	Ma Wei
Ma Yaoming	Qin Dahe	Ren Jiawen	Sun Liguang
Sun Bo	Tian Lide	Wang Genxu	Wang Ninglian
Wei Wenshou	Wu Bingyi	Wu Qingbo	Xiao Cunde
Yang Huigen	Yao Tandong	Ye Baisheng	Zhang Haisheng
Zhang Qiang	Zhang Renhe	Zhang Yili	Zhang Xiaolei
Zhang Jinzhao	Zhao Lin	Zhao Xinquan	Zhu Liping

Secretary General: Ding Yongjian

Vice-Secretary General: Chen Zhenlin Xiao Cunde (executive) Kang Shichang (executive)

Executive secretary: Xie Aihong Yang Jianping Qin Xiang

Working Groups:

1. Ice and Snow
   Leader: Wang Ninglian and Kang Shichang
2. Frozen Ground/Permafrost
   Leader: Wu Qingbai and Zhao Lin
3. Cold Regions Hydrology
   Leader: Deng Mingjiang and Ye Baisheng
4. Cold Regions Ecology
   Leader: Wang Genxu and Zhao Xinquan
5. Cryosphere Change and Climate Predict
   Leader: Luo Yong and Wu Bingyi
6. Remote Sensing, Observation and Data Base
   Leader: Li Xin and Li Zhongqin
7. Polar Science
   Leader: Xiao Cunde and Li Yuansheng
8. Eco-social Sustainability in Cryospheric Regions
   Leader: Zhang Yili and Fang Yiping.